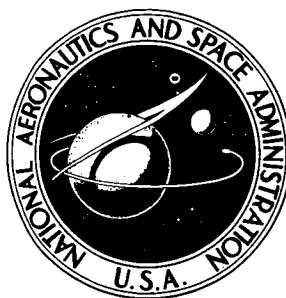


N 73 - 27808

**NASA CONTRACTOR  
REPORT**



**NASA CR-2270**

**NASA CR-2270**

**CASE FILE  
COPY**

**EXTENDED HYDRODYNAMIC THEORY  
OF THE PEAK AND MINIMUM  
POOL BOILING HEAT FLUXES**

*by John H. Lienhard and Vijay K. Dhir*

*Prepared by*

**UNIVERSITY OF KENTUCKY**

Lexington, Ky. 40506

*for Lewis Research Center*

**NATIONAL AERONAUTICS AND SPACE ADMINISTRATION • WASHINGTON, D. C. • JULY 1973**

|  |   |   |                             |
|--|---|---|-----------------------------|
| 1. Report No.<br><b>NASA CR-2270</b>   | 2. Government Accession No.                                 | 3. Recipient's Catalog No.  |                             |
| 4. Title and Subtitle<br><b>EXTENDED HYDRODYNAMIC THEORY OF THE PEAK AND MINIMUM POOL BOILING HEAT FLUXES</b>  |   | 5. Report Date<br><b>July 1973</b>  |                             |
|  |   | 6. Performing Organization Code   |                             |
| 7. Author(s)<br><b>John H. Lienhard and Vijay K. Dhir</b>  |   | 8. Performing Organization Report No.<br><b>None</b>  |                             |
|  |   | 10. Work Unit No.   |                             |
| 9. Performing Organization Name and Address<br><b>University of Kentucky<br/>Lexington, Kentucky 40506</b>   |   | 11. Contract or Grant No.<br><b>NGL 18-001-035</b>  |                             |
|  |   | 13. Type of Report and Period Covered<br><b>Contractor Report</b>   |                             |
| 12. Sponsoring Agency Name and Address<br><b>National Aeronautics and Space Administration<br/>Washington, D. C. 20546</b>   |   | 14. Sponsoring Agency Code  |                             |
|  |   | 15. Supplementary Notes<br><b>Project Manager, Thomas H. Cochran, Chemical Propulsion Division, NASA Lewis Research Center, Cleveland, Ohio</b> |                             |
| 16. Abstract<br><br>The hydrodynamic theory of the extreme pool boiling heat fluxes is expanded to embrace a variety of problems that have not previously been analyzed. These problems include the prediction of the peak heat flux on a variety of finite heaters, the influence of viscosity on the Taylor and Helmholtz instability mechanisms with application to film boiling and to the peak heat flux in viscous liquids, the formalization of the analogy between high-current-density electrolysis and boiling, and the description of boiling in the low-gravity limit. The predictions are verified with a large number of new data. |   |   |                             |
| 17. Key Words (Suggested by Author(s))<br><b>Peak heat flux<br/>Minimum heat flux<br/>Hydrodynamic theory</b>  |   | 18. Distribution Statement<br><b>Unclassified - unlimited</b>   |                             |
| 19. Security Classif. (of this report)<br><b>Unclassified</b>  | 20. Security Classif. (of this page)<br><b>Unclassified</b> | 21. No. of Pages<br><b>194</b>  | 22. Price*<br><b>\$3.00</b> |

## CONTENTS

Page

CHAPTER

|      |   |    |
|------|---|----|
| I.   | INTRODUCTION . . . . .  | 1  |
|      | Hydrodynamic Theory . . . . .   | 1  |
|      | Other Results . . . . .   | 2  |
| II.  | PEAK AND MINIMUM HEAT FLUXES FOR<br>INVISCID LIQUIDS ON INFINITE FLAT PLATES . . . . .          | 4  |
|      | The Original Hydrodynamic Theory . . . . .  | 4  |
|      | Modifications of the Theory. . . . .  | 10 |
|      | The Problem of the Finite Flat Plate . . . . .  | 11 |
|      | Experimental Determination of $q_{max}$ . . . . .   | 12 |
|      | Discussion of Experimental Results . . . . .  | 18 |
|      | Conclusions . . . . .   | 24 |
| III. | THE PEAK AND MINIMUM POOL BOILING<br>HEAT FLUXES ON FINITE HEATERS . . . . .                    | 27 |
|      | General Considerations . . . . .  | 27 |
|      | The Horizontal Cylinder, An Illustrative Example . . . . .                                      | 27 |
|      | The Evaluation of $\lambda_d$ and $A_j/A_h$ . . . . .   | 30 |
|      | Comparison of the Present Modified Theory with<br>Data for Cylinders . . . . .                  | 35 |
|      | Comparison of Theory with Data for Spheres . . . . .  | 35 |
|      | Comparison of Theory with Data for Horizontal<br>Ribbons Oriented Vertically . . . . .          | 42 |
|      | Conclusions . . . . .   | 48 |
| IV.  | A VISCOUS THEORY OF TAYLOR STABILITY<br>WITH APPLICATION TO FILM BOILING . . . . .              | 53 |
|      | Introduction . . . . .  | 53 |
|      | Hydrodynamic Analysis . . . . .   | 53 |
|      | Experimental Determination of Vapor Blanket<br>Thickness, Wavelength, and Growth Rate . . . . . | 64 |
|      | Vapor Blanket Thickness Correlation . . . . .   | 72 |
|      | Comparison of Wavelength Predictions with<br>Experiment . . . . .                               | 78 |
|      | Comparison of Wave Growth Predictions with<br>Experiment . . . . .                              | 82 |

|  |     |
|--|-----|
| Bubble Release Frequency . . . . .                                   | 91  |
| Effect of High Volume Fluxes on the<br>Dominant Wavelength . . . . . | 97  |
| On Predicting the Minimum Heat Flux . . . . .                        | 101 |
| Conclusions . . . . .  | 103 |
| V. THE PEAK HEAT FLUX IN VISCOUS LIQUIDS . . . . .                   | 104 |
| The Maximum Stable Vapor Velocity in a Jet . . . . .                 | 104 |
| Peak Heat Flux Prediction . . . . .                                  | 109 |
| Comparison of Theory . . . . .                                       | 110 |
| Conclusions . . . . .  | 117 |
| VI. HYDRODYNAMIC THEORY OF ELECTROLYSIS . . . . .                    |     |
| Introduction . . . . .   | 118 |
| The Transitions in Electrolysis . . . . .                            | 121 |
| Experiments . . . . .  | 124 |
| Discussion of Results . . . . .                                      | 131 |
| Conclusions . . . . .  | 137 |
| VII. BOILING ON SMALL WIRES . . . . .                                | 138 |
| Introduction . . . . .   | 138 |
| Experiment . . . . .   | 140 |
| The Inception of Boiling . . . . .                                   | 156 |
| Mixed-Mode Boiling . . . . .   | 159 |
| Film Boiling . . . . .   | 166 |
| Conclusions . . . . .  | 168 |
| VIII. CONCLUSIONS . . . . .  | 171 |
| APPENDIX A NOMENCLATURE . . . . .                                    | 174 |
| REFERENCES . . . . .   | 181 |

## SUMMARY

This report describes the last three years work of a five-year NASA-supported study of the interacting effects of gravity and geometry on the peak minimum and pool boiling heat fluxes. The work has generally sought to clarify this interaction by seeking an understanding of the hydrodynamic mechanisms which dictate it. Accordingly, this report emphasizes that portion of the last three year's work which has extended the hydrodynamic theory.

The work in this area, embracing two doctoral dissertations, two masters theses, two special undergraduate projects, and a variety of other studies, represents a major extension of the theory as a whole. The major elements of the report include:

- 1.) An extension of the hydrodynamic theory of the peak heat flux for flat plates of both finite and infinite size, supported by a great deal of new data.
- 2.) A general theory of the peak heat flux on finite bodies of various configurations. The theory is applied to a variety of particular configurations and supported, in these cases, by much new data.
- 3.) Viscous theories of the Helmholtz and Taylor stability problems. These theories are born out in great detail with new data for film boiling and for the peak heat flux, in viscous liquids. A viscous theory of the peak heat flux is developed and verified experimentally.
- 4.) A hydrodynamic theory, fully verified with new data, for high current-density electrolysis.
- 5.) An examination of the deterioration of the conventional boiling curve, that takes place when size or gravity are reduced to the point at which inertia ceases to be of importance. The result is a new phenomenon for which a new set of analyses are developed and corroborated with much original data.

## I. INTRODUCTION

During the past five years, the NASA Lewis Research Center has supported an ongoing study of the hydrodynamically dictated peak and minimum pool boiling heat fluxes at this laboratory. The results of this effort have ranged broadly over many related areas and they are reported in 28 project-related publications [1 to 28]<sup>1</sup>.

The general functional objective of the study was to learn how gravity influenced the peak and minimum pool boiling heat fluxes in various configurations. The primary contribution of the work has been to broaden the hydrodynamic mechanisms of these heat fluxes, as proposed by Zuber [29] and Kutateladze [30], into a general body of theory which can describe a large variety of situations. These mechanisms are the combined result of gravity, inertia, and capillary forces.

The initial stages of this program were summarized in the NASA Contractor Report [7] of the first two year's activity (Sept. 1967 to Sept. 1969). The first extension of the grant (Sept. 1969 to Dec. 1970) was reported by a brief letter listing the publications of that period. Therefore, this final report will detail the work of the first and second (Jan. 1971 to May 1972) extension periods as they relate to the hydrodynamic theory. Those efforts of the project which do not bear directly on the hydrodynamic theory will only be summarized briefly at the end of this chapter.

### Hydrodynamic Theory

The present report presents the following extensions of the hydrodynamic theory of the peak and minimum pool boiling heat fluxes, which have been made since the last contractor report [7] was presented:

Chapter II describes the hydrodynamic theory of the peak and minimum pool boiling heat fluxes on infinite flat plates. The theory, as originally formulated by Zuber, is altered in the light of recent experimental evidence and tested against new data. Chapter III is devoted to the adaptation of the theory to a variety of finite heaters. Many new experimental data are offered in verification of the resulting predictions.

The variable of viscosity is introduced in the IVth Chapter. Here the Taylor and Helmholtz stability theories, which underlie the hydro-

---

<sup>1</sup> Numbers in square brackets denote entries in the REFERENCES section.

dynamic processes, are formulated with consideration of the role of such variables as liquid depth, vapor density, and finally liquid viscosity. Experimental data are provided to verify the theory. In Chapter V, these results are used as the basis for predicting the peak heat flux in viscous liquids. Original  $q_{\max}$  data are given in verification of the prediction.

Chapter VI deals with the application of the hydrodynamic stability concept to high current-density electrolysis processes. Experiments and theoretical considerations show that the peak electrolysis gas flux does not correspond with the Helmholtz-unstable gas removal flux, as is the case in boiling. Rather it occurs at the Moissis-Berenson point of first hydrodynamic transition. A region of film electrolysis is also identified.

An important limitation on the hydrodynamic theory is its failure in situations where surface tension completely overbalances inertial forces. This occurs when heaters are very small or gravity approaches zero. Chapter VII treats the boiling process on very small wires in an attempt to learn how the transition to low-gravity behavior occurs. The peak and minimum heat fluxes are found to vanish completely. They are replaced by a heat flux vs. temperature curve that rises monotonically through a mixed natural convection and film boiling regime.

The objective of learning the role of gravity has been satisfied in that every theoretical result given in Chapters II through VII incorporates gravity explicitly, and every experimental correlation incorporates the variable of gravity in the nondimensionalization.

### Other Results

A great deal of the work done on the project has been essentially omitted from the present account since it would add unduly to the length of the report. We shall therefore describe the deleted material briefly before moving on to the hydrodynamic theory:

Condensation: The practical problem of refluxing boiled liquids within the centrifuge led to theoretical work on condensation and natural convection in variable gravity fields. A first paper on laminar condensation [10] showed how to rewrite Nusselt's equation in a form that will apply when gravity varies along the condenser, and which will handle a variable radius of curvature as well. The equation differs from Nusselt's equation only in that it replaces gravity with an "effective gravity" which takes account of the arbitrarily variable gravity and radius.

A second paper on laminar condensation [23] showed how an arbitrary variation of wall suction could also be incorporated into this sort of analysis.

Convection: A second problem that was motivated by the reflux condenser design was that of predicting natural convection heat transfer in a variable gravity field. This led us to formulate a general integral method for predicting natural convection in a variable gravity field [22]. The method was applied to a variety of rotating, and curved-surface, heaters. A series solution was developed for the full differential equation to provide verification of the accuracy of the integral method.

Fin design: A brief note was written to show how to design a "perfectly effective" fin [8]. By boiling a coolant on a fairly short, isothermal fin, near the peak heat flux, an extraordinarily high heat removal rate can be achieved. Design relations are given for such a fin.

Electrolysis bubbles: An important task within the last grant from NASA was that of exploring the analogy between gas formation and removal in electrolysis and boiling. The task was divided into two portions: a) a study of the analogy between electrolysis and boiling bubble growth, and b) the study of the analogy between the hydrodynamic stability mechanisms in electrolysis and boiling which is treated in Chapter VI.

The bubble growth analogy is dealt with in references [11] and [17]. In these studies, the equations for bubble growth are non-dimensionalized in such a way as to make them identical for either electrolysis or boiling. Comparisons are then made between predictions of electrolysis bubble growth and measurements of vapor bubble growth.

Computer coding: A very large number of data had to be cast into various schemes of non-dimensionalization. For convenience of handling the data, a computer code was developed. The complete data of the project were put on cards and the equations for the physical properties of the boiled liquids were assembled in a subroutine. The routine makes it possible to call forth plots of any appropriate data in any desirable scheme of non-dimensionalization. This code is described fully in reference [13].

## II. PEAK AND MINIMUM HEAT FLUXES FOR INVISCID LIQUIDS ON INFINITE FLAT PLATES

### The Original Hydrodynamic Theory

The hydrodynamic theory of Zuber showed rationally in 1958 [29] why the older correlative equation of Kutateladze [30] for the peak heat flux,  $q_{\max_F}$ , on a horizontal flat plate:

$$q_{\max_F} = (\pi/24) \rho_g^{1/2} h_{fg} [\sigma g (\rho_f - \rho_g)]^{1/4} \equiv q_{\max_Z} \quad (1)$$

was correct<sup>2</sup>. He formalized Kutateladze's suggestion that the peak occurred when the vapor outflow from the plate became enough to obstruct the returning liquid flow: Figure 1 shows his physical idealization of the process.

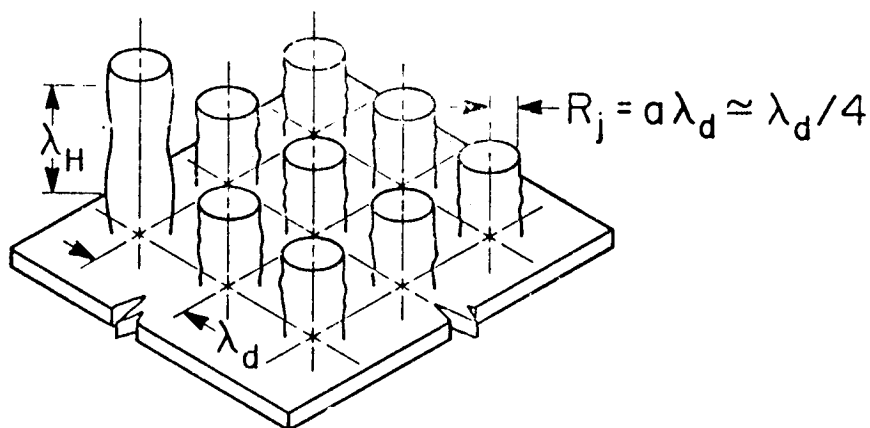


Fig. 1 Zuber's vapor jet configuration for boiling from a horizontal flat plate heater

The square array of jets is spaced on the "most susceptible" or most rapidly growing Taylor unstable wavelength. This is sometimes

<sup>2</sup> Symbols not explained in context are ones in common use. They are explained in the NOMENCLATURE section.

called the "most dangerous" wavelength; hence the symbol,  $\lambda_d$ , is used to identify it. The reason for this choice is that the vapor generated at the plate is lighter than the liquid above it and the configuration is inherently Taylor-unstable.

Zuber had access to no experimental data of a kind that would tell him whether the interface would collapse into jets on the most susceptible wavelength, the "critical" (or shortest unstable) wavelength,  $\lambda_c$ , or some other wavelength entirely. Hence he was forced to guess that the collapse would occur somewhere between  $\lambda_c$  and  $\lambda_d = \sqrt{3} \lambda_c$ . We shall provide a good deal of evidence related to this point in Chapter IV.

The theory of Bellman and Pennington [31] gives  $\lambda_d$  for a horizontal inviscid interface between a liquid (f) and a gas (g) with surface tension,  $\sigma$ , as:

$$\lambda_{d_F} = \sqrt{3} \left[ 2\pi \sqrt{\sigma/g(\rho_f - \rho_g)} \right] = \sqrt{3} \lambda_c \quad (2)$$

where the subscript, F, is added to remind us that this result is restricted to an undisturbed interface that is flat.

The jet pattern is now known to be well-established at heat fluxes far below  $q_{max}$ . In 1962, Moissis and Berenson [32] showed that the jets came into being as the result of a hydrodynamic transition from isolated bubble behavior to continuous columns. They gave an expression for this transition and corroborated it with experimental data. Thus Zuber's proposal that the vapor generated at the wall is carried away in these jets was shown to be true over much of the range of nucleate boiling.

The jets continue to serve as the vapor escape route until the vapor velocity is high enough to make them Helmholtz unstable. This instability causes the entire process to collapse and it defines the maximum attainable heat flux in nucleate boiling. We can then write the peak heat flux as the maximum latent energy transport from the surface:

$$q_{max} = \rho_g h_{fg} (A_j/A_h) U_H \quad (3)$$

where  $A_j$  and  $A_h$  are the cross-sectional area of the jets and the area of the heater, and  $U_H$  is the vapor velocity for which the jets become Helmholtz unstable.

Equation (3) is perfectly general. It applies to any configuration if the right values of  $A_j/A_h$  and  $U_H$  are used. To evaluate  $A_j/A_h$  for a

flat plate one assumption must be made, namely that the radius of a jet is  $\lambda/4$  where  $\lambda$  is the actual wavelength -- be it  $\lambda_d$ ,  $\lambda_c$ , or some other value. This assumption has been supported by some experimental evidence (see e.g. [33] or information presented later in this chapter). Using it we obtain:

$$A_j/A_{h/F} = \pi/16 \quad (4)$$

The critical velocity,  $U_H$ , can be shown (see e.g. [34], pg. 462 or [12] to be

$$U_H = \sqrt{2\sigma/\rho} \lambda_H \quad (5)$$

where  $\lambda_H$  is the disturbance which amplifies and becomes Helmholtz-unstable. This result, like all of the results we shall present in this chapter, is restricted to system pressures that are not near the critical pressure. This means that  $\rho_g/\rho_f$  is  $\ll 1$  and that the liquid inflow velocity is negligible with respect to the vapor outflow velocity.

Finally, we must determine the appropriate value of  $\lambda_H$ . Zuber guessed the critical Rayleigh wavelength to be the dominant existing disturbance in the jet. A vapor jet in a liquid collapses in capillary waves just as a free liquid jet in a gas does. Rayleigh (see [34], pg. 473) showed that this wavelength is equal to the circumference of the jet, or  $\pi\lambda/2$  in the present case.

Finally, Zuber substituted equations (4) and (5) in equation (3). Then, using equation (2) for  $\lambda$  in  $\lambda_H = \pi\lambda/2$ , he obtained equation (1).

In formulating expressions for  $q_{\max}$  and  $q_{\min}$ , Zuber actually began by thinking about the transitional boiling regime and he conceived the peak and minimum heat flux transitions as limiting points of this regime. Throughout the transitional boiling regime, vapor blankets the heater in greater or less degree. The liquid spills through the vapor from time to time, either touching the surface or at least drawing very close to it. As the surface temperature of the heater is reduced, more liquid contact can be sustained and the heat flux is improved. Finally, the Helmholtz-stable jet is re-established at a heat flux equal to  $q_{\max}$ .

An important feature of the transitional boiling regime is that it involves a vapor blanket beneath the liquid bulk. Thus this blanket must constantly collapse in Taylor-unstable waves to release vapor and admit liquid. The vapor escape paths will then be arranged on a rectangular grid of Taylor-wavelength spacing everywhere in the transitional regime.

The minimum heat flux is reached when the heat flux matches the minimum rate of latent heat removal that will sustain the regular formation and collapse of Taylor waves in the interface over the plate. If the heat flux is anything less than this, the interface will collapse onto the plate cooling it and re-establishing nucleate boiling. The minimum appears to occur in practice after the Leidenfrost point (beyond which the surface is too hot to permit direct liquid contact) has been reached.

The minimum heat flux,  $q_{\min}$ , can then be written as

$$q_{\min} = \rho_g h_{fg} \left[ \begin{array}{l} \text{volume of} \\ \text{a bubble} \end{array} \right] \left[ \begin{array}{l} \text{bubbles per cycle} \\ \text{for unit area} \end{array} \right] \left[ \begin{array}{l} \text{minimum wave} \\ \text{frequency} \end{array} \right] \quad (6)$$

Figure 2 shows the vapor removal configuration as it typically appears in reality.

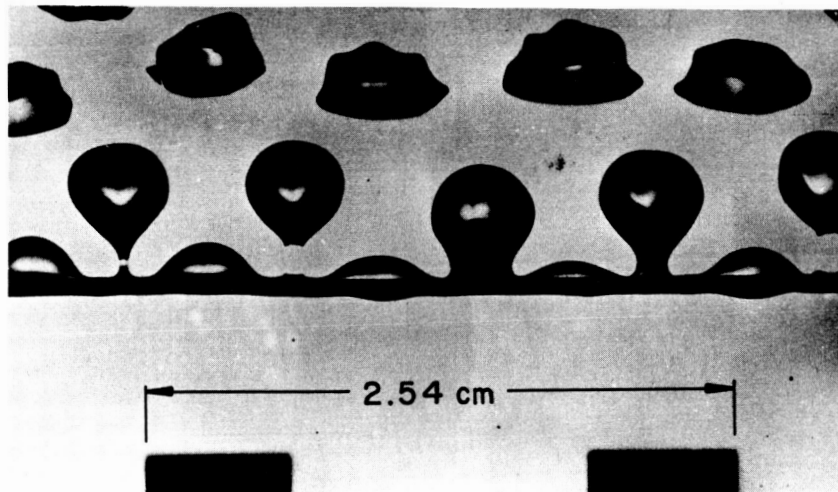


Fig. 2 The film boiling of acetone near the minimum heat flux.  
0.646 mm dia. wire.

Zuber assumed the radius of departing bubbles to be  $\lambda/4$ . This, indeed, was the motivation for his assumption that the jet radius is  $\lambda/4$  and it has subsequently been verified experimentally [33]. The number of bubbles released per cycle in a unit area is  $4/\lambda_d^2$  for the flat plate.<sup>3</sup>

<sup>3</sup>Zuber erred on this point and wrote  $2/\lambda_d^2$  (see [12], pg. 25). However, his number turns out to be correct for a legitimate 3-dimensional interface.

Finally, the minimum wave frequency poses the most serious difficulties since most of the growth of the wave up to the point of bubble release is non-linear. Zuber attempted to guess the relation of the average growth rate to the initial linear growth rate of the wave. Berenson [35] subsequently objected, pointing out that there is insufficient information to predict this average. Additional data is required to get the minimum frequency.

Berenson argued that the minimum wave frequency is directly proportional to  $-i\omega_{\max}$ , where  $\omega_{\max}$  is the frequency of exponential growth of the linear wave, and a pure imaginary number. Using these results and writing the volume of the bubble as  $(4\pi/3)\lambda_d^3/64$ , we get

$$q_{\min F} = \text{constant } \rho_f h_{fg} \lambda_{dF} (-i\omega_{\max}) \quad (7)$$

The theory of Bellman and Pennington [31] includes the expression for  $(i\omega_{\max})_F$

$$(-i\omega_{\max})_F = \sqrt{\frac{2\pi}{\lambda_d}} \left[ \frac{g(\rho_f - \rho_g)}{(\rho_f + \rho_g)} - \frac{4\pi^2 \sigma}{\lambda_d^2 (\rho_f + \rho_g)} \right]^{1/2} \quad (8)$$

combining equations (2), (7), and (8) we obtain at last

$$q_{\min F} = \text{constant } \rho_g h_{fg} \sqrt{\frac{4 \frac{g(\rho_f - \rho_g)}{(\rho_f + \rho_g)}}{(\rho_f + \rho_g)^2}} \quad (9)$$

The constant in equation (9) must really be determined experimentally. Zuber originally suggested a value of 0.177 which is too high. Berenson's experiments subsequently fixed it at 0.09 and that is our best information to date.

While we have gone into detail in describing Zuber's enunciation of the hydrodynamic theory, we shall, for completeness, include a brief chronological review of the overall development of the theory prior to the period covered by this report.

1948: Kutateladze [30] proposes the choking mechanism of the peak heat flux, and uses dimensional analysis to obtain an empirical expression for  $q_{\max}$  on a horizontal flat plate heater.

1956: Borishanski [36] extends the correlation of Kutateladze to include the effect of viscosity. For large flat heaters he finds that

$$q_{\max_F}^{\text{viscous}} = \left[ 1 + 30.5/N^{2/5} \right] q_{\max_F} \quad (10)$$

where  $N$ , the "Borishanski number" is:

$$N = \frac{\rho_f \sigma}{\mu_f} \left[ \sigma/g (\rho_f - \rho_g) \right]^{1/2} \quad (11)$$

1957: Chang [37] observes that the Taylor instability is basic to natural convection from heated horizontal plates, and to film boiling as well.

1958: Zuber and Tribus [29], [38] propose the analytical model of the burnout process that we have discussed here.

1962: Berenson [35] reconsiders Zuber's theory both experimentally and analytically. He supports the  $q_{\max}$  theory with an experimental verification of the predicted insensitivity of  $q_{\max}$  to surface condition. He also shows, both analytically and experimentally, that the constant in equation (9) must be determined empirically and that it can be altered by surface effects.

1963: Lienhard and Wong [33] show how to adapt Zuber's  $q_{\min}$  prediction to a horizontal cylinder configuration. The work involves a prediction of the radius-dependent Taylor-wavelength for this configuration. In 1969 [5], Lienhard and Sun provide an extension of these ideas and a discussion of some of the limitations on them.

1964: Bobrovich, Gogonin, and Kutateladze [39] use dimensional analysis based on the hydrodynamic theory to show that  $q_{\max}$  data for complex geometries can be correlated with:

$$q_{\max} / q_{\max_Z} = \text{fn}(L') \quad (12)$$

where  $L'$  is a scale parameter based on a characteristic length,  $L$ :

$$L' = L \sqrt{g (\rho_f - \rho_g) / \sigma} \quad (13)$$

This work was also done independently by Lienhard and Watanabe [40] in 1965, who also provided some theoretical justification for equation (12).

- 1970: Lienhard and Keeling [4] discuss the inclusion of the Borishanski number in  $q_{\max}$  correlations in general. They show that when heaters are arranged so that the rising vapor induces a secondary flow of liquid into the jets and columns, the influence of  $N$  can be very great.
- 1970: Sun and Lienhard [6] make a successful hydrodynamic prediction of  $q_{\max}$  for horizontal cylindrical heaters.

### Modifications of the Theory

Zuber's theory for  $q_{\max_Z}$  involved assumptions which can be questioned in the light of things that have been learned during the intervening years. These questions will lead to a modified prediction of the peak heat flux on a flat plate, which we designate as  $q_{\max_F}$  as opposed to Zuber's value,  $q_{\max_Z}$ .

Since experimental data [33] verified Zuber's assumption that the jet radius,  $R_j$ , equals  $\lambda_d/4$  for horizontal cylindrical heaters, we shall accept this assumption as being true for infinite flat plates as well.

The length of the Helmholtz unstable wavelength in the vapor jets is very hard to know a priori. It was found in the study of  $q_{\max}$  on horizontal cylinders [6] that Zuber's use of the Rayleigh wavelength is probably valid as long as the heater (and, with it, the jet) is small. Indeed the Rayleigh wavelength can be seen clearly in the jet leaving a small sphere [15]. But on larger bodies, from which the vapor leaves in a larger jet, the Rayleigh wave becomes much longer than  $\lambda_d$ . And  $\lambda_d$  is the dominant disturbance in the liquid-vapor interface. This wavelength is picked up from the interface and carried into the jets in a rather advanced state of development.

Accordingly the jets may collapse at a lower vapor velocity [cf. equation (5)] due to Rayleigh instability but only after the vapor has been carried

far out of harm's way. The collapse will not lead to burnout. At a somewhat higher vapor velocity, however, the shorter disturbances of length,  $\lambda_{dF}$ , will be triggered and the process will collapse at the surface. Thus we pick  $\lambda_H = \lambda_{dF}$  instead of  $2\pi R_j$ , for use in equation (5), when we deal with the relatively large jets above a flat plate. Using equation (2) for  $\lambda_{dF}$  this gives

$$U_H = \sqrt[4]{\sigma_g (p_f - p_g) / 3\rho_g^2} \quad (14)$$

The area ratio  $A_j/A_h$  will be  $\pi/16$  regardless of the exact value of  $\lambda$ . Substituting equations (1), (4) and (14) in equation (3) we then obtain

$$\frac{q_{\max_F}}{q_{\max_Z}} = 1.14 \quad (15)$$

Thus Zuber's original expression gave values about 14% less than we would expect to obtain experimentally.

### The Problem of the Finite Flat Plate

Equation (15) should give good results for finite plates as long as their dimensions greatly exceed  $\lambda_{dF}$ . However, as the plate dimensions approach  $\lambda_{dF}$ ,  $A_j/A_h$  will begin to vary discontinuously with plate size. The reason for this is that a small plate will have, say, one single jet on it. As the plate is increased in size, an additional jet (or jets) will be added, and the peak heat flux (which has been dropping up to this transition point) will suddenly be increased by a factor equal to the new number of jets.

In counting the maximum number of jets that can be accommodated on a plate of a given size, we assume that, if there is more than one jet on a plate, then no jet will lie closer than  $\lambda_d/4$  to the vertical side-wall which must rise from the edge of the plate. Thus (with reference to Fig. 3) a square plate may be any size up to  $4\lambda_d^2$  and it will have only one

jet on it. At this point  $q_{\max}$  will be very small--only a fourth of the predicted value. But now the single jet will give way to an array of four jets and  $q_{\max}$  will once again assume the predicted value.

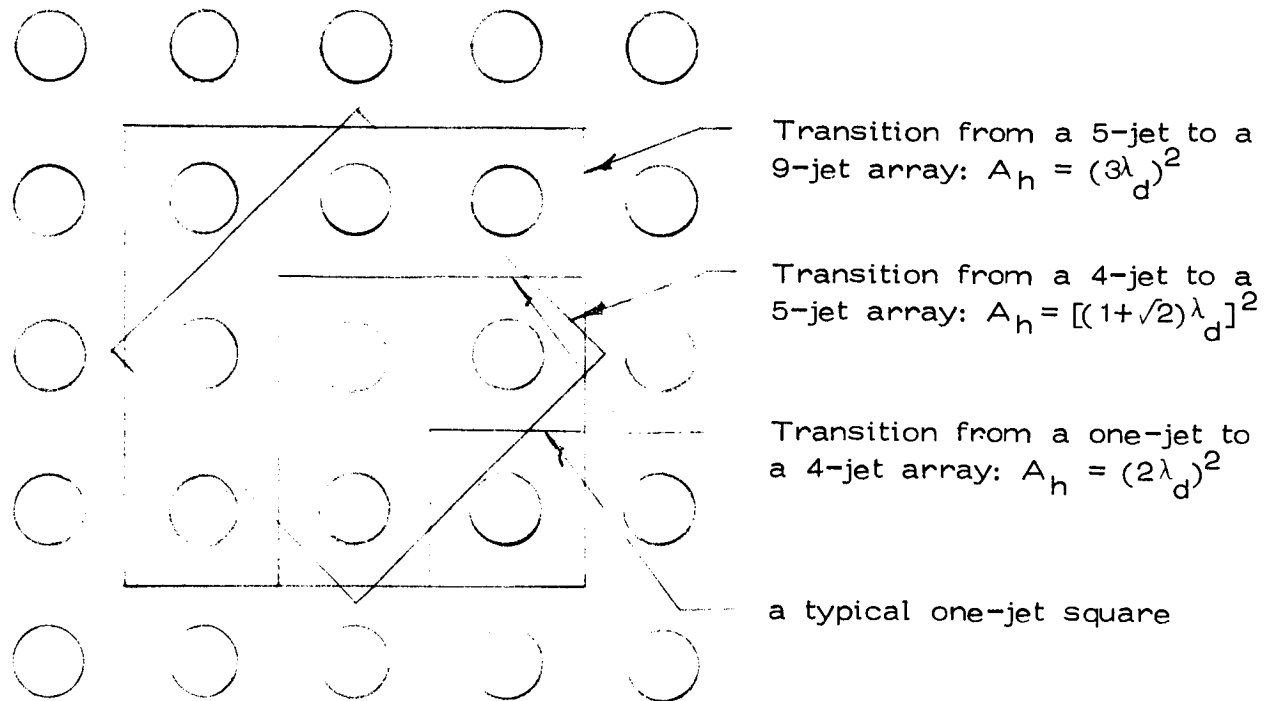


Fig. 3 Jet configurations on square heaters of various sizes.

This rationale can be continued. However, it becomes less satisfactory as larger and larger numbers of jets are considered, because the wavelength can vary somewhat around  $\lambda_d$ . The actual heat flux will equal the infinite flat plate value multiplied by  $(N_j \lambda_d^2 / A_h)$ , where  $N_j$  is the number of jets on the plate. This factor will approach unity as  $N_j$  and  $A_h$  become large. The same rationale can easily be applied to circular, or other shaped, plates.

#### Experimental Determination of $q_{\max_F}$

An important point relative to Zuber's equation is that it was never systematically tested against data obtained in the configuration for which it was intended. To approximate an infinite flat plate experimentally, one must first employ a very clean finite plate, much larger in any dimension than  $\lambda_d$ . Then he must employ vertical side walls to prevent a horizontal

inflow of liquid since this has been shown [41, 4] to seriously influence  $q_{\max}$ .

The data we have located which meet these criteria are few. The vast majority of available flat plate data were obtained with strip or disc heaters in open pools and are hence unusable. The classical data of Cichelli and Bonilla [42] are for the correct configuration--a 9-1/2 cm dia. disc heater which formed the bottom of a tubular container for the boiled liquid. But very many of their data must be eliminated because they were obtained on "dirty" heaters. Most of the remainder are for nominal fluids of extremely low purity--actually mixtures for which properties are not known and correlations cannot be applied. Only a few of their data for ethanol remain for use. Berenson presented similar data for  $\text{CCl}_4$  and n-pentane on 5 cm dia. heaters that were subject to very close control of surface condition.

Owing to the paucity of available data, a program for the experimental determination of the peak heat fluxes on finite and "infinite" flat plates was carried out, both at earth-normal gravity and at elevated gravities. By "infinite" flat plates, we mean ones with dimensions much larger than the "most susceptible" wavelength,  $\lambda_D$ , and one with side walls to avoid any inflow of liquid from the sides. The flat plate we used accommodated more than three wavelengths for the alcohols, and about two for water, at earth-normal gravity; while these numbers increased as  $g^{1/2}$  at higher gravities. The observations were made for both viscous and nearly-inviscid liquids. The reagent grade liquids used were: acetone ( $\text{CH}_3\text{-COCH}_3$ ), benzene ( $\text{C}_6\text{H}_6$ ), isopropanol ( $\text{CH}_3\text{CHOH CH}_3$ ), methanol ( $\text{CH}_3\text{OH}$ ), distilled water and cyclohexanol ( $\text{CH}_2(\text{CH}_2)_4 \text{CHOH}$ ).

A detailed description of the flat plate apparatus is given in reference [27], and we shall only describe some of its major features here. The apparatus consisted of a heater, a heater support, an emergency shut-off mechanism and a reflux condenser. This entire assembly was designed to operate either at earth-normal gravity or to be placed in the Centrifuge Facility of the Boiling and Phase-Change Laboratory at the University of Kentucky. A schematic diagram of the apparatus is shown in Fig. 4.

The heater itself was made of pure copper with a circular bell shaped configuration. It has a diameter of 6.35 cm at the boiling surface, 10.16 cm at the butt end, and a height of 10.8 cm. A pyrex glass cylinder allowing a liquid head of about 6 cm sits on the heater surface and is held in place by two stainless steel flanges. Stainless steel has a much lower thermal conductivity than copper, hence the flanges have a very small cooling effect on the edges of the boiling surface. The total height

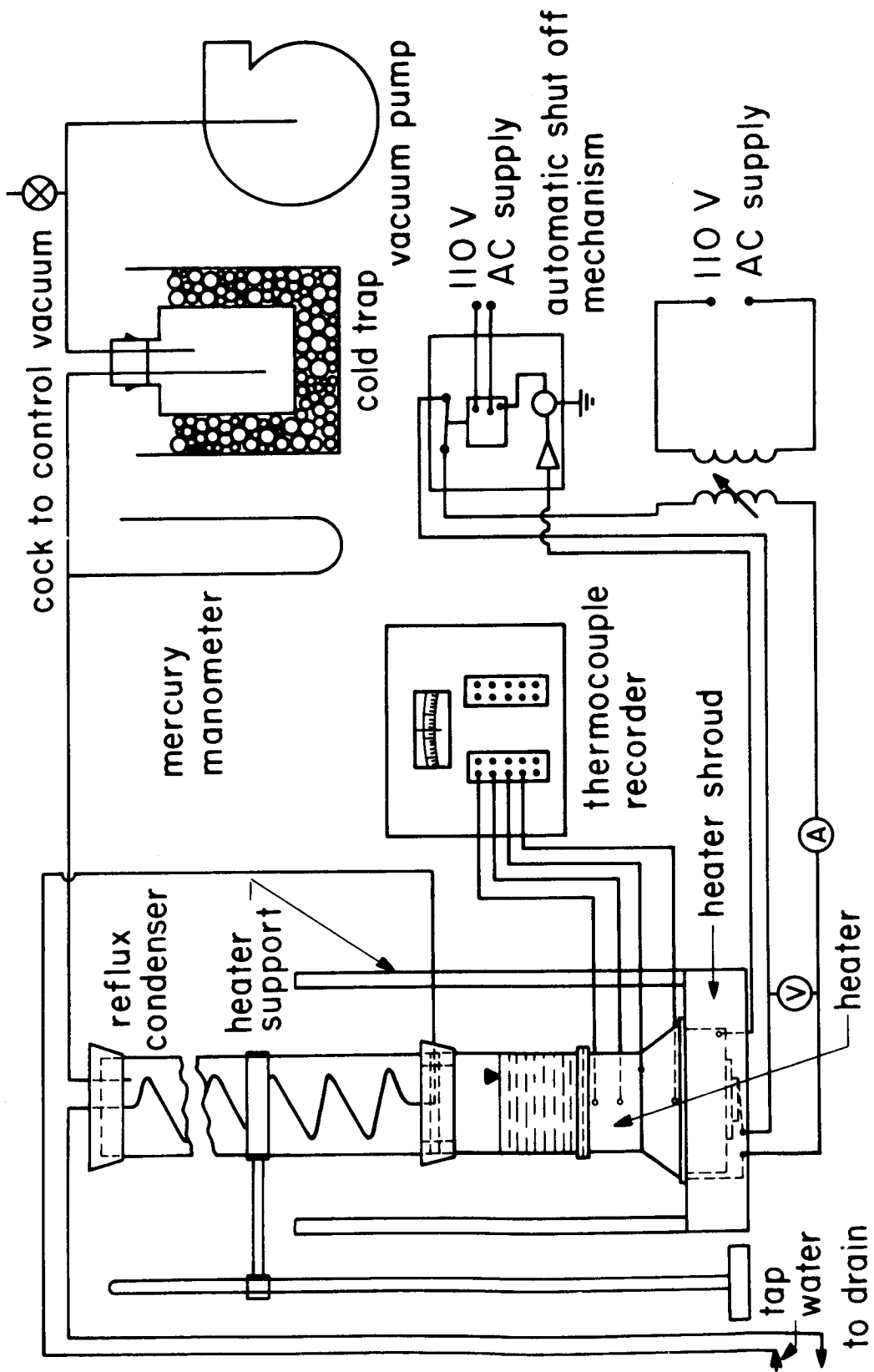


Fig. 4 Schematic diagram of stationary flat plate test.

of the heater with the glass cylinder is about 19 cm and it has a final weight of 5 kg.

Figure 5 shows a sectioned view of the heater. Its lower portion consists of three rings wound with 4 meters of 1.62 mm dia. nichrome wire, capable of dissipating 6 kw of power. Five iron-constantan thermocouples are positioned as shown in the figure to monitor the temperature in various parts of the heater body. The top two thermocouples were used to determine the heat flux to the boiling surface. A third thermocouple was used for a counter-check on the heat flux calculations and a fourth thermocouple to show whether steady state conditions are reached.

The thermocouple in the base monitored the temperature for an electronic emergency shut-off system. This system cut off the power supply after the peak heat flux was reached. This was necessary because this transition effectively insulated the surface and permitted the temperature in the rings to run away. This system is fairly complex and full details are given in reference [27].

Elevated gravity tests were performed on the existing centrifuge facility. Complete details of the centrifuge design are given in reference [1]. Figure 6a shows the centrifuge designed and built to obtain 100 times earth normal gravity at a speed of 360 rpm. When the flat plate heater is put on the centrifuge, its boiling surface is 77.7 cms from the center of rotation.

Electrical connections to the centrifuge are made through slip rings attached to the drive shaft. Those include twelve circuits for power input, voltage measurement, and for thermocouples. The drive shaft also carries a tube which is connected to a vacuum pump through a stationary vacuum seal.

A strobe light is placed on a bracket attached to the stand supporting the centrifuge. It is triggered by a photo-electric pick-off which senses light reflected from a shiny metal piece attached to the centrifuge arm. Thus each revolution of the arm triggers the light and the heater appears to stand still so one can view the boiling process. Figure 6b shows the flat plater heater assembly in position on the centrifuge arm.

Before each test, the boiling surface was polished with 220 grit size emery paper to remove any rust or carbon deposit formed during the previous observation. The surface was then cleaned with soap and warm water and rinsed with the test liquid. This was done to ensure

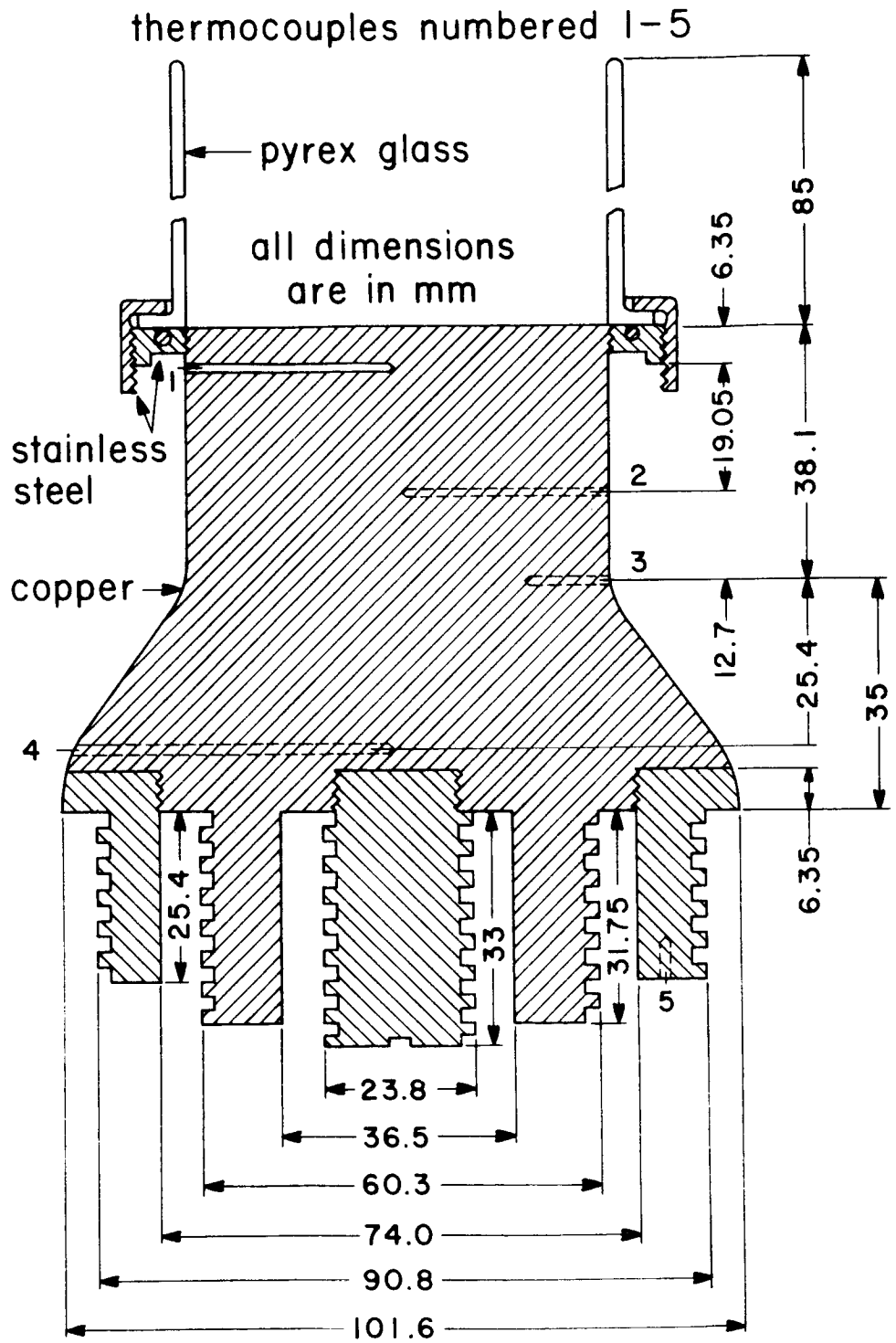
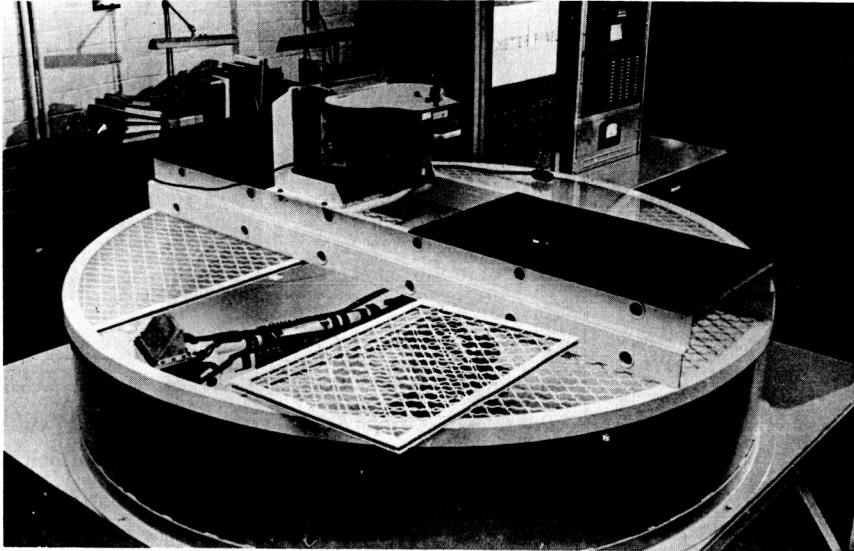
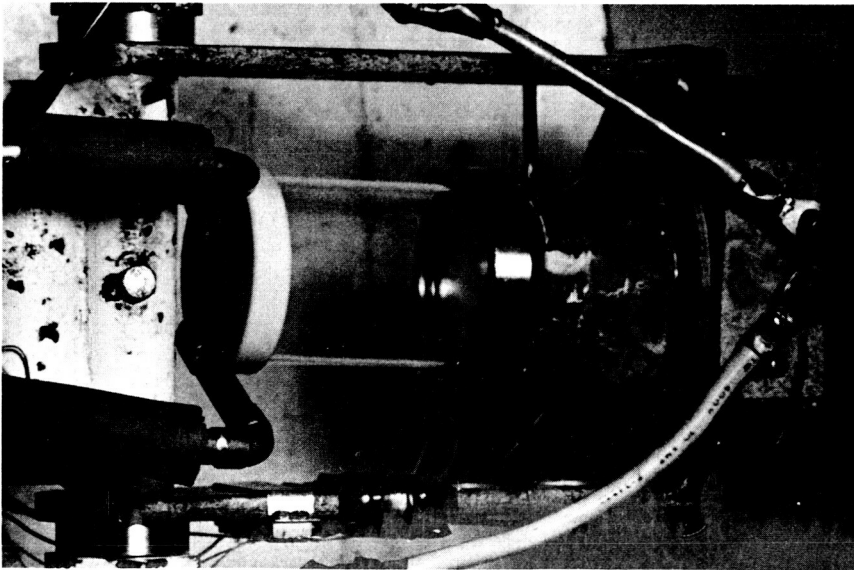


Fig. 5. Sectioned view of the flat plate heater.



a.) Centrifuge facility -- general view



b.) Top view of flat-plate heater assembly installed at end of centrifuge arm.

Fig. 6 Photographs of Apparatus

that there was no uncleanliness on the surface which might affect the wettability and affect the  $q_{\max}$  data. The very careful experiments of Berenson [35] have shown that, in this configuration,  $q_{\max}$  is insensitive to surface conditions and that these precautions are more than ample.

The resistance heating wire was energized and the current was gradually increased in steps. At each step the current and voltage were noted and thermocouple observations were recorded and updated until steady state was reached. It usually took about 5 minutes to reach steady state after the current was increased to the next higher value.

Various regimes of nucleate boiling (e.g. the isolated bubble regime and the transition from single bubbles to slugs and columns) were easily discernable. The transition from nucleate to transitional boiling was identified by noting a slowdown of the boiling process and a sudden continuous increase in the thermocouple reading. The thermocouple reading kept on increasing for a while, even after the power was removed. In most cases, the power was cut off after visual observation of the boiling transition, rather than by triggering of the automatic shut-off mechanism.

The peak heat flux was computed from the observations of the top two thermocouples. Observation of the third thermocouple helped in making a counter check on the heat flux calculations. The maximum probable error of the peak heat flux is calculated in reference [27]. It is found to be 7.7%.

The peak heat flux observations were made for both viscous and inviscid liquids, both in the centrifuge and at earth-normal gravity. A few of the observations were repeated to check for reproducibility of results. Each time a new observation was made the above-mentioned procedure for cleaning the boiling surface was used and fresh test liquid was employed.

### Discussion of Experimental Results

The available  $q_{\max F}$  data from both this and other investigations are plotted against  $L/\lambda_D$  (or  $L'/2\pi\sqrt{3}$ ) in Fig. 7. This abscissa scale gives the heater size in terms of the number of wavelengths that it will accommodate. Data for circular heaters ( $L$  = diameter) and one point for a square heater (reference [41],  $L$  = width) are included in the figure. The original data and details of their reduction to dimensionless form are tabulated in Table I.

Only those data for which the liquid was fairly inviscid are included in the figure. The question of viscous effects on  $q_{\max}$  will be addressed

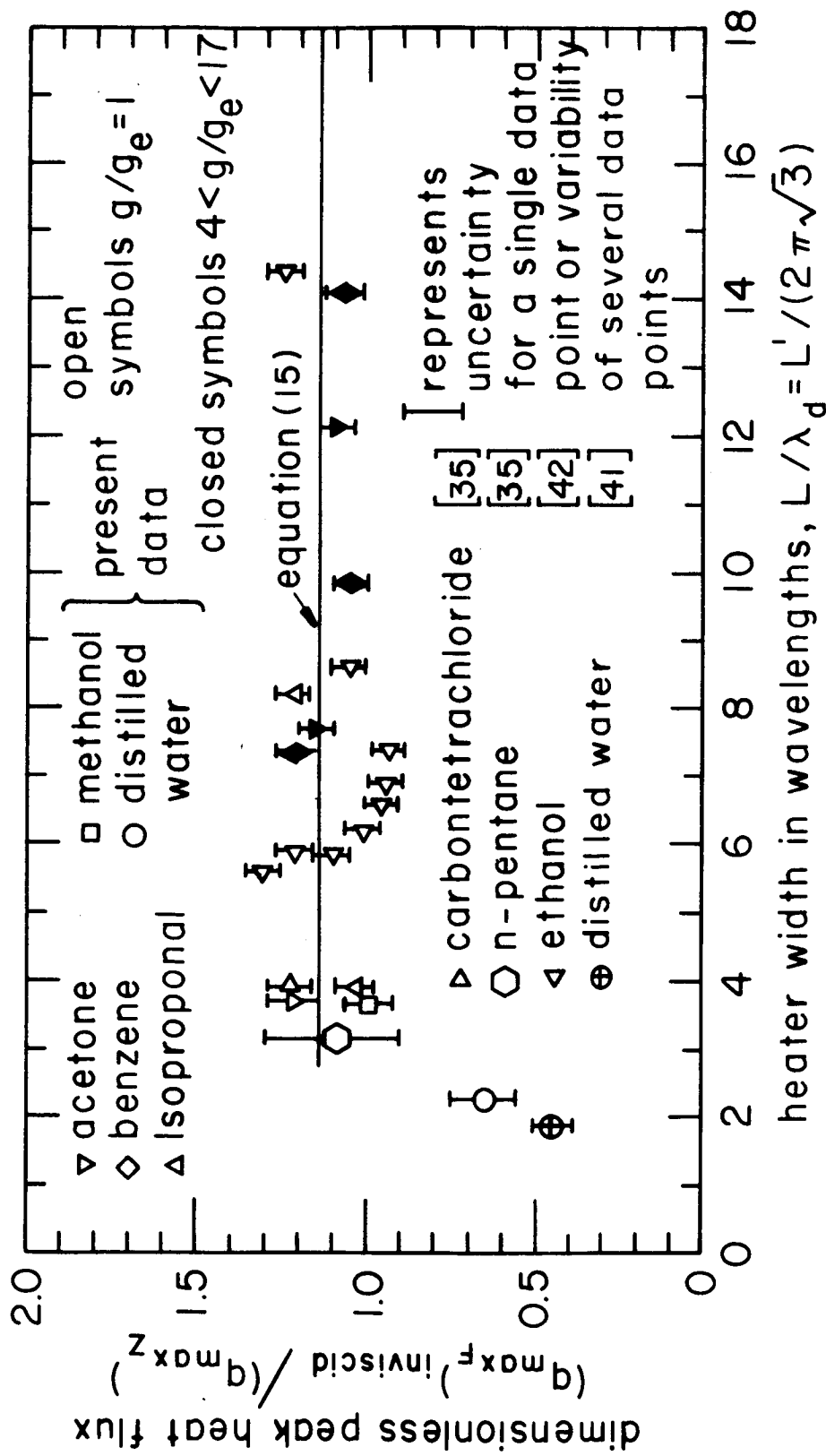


Fig. 7. Peak heat flux on broad flat plate heaters with vertical side walls.

Table I. Peak Heat Flux Data on Circular Flat Plate Heaters

| Liquid                        | $g/g_e$ | P<br>(k Pa) | M     | $\frac{L'}{2\pi\sqrt{3}}$ | $q_{\max} \times 10^{-5}$<br>$\left(\frac{W}{m^2}\right)$ | $\frac{q_{\max}}{(q_{\max})_Z}$ |
|-------------------------------|---------|-------------|-------|---------------------------|---|---------------------------------|
| Acetone                       | 1       | 98.58       | 599   | 3.71                      | 3.94  | 1.18                            |
|                               | 1       | 98.93       | 599   | 3.71                      | 4.10  | 1.22                            |
|                               | 4.97    | 23.99       | 548   | 7.69                      | 3.44  | 1.14                            |
|                               | 12.30   | 25.37       | 548   | 12.07                     | 4.19  | 1.07                            |
| Benzene                       | 4.97    | 18.06       | 384   | 7.36                      | 2.98  | 1.21                            |
|                               | 8.72    | 24.88       | 410   | 9.85                      | 3.31  | 1.05                            |
|                               | 17.5    | 27.09       | 413   | 14.07                     | 4.19  | 1.07                            |
| Iso-<br>propanol <sup>+</sup> | 1       | 22.75       | 138   | 3.68                      | 2.08  | 0.79                            |
|                               |         | 46.53       | 182   | 3.78                      | 3.34  | 1.0                             |
|                               |         | 73.21       | 233   | 3.85                      | 3.82  | 0.98                            |
|                               |         | 88.52       | 243   | 3.88                      | 4.54  | 1.10                            |
|                               |         | 98.72       | 254   | 3.91                      | 4.26  | 1.0                             |
|                               |         | 4.97        | 18.06 | 83                        | 8.2   | 5.39                            |
| Methanol                      | 1       | 44.60       | 370   | 3.56                      | 3.69  | 0.94                            |
|                               |         | 47.43       | 377   | 3.56                      | 4.13  | 1.02                            |
|                               |         | 88.04       | 420   | 3.72                      | 5.33  | 1.04                            |
|                               |         | 96.38       | 435   | 3.75                      | 5.33  | 1.01                            |
|                               |         | 96.52       | 435   | 3.75                      | 5.33  | 1.01                            |
|                               |         | 98.10       | 439   | 3.75                      | 5.33  | 1.0                             |
| Distilled<br>Water            | 1       | 14.48       | 757   | 2.24                      | 3.34  | 0.70                            |
|                               |         | 25.37       | 930   | 2.27                      | 4.45  | 0.72                            |
|                               |         | 29.51       | 976   | 2.28                      | 4.26  | 0.66                            |
|                               |         | 36.54       | 1040  | 2.29                      | 4.82  | 0.67                            |
|                               |         | 39.16       | 1060  | 2.29                      | 4.54  | 0.62                            |
|                               |         | 42.74       | 1079  | 2.30                      | 4.54  | 0.59                            |

<sup>+</sup> While plotting the data for iso-propanol in Fig. 7, a small correction for the effect of liquid viscosity was made using Fig. 50.

in Chapter V, and some data for moderately viscous isopropanol are included but are corrected for viscosity in Fig. 7. Suffice it to say for the moment that a liquid is inviscid for this purpose when a viscosity parameter,  $M$ , is on the order of 400 or larger.

With reference to Fig. 7, we see that all the data are very closely represented by our version of Zuber's flat-plate prediction, equation (15), when  $L/\lambda_d$  exceeds about 3. The two data for smaller  $L/\lambda_d$  deviate sharply below the predicted value of  $q_{\max_F} = 1.14 q_{\max_Z}$ , however,

These deviant data--one is our own for a circular heater, the other was obtained years ago by Costello [41] for a square heater--these data serve strongly to support our present case. In Fig. 8 we give the peak heat flux for various numbers of jets using the expression suggested earlier.

$$q_{\max} = \frac{N_j \lambda_d^2}{A_h} (1.14 q_{\max_Z}) \quad (16)$$

Lines have been sketched in for various numbers of jets. No line has been carried back beyond the point at which the preceding curve also rises above  $1.14 q_{\max_Z}$ . Likewise, no line has been carried forward beyond the point at which the following curve also falls below  $1.14 q_{\max_Z}$ . We note that as  $L/\lambda_d$  goes to about 3 and more, less variation in  $q_{\max}$  is encountered.

The data point for  $L/\lambda_d \sim 2.3$ , which actually represents 6 individual observations, corresponds very closely with one of the possible predictive curves. This success in rationalizing such a startling deviation from conventional expectation suggests that a more extensive comparison with experimental data would be warranted.

Therefore, since we have only one other data point for small  $L/\lambda_d$ , it is necessary to acquire additional experimental data. We turn to an unpublished study by D. M. Rihard [43], details of which we shall summarize briefly here.

The apparatus is shown in Fig. 9. It consists quite simply of a pair of electrodes positioned to accommodate nichrome resistance heater plates of varying width. Enough of each plate is short-circuited, as shown in the figure, so that the remaining active area is square. A chimney is fitted over the plate to contain the boiled liquid. Within the chimney are included spacers so the inside area of the chimney rises

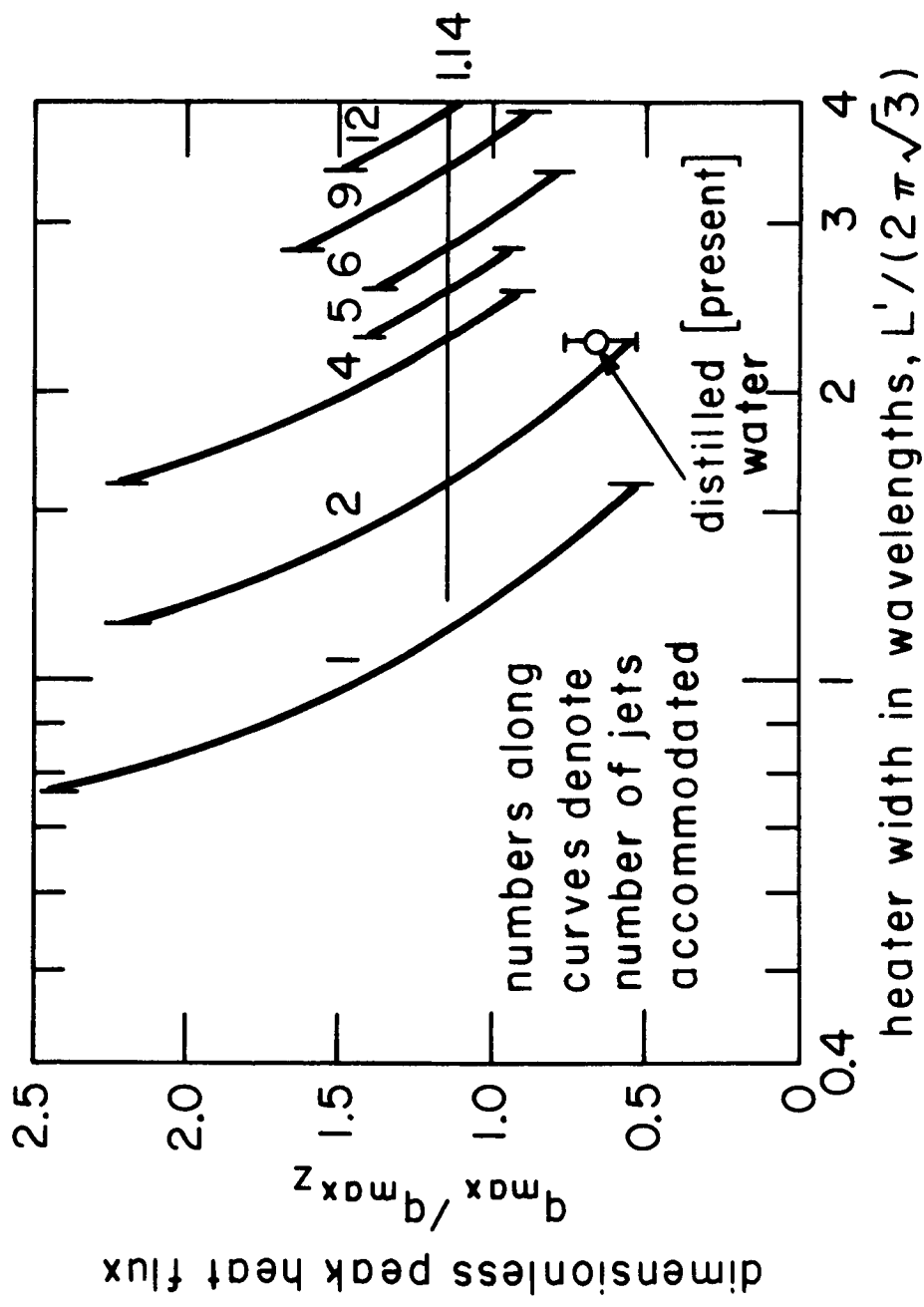


Fig. 8. Peak heat flux on a circular finite flat plate with vertical side walls.

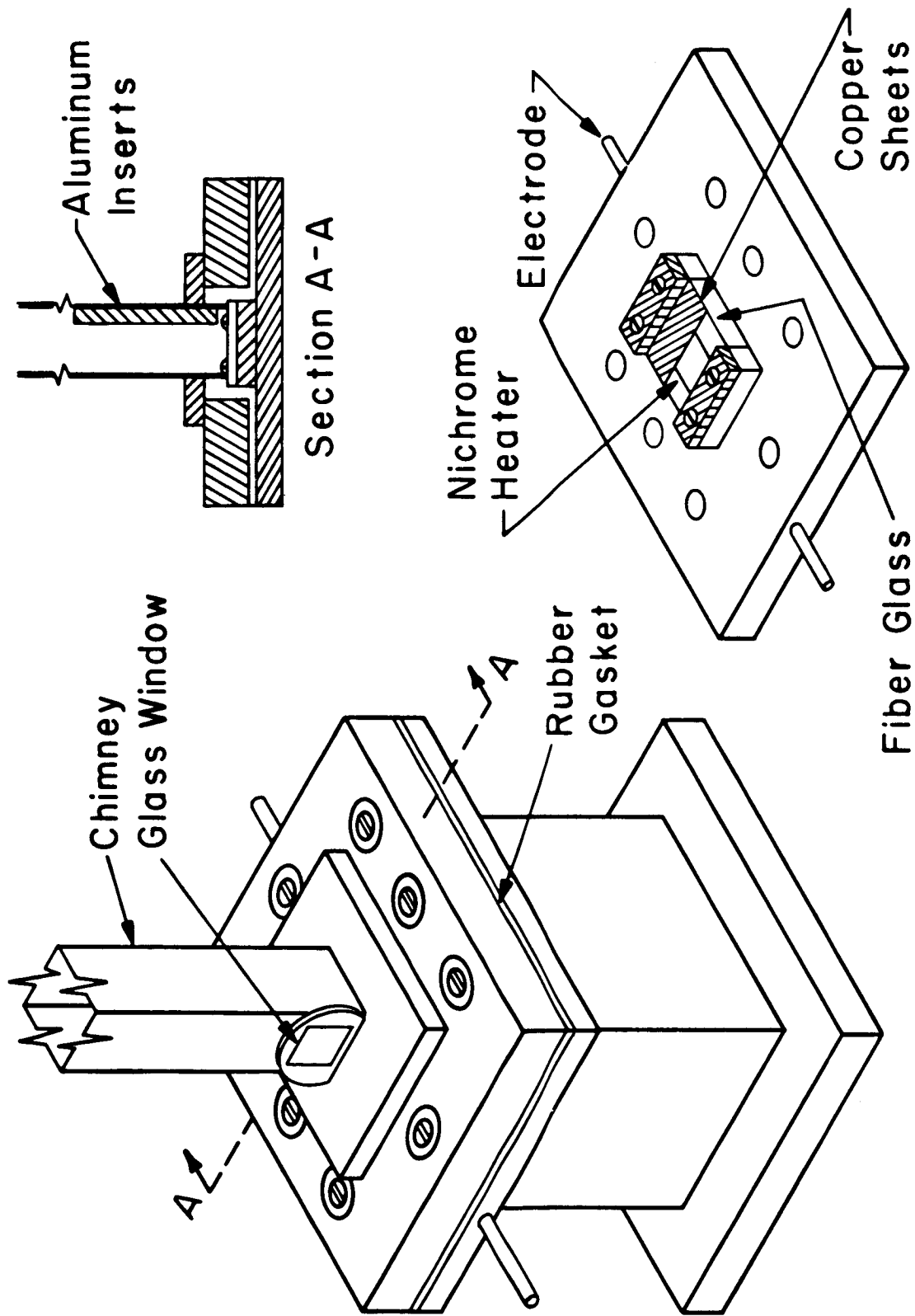


Fig. 9 Small plate heater apparatus (Riherd's experiment)

directly upward from the active heater area.

Each plate was washed with soap and warm water after it was installed, and then rinsed with the test liquid. This was done before each set of observations was made on the plate. The results of these observations are presented in both raw and reduced form in Table II. The test liquids included reagent grade isopropanol and methanol, and 95% pure ethanol.

In Fig. 10 we have combined Riherd's data for square plates with Costello's point for a square plate. We also include equation (16) for  $N_j = 1, 4, 5, 9, 13,$  and  $16$ .

This figure shows very clearly the effect of finite heater size on  $q_{\max}$ . The data cling very closely to the line, between  $L/\lambda_d = 1.0$  and  $2.0$ , indicating that only one jet can be accommodated on the plate. This was substantiated by the scorch-marks on the used plates. Circular marks,  $\lambda_d/2$  in diameter, were observed repeatedly.

As the plate is shrunk to  $L = \lambda_d/2$  we see that the data fall away from the curve. This is no surprise since the simple inviscid model no longer applies. The liquid return route is being squeezed into a viscous film crowded against the chimney, and considerations not included in the theory dictate  $q_{\max}$ .

This result provides a dramatic verification of the hydrodynamic theory. It reveals a 5-fold variation of  $q_{\max}$  in conformity with the theory. It is, perhaps, ironic that Costello used the data point shown in the figure to support his own doubts as to the validity of the theory.

### Conclusions

1.) The peak pool boiling heat flux on an infinite flat plate is given by

$$q_{\max_F} = \frac{1.14\pi}{24} \sqrt{\rho_g} h_{fg} \sqrt[4]{\sigma g(\rho_f - \rho_g)} = 1.14 q_{\max_Z}$$

2.) If the plate is fewer than 3 wavelengths in width, the variations in  $q_{\max}$  as jets are added or removed becomes very important. In this case:

$$q_{\max} = \frac{N_j \lambda_d^2}{A_h} (1.14 q_{\max_F})$$

Table II Riherd's  $q_{\max}$  Observations for Finite Horizontal Square Plates

| Liquid      | width<br>(cm) | Power<br>(watts) | $\frac{L}{\lambda_d}$ | $\frac{q_{\max}}{q_{\max Z}}$ |
|-------------|---------------|------------------|-----------------------|-------------------------------|
| Isopropanol | 2.16          | 156              | 1.32                  | 0.777                         |
|             |               | 148              |                       | 0.738                         |
|             | 1.52          | 156              | .93                   | 0.777                         |
|             |               | 102              |                       | 1.021                         |
|             |               | 105              |                       | 1.049                         |
| Methanol    |               | 132              | .89                   | 1.048                         |
|             |               | 125              |                       | .991                          |
|             |               | 127              |                       | 1.010                         |
|             |               | 130              |                       | 1.029                         |
| Ethanol     |               | 130              | .90                   | 1.207                         |
|             |               | 130              |                       | 1.207                         |
|             |               | 130              |                       | 1.204                         |
| Isopropanol | 1.84          | 119              | 1.12                  | 1.103                         |
|             |               | 110              |                       | 0.756                         |
|             |               | 108              |                       | 0.743                         |
| Methanol    |               | 111              | 1.07                  | 0.759                         |
|             |               | 146              |                       | 0.789                         |
|             |               | 152              |                       | 0.825                         |
| Isopropanol | 0.89          | 147              | .54                   | 0.800                         |
|             |               | 74               |                       | 2.183                         |
|             |               | 80               |                       | 2.354                         |
| Methanol    |               | 78               | .52                   | 2.292                         |
|             |               | 74               |                       | 1.726                         |
|             |               | 78               |                       | 1.817                         |
| Ethanol     |               | 74               | .33                   | 1.726                         |
|             |               | 80               |                       | 2.178                         |
|             |               | 82               |                       | 2.238                         |
| Methanol    | 1.21          | 100              | .70                   | 1.266                         |
|             |               | 100              |                       | 1.266                         |
|             |               | 100              |                       | 1.266                         |
| Isopropanol |               | 101              | .73                   | 1.614                         |
|             |               | 94               |                       | 1.506                         |
|             |               | 101              |                       | 1.614                         |
| Methanol    | 2.16          | 118              | 1.26                  | 0.467                         |
|             |               | 114              |                       | 0.451                         |
|             |               | 110              |                       | 0.435                         |
|             |               | 116              |                       | 0.459                         |

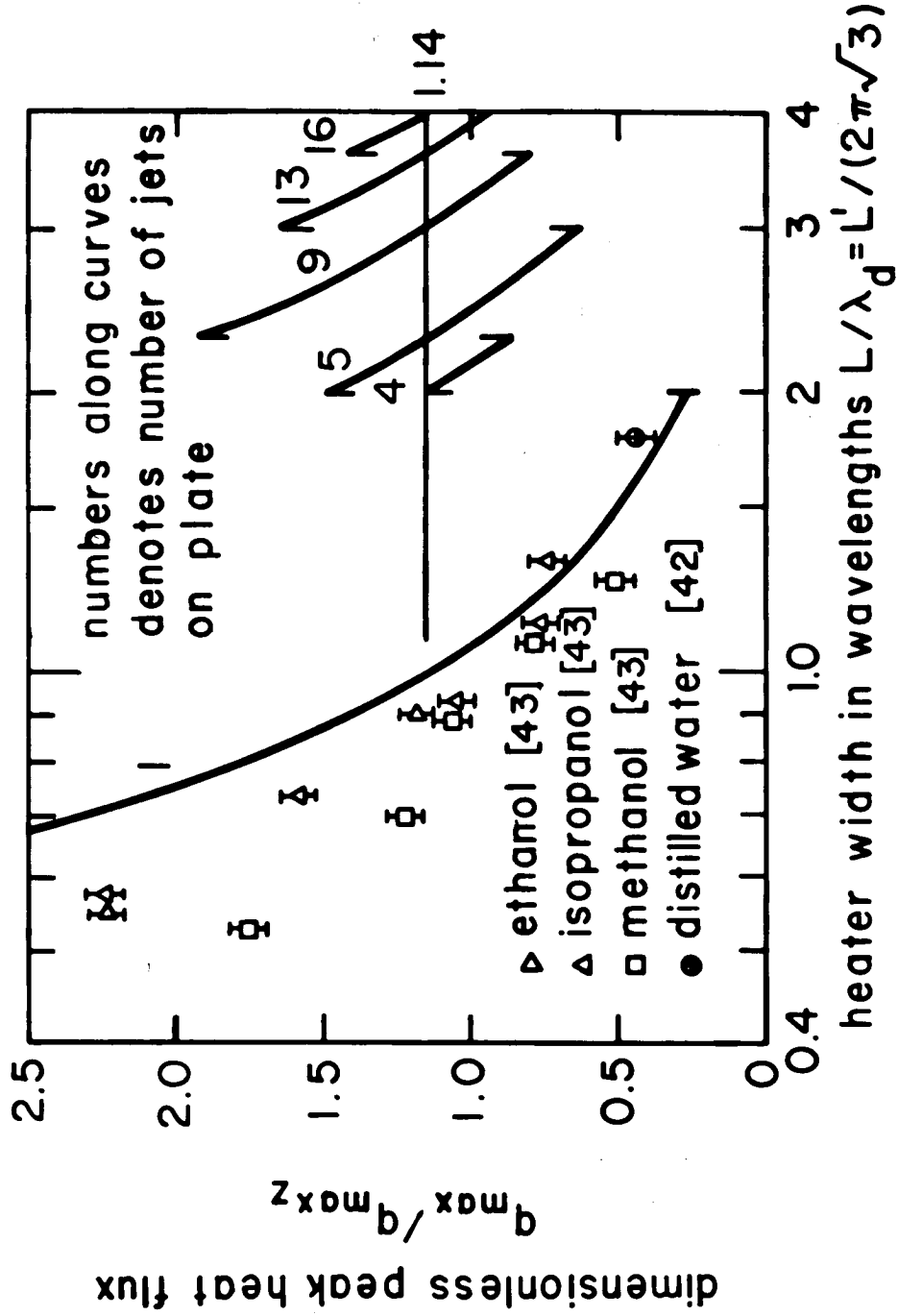


Fig. 10. Peak heat flux on a square finite flat plate with vertical side walls.

### III. THE PEAK AND MINIMUM POOL BOILING HEAT FLUXES ON FINITE HEATERS

#### General Considerations

The hydrodynamic method can be applied to the sort of finite heaters which are totally encompassed by a liquid bath, but some serious complications are introduced to the problem. References [5], [15], and [24] deal with such heaters and provide the basis of the present discussion.

The present considerations all begin with a general peak heat flux expression obtained by combining equations (3), (5), and (1), namely

$$\frac{q_{\max}}{q_{\max Z}} = \frac{24}{\pi} \sqrt{\frac{2\pi}{\lambda_H \sqrt{g(\rho_f - \rho_g)/\sigma}}} \frac{A_j}{A_h} \quad (16)$$

When  $\lambda_H = \lambda_d$  and  $A_j/A_h = \pi/16$  this reduces to equation (15), however for finite heaters we must reopen the question as to what  $\lambda_d$  and  $A_j/A_h$  are. These questions caused no problems in dealing with either the infinite or the bounded flat plates.

Figure 11 shows the finite configurations under consideration here. They include cylinders, spheres, and horizontal ribbons oriented vertically with and without insulation on one side. Each of these introduces different ramifications to the problem. Much of this complication can be clarified by reviewing the derivation of  $q_{\max}$  on the horizontal cylinder.

#### The Horizontal Cylinder, An Illustrative Example

The geometry of a finite body exerts an important influence both on the size and the arrangement of the vapor jets. Photographic observations of boiling on cylinders indicate--at least on the larger cylinders--that the jets adjust approximately to the width of the cylinder (plus the thickness of the vapor blankets,  $2\delta$ ) as shown in Fig. 11. If the cylinder is small the jets are small and the assumed spacing can reasonably be assumed equal to  $\lambda_d$ . As the cylinder increases in size the spacing must eventually spread to beyond  $\lambda_d$  to accommodate jets which now exceed



$\lambda_d/2$  in diameter<sup>4</sup>. Sun showed that the spacing was about two jet diameters or about  $4(R+\delta)$  in this case. Thus

$$\frac{A_j}{A_h} \approx \frac{(R+\delta)^2}{2R\lambda_d} \left| \begin{array}{l} \text{small} \\ \text{cyls.} \end{array} \right. ; \quad \frac{A_j}{A_h} \approx \frac{R+\delta}{8R} \left| \begin{array}{l} \text{large} \\ \text{cyls.} \end{array} \right. \quad (17)$$

Of course, equations (17) are true only insofar as  $R_j \approx R + \delta$ .

Furthermore the wavelength,  $\lambda_d$ , is the dominant disturbance in the interface between the jets on large cylinders and it is picked up by the jets. The minimum Rayleigh disturbance,  $2\pi R_j$ , is longer than  $\lambda_d$  and would normally become Helmholtz unstable at a lower vapor velocity,  $U_H$ . However, photographic evidence confirmed that vapor jets on large cylinders were much too short to have collapsed by virtue of the Rayleigh disturbance. This means that the shorter waves of length,  $\lambda_d$ , are already well developed at the outset, while the Rayleigh waves require some distance to develop. Accordingly, Sun used  $\lambda_H = 2\pi R_j \approx 2\pi(R+\delta)$  for the small cylinders and  $\lambda_H = \lambda_d$  for the large ones. Using these  $\lambda_H$ 's and equation (17) in equation (16), gives

$$\frac{q_{\max}}{q_{\max_Z}} = \frac{6}{\pi^2 \sqrt{3}} \frac{(R'+\Delta)^{3/2}}{R} \quad \text{and} \quad \frac{3^{3/4}}{\pi} \frac{R'+\Delta}{R'} \left| \begin{array}{l} \text{small} \\ \text{cyls.} \end{array} \right. \quad \left| \begin{array}{l} \text{large} \\ \text{cyls.} \end{array} \right. \quad (18)$$

where  $\Delta \equiv \delta \sqrt{g(\rho_f - \rho_g)/\sigma}$ , a dimensionless blanket thickness. The transition between small and large cylinders occurs somewhere in the neighborhood of  $\lambda_d = 4(R+\delta)$  or  $R' \approx 2.5$  depending on the magnitude of  $\delta$ .

The parameter  $R'$ , which has been variously named "the Laplace number," "the Rayleigh number," and the square root of "the Bond number", characterizes the ratio of buoyant forces to capillary forces in a system. As  $R'$  becomes very large, the system should approach

---

<sup>4</sup> The most susceptible wavelength used here is that for a flat interface. We do not include the correction for circumferential curvature [33,6] because that effect becomes lost in the irregularities of the interface near  $q_{\max}$ .

a state in which it is no longer subject to capillary forces. In this state we would expect to see no further influence of  $R'$  upon  $q_{\max}/q_{\max Z}$ . This is what was found to be the case in [6]. As  $R'$  became large, Sun measured  $\delta \approx 0.233 R$  so equation (17) gave  $A_j/A_h \approx 0.155$  and  $q_{\max}/q_{\max Z}$  approached a constant value of 0.894.

For small cylinders Sun approximated the measured values of  $\delta$  with a fairly complicated equation in the form  $\Delta = \Delta(R')$ . Substitution of this expression in equation (18) gave:

$$\frac{q_{\max}}{q_{\max Z}} \Bigg|_{\substack{\text{small} \\ \text{cyls. [8]}}} = 0.89 + 2.27 \exp(-3.44\sqrt{R'}) \quad (19)$$

which represented approximately 900 data from a large variety of sources with very good accuracy.

#### The Evaluation of $\lambda_H$ and $A_j/A_h$

The fact that  $\lambda_d$  is the correct value of  $\lambda_H$  for use with large cylinders can be used with any other large heater configuration since the situation in the upper interface is similar. Accordingly we can enter equation (16) with  $\lambda_H = \lambda_d$  and obtain in general:

$$\frac{q_{\max}}{q_{\max Z}} \Bigg|_{\substack{\text{large} \\ \text{heater}}} = \frac{24}{\pi} \frac{A_j}{A_h} \quad (20)$$

Likewise we may enter equation (16) with  $\lambda_H = 2\pi R_j$  for any small heater. Then, using the fact that  $R_j$  must equal  $\sqrt{(A_h/\pi)(A_j/A_h)}$ , we obtain

$$\frac{q_{\max}}{q_{\max Z}} \Bigg|_{\substack{\text{small} \\ \text{heater}}} = \frac{24}{\pi} \sqrt[4]{\frac{\pi \sigma}{A_h g(\rho_f - \rho_g)}} \left(\frac{A_j}{A_h}\right)^{3/4} \quad (21)$$

The problem of making general predictions of  $q_{\max}$  on finite heaters

then reduces to the problem of estimating  $A_j/A_h$  for any given situation.

As a first step to determining  $A_j/A_h$  we shall assume that the speed of the vapor passing through the blanket equals that in the escaping jet. For the speeds to differ would require the existence, both of pressure differences within the vapor escape path, and of significant dissipative mixing processes in the jet. We do not believe it is reasonable to look for either, and therefore assume that  $\delta$  simply adjusts to give equal velocities in both passages.

For the large cylinder, this assumption, combined with a simple continuity statement (velocity times cross-sectional area is constant) gives

$$2[4(R+\delta)\delta] = A_j/2 \quad (22)$$

and for any sphere, large or small, it gives

$$2\pi(R+\delta/2)\delta = A_j/2 \quad (23)$$

For the small cylinder such a balance is not feasible since the vapor must flow horizontally in a long annulus subject to pressure drops. But for the small sphere equation (23) will still be true. From this point two paths can be followed:

The path followed in reference [6] was to assume a jet configuration in terms of  $\delta$ , and then to complete the derivation using observed values of  $\delta$ . References [6] and [15] give the needed measurements of  $\delta$  for both cylinders and spheres as scaled from photographs. These data, and two additional points scaled from photographs in other papers [44,45,46] are combined in Fig. 12. Approximate lines have been fit through the data in both the large and small  $R'$  ranges. The results are:

$$\Delta \text{ small cylinders} = (\sqrt{3.72/R'} - 1) R' \quad (24)^5$$

$$\Delta \text{ large cylinders} = 0.244 R' \quad (25)^6$$

$$\Delta \text{ small spheres} = 0.20 R' \quad (26)$$

$$\Delta \text{ large spheres} = 0.134 R' \quad (27)$$

<sup>5</sup> Sun used a more complex fit to the data--one which fit well in the mid-range but was very nearly equal to equation (24) for  $R' \leq 1$ . We are presently more interested in low  $R'$  behavior than in transitional behavior at higher  $R'$ .

<sup>6</sup> This result is a little higher than Sun's and represents a slightly better fit.

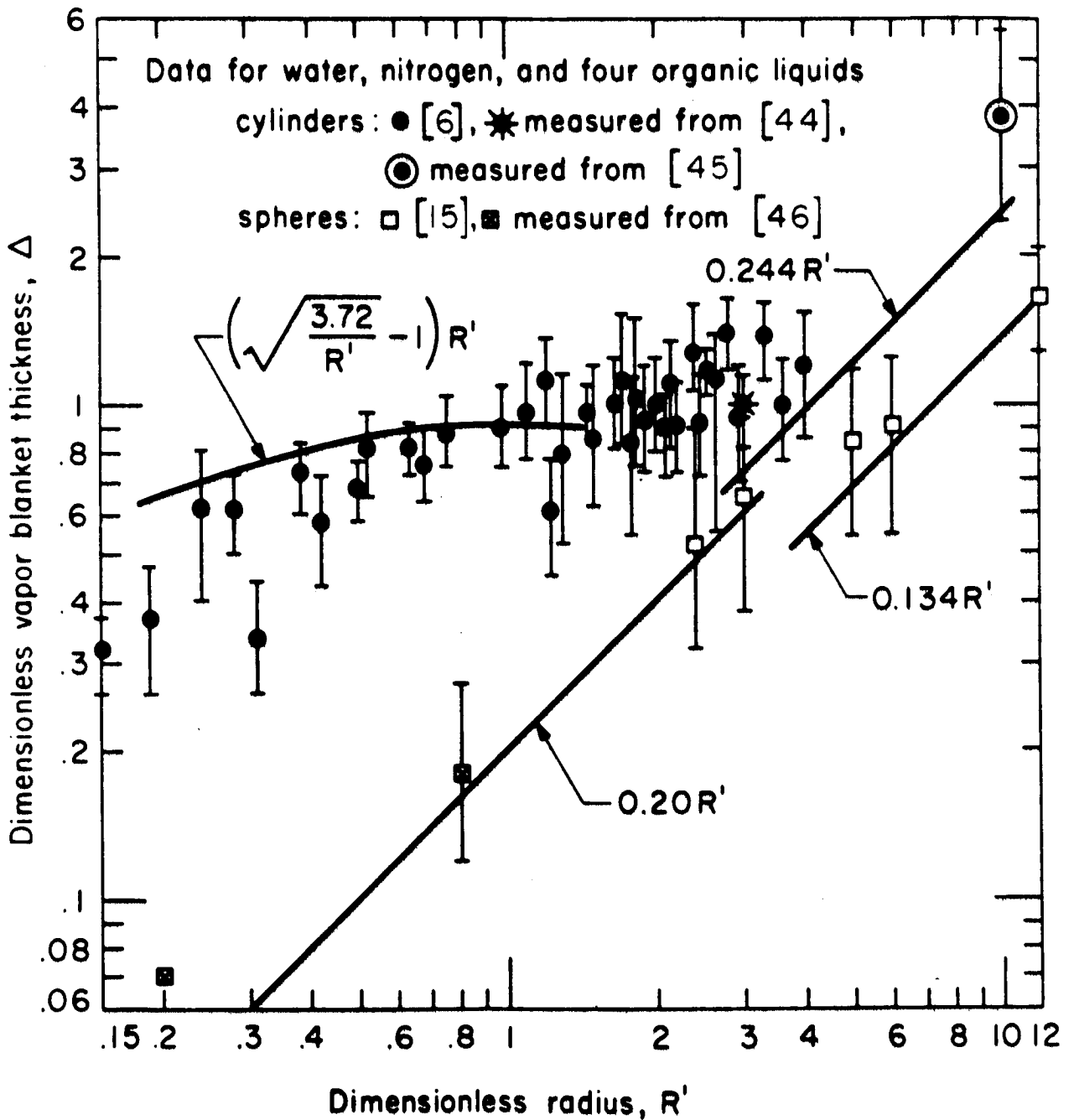


Fig. 12 Vapor blanket thickness measured on spheres and cylinders.

Using these equations in equations (22) and (23) leads to:

$$\frac{A_j}{A_h} \left| \begin{array}{l} \text{large} \\ \text{cyls.} \end{array} \right. = 0.155 \quad (28)$$

$$\frac{A_j}{A_h} \left| \begin{array}{l} \text{large} \\ \text{spheres} \end{array} \right. = 0.143 \quad (29)$$

$$\frac{A_j}{A_h} \left| \begin{array}{l} \text{small} \\ \text{spheres} \end{array} \right. = 0.220 \quad (30)$$

The other approach is to combine the description of the assumed configuration of the jets with equations (22) and (23), solve the result for  $\delta$ , and then obtain  $q_{\max}/q_{\max_Z}$  from equation (18). This is reasonably safe to do in the case of large cylinders since the physical model ( $R_j = R + \delta$ ) is consistent with Sun's photographs. The result,  $\delta = 0.244R$ , corresponds precisely with the experimental value given in equation (25) and leads to

$$\frac{q_{\max}}{q_{\max_F}} \left| \begin{array}{l} \text{large} \\ \text{cyls.} \end{array} \right. = 0.904 \quad (31)$$

This is negligibly higher than Sun's result of 0.894, and it is a completely theoretical expression. While this result is accurate, the minor errors in the assumed characteristics of the vapor escape configuration accumulate more than we would like, in other cases. Such errors are particularly troublesome for the small heater configurations.

Using the first approach, we combine the first of equations (17) with equation (24) and obtain

$$\frac{A_j}{A_h} \left| \begin{array}{l} \text{small} \\ \text{cyls.} \end{array} \right. = 0.171 \quad (32)$$

It appears from these  $A_j/A_h$  results, that for all finite heaters except small bluff bodies (such as spheres), we can anticipate that:

$$\frac{A_j}{A_h} \approx 0.155 \pm 10\% \quad (33)$$

Accordingly equation (20) gives

$$\frac{q_{\max}}{q_{\max Z}} \Big|_{\substack{\text{large} \\ \text{heater}}} \approx 0.9 \quad (34)$$

If we note that  $A_h$  for long slender heaters is  $\lambda_d$  times the perimeter,  $P$ , then equations (21) and (33) give

$$\frac{q_{\max}}{q_{\max Z}} \Big|_{\substack{\text{long} \\ \text{slender} \\ \text{heater}}} \approx \frac{1.4}{4\sqrt{P'}} \quad (35)$$

where  $P' \equiv P\sqrt{g(\rho_f - \rho_g)/\sigma}$

For small bluff heaters,  $A_h \sim L^2$ , where  $L$  is an appropriate characteristic length. Accordingly equation (21) gives

$$\frac{q_{\max}}{q_{\max Z}} \Big|_{\substack{\text{small} \\ \text{bluff} \\ \text{heater}}} = \frac{\text{constant}}{\sqrt{L'}} \quad (36)$$

where the constant can be determined by the correlation of a few available data. If  $A_j/A_h$  can be predicted, then there is no advantage to equation (35); a direct prediction can be obtained from equation (21).

With these generalizations in hand, we now return to the specific geometrical configurations shown in Fig. 11.

## Comparison of the Present Modified Theory With Data for Cylinders

The present formulation will differ very slightly from that of Sun. The difference lies only in the fact that we do not use exactly the same description of his  $\delta$  data as he did. Using equation (32) in equation (21) we obtain

$$\frac{q_{\max}}{q_{\max Z}} \Bigg|_{\substack{\text{small} \\ \text{cylinders}}} = 0.94 / \sqrt[4]{R'} \quad (37)$$

(while if we had substituted  $P' = 2\pi R'$  into the simplified expression, equation (35), we would have obtained  $0.885/\sqrt[4]{R'}$  -- only 6% below the more accurate result).

In Fig. 13 we compare equations (37) and (31) with the data given in reference [6]. The predictions are upheld perfectly. However, two general warnings are made evident in the figure:

1.) Neither prediction should be applied beyond the point of where they join. This junction occurs a little beyond  $R' = 1$  in this case, and at  $R'$  between 1 and 6 in all the cases we shall consider here. Thus, the transition generally occurs when the Taylor wavelength is comparable to the characteristic length of the heater. We also note that the sharp break between the two predictions represents the actual transition fairly well even though the actual transition is smooth. This will also prove to be true in the other cases we shall treat.

2.) The prediction fails to be valid when  $R'$  is less than about 0.15. The reason for this will be treated at length in Chapter VII. Briefly, when  $R' \ll 1$ , inertia proves to be no longer important in the peak heat flux mechanism. The hydrodynamic instability processes break down and the present predictions no longer apply. For that reason we claim no validity for any of the predictions when  $R' \leq 0.1$ .

## Comparison of Theory with Data for Spheres

For large spheres we can substitute equation (29) into equation (20) to obtain:

$$\frac{q_{\max}}{q_{\max Z}} \Bigg|_{\substack{\text{large} \\ \text{spheres}}} \simeq 0.84 \quad (38)$$

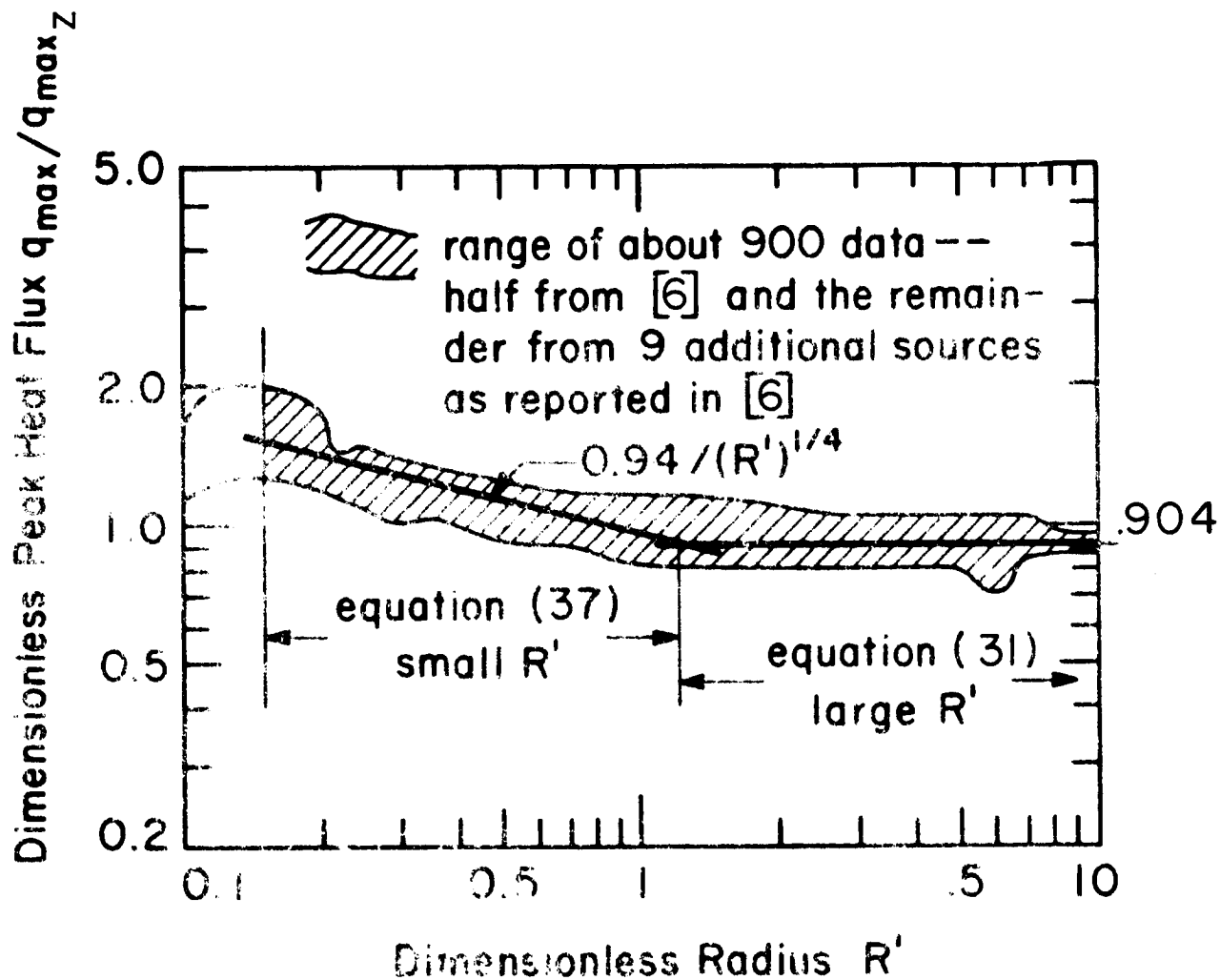


Fig. 13 The peak heat flux on horizontal cylinders

(which is within about 6% of the simplified approximate expression, equation (34).

For small spheres we substitute equation (30) and  $A_h = 4\pi R^2$  into equation (21) and obtain:

$$\frac{q_{\max}}{q_{\max,z}} \Big|_{\text{small spheres}} = \frac{1.734}{\sqrt{R^*}} \quad (39)$$

which is a special case of equation (36).

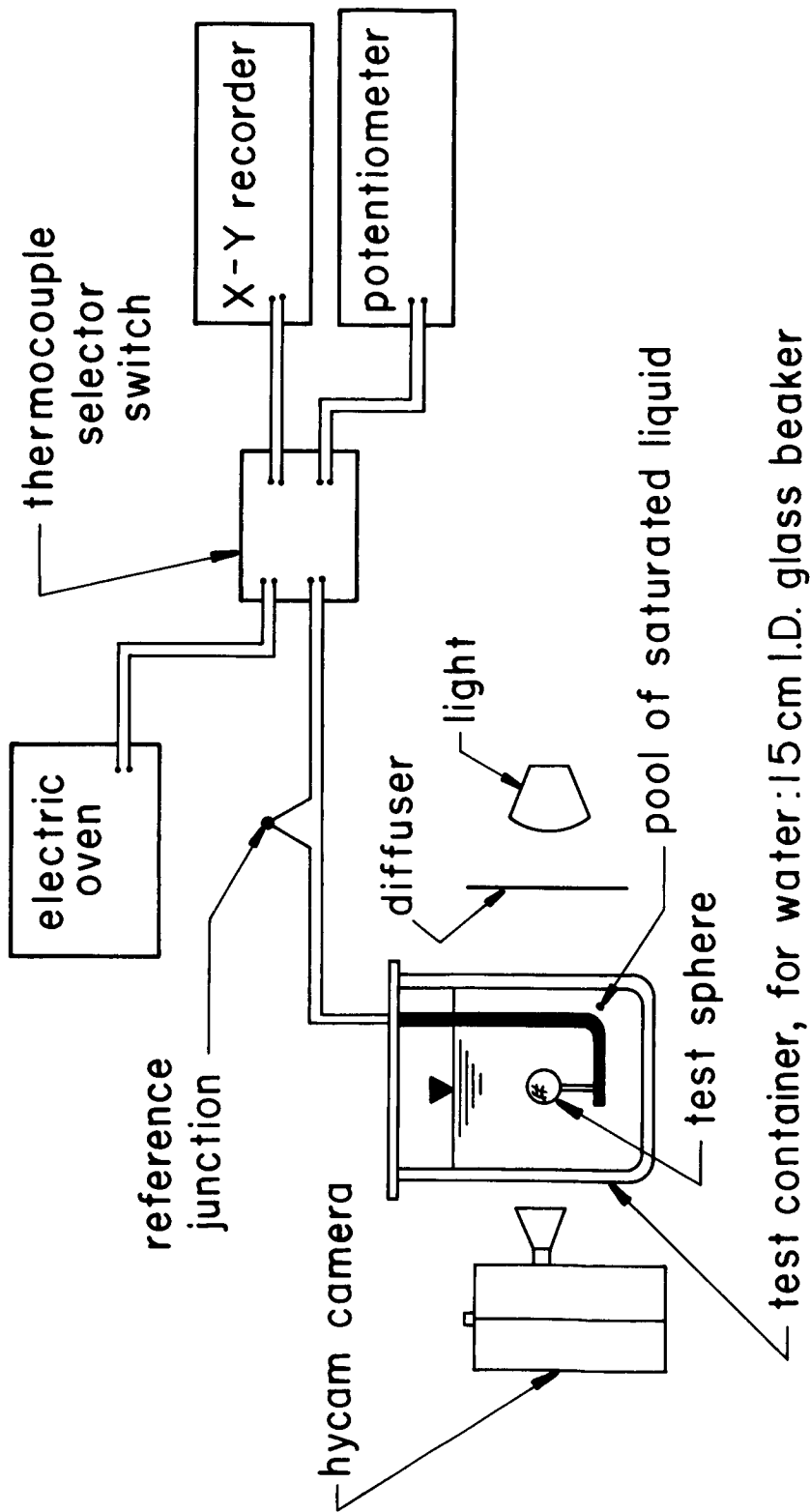
Since there were insufficient data in the literature to test these expressions adequately, Ded had to do his own set of experiments. We have already alluded to this work in the context of equations (26) and (27), and we should now describe it more fully.

Figure 14 shows the general layout of the experiment used by Ded to measure  $q_{\max}$  and  $\delta$  in both nitrogen and double-distilled water. The test heaters were 0.635, 1.27, and 2.54 cm dia. copper spheres with ion-constantan thermocouples mounted in the center. The water-quenched spheres were heated to 510°C in the oven shown, and the nitrogen-quenched spheres were stabilized at room temperature. In both cases the spheres were then quenched in the test beaker.

For boiling in water, a 12.7 cm I.D. glass beaker was placed on a hot-plate which kept the water saturated. A 15.2 cm I.D. double-walled, clear-glass, vacuum-insulated Dewar was used to hold the liquid nitrogen. It was kept saturated by heat leakage from the atmosphere, and the double wall prevented condensation on the outside so that clear photographs could be made.

Details of the sphere mounting are shown in Fig. 15. An additional thermocouple was placed near the surface of the largest sphere for use in some of the water runs. This facilitated an experimental indication of the extent of the failure of the lumped-capacity (or uniform sphere temperature) assumption. The worst case (in water) yielded only a 2% temperature difference between the two thermocouples.

The spheres were polished with 500 grit emery cloth and the surface was cleaned carefully before each run. Since runs made with a sphere cleaned in acetone, and runs made with one simply sanded and then washed in water, gave identical results, both procedures were used. The



test container, for water: 15 cm I.D. glass beaker  
 for liquid nitrogen: 13 cm I.D. double glass clear  
 Dewar.

Fig. 14 Schematic diagram of the experiment.

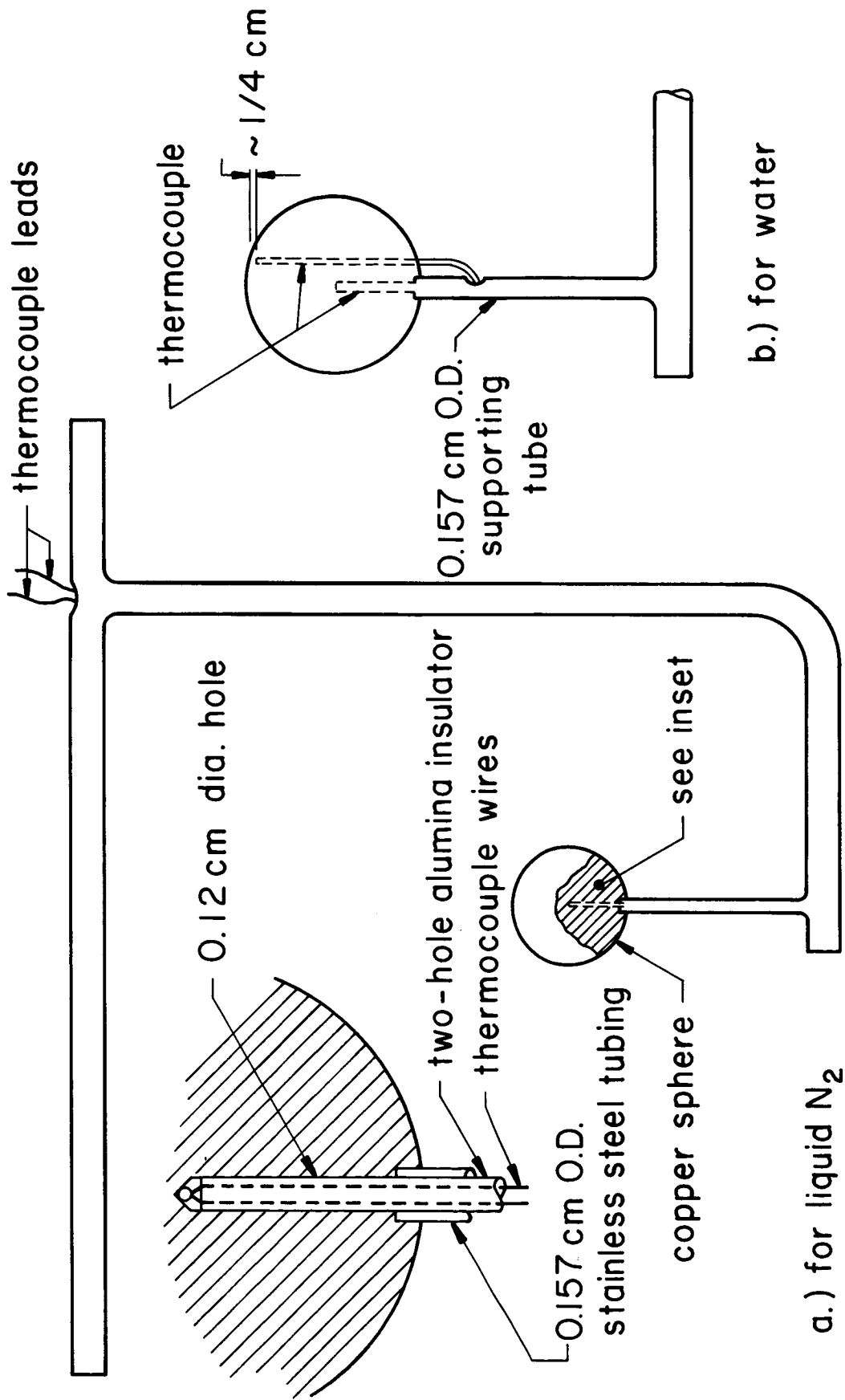


Fig.15 Test spheres for water and liquid nitrogen.

acetone rinse procedure was used in obtaining most of the data available in the literature.

The basic output of the experimental runs were temperature-time curves. The heat flux was obtained from these curves by noting that

$$q = -\rho_h \frac{\frac{4}{3}\pi R^3}{4\pi R^2} c_p(T) \frac{dT}{dt} = -\rho_h c_p(T) \frac{R}{3} \frac{dT}{dt} \quad (40)$$

This method is called the "transient calorimeter" technique. Its use involves making the tacit assumptions that the Biot Number,  $Bi = hR/k_w$ , is small and that the process is quasi-static. Bergles and Thompson [47], quoting from earlier sources, suggest that  $Bi$  at  $q_{max}$  should not be much more than 0.4 for accuracy, and they warn against the second possible source of error -- namely that the boiling process might not be quasi-static during the quench.

A subsequent paper by Veres and Florschuetz [48] provided evidence that the present data were obtained under conditions for which the cooling can legitimately be assumed quasistatic<sup>7</sup>. When  $Bi$  exceeded 0.4 in the present tests, equation (40) was abandoned in favor of the following computational method:

The transient heat conduction equation for a spherically symmetrical body was solved numerically beginning with a known uniform temperature distribution at  $t = 0$ , and using the boundary conditions of zero temperature gradient and  $T$  equal to a measured function of time, at the center. A simple Euler's method was used and the increments were chosen so that  $\alpha\Delta t/\Delta r^2 = 0.139$ . Rerunning the program with larger and smaller values of  $\alpha\Delta t/\Delta r^2$  did not alter the results. The instantaneous temperature distribution was then averaged over the volume and  $T$  in equation (40) was replaced with this average value. An error analysis [14] gave 6.5 percent maximum probable error for the  $q_{max}$  data we present here. The maximum probable errors for  $q_{max_F}$  and  $R^1$  were only 1.2 and 2.3 percent, respectively.

Ded's  $q_{max}$  data are presented in Table III. The temperature difference observed at  $q = q_{max}$  is also reported for the reader's interest. With these data we include six points which he reduced from

---

<sup>7</sup> The rationalization of references [47] and [48] is somewhat intricate. It is discussed in [15].

Table III. Peak Heat Flux Data for Spheres

| R<br>(cm)   | $q_{\max} \times 10^{-5}$ (W/m <sup>2</sup> ) | $\Delta T_{\max}$<br>(°C) | R'     | $\frac{q_{\max}}{q_{\max Z}}$ |
|---|---|---------------------------|--------|-------------------------------|
| Liquid Nitrogen, $q_{\max F} = 156,000 \text{ W/m}^2$ |   |                           |        |                               |
| 1.27*   | 1.18  | 8.1                       | 12.01  | 0.75                          |
| 1.27  | 1.25  | 7.0                       |        | 0.80                          |
| 1.27*   | 1.39  | 8.9                       |        | 0.885                         |
| 1.27  | 1.15  | 9.5                       |        | 0.73                          |
| 1.27  | 1.06  | 10.5                      |        | 0.675                         |
| .635*   | .95   | 11.1                      | 6.0    | 0.606                         |
| .635  | 1.14  | 11.7                      |        | 0.73                          |
| .635*   | 1.12  | 9.4                       |        | 0.71                          |
| .635  | 1.23  | 10.0                      |        | 0.784                         |
| .635*   | 1.33  | 9.2                       |        | 0.848                         |
| .635  | 1.38  | 10.6                      |        | 0.883                         |
| .318*   | 1.43  | 11.7                      | 3.0    | 0.91                          |
| .318  | 1.79  | 10.5                      |        | 1.12                          |
| .198 <sup>H</sup>                                     | 1.80  | 8.9                       | 1.87   | 1.14                          |
| .198 <sup>H</sup>                                     | 2.50  | 9.7                       |        | 1.59                          |
| .0794*, <sup>H</sup>                                  | 2.43  | 7.0                       | 0.75   | 1.55                          |
| .0794 <sup>H</sup>                                    | 3.04  | 9.2                       |        | 2.14                          |
| .0397*, <sup>H, T</sup>                               | 4.06  | 7.8                       | 0.375  | 2.60                          |
| .0198 <sup>H, T</sup>                                 | 4.98  | 7.5                       | 0.1875 | 3.19                          |
| Water, $q_{\max F} = 1,108,000 \text{ W/m}^2$         |   |                           |        |                               |
| 1.27*   | 8.20  | 38.9                      | 5.06   | .739                          |
| 1.27  | 9.10  | 43.9                      |        | .82                           |
| 1.27*   | 10.09   | 47.2                      |        | .91                           |
| 1.27  | 8.76  | 40.5                      |        | .79                           |
| .635  | 7.76  | 45.5                      | 2.53   | .69                           |
| .635*   | 8.93  | 41.6                      |        | .80                           |
| .635  | 11.10   | 40.0                      |        | 1.01                          |

\* denotes runs for which motion pictures were made

H denotes results from time-temperature data of Hendricks [19]

T denotes tungsten-carbide sphere (all other spheres were copper)

temperature-time plots made by Hendricks and Baumeister in connection with a recent study of film boiling from small spheres [46] of both copper and tungsten carbide.

These results have been nondimensionalized in accordance with equation (2), using property values as assembled by Reich and Lienhard [13]. The resulting  $q_{\max}/q_{\max Z}$  values are plotted against  $R'$  in Fig. 16 along with the  $q_{\max}$  of Merte and Clark [49], Veres and Florschuetz, and Bradfield [50].

The predictions for spheres, equations (38) and (39), are also included in the figure. The comparison between theory and data is once again very good, indeed.

The visual observations also serve to bear out the analytical models. Figure 17 shows typical photographs of boiling from spheres of increasing  $R'$ . The first picture, Fig. 17a, was taken from a motion picture supplied by Hendricks. The remaining three were obtained from Hycam movies (100 pps at 1/5000 sec exposure time.)

In Fig. 17a one-half of a Rayleigh wave is apparent in the escaping jet. This wavelength is comparable with  $2\pi R$  as we anticipated. Figures 17c and 17d provide a side-view of the anticipated four-jet pattern for large  $R'$  although the jets are very blunt--much too short to contain a Rayleigh wave. Figure 17b is for a case close to the transitional range of  $R'$  and the single-jet configuration has deteriorated into an ambiguous conglomerate between the two models. These pictures are, of course, only static representations of processes that were repeatedly clear to eye when the movies were screened. The measurements of  $\delta$  mentioned on page 31 were also made from these movies.

#### Comparison of Theory with Data for Horizontal Ribbons Oriented Vertically

Consider next the case of a thin horizontal ribbon heater with the broad side of height,  $H$ , oriented vertically, as shown at the bottom of Fig. 11. We shall also give brief attention to such a ribbon with one side insulated. When  $H'$  is small equation (35) will apply, and the dimensionless perimeter will equal  $2H'$ . When one side is insulated,  $P' = H'$ . Thus we obtain

$$\frac{q_{\max}}{q_{\max Z}} \left| \begin{array}{l} \text{small} \\ \text{horiz. ribbons} \\ \text{vert. orient.} \end{array} \right. = \frac{1.18}{\sqrt[4]{H'}} \quad (41)$$

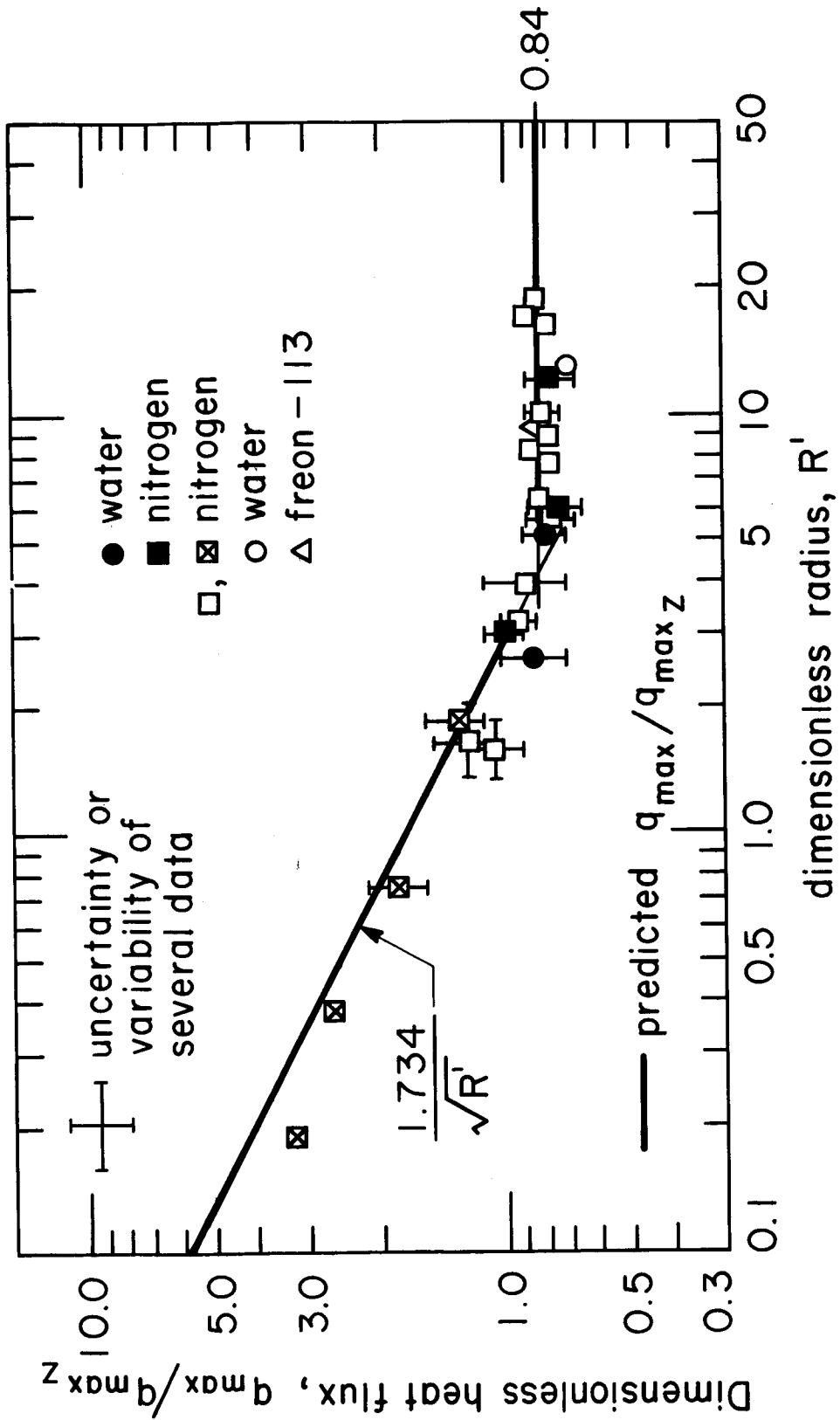
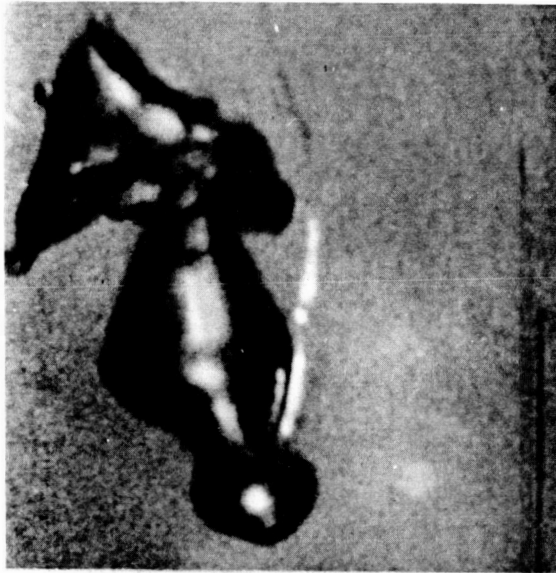


Fig. 16  $q_{\max}$  on spheres.



a)  $R = .0795$  cm  $R' = .75$   
liquid nitrogen



b)  $R = .635$  cm  $R' = 3.0$   
liquid nitrogen



c)  $R = 2.54$  cm  $R' = 5.06$   
water



d)  $R = 2.54$  cm  $R' = 12.0$   
liquid nitrogen

Figure 17 Photographs of vapor jets near  $q_{\max}$  on spheres of increasing diameters in liquid nitrogen and water

and

$$\frac{q_{\max}}{q_{\max Z}} \left| \begin{array}{l} \text{small} \\ \text{horiz. ribbon} \\ \text{vert. orient.} \\ \text{1 side insul.} \end{array} \right. = \frac{1.4}{4\sqrt{H'}} \quad (42)$$

For large  $H'$ 's we shall expect equation (34) to apply in either case.

Table IV includes original data for vertically oriented ribbon heaters in four liquids: acetone, benzene, methanol, and isopropanol. The ribbons were all of nichrome, 0.023 cm thick, about 10 cm in length, and they varied in height,  $H$ , from 0.104 cm to 0.478 cm. They were operated as electrical resistance heaters and were connected to the heavy power supply electrodes through brass ribbon attachments which served to prevent vapor hangup by providing a smooth transition section. The range of  $H'$  ( $\equiv H \sqrt{g(\rho_f - \rho_g)/\sigma}$ ) was greatly increased by observing  $q_{\max}$  both at elevated gravity in the University of Kentucky Gravity-Boiling Centrifuge Facility, as well as at earth normal gravity,  $g_e$ .

Complete details of the experimental method and apparatus can be obtained from [5] and [6], since exactly the same equipment and procedure were employed. The probable experimental error in  $q_{\max}$  was about  $\pm 4$  percent although intrinsic variability of the data was  $\approx \pm 15$  percent which is typical for such results. All ribbons had a smooth cold rolled finish (as delivered). Before each test the ribbons were carefully washed in soap and hot water, and then rinsed in the test fluid.

We can be sure that, even on these small ribbons,  $q_{\max}$  did not occur prematurely by virtue of low thermal capacity effects such as Houchin [59] observed, since he was only able to observe the phenomenon in water. Even though he used much thinner ribbons than we, he never witnessed the early burnout in organic liquids.

These data are presented in dimensionless form in Fig. 18. Twelve additional cyclohexane data for this situation which were given in [52] are also included in the figure. Equations (34) and (41) once again characterize the data perfectly.

The peak heat flux was also measured on two 0.023 cm thick horizontal nichrome ribbons, vertically oriented, but with one side

Table IV Peak Heat Flux on a Vertically Oriented Horizontal Ribbon

| fluid       | H (cm)     | g/g <sub>e</sub> | q <sub>max</sub> × 10 <sup>-5</sup> (W/m <sup>2</sup> ) | H'    | $\frac{q_{max}}{q_{maxZ}}$ |
|-------------|------------|------------------|---|-------|----------------------------|
| Acetone     | 0.104      | 1                | 4.46 ± .16  | 0.65  | 1.34                       |
|             | 0.130      | 1                | 4.90 ± .19  | 0.80  | 1.47                       |
|             | 0.207      | 1                | 3.70 ± .09  | 1.27  | 1.12                       |
|             | 0.354      | 1                | 3.36 ± .09  | 2.21  | 1.01                       |
|             | 0.480      | 1                | 3.07 ± .09  | 2.98  | 0.93                       |
|             | 0.366      | 4.01             | 4.42 ± .03  | 4.56  | 0.94                       |
|             |            | 8.30             | 5.08 ± .06  | 6.56  | 0.92                       |
|             |            | 17.84            | 7.10 ± .03  | 9.62  | 1.03                       |
| 32.32       |            | 8.40 ± .13       | 12.95   | 1.06  |                            |
| 49.49       | 9.06 ± .09 | 16.03            | 1.08  |       |                            |
| Benzene     | 0.104      | 1                | 3.96 ± .06  | 0.64  | 1.31                       |
|             | 0.140      | 1                | 3.70 ± .13  | 0.85  | 1.23                       |
|             | 0.217      | 1                | 3.02 ± .09  | 1.32  | 1.00                       |
|             | 0.366      | 4.01             | 4.24 ± .06  | 2.65  | 0.99                       |
|             |            | 7.98             | 5.18 ± .08  | 3.70  | 1.02                       |
|             |            | 18.32            | 6.36 ± .09  | 5.60  | 1.02                       |
|             |            | 31.68            | 7.45 ± .06  | 7.35  | 1.03                       |
|             | 49.49      | 8.55 ± .19       | 9.25  | 1.06  |                            |
| Methanol    | 0.140      | 1                | 6.32 ± .13  | 0.88  | 1.19                       |
|             | 0.252      | 1                | 5.05 ± .09  | 1.59  | 0.95                       |
|             | 0.354      | 1                | 4.40 ± .13  | 2.25  | 0.83                       |
|             | 0.480      | 1                | 3.90 ± .13  | 3.03  | 0.74                       |
|             | 0.366      | 4.01             | 5.72 ± .19  | 4.63  | 0.75                       |
|             |            | 7.98             | 6.95 ± .05  | 6.54  | 0.78                       |
|             |            | 18.32            | 8.86 ± .25  | 9.91  | 0.80                       |
|             |            | 32.32            | 9.85 ± .25  | 13.16 | 0.77                       |
| Isopropanol | 0.354      | 1                | 3.17 ± .09  | 2.34  | 0.76                       |
|             | 0.480      | 1                | 3.10 ± .13  | 3.16  | 0.74                       |
|             | 0.366      | 4.11             | 4.81 ± .16  | 4.90  | 0.81                       |
|             |            | 8.3              | 5.66 ± .22  | 6.96  | 0.80                       |
|             |            | 18.56            | 6.60 ± .06  | 10.40 | 0.76                       |
|             |            | 32.32            | 8.04 ± .19  | 13.74 | 0.81                       |

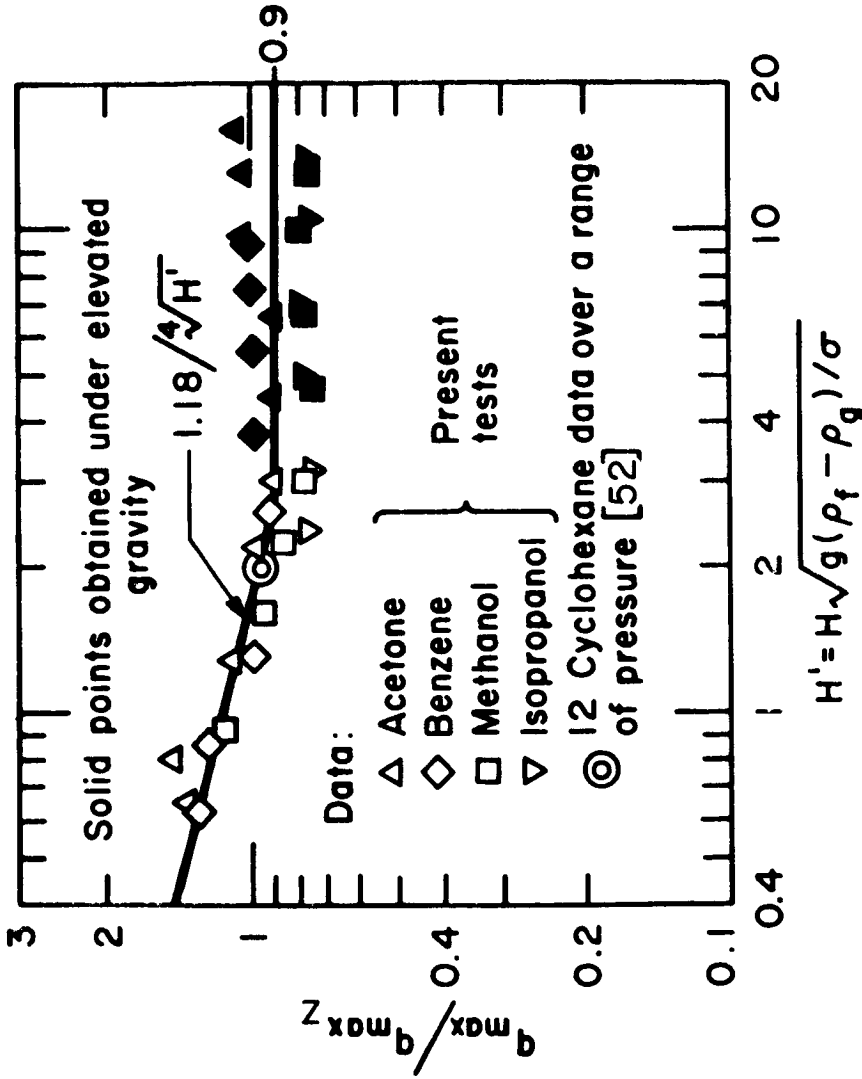


Fig. 18  $q_{max}$  on horizontal ribbon heaters oriented vertically.

heavily insulated with Sauereisen cement. A 0.252 cm ribbon was observed in methanol and a 0.478 cm ribbon was observed in acetone. The results were:

$$\text{at } H' = 1.59, \quad 1.19 \leq \frac{q_{\max}}{q_{\max Z}} \leq 1.30$$

$$\text{at } H' = 2.98, \quad 1.03 \leq \frac{q_{\max}}{q_{\max Z}} \leq 1.07$$

respectively. These data are plotted in Fig. 19 along with some high gravity data given by Adams [53] for higher values of  $H'$  in the same geometry.

In this case we find that equations (34) and (42) give an excellent representation of the data.

Both equations (41) and (42) correspond with  $A_j/A_h = 0.155$ . The transition from large to small  $H'$  occurs at 6 when the ribbon is insulated and at 2.6 when it is not.

## CONCLUSIONS

1. The method of hydrodynamic prediction of the peak heat flux on finite heaters is discussed in detail and certain general guidelines are set up for making such predictions. The assumption that the vapor velocities in the vapor blanket and in the jets must match, greatly streamlines prior descriptions and simplifies these guidelines. The guidelines can be summarized as follows:

$$\text{a.) } q_{\max}/q_{\max Z} = \frac{24}{\pi} \sqrt[4]{\frac{\pi}{A_h}} \frac{\sigma}{g(\rho_f - \rho_g)} \left( \frac{A_j}{A_h} \right)^{3/4} \text{ for small heaters}$$

$$\text{b.) } q_{\max}/q_{\max Z} = \frac{24}{\pi \sqrt[4]{3}} \frac{A_j}{A_h} \text{ for large heaters}$$

$$\text{c.) } \lambda_H \approx 2\pi R_j \text{ for small heaters}$$

$$\text{d.) } \lambda_H = \lambda_d \text{ for large heaters including the flat plate}$$

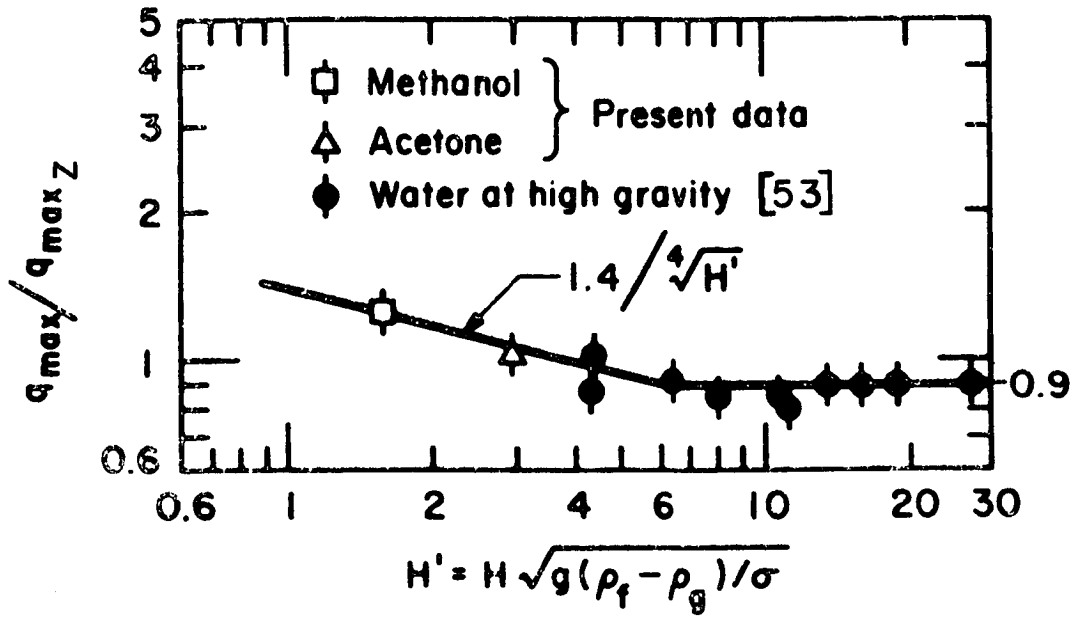


Fig. 19  $q_{max}$  on horizontal ribbon heaters oriented vertically with one side insulated.

e.) For small bluff bodies,  $A_h \sim L^2$  and

$$\frac{q_{\max}}{q_{\max_Z}} \Bigg|_{\substack{\text{small bluff} \\ \text{bodies}}} = \frac{\text{constant}}{\sqrt{L^*}}$$

where the constant must be determined experimentally because  $A_j/A_h$  is only known in one configuration (small spheres).

f.) Except for the case of small spheres,  $A_j/A_h$  seems to be a constant, very nearly independent of configuration. For the known cases (within about 10 percent)

$$\frac{A_j}{A_h} \simeq 0.155 ,$$

g.) Therefore,

$$\frac{q_{\max}}{q_{\max_Z}} \Bigg|_{\substack{\text{large} \\ \text{heaters}}} \simeq 0.9$$

h.)  $q_{\max}/q_{\max_Z} = \frac{1.4}{4\sqrt{P^*}}$  for long slender heaters.

2.) Some special cases of the above generalizations include the following predictions:

a.)  $q_{\max}/q_{\max_Z} = 0.94/\sqrt[4]{R^*}$  for small cylinders

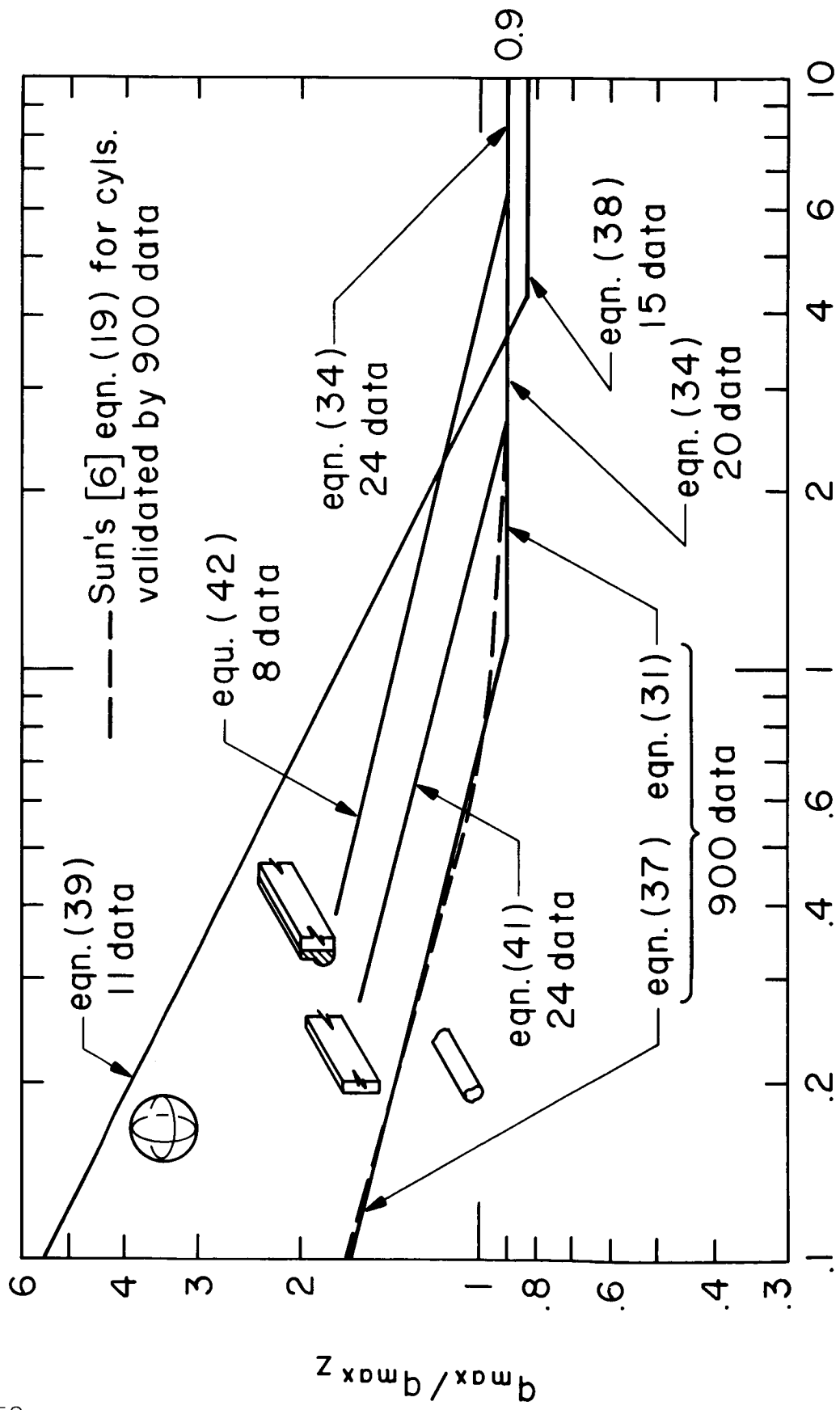
b.)  $q_{\max}/q_{\max_Z} = 0.904$  for large cylinders

c.)  $q_{\max}/q_{\max_Z} = 1.754/\sqrt{R^*}$  for small spheres

d.)  $q_{\max}/q_{\max_Z} = 0.84$  for large spheres

- e.)  $q_{\max}/q_{\max_Z} = 1.18/4\sqrt{H'}$  for small horizontal ribbons,  
oriented vertically
- f.)  $q_{\max}/q_{\max_Z} = 1.4/4\sqrt{H'}$  for small horizontal ribbons  
oriented vertically with one side insulated
- g.)  $q_{\max}/q_{\max_Z} = 0.90$  for large horizontal ribbons oriented  
vertically, one side insulated or not.

3.) The existing hydrodynamic  $q_{\max}$  predictions for finite bodies are summarized in Fig. 20. The figure includes an indication of the number of data by which each has been verified. This number exceeds the number of points actually shown in Fig. 18 and 19, since more than one observation has been lumped in some of the points. The curves have all been terminated at  $L' = 0.1$  on the left side since hydrodynamic predictions are known to deteriorate for  $L' \lesssim 0.1$ .



$$L' = L \sqrt{g(\rho_f - \rho_g) / \sigma}$$

Fig. 20. Collected predictions of  $q_{max}$  for four finite heater configurations.

## IV. A VISCOUS THEORY OF TAYLOR STABILITY WITH APPLICATION TO FILM BOILING

### Introduction

We now turn to the question of the influence of viscosity in the hydrodynamic theory. As we indicated in Chapter II, a Taylor unstable process is common to both the peak and the minimum heat fluxes. Thus our study of the influence of viscosity in the hydrodynamic theory should begin with a viscous theory of Taylor stability.

In 1950, G.I. Taylor [54] discussed the instability of the horizontal interface between two ideal incompressible fluids of infinite depth. He showed that irregularities at the interface tended to grow if the acceleration was directed from the less dense to the more dense medium. Bellman and Pennington's contribution [31] was to extend his problem and showed how to take into account the interfacial surface tension and fluid viscosity. They gave closed form expressions only for the "most susceptible" wavelength (i.e., the wavelength for which the growth rate for a small disturbance at the interface is maximum) and the corresponding frequency. They obtained solutions for the situation in which only the surface tension at the interface was considered, but they were unable to solve the more general problem in which both the liquid viscosity and interfacial surface tension were considered.

We shall begin with formulation of the instability problem similar to that made by Bellman and Pennington; we shall then incorporate the pressure contribution of curvature of a cylindrical surface as was done by Lienhard and Wong [33] for the inviscid case. Thus we shall attempt to obtain numerical values of the "most susceptible" frequency and corresponding wavelength as a function of liquid viscosity, as well as radius of curvature of a cylindrical heater. Finally, we shall discuss the use of this evaluation in predicting the minimum heat flux.

### Hydrodynamic Analysis

Before dwelling on the instability theory it is appropriate to state the various assumptions we are going to make:

- 1) The fluids are incompressible
- 2) The fluids are Newtonian

- 3) The fluid depths are large as compared to wavelength. This is not exactly valid for the vapor blanket thickness in film boiling, but we shall show later that the above assumption is not unrealistic.
- 4) The upper fluid layer is a liquid and the lower fluid layer is a gas. We thus envision that the acceleration at the interface is always directed from the lighter to the heavier fluid. We assume this is so, because it is the situation encountered in all film boiling cases we will treat.
- 5) Nonlinear effects are negligible.

Figure 21 shows the interface between two incompressible viscous fluids of infinite depth. The linearized equations governing the motion are:

$$u_x + v_y = 0 \quad (43)$$

$$u_t = -\frac{1}{\rho} p_x + \frac{\mu}{\rho} (u_{xx} + u_{yy}) \quad (44)$$

$$v_t = -\frac{1}{\rho} p_y - g + \frac{\mu}{\rho} (v_{xx} + v_{yy}) \quad (45)$$

These equations are satisfied by

$$u = -\phi_x - \psi_y \quad (46)$$

$$v = -\phi_y + \psi_x \quad (47)$$

and

$$p = p_0 - \rho g y + \rho \phi_t \quad (48)$$

provided that

$$\phi_{xx} + \phi_{yy} = 0 \quad (49)$$

and

$$\frac{\mu}{\rho} (\psi_{xx} + \psi_{yy}) = \psi_t \quad (50)$$

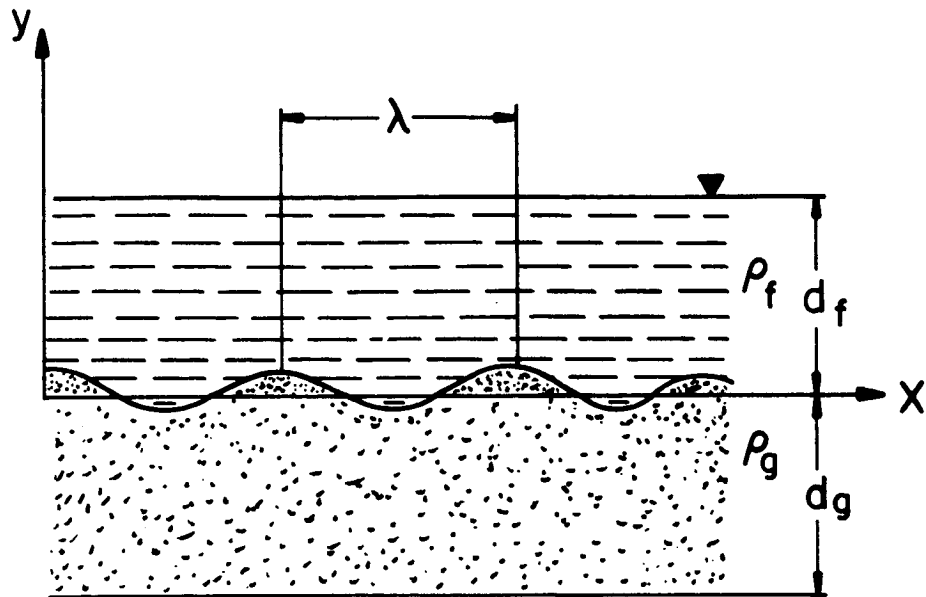


Fig. 2|a. Interface between two incompressible viscous fluids of infinite depth.

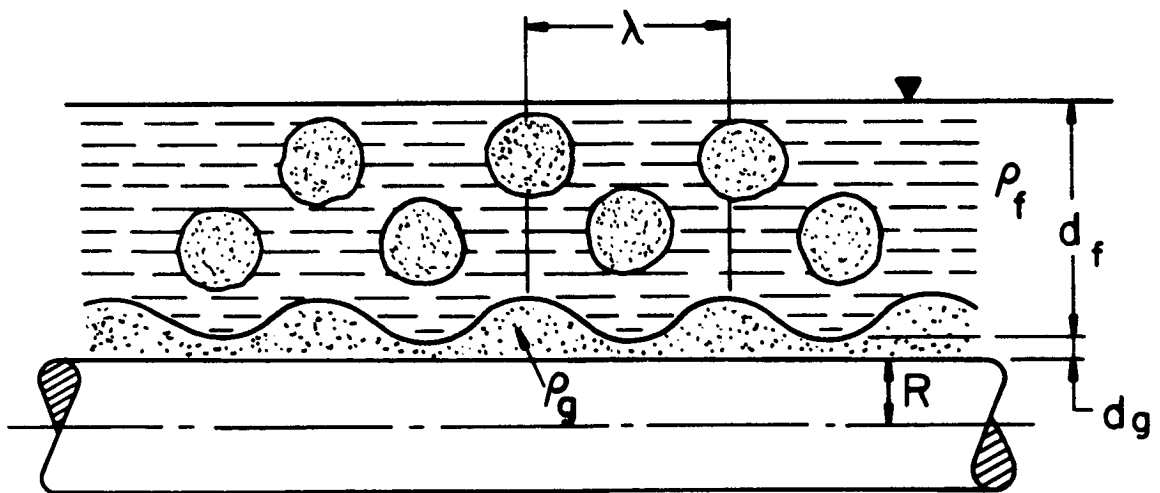


Fig. 2|b. Schematic diagram of a typical configuration of film boiling on cylinders.

where  $u$  and  $v$  are the velocities in the  $x$  and  $y$  directions, respectively;  $p$  is the static pressure;  $p_0$  is the total pressure; and  $\rho$  is the density of the fluid.

Let us take, for the liquid phase:

$$\varphi_f = A_f e^{-ky+\omega t} \cos kx \quad (51)$$

$$\psi_f = B_f e^{-m_f y+\omega t} \sin kx \quad (52)$$

$$p_f = p_0 - \rho_f g y + \rho_f (\varphi_f)_t \quad (53)$$

where  $k$  is the wave number,  $\omega$  is the growth rate<sup>8</sup>, and:

$$m_f^2 = k^2 + \rho_f \omega / \mu_f \quad (54)$$

Similarly for the gaseous phase:

$$\varphi_g = A_g e^{ky+\omega t} \cos kx \quad (55)$$

$$\psi_g = B_g e^{m_g y+\omega t} \sin kx \quad (56)$$

$$p_g = p_0 - \rho_g g y + \rho_g (\varphi_g)_t \quad (57)$$

and

$$m_g^2 = k^2 + \rho_g \omega / \mu_g \quad (58)$$

The real part of  $m_f$  or  $m_g$  has to be positive so the velocity remains finite as  $y \rightarrow \pm \infty$ .

---

<sup>8</sup> In Chapter II, we used  $\omega$  to designate a true cyclic frequency. Thus the real part of  $\exp(-i\omega t)$  was the cosine of the phase angle, and when exponential growth occurred,  $\omega$  was a pure imaginary number. Here we designate as  $\omega$ , what we formerly wrote as  $(-i\omega)$ . Henceforth  $\omega$  will designate a real growth rate--not a real frequency.

Considering that waves of height  $y = \eta(x,t)$  are propagated, we obtain for the linearized kinematic condition at the interface:

$$\eta_t = v_f \quad (59)$$

or

$$\eta = \eta_0 e^{i\omega t} \cos kx \quad (60)$$

where

$$\eta_0 = \frac{k(A_f + B_f)}{\omega} \quad (61)$$

The boundary conditions at the interface, i.e., at  $y=\eta$ , are:

$$u_f = u_g \quad (62)$$

$$v_f = v_g \quad (63)$$

$$-p_f + 2\mu_f(v_f)_y = -p_g + 2\mu_g(v_g)_y - \sigma\eta_{xx} \quad (64)$$

$$\mu_f[(v_f)_x + (u_f)_y] = \mu_g[(v_g)_x + (u_g)_y] \quad (65)$$

The substitution of equations (51) through (53); (55) through (57) and (60) in equations (62) to (65) gives four linear and homogeneous equations in the four constants,  $A_f$ ,  $B_f$ ,  $A_g$ , and  $B_g$ :

$$kA_f + m_f B_f - kA_g + m_g B_g = 0 \quad (66)$$

$$A_f + B_f + A_g - B_g = 0 \quad (67)$$

$$\left[ \frac{g(\rho_f - \rho_g)k}{\omega} - \frac{\sigma k^3}{\omega} - \rho_f \omega - 2\mu_f k^2 \right] A_f + \left[ \frac{g(\rho_f - \rho_g)k}{\omega} - \frac{\sigma k^3}{\omega} - 2\mu_f k m_f \right] B_f$$

$$+ [\rho_g \omega + 2\mu_g k^2] A_g - [2\mu_g k m_g] B_g = 0 \quad (68)$$

and

$$2\mu_f k^2 A_f + \mu_f (k_f^2 + m_f^2) B_f + 2\mu_g k^2 A_g - \mu_g (k_g^2 + m_g^2) B_g = 0 \quad (69)$$

The above equations have a non-trivial solution if and only if the determinant of the coefficient matrix is zero, i.e.:

$$\begin{vmatrix} k & m_f & -k & m_g \\ 1 & 1 & 1 & -1 \\ \left\{ \frac{g(\rho_f - \rho_g)k}{w} - \frac{\sigma k^3}{w} \right\} & \left\{ \frac{g(\rho_f - \rho_g)k}{w} - \frac{\sigma k^3}{w} \right\} & \rho_g w + 2\mu_g k^2 & -2\mu_g k m_g \\ -\rho_f w - 2\mu_f k^2 & -2\mu_f k m_f & 2\mu_g k^2 & -\mu_g (k^2 + m_g^2) \\ 2\mu_f k^2 & \mu_f (k_f^2 + m_f^2) & & \end{vmatrix} = 0 \quad (70)$$

Equation (70) should be valid only when the fluid depths are infinite and there is no curvature in the transverse direction at the interface. In film boiling on horizontal cylinders the depth of the vapor blanket is finite and there is a curvature in the transverse direction. A typical configuration is shown in Figure 21b.

Recently, Hsieh [55] analyzed the inviscid instability problem in the presence of heat and mass transfer. His analysis also incorporated a finite depth of fluids. Commenting on his work as applied to film boiling, we [56] showed that there was no effect of finite vapor depth on the "most susceptible" wavelength, while the effect on the corresponding frequency was to decrease it by a small amount.

As proposed earlier by Lienhard and Wong [33], a two dimensional model can be used for cylindrical geometries. The effect of transverse curvature is treated in the form of an additional oscillating pressure difference component across the interface, as shown in Figure 22.

The expression for the transverse pressure may easily be written as:

$$\Delta p_{tr} = \frac{\sigma}{2R^2(1+d_g/R)^2} \eta \quad (71)$$

where  $d_g$  is the depth of the vapor blanket over the wire.

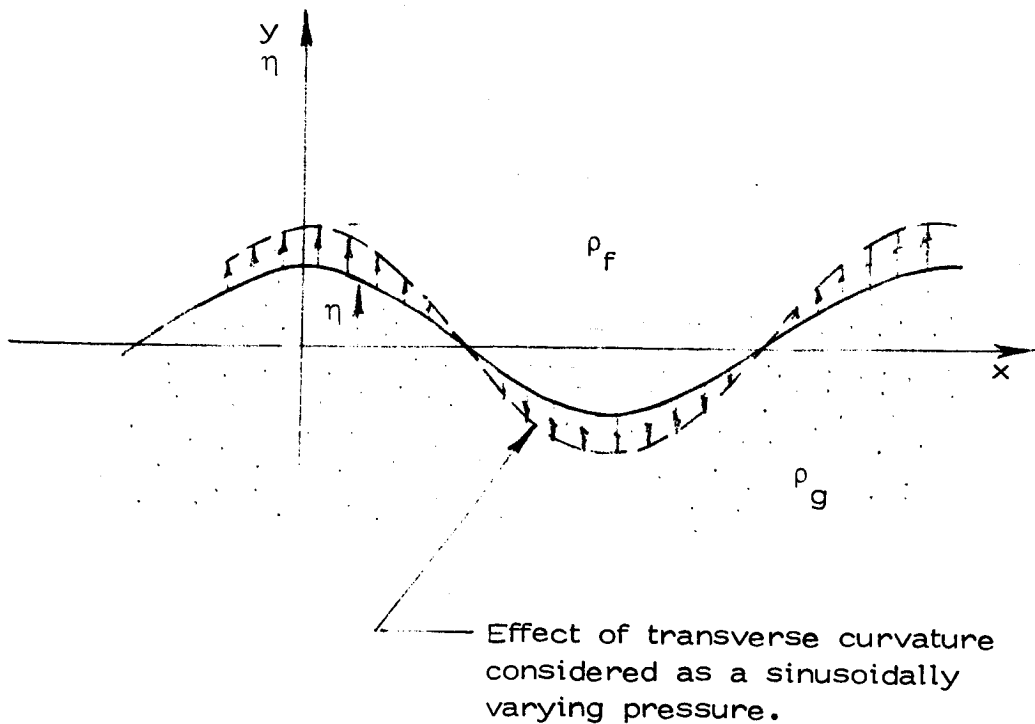


Figure 22 Contribution of transverse curvature on a two dimensional wave

If we define a corrected radius,  $R_c \equiv R[1+d_g/R]$ , we can write equation (64) as:

$$-p_f + 2\mu_f v_f y = -p_g + 2\mu_g v_g y - \sigma \eta_{xx} - \frac{\sigma}{2R_c} \eta \tag{64a}$$

Consequently equation (70) becomes

$$\begin{vmatrix} k & m_f & -k & m_g \\ 1 & 1 & 1 & -1 \\ \left\{ \frac{g(\rho_f - \rho_g)k}{\omega} - \frac{\sigma k^3}{\omega} \right\} & \left\{ \frac{g(\rho_f - \rho_g)k}{\omega} - \frac{\sigma k^3}{\omega} \right\} & (\rho_g \omega + 2\mu_g k^2) & -2\mu_g k m_g \\ \left\{ -\rho_f \omega - 2\mu_f k^2 + \frac{\sigma k}{2R_c \omega} \right\} & \left\{ -2\mu_f k m_f + \frac{\sigma k}{2R_c \omega} \right\} & 2\mu_g k^2 & -\mu_g (k^2 + m_g^2) \end{vmatrix} = 0 \tag{70a}$$

The evaluation of the determinant equation, (70a) gives:

$$\left[ -g(\rho_f - \rho_g)k + \sigma k^3 - \frac{\sigma k}{2R_c} + (\rho_f + \rho_g)\omega^2 \right] [\mu_f(k+m_f) + \mu_g(k+m_g)] + 4\omega k [\mu_f k + \mu_g m_g] [\mu_g k + \mu_f m_f] = 0 \quad (70b)$$

Our next step is to put equation (70b) in a more usable form, so that it can be solved explicitly for frequency and wave number, or wavelength. The vapor viscosity  $\mu_g$  is much less than  $\mu_f$  so it may be neglected in comparison to liquid viscosity. Thus we may write, for the growth rate,  $\omega$ ,

$$\omega = f(\rho_f + \rho_g, \rho_f - \rho_g, \mu_f, \sigma, k, g, R_c) \quad (72)$$

This expression relates eight quantities which are expressible in three dimensions. Using the Buckingham Pi-Theorem, we can recast this problem in terms of five dimensionless groups. For these groups we choose:

- (i) a dimensionless growth rate or "frequency"

$$\Omega \equiv \omega \left[ \frac{\sigma}{g(\rho_f - \rho_g)} \right]^{1/4} \quad (73)$$

- (ii) a dimensionless wave number

$$K \equiv k \left[ \frac{\sigma}{g(\rho_f - \rho_g)} \right]^{1/2} \quad (74a)$$

or a dimensionless wavelength,  $\Lambda$ , defined as

$$\Lambda = 1/(\sqrt{3} K) \quad (74b)$$

(iii) a dimensionless liquid viscosity parameter

$$M \equiv \frac{\rho_f \sigma^{3/4}}{\mu_f g^{1/4} (\rho_f - \rho_g)^{3/4}} \quad (75)$$

The square of this group is very nearly the Borishanski number,  $N$ , as defined in equation (11).

(iv) a dimensionless density

$$\Gamma \equiv \frac{\rho_f - \rho_g}{\rho_f + \rho_g} \quad (76)$$

(v) a non-dimensional cylinder radius

$$R'_c \equiv R_c \left[ \frac{g(\rho_f - \rho_g)}{\sigma} \right]^{1/2} \quad (77)$$

This number is related to the Bond number,  $Bo$ , by  $Bo \equiv R'_c{}^2$ .

Using these dimensionless numbers, we may write equation (70b) as:

$$1 - K^2 + \frac{1}{2Bo} - \frac{\Omega^2}{\Gamma K} + \frac{K}{(K^2 + \Omega M)^{1/2}} - \frac{K^3}{(K^2 + \Omega M)^{1/2}} - \frac{\Omega^2}{\Gamma(K^2 + \Omega M)^{1/2}} - \frac{4\Omega K}{M\Gamma} + \frac{K}{2Bo(K^2 + \Omega M)^{1/2}} = 0 \quad (78)$$

Equation (78) gives a relation between growth rate and wave number for an unstable disturbance (corresponding to  $\Omega$  positive and real), when the interfacial surface tension, transverse curvature and liquid viscosity are taken into account.

From equation (78) it is clear that when the wave propagation velocity is zero, there is no effect of liquid viscosity on the critical wavelength. Also, when  $M \rightarrow \infty$  (i.e., the liquid is inviscid) equation (78) reduces to the same equation as obtained by Lienhard and Wong [33] for the inviscid case.

We are interested in the "most susceptible frequency", or the value of  $\omega$  for which growth rate of the disturbance is maximum (i.e., the one for which  $\frac{d\Omega}{dk} = 0$ ). Differentiating equation (78) with respect to  $k$  and setting  $\frac{d\Omega}{dk} = 0$ , gives

$$\begin{aligned}
 & -2K + \frac{\Omega^2}{\Gamma K^2} + \frac{1}{(K^2 + \Omega M)^{1/2}} - \frac{K^2}{(K^2 + \Omega M)^{3/2}} - \frac{3K^2}{(K^2 + \Omega M)^{1/2}} \\
 & + \frac{K^4}{(K^2 + \Omega M)^{3/2}} + \frac{\Omega^2 K}{\Gamma (K^2 + \Omega M)^{3/2}} - \frac{4\Omega}{M\Gamma} + \frac{1}{2Bo(K^2 + \Omega M)^{1/2}} \\
 & - \frac{K^2}{2Bo(K^2 + \Omega M)^{3/2}} = 0
 \end{aligned} \tag{79}$$

Thus we have two nonlinear equations (78) and (79) in two unknowns,  $\Omega$  and  $K$ . The two equations were solved numerically on an IBM/360 computer using a subroutine: XFNLES, which solves a system of nonlinear equations. This subroutine is available in the Numerical Analysis Library [57] for the S/360.

For the physical cases that we shall consider subsequently,  $\Gamma$  is approximately 0.9995. This is the value that we used in the calculations. We might just as well have set  $\Gamma = 1$ , however, since  $\Gamma$  would have to be much farther from unity to alter the computations noticeably.

The "most susceptible frequency" and corresponding wavelength are plotted in Figs. 23 and 24, respectively, as a function of the viscosity parameter  $M$  and Bond number,  $Bo$ . As evident from these figures, the effect of liquid viscosity is to increase the wavelength and to decrease the corresponding frequency.

Figures 25 and 26 show the effect of Bond number and liquid viscosity separately on the frequency-wavelength relationship equation (78). Transverse curvature of the cylindrical heater reduces the "most susceptible" wavelength and increases the frequency. Figure 26 shows that apart from increasing the wavelength, viscosity also tends to increase the region of near neutral stability slightly. By "region of near neutral stability" we mean the range of wavelengths that can exist within any specified range of frequency close to the maximum frequency.

#### Experimental Determination of Vapor Blanket Thickness, Wavelength, and Growth Rate

An experimental program was carried out to observe the wavelength, its rate of growth, and the thickness of the vapor blanket surrounding the wire heater during film boiling in viscous liquids. Since the viscosity of most of the liquids is fairly low when they boil at normal pressures, the experiments had to be performed at very low pressures to illuminate significant viscous effects.

With the limitations of attaining maximum vacuum in the existing boiling apparatus in mind, a survey of various available chemicals was made. It was found that Cyclohexanol,  $CH_2(CH_2)_4$  CHOOH, and Propylene Glycol,  $CH_3(CHOH)CH_2OH$ , were best suited for the purpose. However, nearly all the experiments reported here were performed with cyclohexanol as the boiling liquid. Complete information regarding the relevant physical properties of cyclohexanol are presented in reference [27].

The basic element of the apparatus was a test capsule 8.9 cm wide, 8.9 cm high and 17.8 cm long, with glass windows in the 8.9 by 17.8 cm walls. It was made of brass and insulated on the sides with 0.63 cm thick styrofoam sheet. An electric preheater and 0.63 cm diameter brass holders to support the test heaters were fitted to the capsule. Nichrome wires were used as test heaters and copper hooks were attached to their ends so they could be mounted in the brass holders. The hooks were attached in such a manner as to minimize the end effects. A 2.54 cm marker was mounted on the bottom of the capsule to provide a reference dimension for the

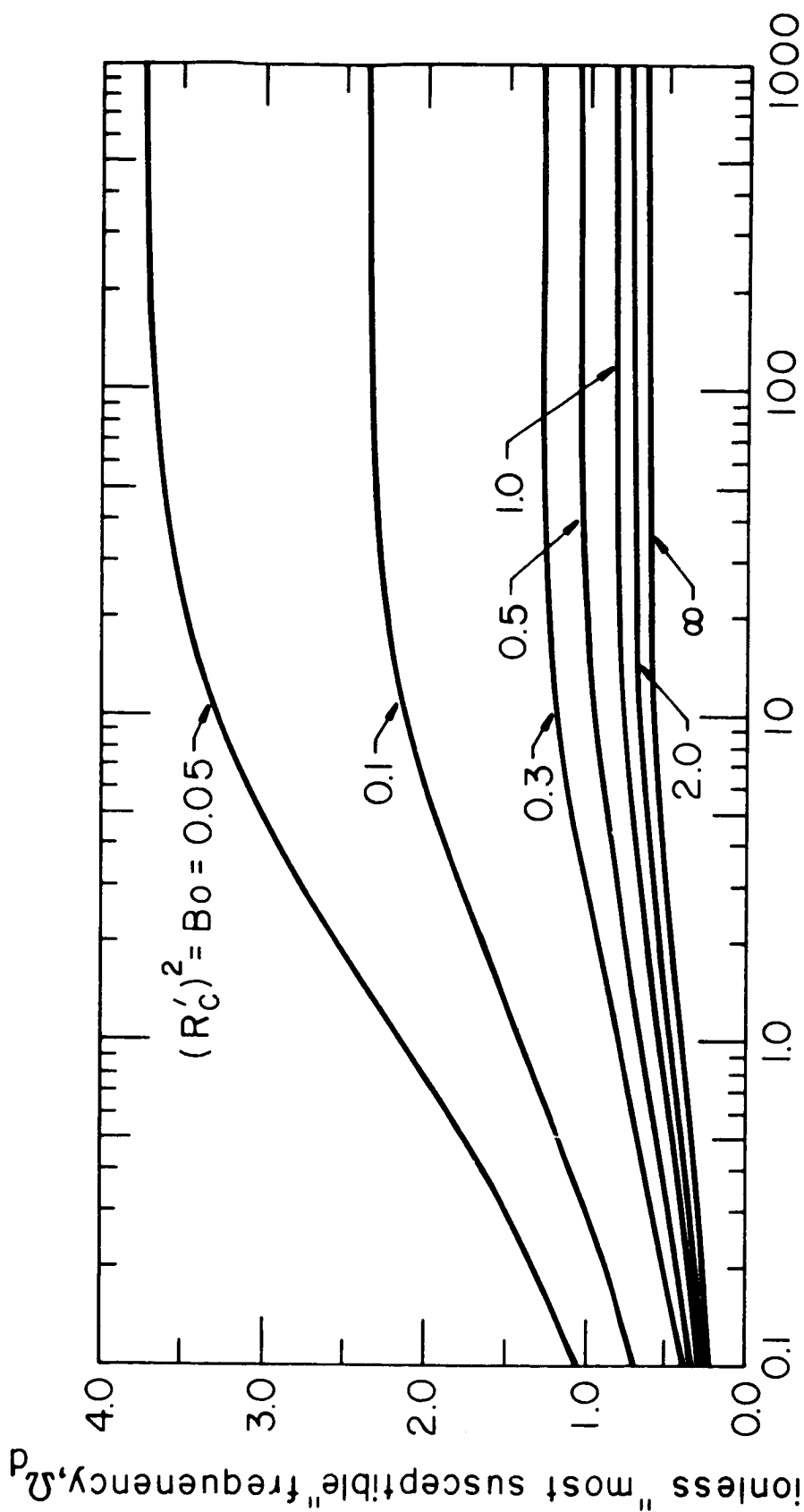


Fig. 23 Variation of  $\Omega_d$  with  $M$  for various Bond numbers

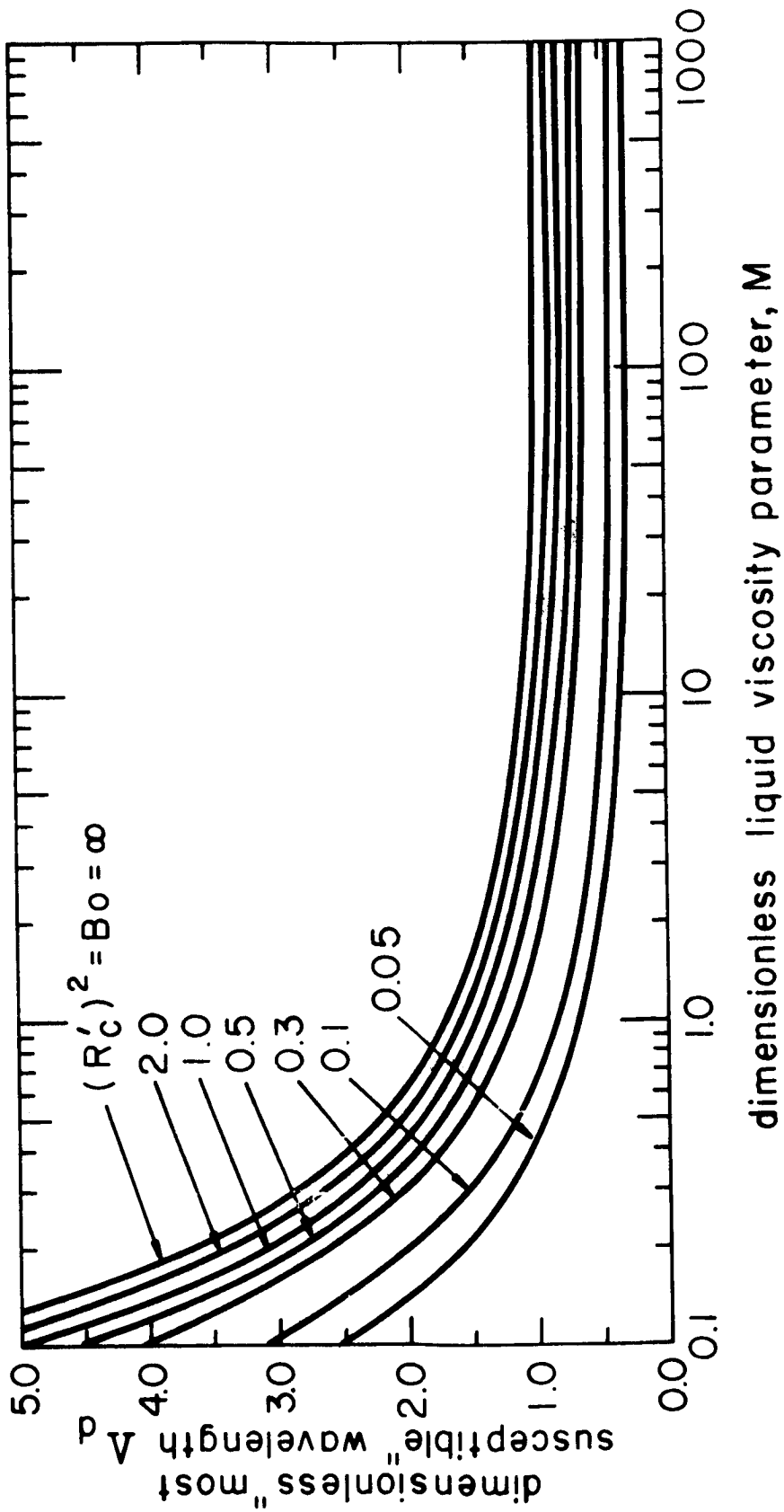


Fig. 24 Variation of  $\Delta_D$  with  $M$  for various Bond numbers

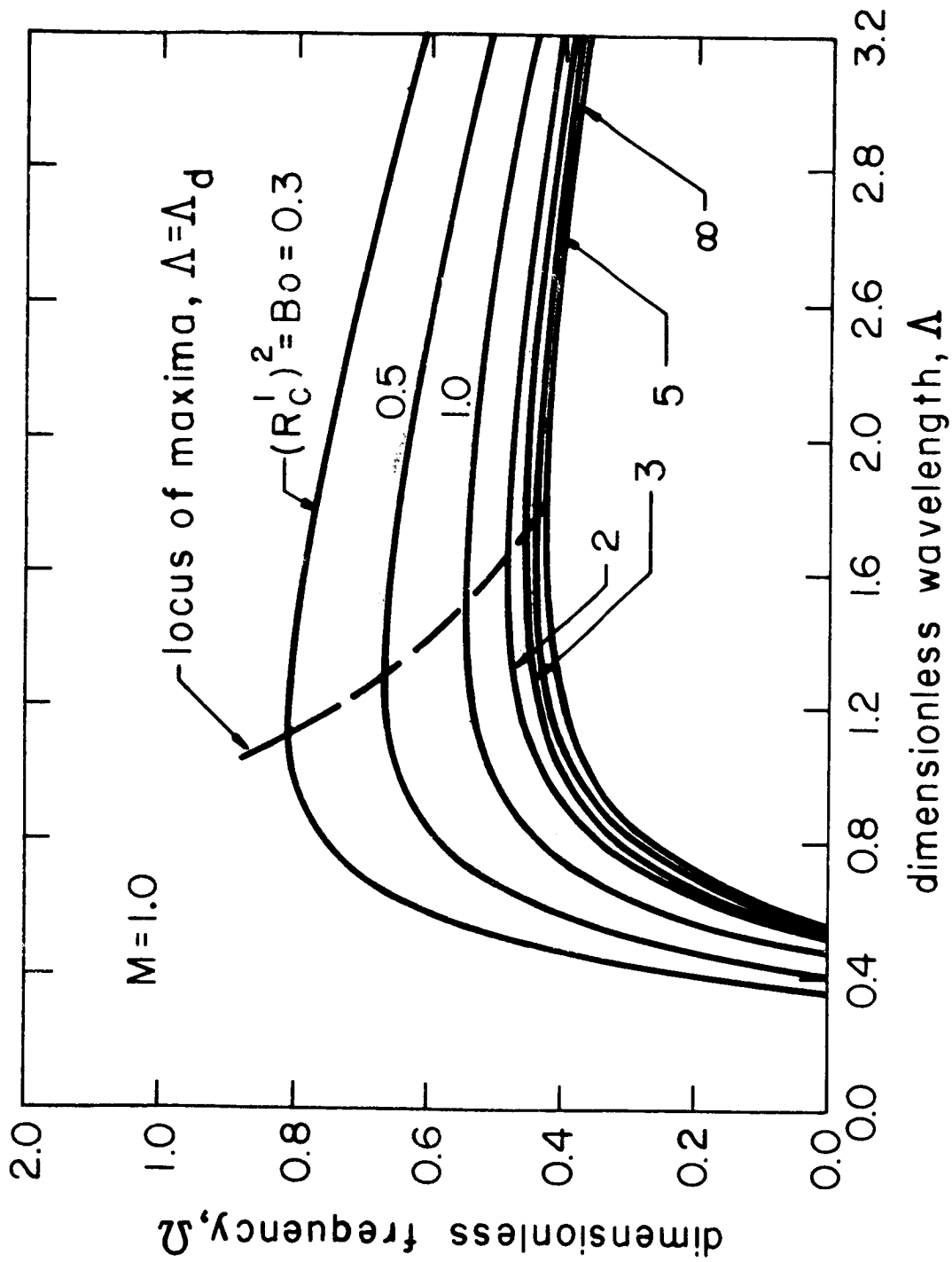


Fig. 25 Effect of radius on dispersion relation for cylinders

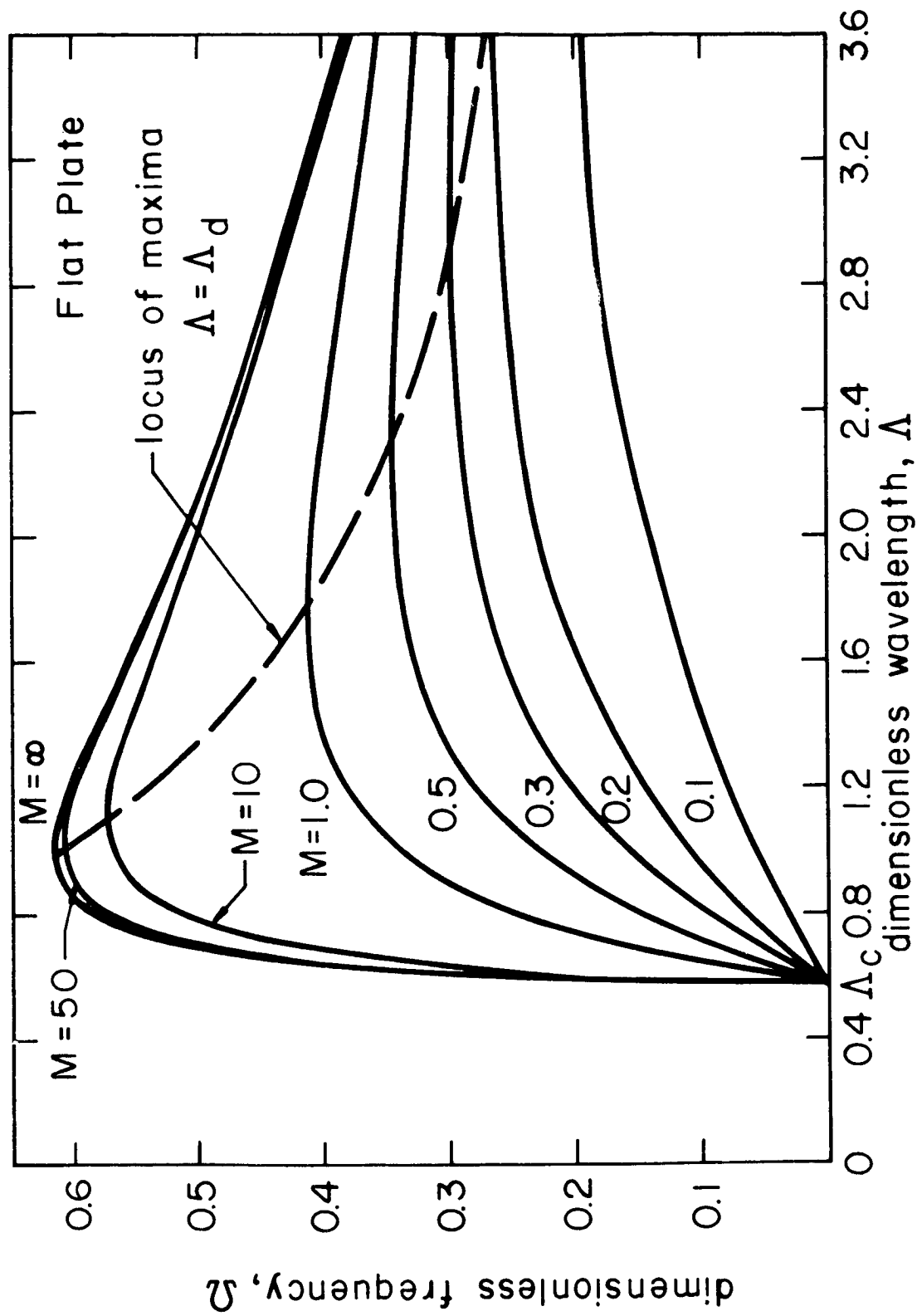


Fig. 26 Effect of viscosity on dispersion relation for a flat plate

reduction of photographic data.

Figure 27 shows a schematic diagram of the apparatus. AC power was employed in most of the experiments. The power supply to the wire was calculated from the measured current and voltage in the wire. A mercury manometer or a vacuum gage was used to note pressure inside the capsule. This pressure was corrected to take into account the head of liquid above the wire. An identical apparatus was used by Lienhard and Sun to make similar measurements. Full details are given in reference [5].

Nichrome wires, about 10 cm long, were cleaned with soap and hot water to remove any grease or oily matter and then rinsed with the test liquid. The wire surfaces were smooth and had a cold-rolled finish (as supplied by the manufacturer). The wires were mounted in the brass holders and the glass windows were positioned. The capsule was filled with reagent grade test liquid to a level of about 2.5 cm above the wire. The vacuum pump was started and the preheater was turned on to heat the liquid to saturation temperature. The preheater was turned off before energizing the wire. This was done to avoid any effects of convective currents and electric fields.

The current in the wire was steadily increased until the peak heat flux was reached and the transition from nucleate to film boiling was observed. Thereafter the current was reduced until film boiling started to disappear at the ends. This insured that the heat flux was close to minimum.

Still pictures of the film boiling phenomenon were taken and observations of the temperature and pressure were also made. The heat flux was again increased in steps. At each step a photograph was taken and other corresponding observations were made. This procedure was continued until the heat flux was such that the wire started glowing or the bubble merger mechanism was evident. By "bubble merger" we mean that two neighboring bubbles growing in the first half of the cycle come into contact with the adjoining bubble from the second half of the cycle. Again the heat flux was decreased in steps and the process repeated.

This procedure was repeated for wires of different sizes and various pressures. Each time a new wire was used, the liquid in the capsule was also replaced. In some cases high speed movies were made, to facilitate study of the growth rate of the disturbance, with a Hycam motion picture camera at a speed of 500 frames per second and

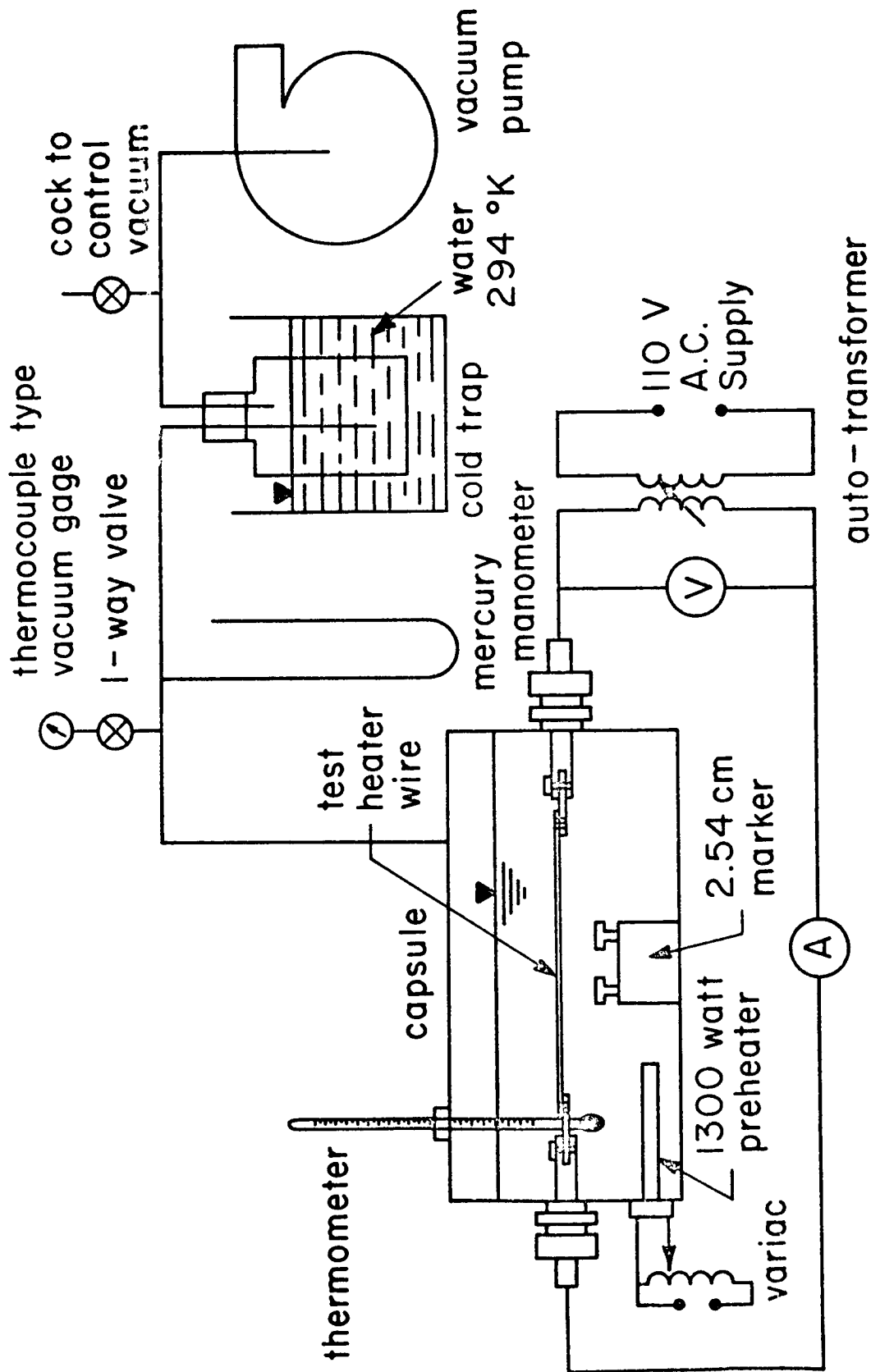


Fig.27 Schematic diagram of the apparatus.

an exposure time of 1/1250 second.

Photographic information was used to make three different kinds of observations. We describe them under three separate subtitles:

Wavelength measurements -- Still pictures were taken with a 2.54 cm marker as a reference dimension, so the wavelengths could be scaled from them. Care was taken to avoid situations where bubble merger or deformation of the wave pattern had taken place. This deformation may be caused by drift in the phase angle along the wire or by oscillations generated through the movement of the outgoing bubbles. The probable error in the measurements of the shortest wavelengths was only about  $\pm 4.5$  percent. The error was less for larger wavelengths.

Vapor blanket thickness measurements -- In film boiling, a vapor blanket of finite thickness always surrounds the heater and there is no liquid contact with the surface of the heater. The instability of the upper boundary of this vapor blanket causes a steady release of bubbles. For the application of the theory developed in the previous section we must obtain the corrected radius of the heater wire by adding the minimum blanket thickness to R.

To observe the vapor blanket thickness, representative pictures of film boiling were enlarged. The minimum diameter of the vapor blanket surrounding the wire was measured, using the 2.54 cm marker again as a reference. This was done to avoid any refraction effects that might creep in if the wire diameter were chosen as a reference. Furthermore, the wire diameter could not be seen clearly through the vapor blanket. The wire diameter was subtracted from this measurement to give twice the vapor blanket thickness. In other words, we anticipated that vapor surrounded the wire equally on the top and the bottom. Sometimes a cusp appeared on the blanket in the wake of a departing bubble, and we have ignored it.

Measurements of growth rate of disturbance -- Hycam movies were viewed on a microfilm viewer. At first, a preliminary survey was made to sort out those bubbles which grew undisturbed by other adjoining bubbles. Starting with a frame in which a bubble had just broken away from the interface, the height of the interface was measured from the lowest boundary of the vapor blanket. Later, the minimum diameter of the vapor blanket tube surrounding the wire was subtracted from each of the above observations to give the amplitude of the wave.

The minimum height of the interface was used as a reference dimension for obtaining dimensionless amplitude. Thus, at a particular value of  $x$ , say  $x=0$ , one may write

$$\eta = \eta_0 \exp(\omega t) \quad (80)$$

or

$$\frac{\eta}{\eta_0} = \exp \left[ \Omega t \sqrt[4]{g^3 (\rho_f - \rho_g) / \sigma} \right] \quad (81)$$

but we can easily show that  $\sqrt[4]{g^3 (\rho_f - \rho_g) / \sigma} = 1.612 \omega_{dF}$ ,

so

$$\ln \left( \frac{\eta}{\eta_0} \right) = \Omega (1.612 \omega_{dF} t) \quad (81a)$$

where  $\eta_0$  is the minimum depth,  $d_g$ , of the vapor and  $\omega_{dF}$  is the "most susceptible" frequency (or growthrate) for the disturbance in the inviscid fluid in the absence of any geometrical effects of the heater. In all cases the dimensionless amplitude,  $\eta/\eta_0$ , was plotted against dimensionless time,  $\omega_{dF} t$ , on semi-logarithmic graph paper. The slope of the curve at any instant gave the dimensionless frequency  $\Omega$ . The probable error in the observation of the linear growth rate was  $\pm 10$  percent.

Now we would like to compare the experimental observations of wavelength and frequency with the theoretical predictions. However before we can do this it is necessary to present some sort of correlation for vapor blanket thickness, because the wire radius has to be corrected for it.

### Vapor Blanket Thickness Correlation

Baumeister and Hamill [58], while analyzing heat transfer from wires in film boiling, developed an expression for vapor blanket thickness. Their theoretical model for the film boiling configuration was a fairly approximate one; a sequence of spherical domes connected by annular passages. Neglecting inertia, they solved the equations of motion and energy with the assumption that the heat transfer rate is maximum.

For the heat transfer coefficient for film boiling on wires they got:

$$h_w = 0.23 \left[ \frac{k_g^3 h_{fg}^* g(\rho_f - \rho_g) \rho_g}{\mu_g \Delta T \sqrt{\frac{\sigma}{g(\rho_f - \rho_g)}}} \right]^{1/4} \times \left[ \left( \frac{1}{2R'} \right)^3 + 2.25 \left( \frac{1}{2R'} \right) (1 + \Delta)^2 \right]^{1/4} \quad (82)$$

where  $\Delta \equiv d_g/R$ . All the physical properties of the vapor in the above equation are evaluated at the mean film temperature, i.e., at  $T = T_{\text{sat}} + \Delta T/2$ . The latent heat of vaporization has been corrected to take into account any sensible heat required to heat the vapor above its saturation temperature. Assuming a parabolic velocity profile and mean film temperature for vapor in the vapor blanket, Breen and Westwater [59] gave a corrected expression for  $h_{fg}$ :

$$h_{fg}^* = h_{fg} \left[ 1 + \frac{0.34 c_p \Delta T}{h_{fg}} \right]^2$$

Baumeister and Hamill' changed the constant in equation (82) from 0.23 to 0.35 for small wires ( $R' \leq 0.05$ ) to take into account any heat transfer from the domes. This constant was further corrected to 0.485 for larger wires ( $R' \geq 0.05$ ) to fit the experimental data. Essentially, the constant in equation (61) was fixed from experimental results. This was necessary owing to their necessarily simplified model of the film boiling process.

Their theoretical expression for the vapor blanket thickness was

$$\Delta = \exp \left\{ 4.35 \left[ \frac{k_g \mu_g \Delta T}{h_{fg}^* 2R' \rho_g \sigma} \right]^{1/4} \left[ \frac{1}{1 + 9R'^2 (1 + \Delta)^2} \right]^{1/4} \right\} - 1 \quad (83)$$

where the term in the second square bracket is close to unity for small values of  $R'$  and  $\Delta$ .

If heat flux,  $q$ , is taken to be an independent variable; the temperature difference,  $\Delta T$ , between the heater wall and the surrounding liquid can be written as  $q/h_w$  so equations (82) and (83) yield:

$$\Delta = \exp \left\{ 7.05 \left[ \frac{q \mu_g}{h_{fg}^* \rho_g \sigma} \right]^{1/3} \left[ \frac{1}{1 + 9R^2 (1 + \Delta)^2} \right]^{1/3} \right\} - 1 \quad (84)$$

The group  $\mu_g/h_{fg}^* \rho_g$  is a weak function of temperature. We took  $\Delta T = 425^\circ K$ , which is typical of the film boiling situation, and plotted the present data for cyclohexanol, as well as some old data of Sun for acetone [1] against equation (84). The predictions were too high and did not correlate the data well for various dimensionless radii. This suggests that we should take another look at the various factors influencing vapor blanket thickness.

The vapor blanket thickness will primarily depend on seven independent variables,  $q$ ,  $\rho_g$ ,  $h_{fg}^*$ ,  $g(\rho_f - \rho_g)$ ,  $\sigma$ ,  $\mu_g$  and  $R$ . The heat flux  $q$  is imagined to be transferred by conduction and used fully in the phase transformation. The eight variables, including vapor blanket thickness,  $d_g$ , can be written in four dimensions: joule, kg, meter, and sec. Thus, in accordance with Buckingham Pi Theorem, we expect the problem to be reducible to a relation among four dimensionless groups. For these we choose:

- a) The dimensionless vapor blanket thickness,  $\Delta$ .
- b) The Bond number,  $Bo$ , or ratio of buoyant to surface tension forces.
- c) A ratio of viscous to surface tension forces,

$$B \equiv \frac{q \mu_g}{\rho_g h_{fg}^* \sigma} \quad (85)$$

- d) A ratio of inertial to viscous forces--a kind of Reynolds number based on the vapor velocity,

$$Re \equiv \frac{qR\Delta}{\mu_g h_{fg}^*} \quad (86)$$

Baumeister and Hamill's equation (84) involved the first three groups but the fourth group was missing because they neglected inertial terms in their equation of motion. Their assumption was realistic as long as either the wire radius, or the heat flux, or the vapor blanket thickness is small; but the ratio of inertial to viscous forces might be of

the order of magnitude of unity when the heat flux is high or the vapor blanket thickness is large.

Radiation losses can also form a significant portion of the total heat transfer from a wire in film boiling. We employed nichrome wires in all the experiments performed. The total hemispherical emittance for slightly oxidized nichrome at a temperature of 750°K has been given by Touloukian [60] as 0.65. Thus the radiative heat flux may be written as:

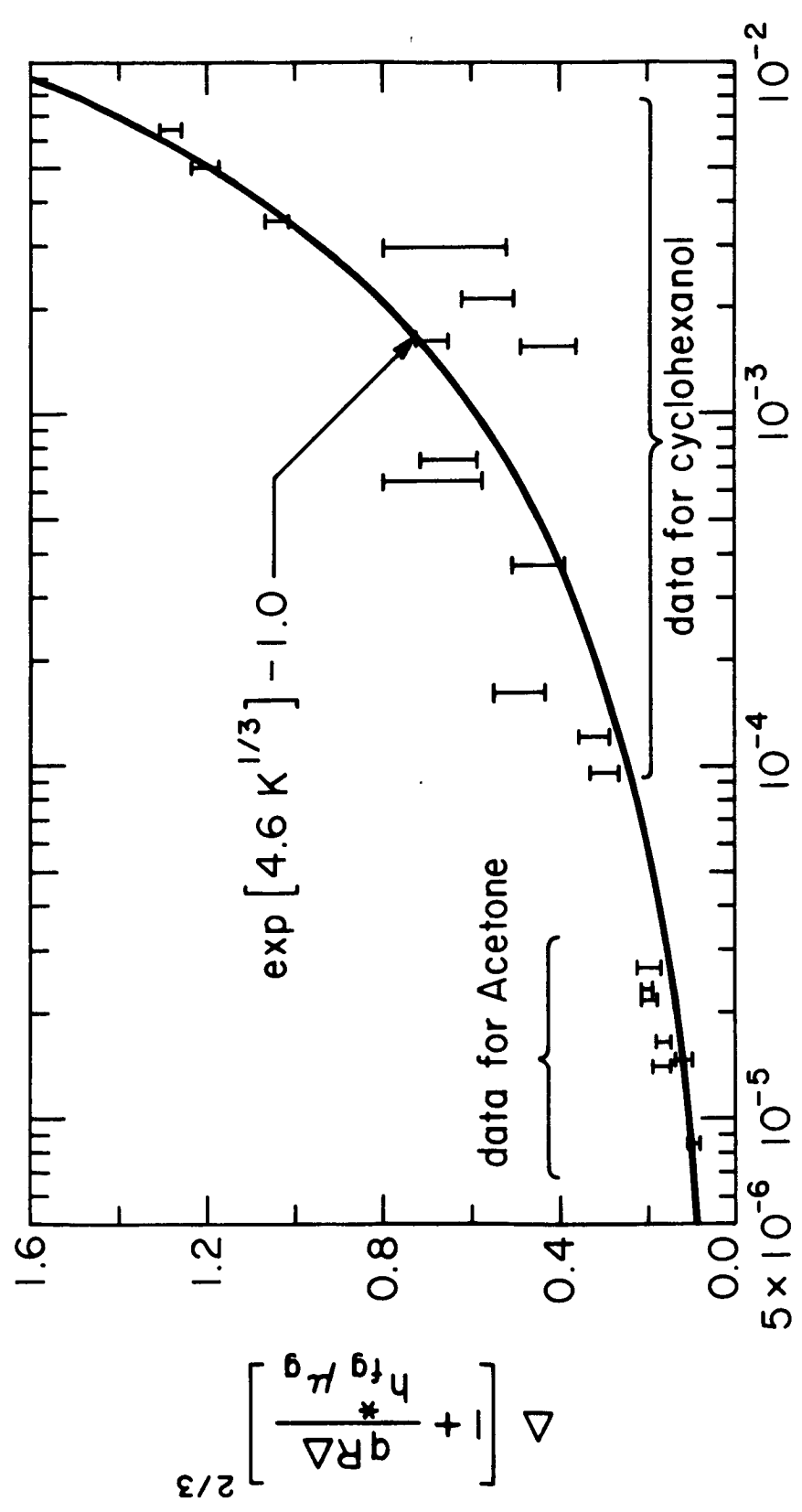
$$q_r = 0.65 \sigma (T_w^4 - T_{sat}^4) \quad (87)$$

For  $\Delta T \approx 425^\circ\text{K}$ , which is typical for our wires, equation (87) gives  $0.132 \times 10^5$  watts/meter<sup>2</sup>. This heat flux may form as much as 10–20 percent of the total heat flux, and it is absorbed by the liquid.

To know the depth of penetration of this radiant heat flux, absorptive properties of liquid cyclohexanol are needed. However, this information is not available in the existing literature. Values of the absorption or extinction coefficient for water [61] indicate that all the radiant energy is absorbed in a very thin layer of liquid. Even if absorption is considerably less for cyclohexanol, the radiant energy absorbed by the liquid adjoining the interface will largely find its way back to the interface where it will be utilized in generating additional amounts of vapor. Thus we incorporate all of  $q_r$  in  $q$  for use in equation (84).

Depending upon the total amount of vapor generated, the vapor blanket thickness and vapor velocity in the vapor blanket, will adjust themselves in such a way as to optimize the process. The Reynolds number,  $Re$ , as defined in equation (86) incorporates the vapor velocity and the vapor blanket thickness, hence it is an important correlation parameter.

In Figure 28, we have plotted 20 data points for vapor blanket thickness on wires in the range  $0.11 \leq R' \leq 0.65$  during the film boiling of acetone and cyclohexanol. While the abscissa is the same as Baumeister and Hamill's, the vapor blanket thickness has been correlated with the Reynolds number as an additional parameter. This correction has been obtained by trial and error procedure and as yet, no theoretical reason is offered for taking the exponent in the inertia correction term to be 2/3. In forming the vapor blanket thickness correlation, all of the vapor properties have been evaluated at the mean film temperature. The raw data are presented in Table V.



$$K = q\mu_g / \left\{ \rho_g h_{fg}^* \sigma \left[ 1 + 9R^{1/2} (1 + \Delta)^2 \right] \right\}$$

Fig. 28. Correlation for vapor blanket thickness.

Table V Vapor Blanket Thickness Data for Horizontal  
Cylindrical Heaters at Earth Normal Gravity

| R<br>(mm)            | R'    | $q \times 10^{-5}$<br>$\left(\frac{W}{m^2}\right)$ | $\frac{q \mu_g}{g h \sigma} \times 10^4$ | $\frac{qR}{\mu_g h \sigma}$ | Observed Vapor Blanket<br>Thickness<br>(minimum - maximum) |                  |
|----------------------|-------|--|--|-----------------------------|--|------------------|
|                      |       |  |  |                             | $d_b$ (mm)   | $\Delta = d_b/R$ |
| Cyclohexanol         |       |  |  |                             |  |                  |
| 0.2667               | 0.144 | 0.85   | 10                                       | 1.25                        | 0.12-0.15  | 0.45-0.55        |
| 0.4128               | 0.216 | 1.16   | 64                                       | 3.42                        | 0.12-0.16  | 0.28-0.38        |
| ↓                    | ↓     | 1.70   | 104                                      | 5.55                        | 0.18-0.21  | 0.44-0.51        |
| ↓                    | ↓     | 2.12   | 130                                      | 6.86                        | 0.19-0.23  | 0.47-0.56        |
| ↓                    | 0.227 | 1.01   | 11.6                                     | 2.30                        | 0.17-0.24  | 0.40-0.58        |
| 0.5144               | 0.268 | 0.96   | 53                                       | 3.60                        | 0.13-0.17  | 0.26-0.34        |
| ↓                    | ↓     | 1.68   | 92                                       | 6.00                        | 0.21-0.26  | 0.41-0.51        |
| ↓                    | 0.278 | 0.67   | 7.8                                      | 1.90                        | 0.15-0.19  | 0.29-0.37        |
| ↓                    | 0.287 | 0.79   | 3.4                                      | 2.64                        | 0.17-0.22  | 0.33-0.43        |
| ↓                    | 0.294 | 0.79   | 1.8                                      | 2.54                        | 0.11-0.13  | 0.22-0.26        |
| ↓                    | ↓     | 1.02   | 2.4                                      | 3.30                        | 0.10-0.13  | 0.20-0.26        |
| 0.6540               | 0.343 | 0.84   | 46                                       | 3.86                        | 0.13-0.17  | 0.20-0.26        |
| ↓                    | ↓     | 0.92   | 50                                       | 4.25                        | 0.21-0.26  | 0.32-0.40        |
| Acetone <sup>†</sup> |       |  |  |                             |  |                  |
| 0.2667               | 0.161 | 1.04   | 0.33                                     | 1.44                        | 0.04-0.05  | 0.15-0.19        |
| 0.3200               | 0.203 | 1.30   | 0.45                                     | 2.27                        | 0.04-0.05  | 0.13-0.19        |
| 0.4128               | 0.257 | 1.19   | 0.42                                     | 2.63                        | 0.07-0.08  | 0.17-0.18        |
| 0.6440               | 0.409 | 1.01   | 0.35                                     | 3.55                        | 0.05-0.06  | 0.08-0.1         |
| 0.6540               | 0.458 | 0.88   | 0.31                                     | 3.10                        | 0.07-0.10  | 0.11-0.16        |
| 0.8250               | 0.514 | 1.17   | 0.41                                     | 5.16                        | 0.09-0.11  | 0.11-0.14        |
| 1.0280               | 0.650 | 1.11   | 0.39                                     | 6.20                        | 0.05-0.09  | 0.06-0.09        |

<sup>†</sup> Data reduced from observations of Sun as reported by Lienhard and Carter [1].

The group,  $qR\Delta/\mu_g h_{fg}^*$ , varied approximately from 0.2 to 2.5 in all the observations. Smaller values of this group usually occur near the left hand side of the figure. The data scatter represents minimum and maximum measurements of vapor blanket thickness. The accuracy of these measurements is  $\pm 10$  percent. The data seem to be correlated well by the solid line whose governing equation is:

$$\Delta = \frac{\left\{ 4.60 \left[ \frac{q\mu_g}{\rho_g h_{fg}^* \sigma} \right]^{1/3} \left[ \frac{1}{1 + 9R^2 (1 + \Delta)^2} \right]^{1/3} \right\} - 1}{\left[ 1 + \frac{qR\Delta}{\mu_g h_{fg}^*} \right]^{2/3}} \quad (88)$$

The constant, 4.60, in equation (88) would correspond to a value of 0.32 instead of 0.23 for the constant in front of equation (82).

#### Comparison of Wavelength Predictions with Experiment

Observed wavelengths for cyclohexanol boiling at a temperature of  $302.5^\circ\text{K}$ , corresponding to absolute pressure of 0.296 kPa, are displayed in Figure 29. The value of the liquid viscosity parameter,  $M$ , is close to 5. The theoretical prediction for the viscous and inviscid cases is also shown in the figure. The wire radius has been corrected to  $R_C$  to take into account the thickness of the vapor blanket surrounding it. The raw wavelength data are presented in Table VI.

Although wavelengths were measured for various heat fluxes, those displayed in Figure 29 correspond to the lowest heat flux. This is done to avoid the longer wavelengths which may, as we will see shortly, be favored at higher heat fluxes. The data show a wide variability, but the lowest points in the range of the data scatter do embrace the theoretical prediction which takes the dominant wavelength to be the "most susceptible" one. The inviscid predictions would have suggested wavelengths about 28 percent too short.

Figure 30 shows photographs of film boiling for two of the data points in Figure 29. Although there is slight phase difference across the length of the wire, the Taylor wave is very well developed. The bubble release pattern is good. The process is slower and viscosity seems to have dampened the small interfacial disturbances which may be observed in less viscous liquids.

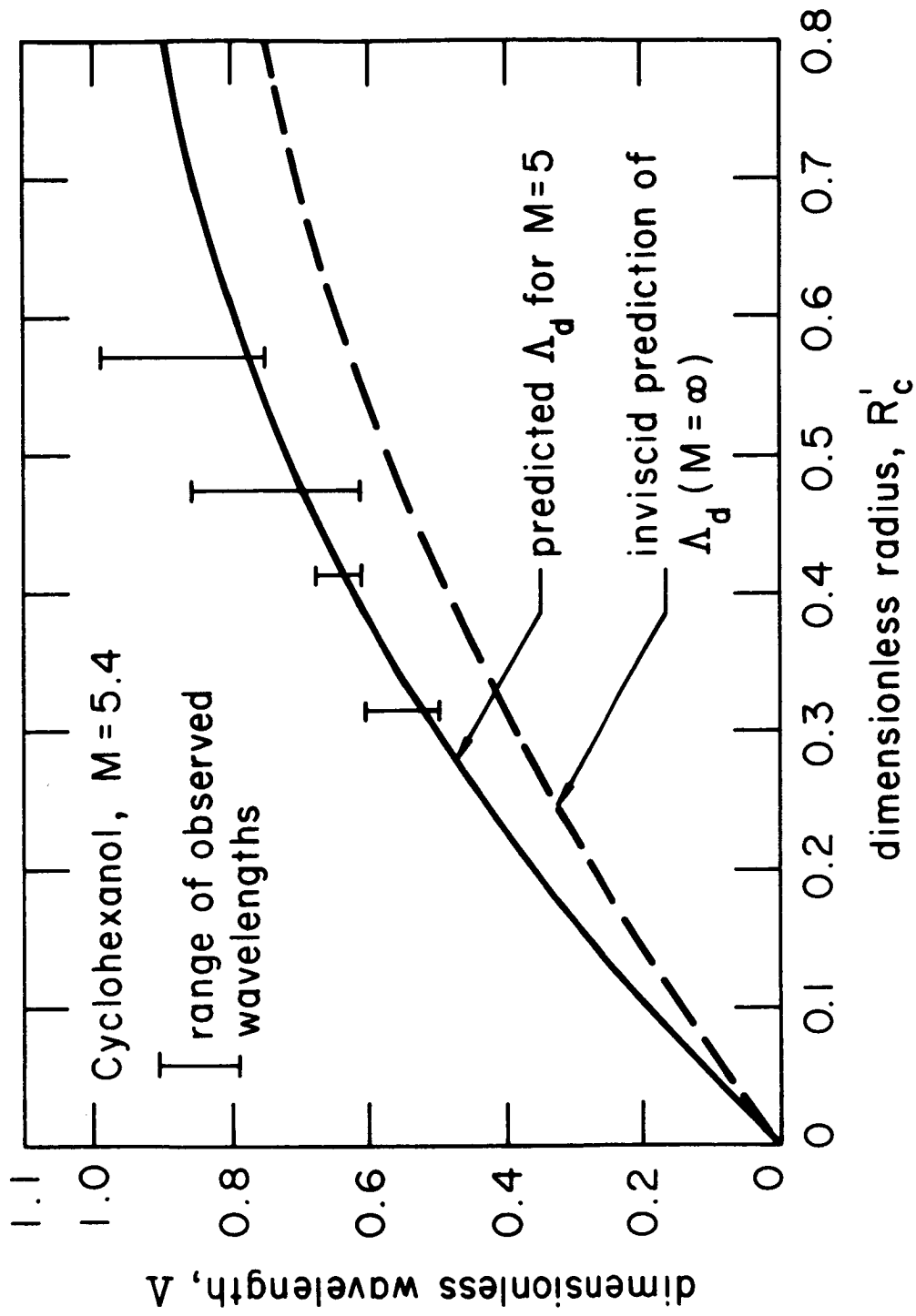
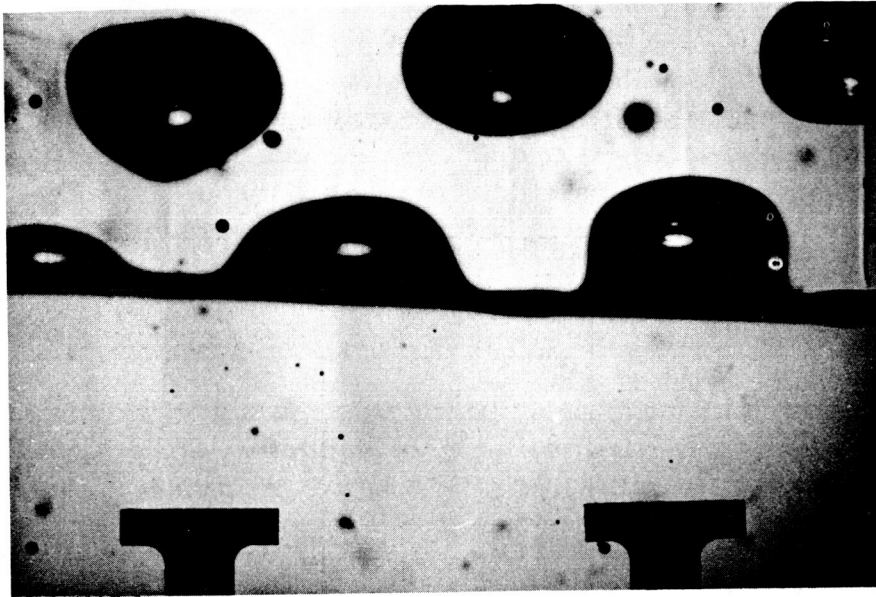


Fig. 29. Wavelengths on horizontal cylinders.

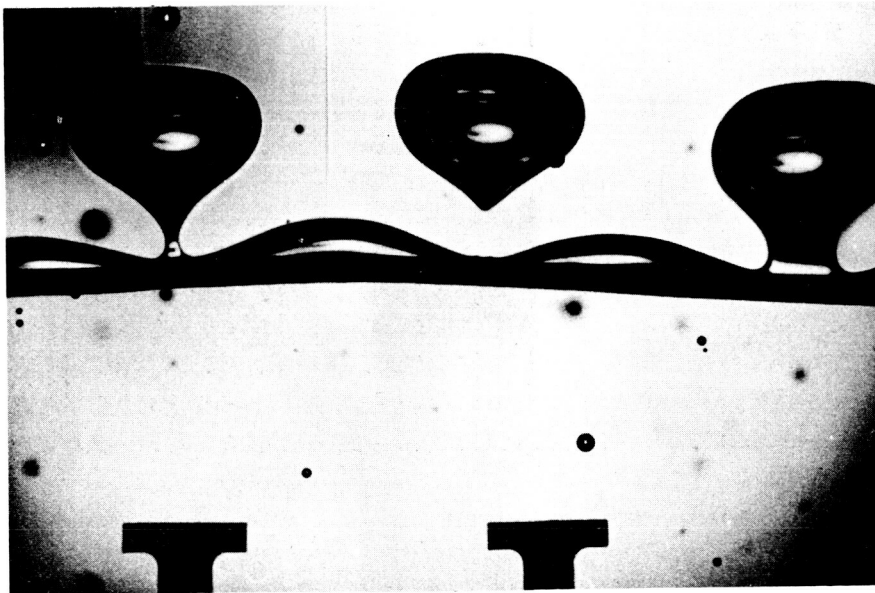
Table VI Wavelength Data of Cyclohexanol for Horizontal Cylindrical Heaters at Earth Normal Gravity

| R<br>(mm) | R'    | P<br>(kPa) | M   | $q \times 10^{-5}$<br>$\left(\frac{W}{m^2}\right)$ | Observed Wavelength<br>(minimum-maximum) |           |
|-----------|-------|------------|-----|--|--|-----------|
|           |       |            |     |  | $\lambda$ (mm)                           | $\Lambda$ |
| 0.4128    | 0.216 | 0.296      | 5.4 | 0.93   | 10.41-11.93                              | 0.50-0.58 |
| ↓         | ↓     |            |     | 0.96   | 11.93-13.97                              | 0.58-0.67 |
| 0.4128    | 0.216 | 0.296      | 5.4 | 1.16   | 11.18-15.75                              | 0.54-0.76 |
| 0.5144    | 0.268 | ↓          | ↓   | 0.74   | 12.70-14.22                              | 0.61-0.68 |
| ↓         | ↓     |            |     | 0.81   | 12.70-15.24                              | 0.61-0.73 |
| ↓         | ↓     |            |     | 0.82   | 14.22-16.76                              | 0.68-0.80 |
| ↓         | ↓     |            |     | 0.88   | 12.70-13.32                              | 0.61-0.64 |
| ↓         | ↓     |            |     | 0.95   | 13.46-16.00                              | 0.65-0.77 |
| 0.6540    | 0.343 | ↓          | ↓   | 1.00   | 14.98-17.53                              | 0.72-0.84 |
| ↓         | ↓     |            |     | 0.69   | 13.97-17.02                              | 0.67-0.82 |
| ↓         | ↓     |            |     | 0.75   | 12.70-17.78                              | 0.61-0.86 |
| ↓         | ↓     |            |     | 0.82   | 14.48-18.54                              | 6.70-0.89 |
| 0.8000    | 0.433 | ↓          | ↓   | 0.84   | 13.97-18.54                              | 0.67-0.89 |
| ↓         | ↓     |            |     | 0.50   | 15.49-20.57                              | 0.75-0.99 |
| 0.4128    | 0.224 | 1.06       | 16  | 0.69   | 20.06-21.08                              | 0.96-1.01 |
| ↓         | ↓     | ↓          | ↓   | 1.11   | 11.93-13.72                              | 0.59-0.68 |
| 0.5144    | 0.278 | ↓          | ↓   | 1.43   | 13.72-14.48                              | 0.68-0.72 |
| ↓         | ↓     |            |     | 0.67   | 13.46-16.76                              | 0.67-0.83 |
| 0.6540    | 0.354 | ↓          | ↓   | 0.62   | 13.46-16.76                              | 0.67-0.83 |
|           |       |            |     | 0.72   | 15.24-18.54                              | 0.75-0.92 |



$$R' = 0.23$$

$$R'_c = 0.33$$



$$R' = 0.34$$

$$R_c = 0.43$$

Fig. 30 Film Boiling of Cyclohexanol.  $M = 5.4$

Wavelength data for  $M = 16$  are plotted in Figure 31. Here the absolute pressure is 1.06 kPa and the saturation temperature is 329°K. In this case, observed wavelengths are higher and the data again show wide variability. This variability in data could be explained from the dispersion relation shown in Figure 25. Near the maximum frequency there is a wide region of near-neutral stability. Thus, for frequencies slightly less than the maximum, a large range of wavelengths close to  $\lambda_d$  is possible.

### Comparison of Wave Growth Rate Predictions with Experiment

Figures 32, 33 and 34 display plots of dimensionless wave amplitude versus time on semi-logarithmic coordinates in an increasing order of  $R'$ . In all cases, the liquid viscosity parameter,  $M$ , for cyclohexanol is 16. The data contained in each figure is for two to three randomly-picked, regularly-growing waves during 5 to 10 seconds of motion pictures of film boiling.

All the figures reveal that bubbles grow linearly during the first 12 percent or so of growth. This is the period during which we would expect our theoretical predictions of the frequency to be valid. Occasionally during the early growth of a bubble, an oscillation of the interface was observed. This was probably caused by the superposition of a disturbance left in the wake of a departing bubble. Such a disturbance is evident in the wake of the left-hand bubble in the bottom picture in Figure 30. Data corresponding to such disturbances have been identified with dotted symbols in the wave growth rate diagrams. One may also note that the bubble grows in height to about 75 or 80 percent of the wavelength before it leaves the interface.

Having measured the frequency corresponding to a linear growth rate and the dominant wavelength, we next wish to see how well the two compare with the predicted dispersion relation. In Figures 35, 36 and 37 we trace the dispersion relations for the three dimensionless corrected radii and  $M=16$ , and we display the experimental points on them. The relation between wavelength and frequency is borne out quite well in each case. It is clear that wavelengths with frequencies slightly less than the "most susceptible" frequency can easily occur. In Figure 38, observed frequencies are plotted as a function of  $R_c'$  along with the viscous and inviscid predictions. The data fall slightly below the viscous predictions, but the inviscid theory would have predicted still higher frequencies.

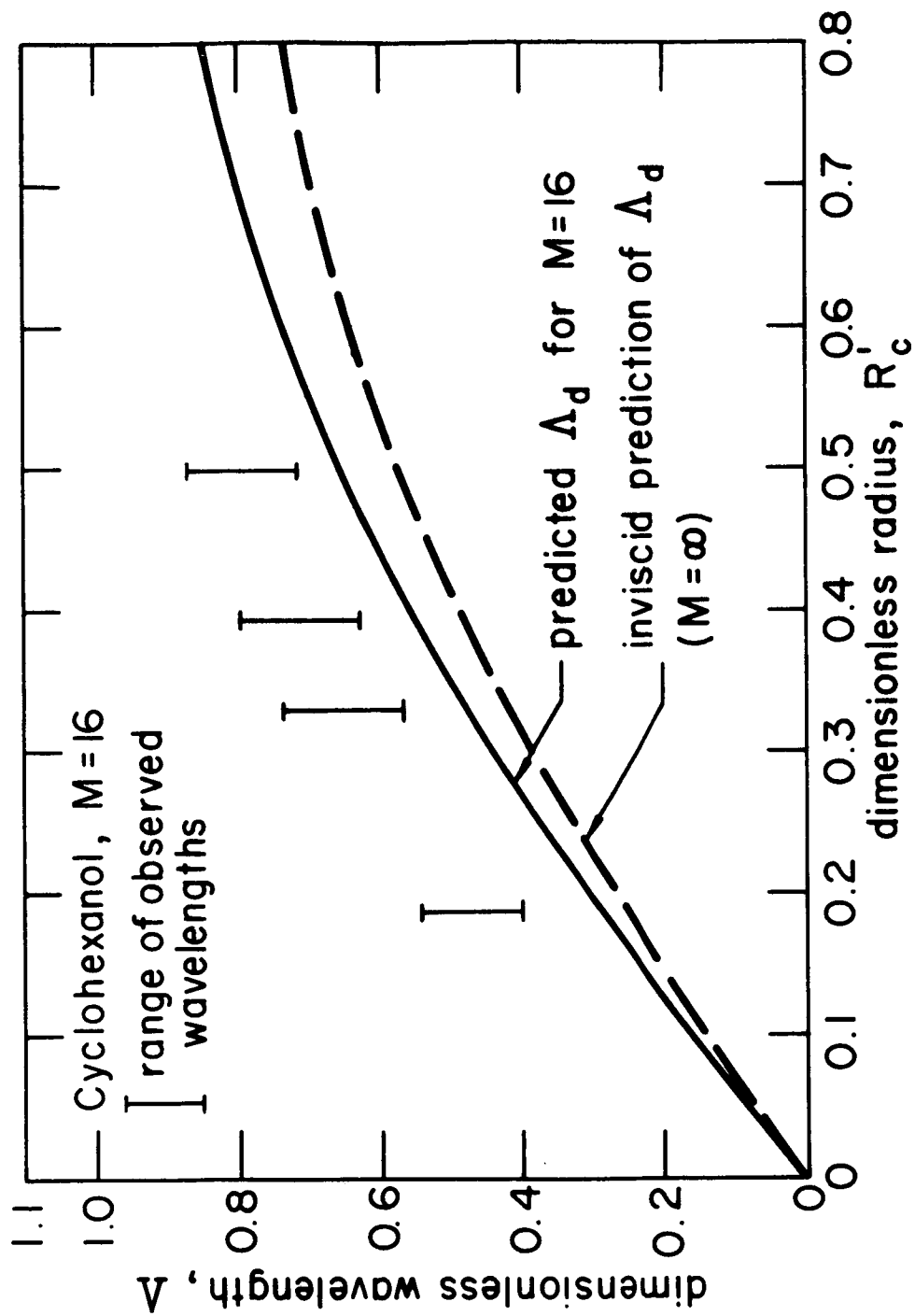


Fig. 31. Wavelengths on horizontal cylinders.

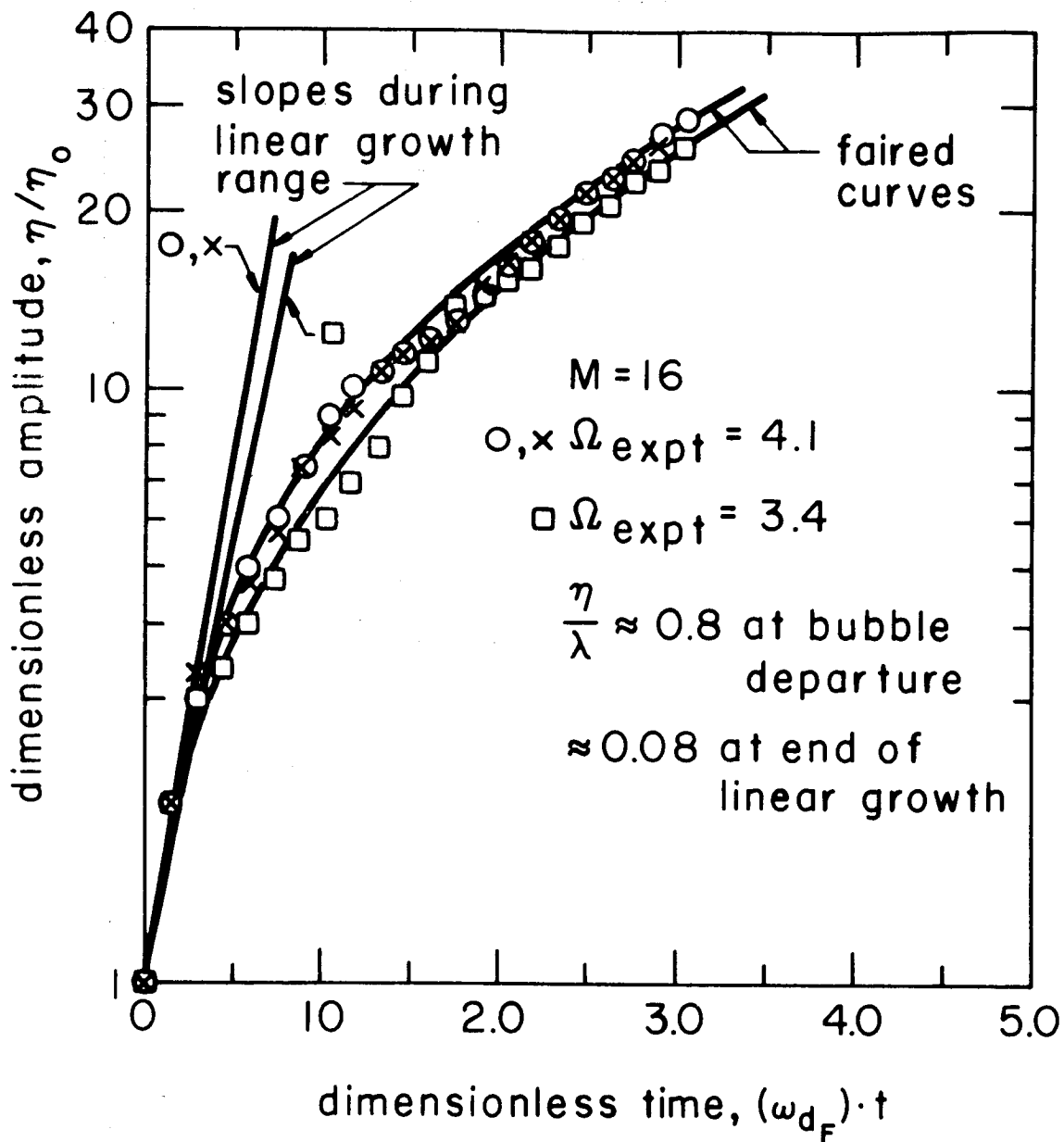


Fig. 32 Growth of waves on a 0.406 mm dia wire heater in cyclohexanol.  $P = 1.06$  kPa,  $q = 0.85 \times 10^5$  watt/meter<sup>2</sup>,  $f_b = 23$  bubble/sec.,  $\omega_{d_F} = 45.5$  hertz,  $R' = 0.11$ ,  $R'_c = 0.185$ .

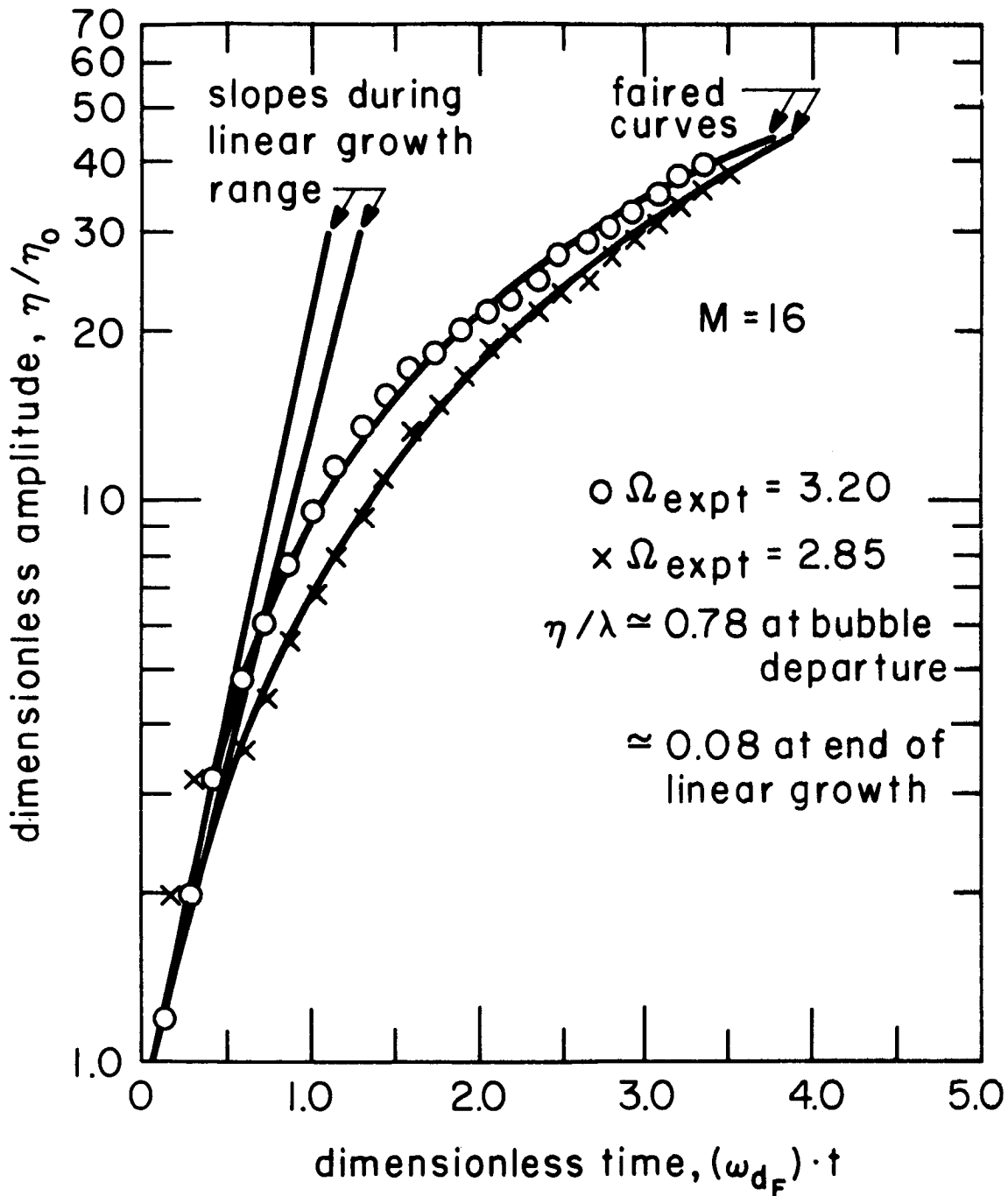


Fig. 33. Growth of waves on a 0.51mm dia wire heater in cyclohexanol.  $P=1.06$  k Pa,  $q=0.86 \times 10^5$  watt/meter<sup>2</sup>,  $f_b = 20$  bubble/sec,  $\omega_{dF} = 45.5$  hertz,  $R'_i = 0.14$ ,  $R'_c = 0.22$

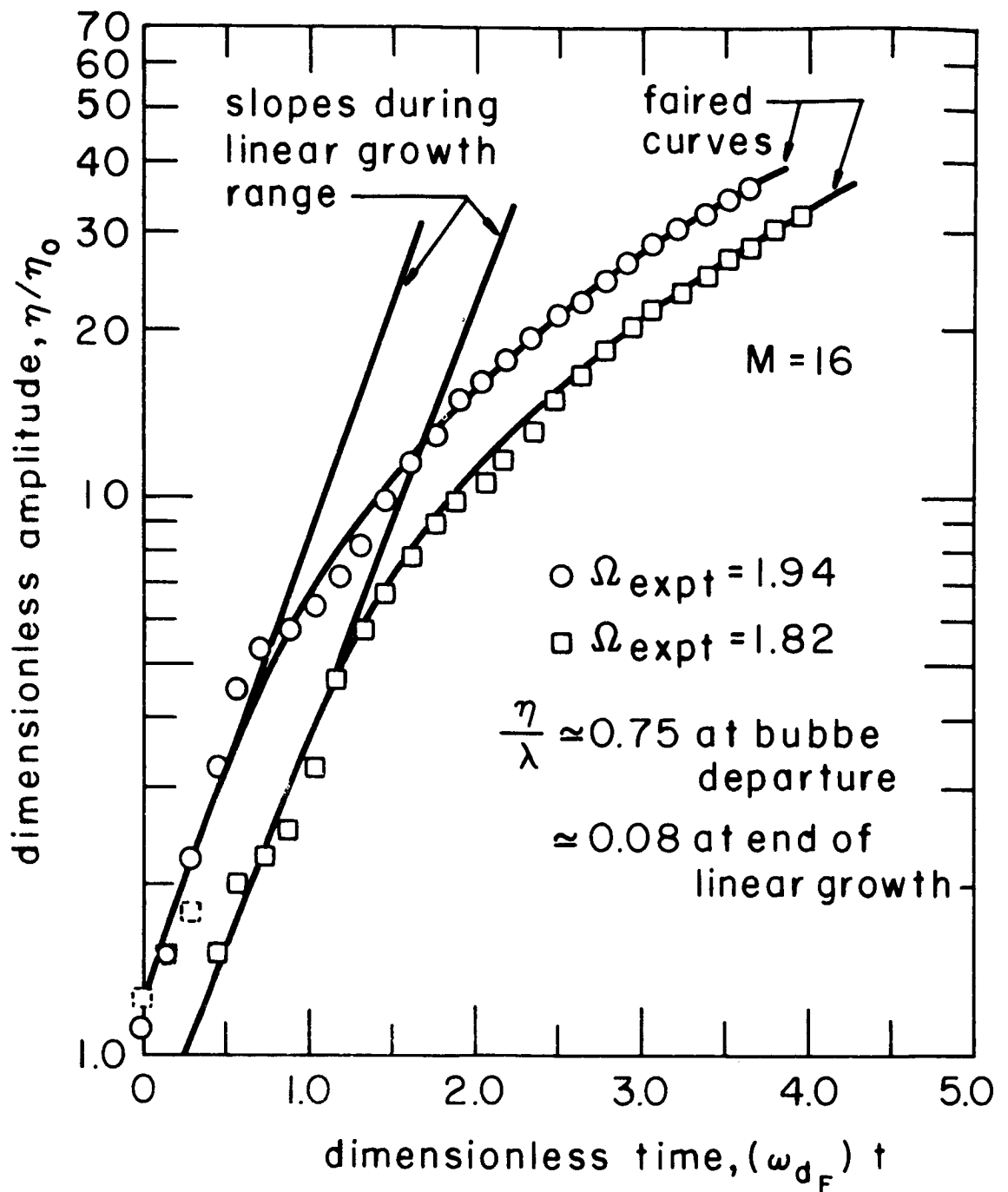


Fig.34 Growth of waves on a 0.825 mm dia wire heater in cyclohexanol.  $P = 1.06$  kPa,  $q = 1.01 \times 10^5$  watt/meter<sup>2</sup>,  $f_b = 18$  bubble/sec,  $\omega_{d_F} = 45.5$  hertz,  $R' = 0.22$ ,  $R'_C = 0.33$

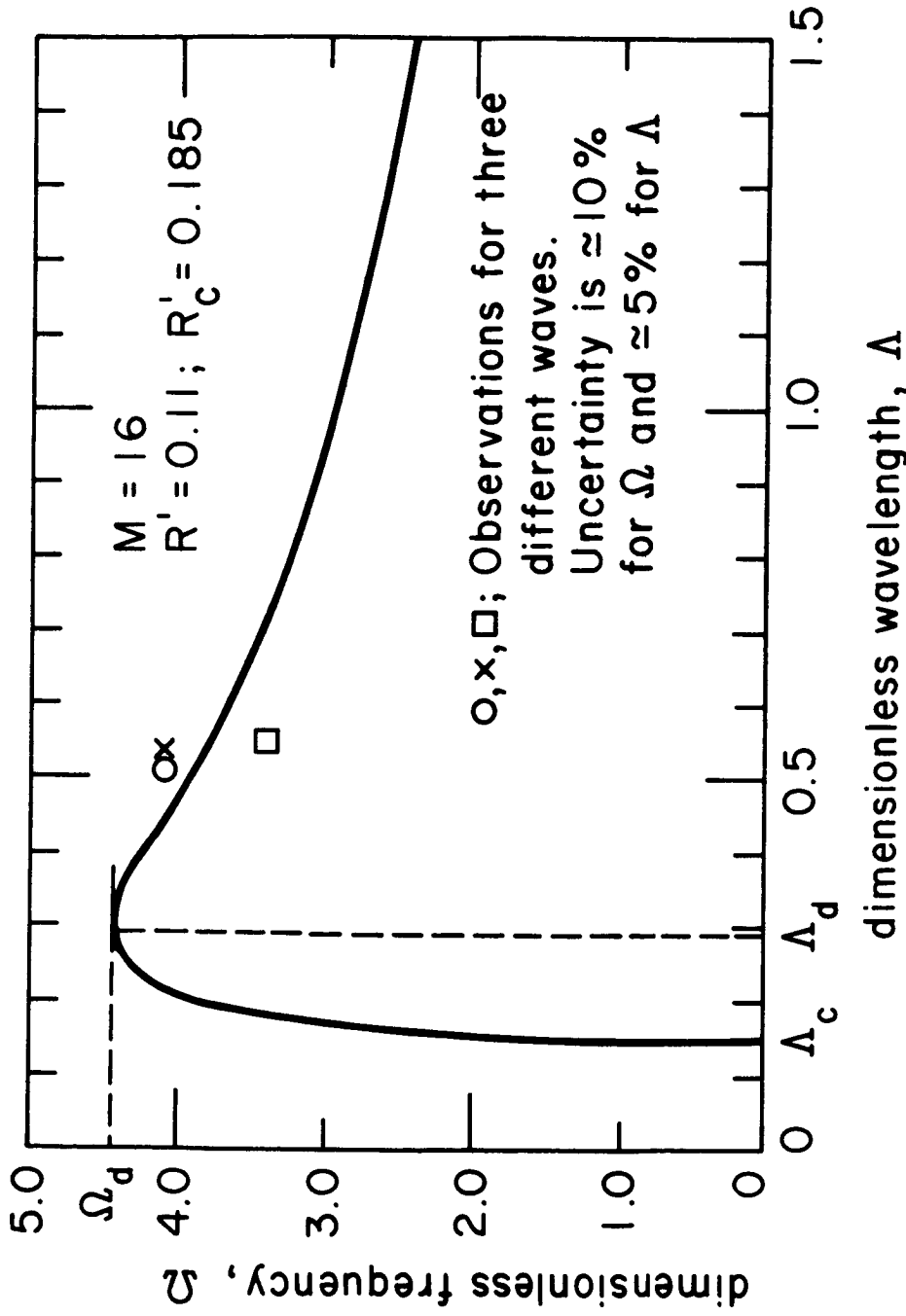


Fig. 35. Experimental verification of dispersion relation for cyclohexanol at 1.06 kPa.  $q = 0.85 \times 10^5$  watt/meter<sup>2</sup>.

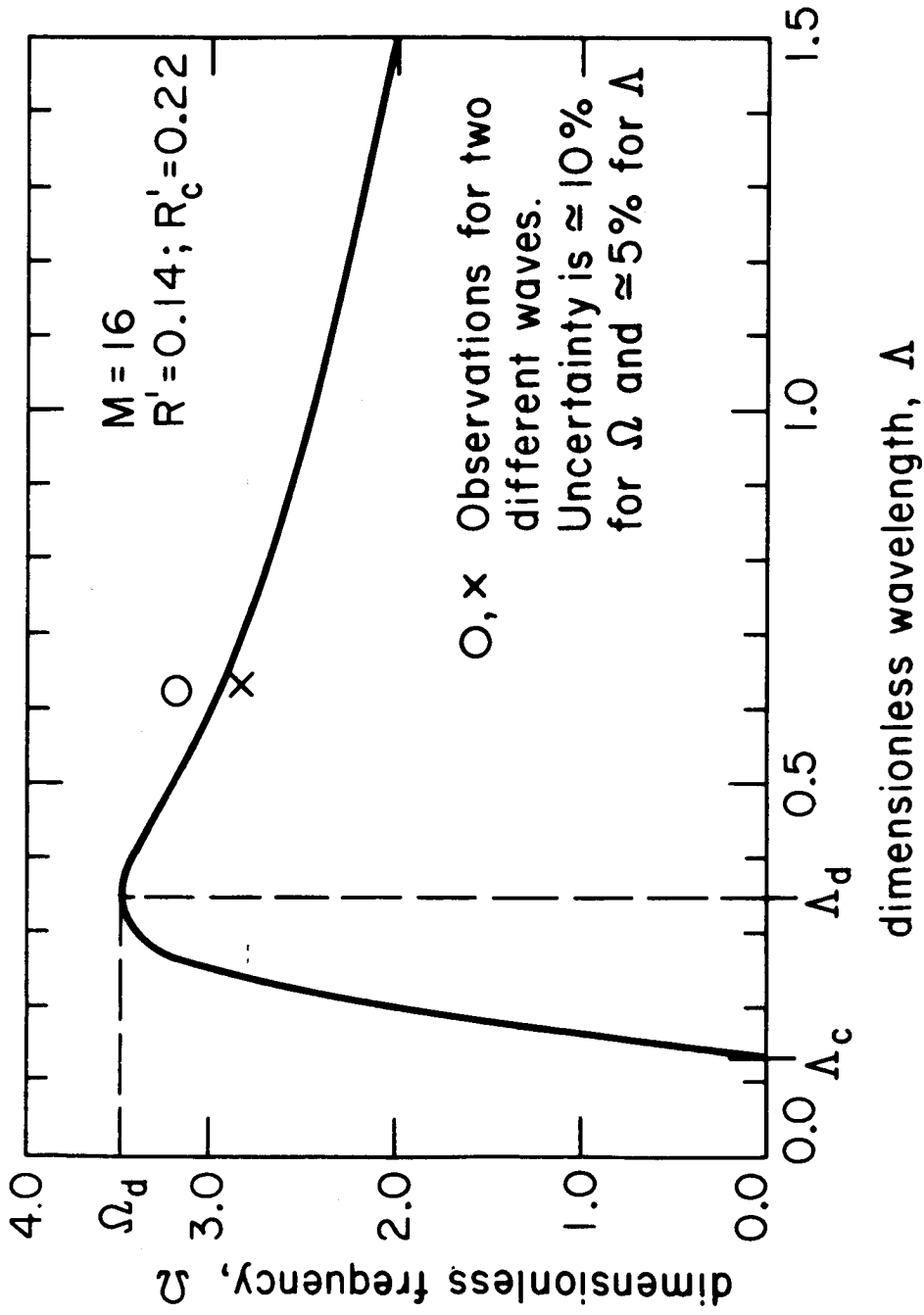


Fig. 36. Experimental verification of dispersion relation for cyclohexanol at 1.06 kPa.  
 $q = 0.86 \times 10^5$  watt/meter<sup>2</sup>.

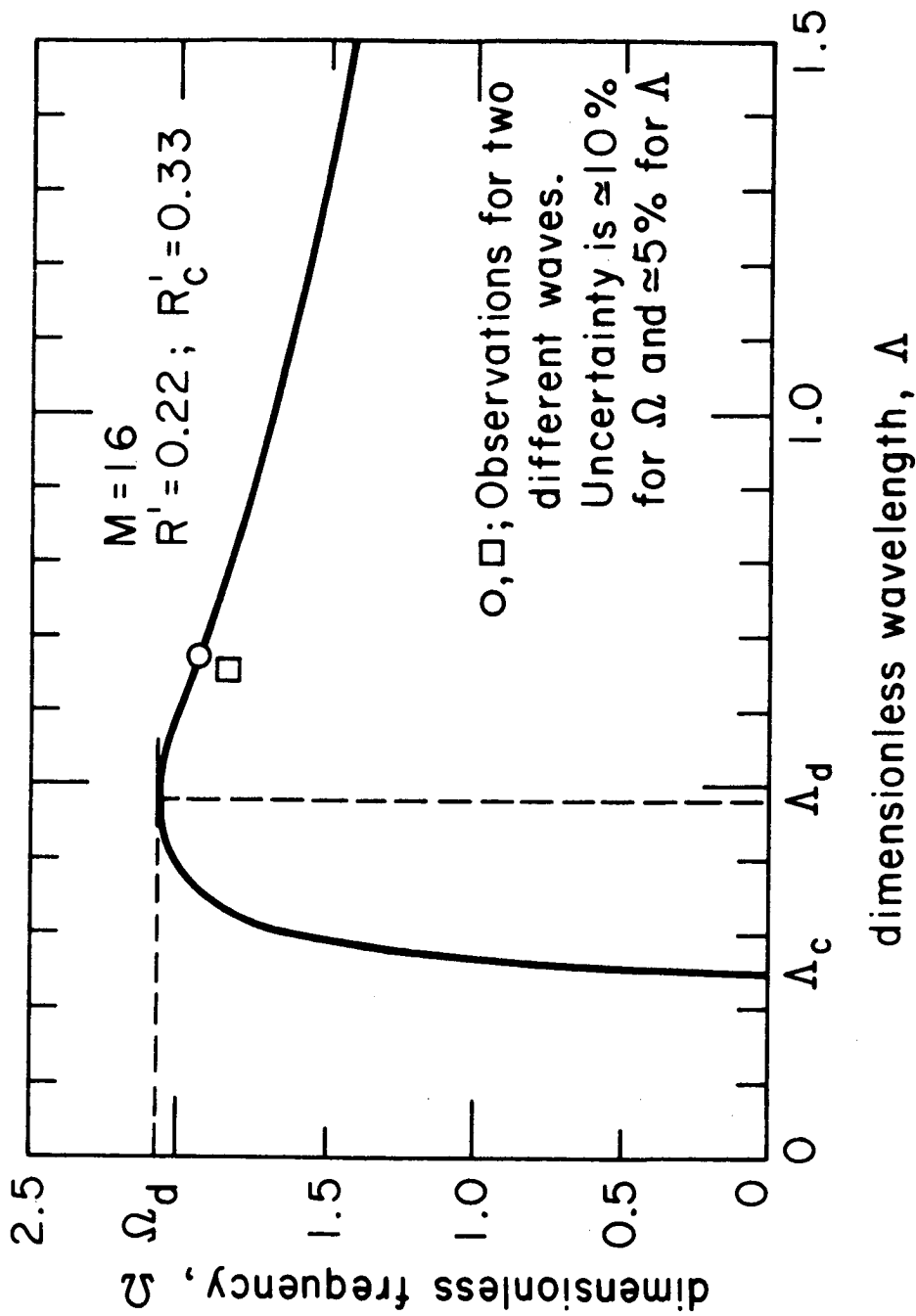


Fig. 37. Experimental verification of dispersion relation for cyclohexanol at 1.06 kPa.  $q=1.01 \times 10^5$  watt / meter<sup>2</sup>.

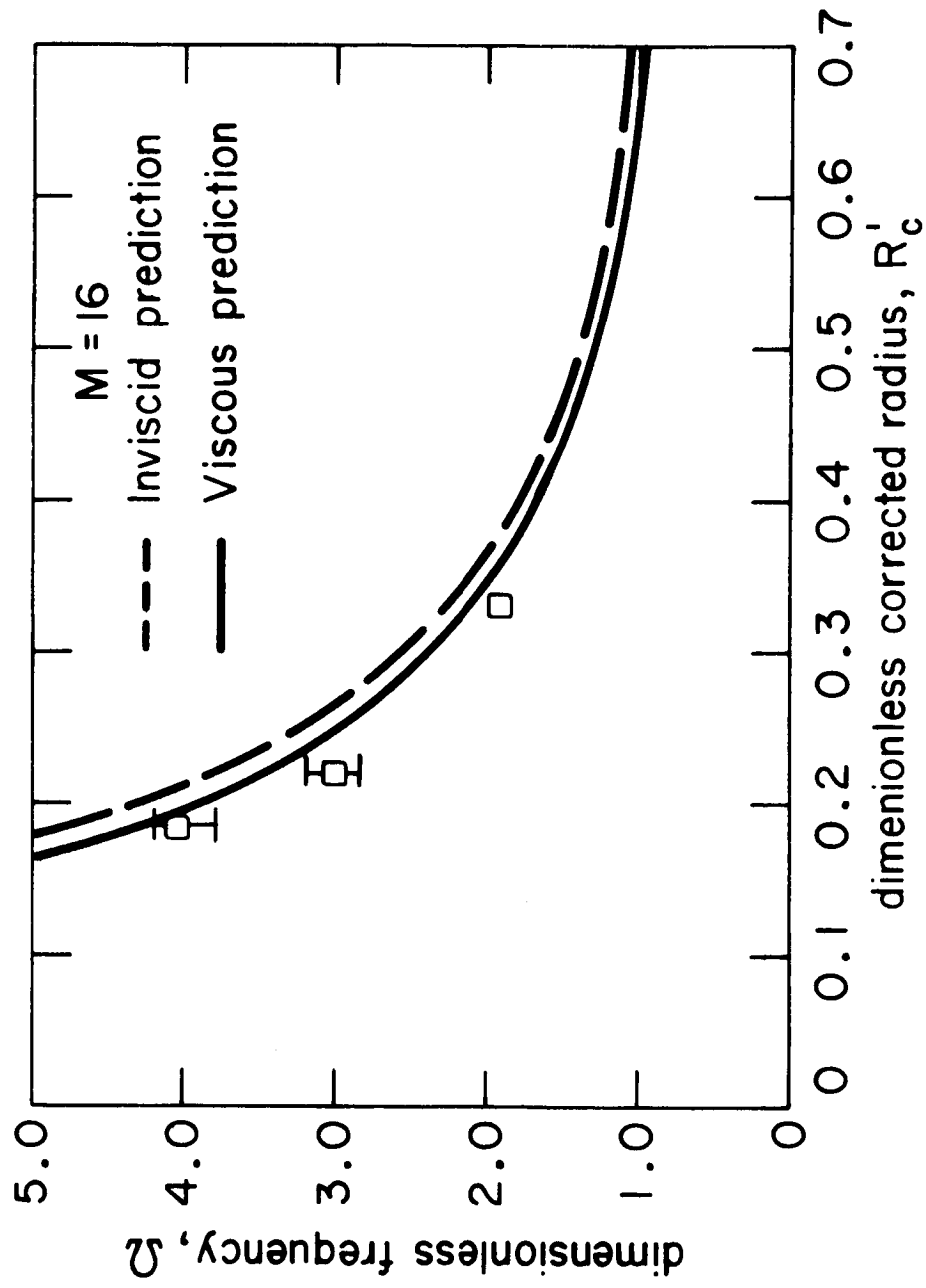


Fig. 38. Experimental observation of frequency of dominant wavelength on cylinders.

The inviscid theory shown in Fig. 38 can be obtained by reducing equations (78) and (79) to the Lienhard-Wong relations. This in turn can be done by letting  $M \rightarrow \infty$ . Figs. 23, 24, and 26 show that when  $M > 50$  viscous effects cease to be important. The results are

$$1 - K^2 + 1/2 R'_c{}^2 = \Omega^2/\Gamma K \quad (78a)$$

and at the maximum  $\Omega$ ,

$$2K = \Omega^2/\Gamma K^2 \quad (79a)$$

The desired relation between  $R'_c$  and  $\Omega$  for low viscosity fluids is obtained by eliminating  $K$  between these two equations.

Figures 39 through 42 show the growth of waves in low viscosity fluids. Figures 39 and 40 for  $M = 52$  and  $68$ , respectively, were obtained from the present motion pictures while Figs. 41 and 42, ( $M = 264$ ) were reduced from a movie by Lienhard and Wong [62]. The growth rates from these figures are compared with the inviscid theory in Fig. 43. The comparison is very satisfactory. That the growth rates do not exceed  $\Omega_{\max}$  is encouraging, since we have already seen that  $\Omega$  should be equal to or slightly less than its maximum value.

As a matter of interest, Fig. 42 shows an oscillatory behavior of the interface during early growth, probably due to superimposition of a disturbance caused by the preceding departing bubble. We have attempted to ignore the disturbance again and to draw the line through the average growth curve.

From the previous observations of growth rates, one may also note that the range of non-linear behavior starts earlier on smaller waves than it does on larger ones, and this effect seems to be enhanced by viscosity.

### Bubble Release Frequency

Up to this point we have dealt with a quantity,  $\omega$ , which we have called either the "wave growth rate" to designate its functional meaning, or the "wave frequency" to indicate its relationship to a stable travelling wave.

Now we wish to define an almost unrelated variable, the bubble release frequency,  $f_b$ . As we can see from Figs. 42, 43, 44, 49, 50, 51, and 52, the linear portion of wave growth is only a small fraction

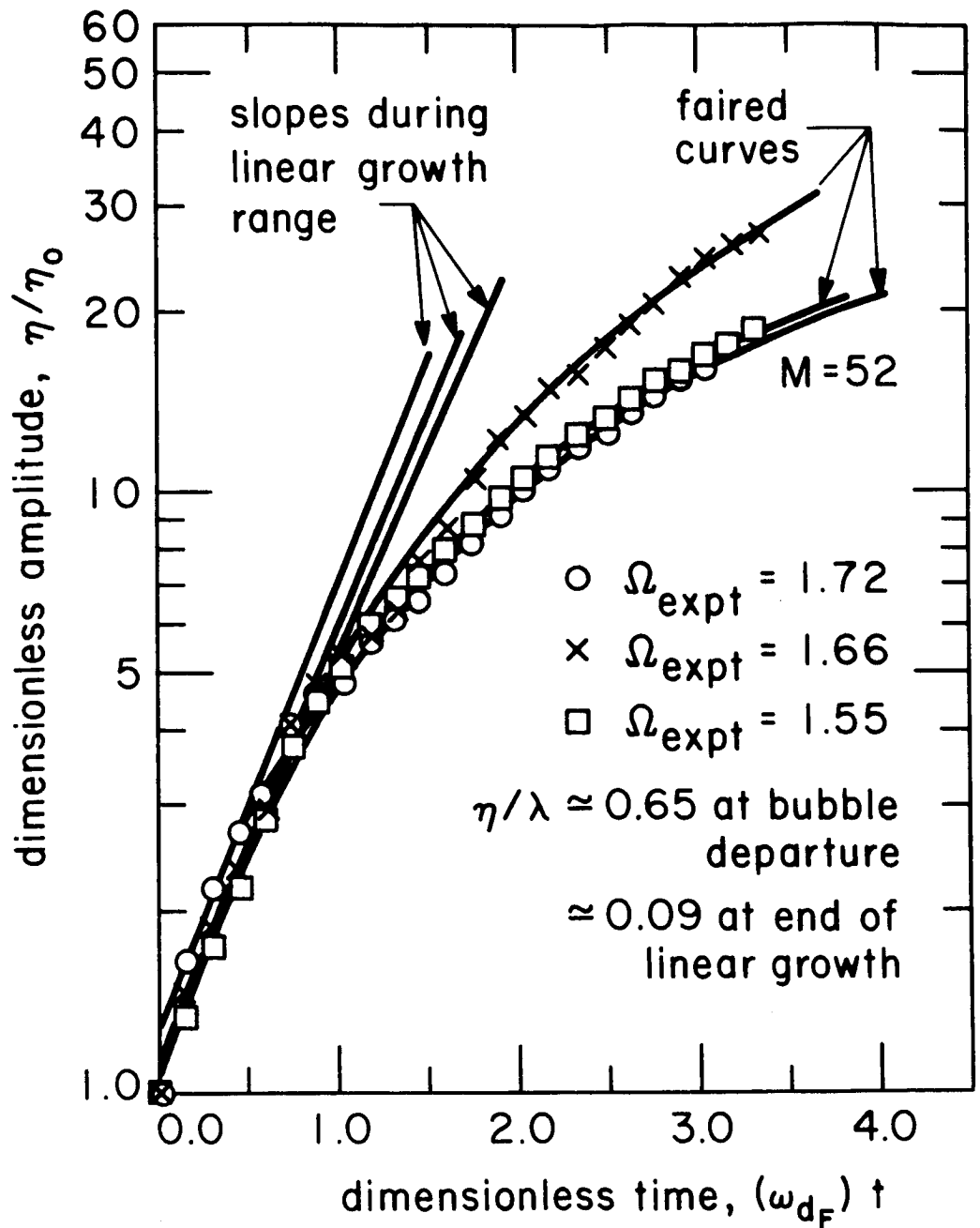


Fig. 39 Growth of waves on a 1.03 mm dia wire heater in cyclohexanol.  $P=4.9$  kPa,  $q=0.85 \times 10^5$  watt/meter<sup>2</sup>,  $f_b = 21$  bubble/sec,  $\omega_{dF} = 46.3$  hertz,  $R' = 0.29$ ,  $R'_c = 0.41$ .

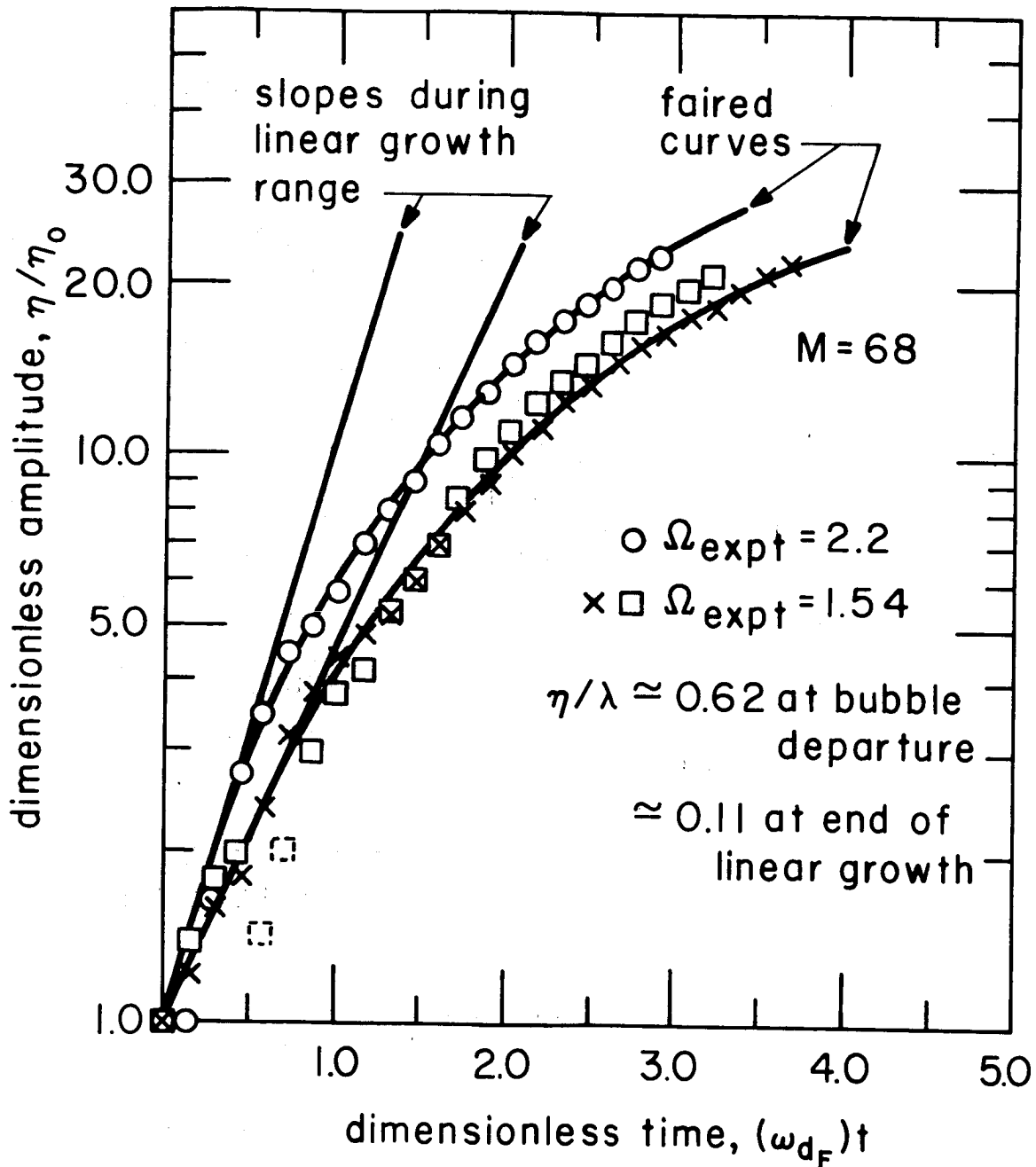


Fig. 40 Growth of waves on a 1.03 mm dia wire heater in cyclohexanol.  $P = 8.05$  k pa,  $q = 0.98 \times 10^5$  watt/meter<sup>2</sup>,  $f_b = 22$  bubble/sec,  $\omega_{dF} = 46.5$  hertz,  $R' = 0.295$ ,  $R'_C = 0.41$

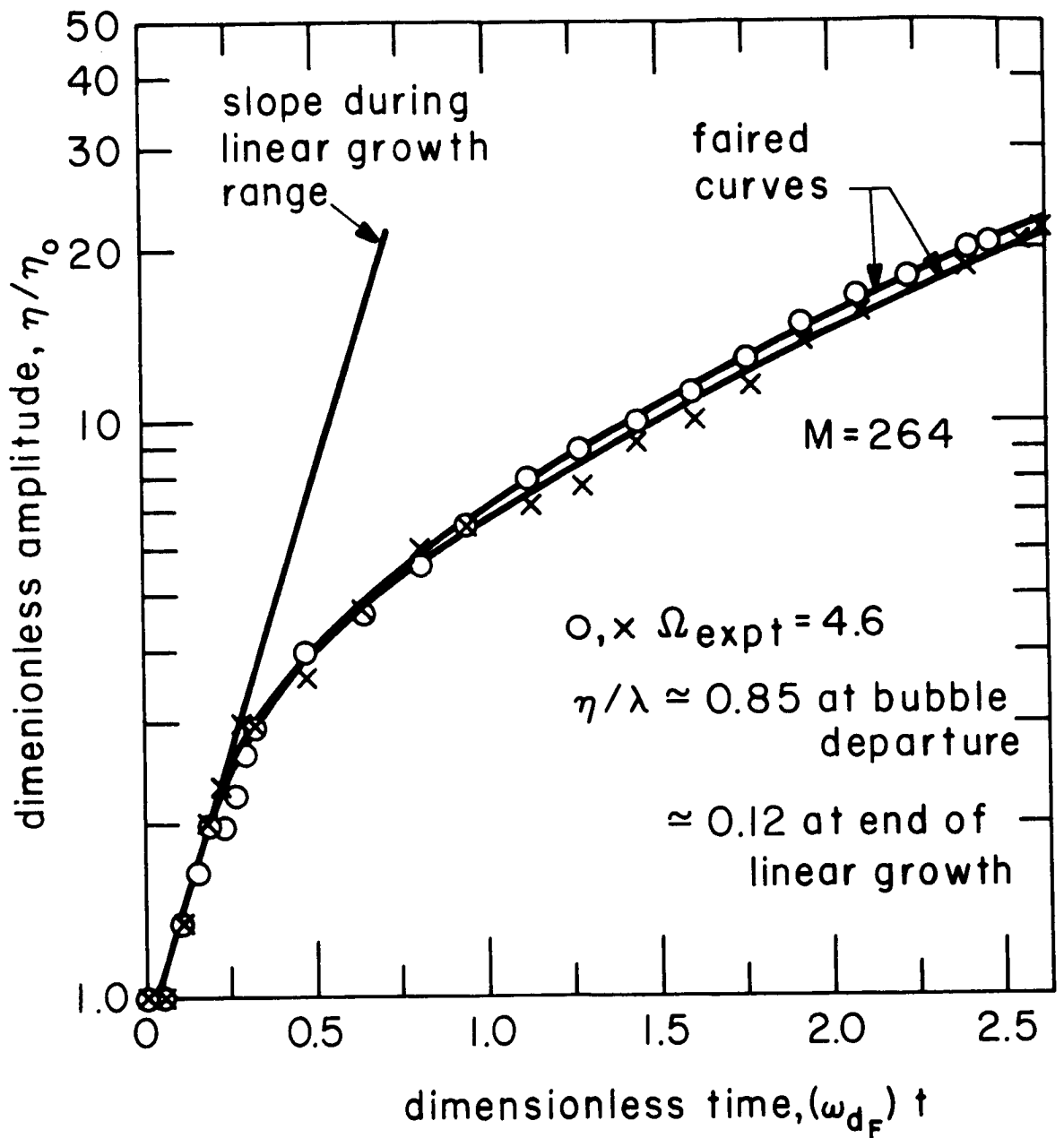


Fig. 41 Growth of waves on a 0.406 mm dia wire heater in Iso-propanol.  $P=98.5$  k pa,  $q=1.7 \times 10^5$  watt/meter<sup>2</sup>,  $f_b=31$  bubble/sec,  $\omega_{dF}=50.0$  hertz,  $R'_c=0.13$ ,  $R'_c=0.17$ .

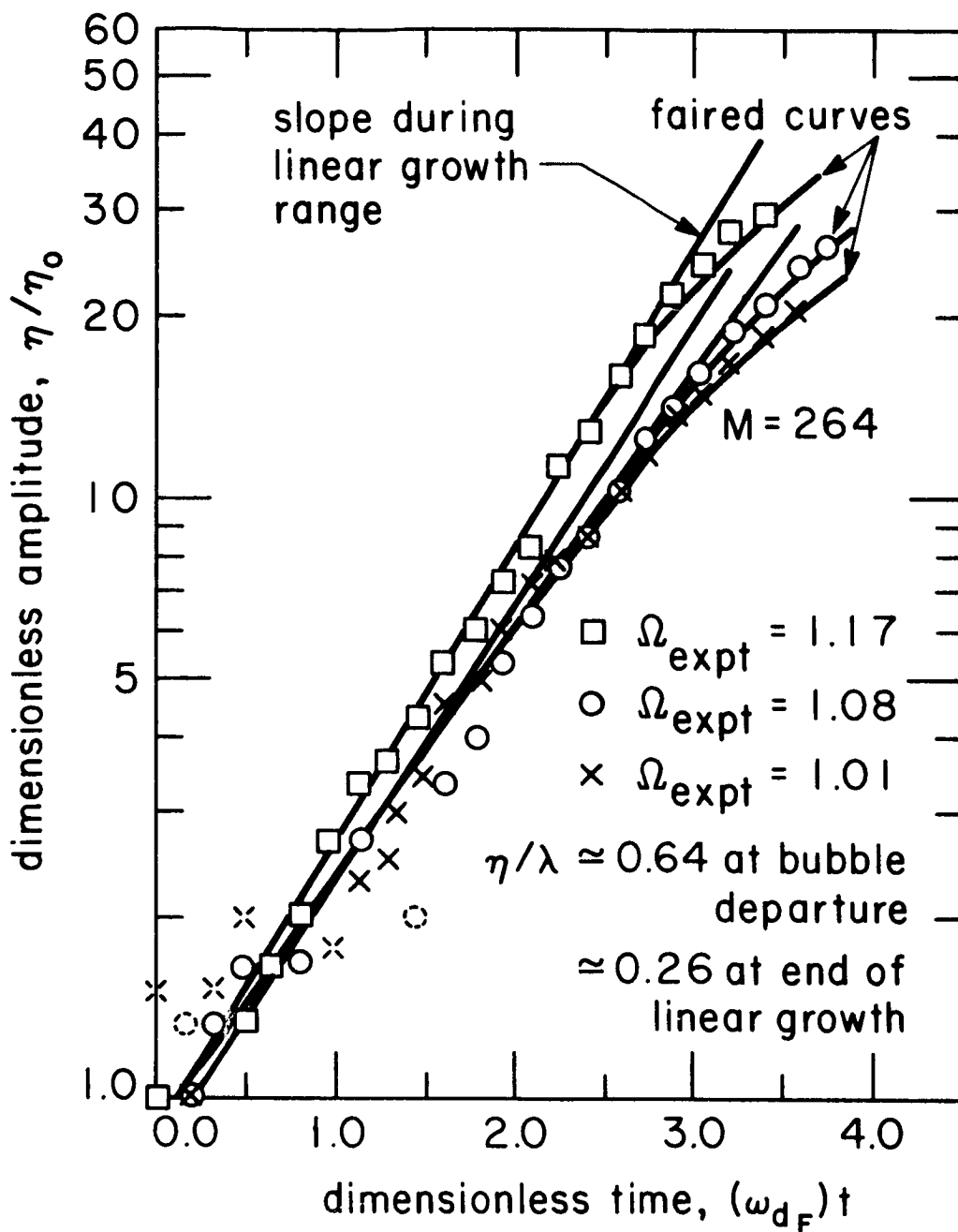


Fig. 42 Growth of waves on a 1.295 mm dia wire heater in cyclohexanol.  $P=98.5$  kPa,  $q=0.514 \times 10^5$  watt/meter<sup>2</sup>,  $f_b = 21$  bubble/sec,  $\omega_{dF} = 50.0$  hertz,  $R' = 0.425$ ,  $R'_c = 0.54$ .

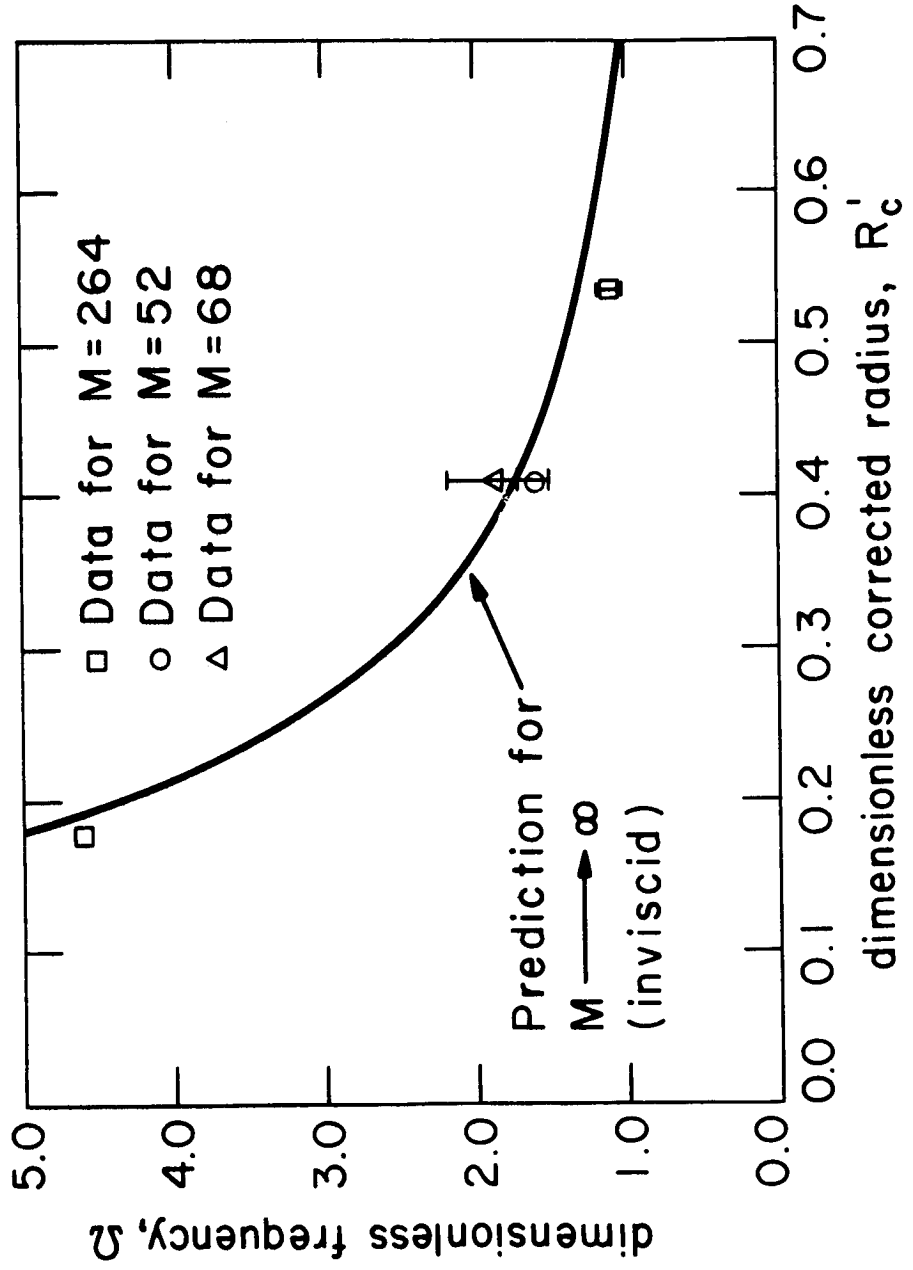


Fig. 4.3 Experimental observation of frequency of dominant wavelength on cylinders.

of the entire growth process. Furthermore, we haven't even attempted to record the recovery of the interface after the bubble leaves. It is clear that the periodicity of bubble growth is very weakly related to  $\omega$ . Indeed we have already noted that Berenson's major contribution to the hydrodynamic theory of  $q_{\min}$  was to reject Zuber's suggestion that  $f_b$  might be expressible as a simple function of  $\omega$ .

Our wave growth rate observations give us both  $f_b$  and  $\omega$  for different wavelengths and liquid viscosities. We plot this information in Fig. 44. The wavelength and the liquid viscosity seem to strongly affect the ratio of bubble release frequency and linear growth rate. This effect is introduced by the non-linear growth of the wave. The chained line shows the value of  $f_b/\omega$  assumed by Zuber in his prediction of the minimum heat flux on flat plates. The dotted line shows the value of  $f_b/\omega$  as proposed by Berenson. He fixed this ratio so that it was consistent with his observations of the minimum heat flux on flat plate heaters.

Clearly, there remains much to be learned about the general dependence of  $f_b$  on  $M$  and  $R'$ , and we have not even addressed the very important influence of varying heat flux on  $f_b$  in this study.

#### Effect of High Volume Fluxes on the Dominant Wavelength

In the previous sections we saw that wavelengths longer than the "most susceptible" wavelength occur frequently in real systems. These waves obeyed the dispersion relation well, but they did not assume exactly the maximum frequency. Since most of our experiments were conducted at very low pressures, we presume that the longer, slower-moving waves are preferred when large vapor volume fluxes are generated. This presumption is reasonable since we also find a stretching of the wavelength when the heat flux is substantially above  $q_{\min}$  (see, e.g. [63] and a discussion of these results in [5]).

It also turns out that we might well expect to find wavelengths shorter than  $\lambda_d$  under certain conditions in which the volume fluxes are very small. The film boiling studies of carbon dioxide near its critical point by Abadzić, Grigull, and Goldstein [64, 65] show the presence of nearly stationary waves with wavelengths close to the critical value. In this case the volume flux is quite low.

In Figure 45 we display dimensionless wavelength as a function of volume flux for horizontal cylinders. Wavelength data have been obtained both at low pressures and high heat fluxes and are given in Table VII. The coordinates have been reduced to dimensionless inviscid

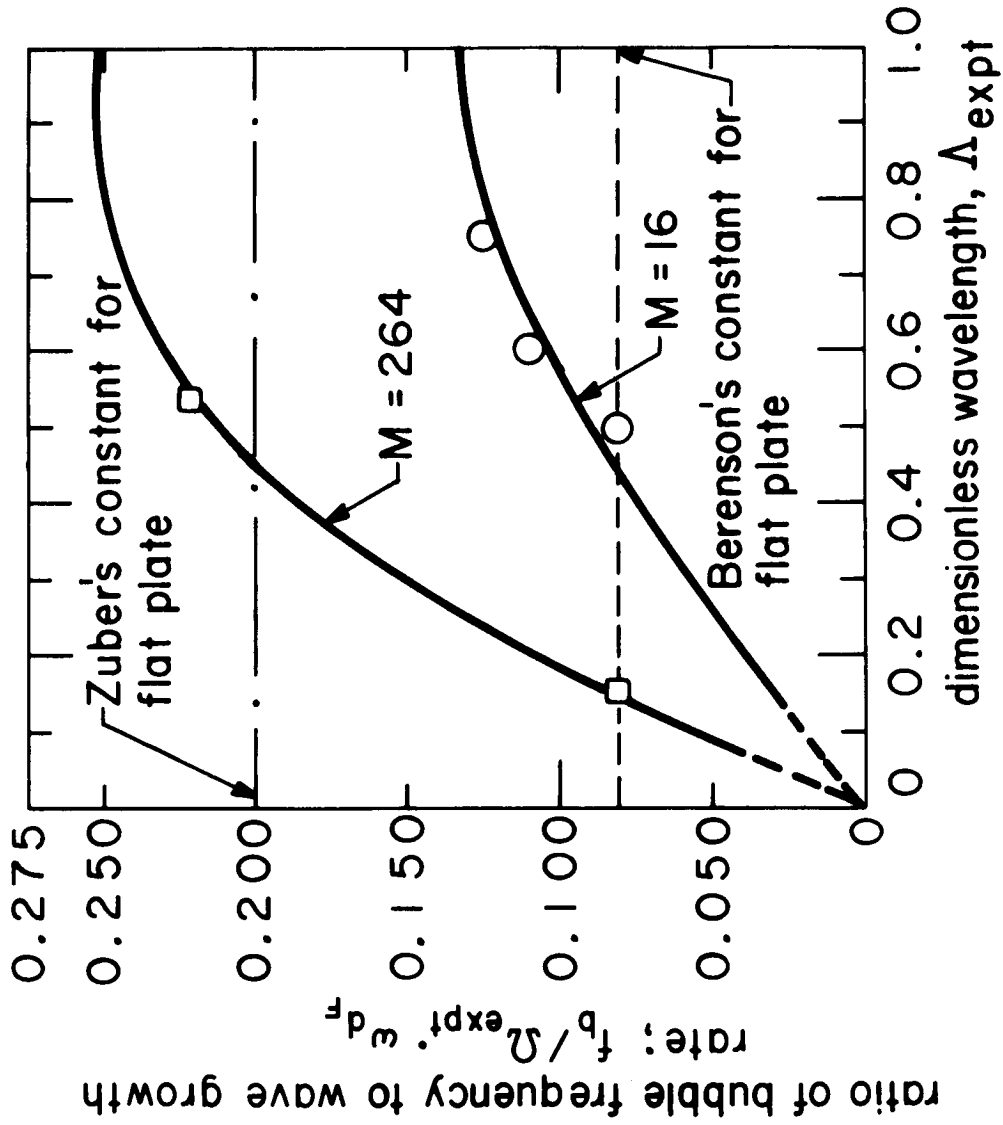


Fig. 4.4. Effect of viscosity and wavelength on bubble departure frequency.

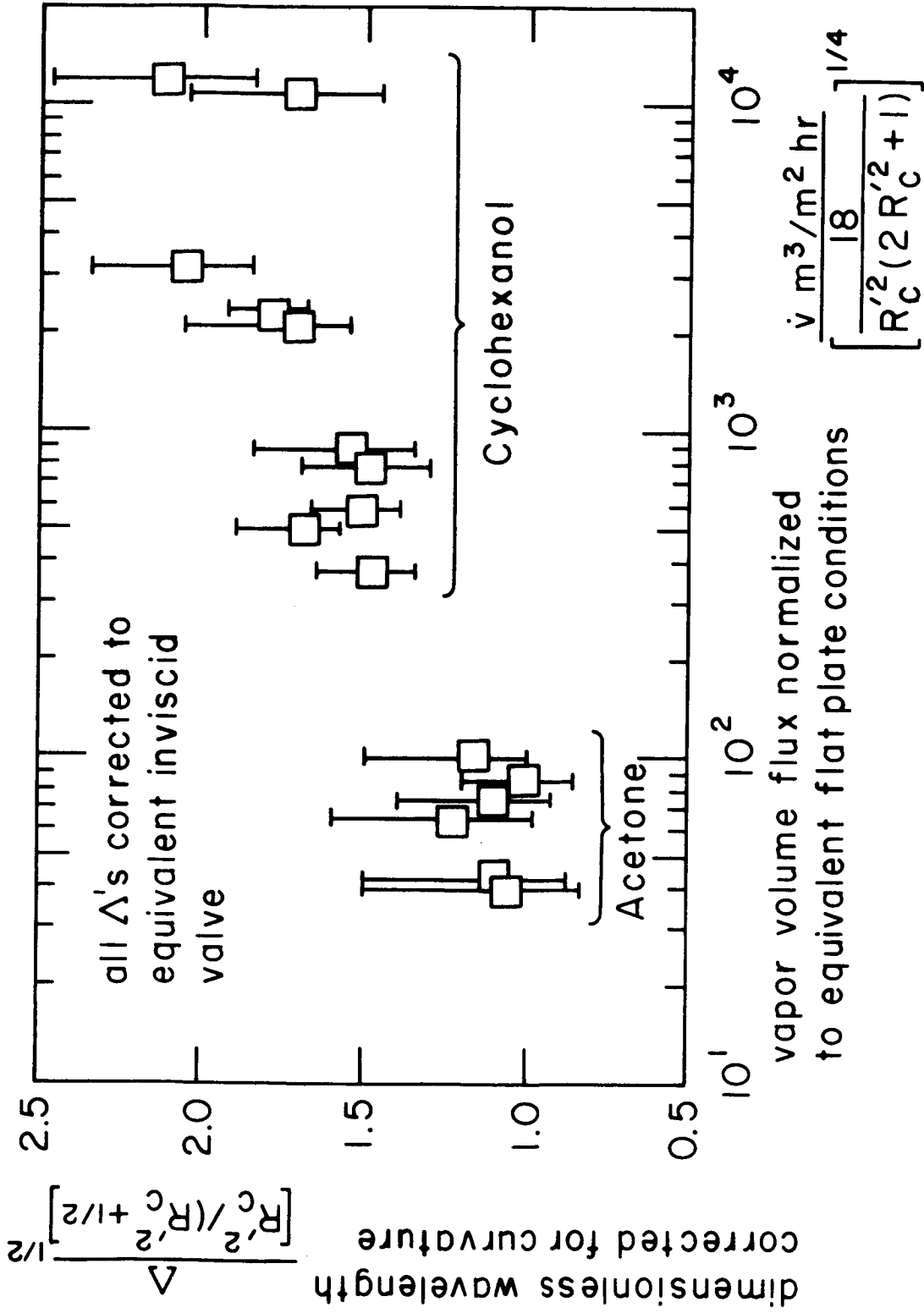


Fig. 45 Effect of volume flux on the dimensionless dominant wavelength.

Table VII Data Used to Obtain Effect of Large Vapor  
Volume Fluxes on Dominant Wavelength

| R<br>(mm)            | R'    | R' <sub>c</sub> | M   | $\dot{v} \times 10^{-2}$<br>(m <sup>3</sup> /m <sup>2</sup> hr) | Observed Wavelength<br>(minimum - maximum) |           |
|----------------------|-------|-----------------|-----|---|--|-----------|
|                      |       |                 |     |   | $\lambda$ (mm)                             | $\Lambda$ |
| Cyclohexanol         |       |                 |     |   |  |           |
| 0.203                | 0.11  | 0.18            | 16  | 21  | 8.89-10.67                                 | 0.44-0.53 |
| ↓                    | ↑     | ↑               |     | 31  | 10.67-13.46                                | 0.53-0.67 |
| 0.514                | 0.276 | 0.36            |     | 104   | 16.00-21.34                                | 0.80-1.06 |
| ↓                    | ↑     | ↑               | ↑   | 118   | 18.80-25.40                                | 0.94-1.27 |
|                      | 0.280 | 0.35            | 52  | 3.7   | 12.70-15.20                                | 0.67-0.80 |
|                      | ↓     | ↓               | ↑   | 5.8   | 14.73-17.27                                | 0.77-0.91 |
|                      | ↑     | 0.38            | 16  | 23  | 18.03-19.56                                | 0.90-0.97 |
|                      | ↑     | 0.39            | 35  | 7.8   | 13.97-19.56                                | 0.71-1.00 |
|                      | 0.290 | 0.41            | ↑   | 8.8   | 13.97-16.76                                | 0.73-0.88 |
| ↓                    | 0.295 | 0.42            | 52  | 5.0   | 13.97-17.02                                | 0.73-0.89 |
| Acetone <sup>+</sup> |       |                 |     |   |  |           |
| 0.152                | 0.101 | 0.13            | 599 | 0.40  | 2.69- 4.83                                 | 0.16-0.28 |
| 0.267                | 0.161 | 0.19            |     | 0.42  | 3.88- 6.78                                 | 0.22-0.39 |
| 0.413                | 0.257 | 0.30            |     | 0.62  | 6.56-11.12                                 | 0.38-0.64 |
| 0.654                | 0.458 | 0.60            |     | 0.70  | 9.40-14.24                                 | 0.54-0.82 |
| 0.826                | 0.514 | 0.59            |     | 0.97  | 10.82-15.29                                | 0.63-0.89 |
| 1.028                | 0.650 | 0.70            | ↑   | 0.82  | 12.44-18.41                                | 0.72-1.07 |

<sup>+</sup> Data reduced from observations of Sun as reported by Lienhard and Carter [1].

flat plate values so that the data obtained at different situations can be compared. The vapor volume flux has been normalized with Lienhard and Wong's correction for the effect of radius of curvature of the cylindrical heater on the minimum heat flux. Similarly the wavelength data have been normalized with their expression representing the effect of heater radius on the wavelength.

There is a definite increase in the dominant wavelength with increasing vapor volume flux. Photographs of the film boiling process at different heat fluxes are shown in Figure 46. The longer wavelengths at the larger volume flux in the bottom picture can easily be distinguished from the shorter wavelength in the top picture.

### On Predicting the Minimum Heat Flux

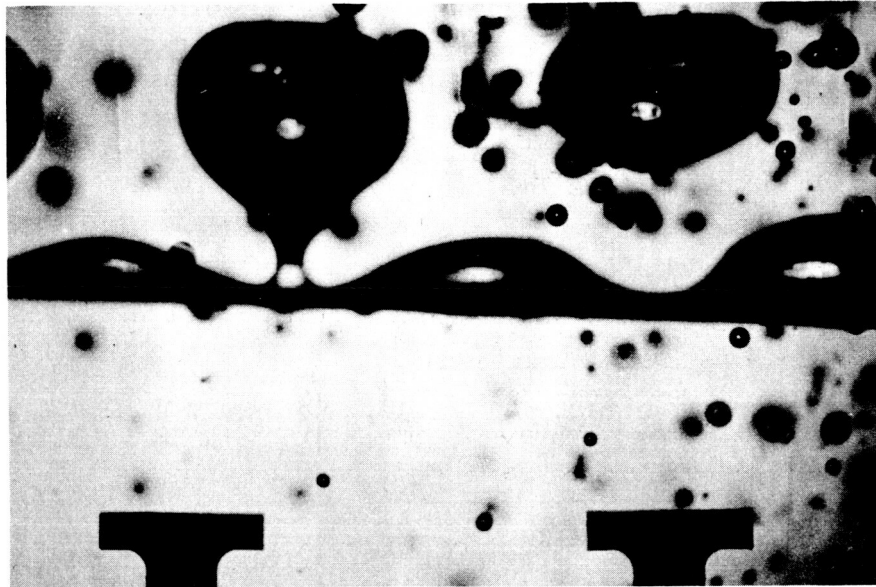
We should now like to refer back to pages 7 and 8 in which we discussed Zuber's prediction of  $q_{\min}$  for a horizontal flat plate. Equation (6) was the general starting point for any  $q_{\min}$  prediction.

For the horizontal flat plate, we can accept everything that Zuber and Berenson did up to equation (7). Using the notation of the present Chapter in which  $\omega$  is a real quantity--the exponential growth rate, we have:

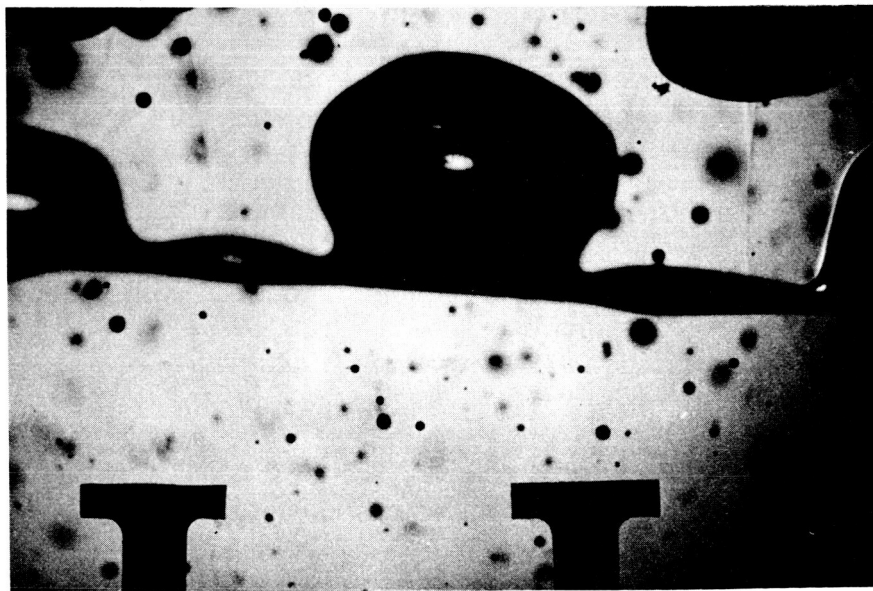
$$q_{\min} = \text{constant } \rho_f h_{fg} \lambda_{dF} \omega_{\max} \quad (7a)$$

There are two difficulties with this result. The first is that  $\lambda_{dF}$  will increase if the fluid is very viscous. The second is that it is based on the presumption that the minimum  $f_b$  is proportional to  $\omega_{\max}$ . The previous section on bubble frequency cast some doubts on this idea and it showed that viscosity tends to slow  $\omega$ . Thus  $q_{\min}$  could either increase or decrease with viscosity. The same sort of difficulties are inherent in predictions of  $q_{\min}$  for cylinders.

Furthermore, various previous authors [66], [5] have pointed out that many physical variables, such as material of the wire, the end mountings, the material and size of the wireholders, and the way the end mountings are attached to the wire, can seriously affect the observations of minimum heat flux. Data obtained under different conditions have been found to differ with each other by as much as 100 to 200 percent. With so many variables affecting the true location of the minimum heat flux, an elaborate experimental program would be needed to provide reproducible and meaningful results. Therefore, we did not make any special effort toward measuring the minimum heat



$$R' = 0.23, R'_c = 0.32, \dot{v} = 4.95 \times 10^4 \text{ m}^3/\text{m}^2 \text{ hr}$$



$$R' = 0.23, R'_c = 0.35, \dot{v} = 8.4 \times 10^4 \text{ m}^3/\text{m}^2 \text{ hr}$$

Fig. 46 Stretching of wavelengths at higher vapor volume fluxes.

flux in the present work.

We thus leave the question of predicting  $q_{\min}$  as an open one. At this time it is very difficult to say quantitatively what the net effect of viscosity is on the minimum heat flux.

### Conclusions

- 1.) An analysis of the Taylor stability of both plane and cylindrical interfaces has been completed.
- 2.) An increase of wavelength with the liquid viscosity has been measured and found to compare well with the theoretical predictions.
- 3.) The wavelength and frequency measurements are faithful to the predicted dispersion relation.
- 4.) A successful correlation for the vapor blanket thickness around a cylindrical heater has been established.
- 5.) The bubble release frequency seems to depend upon both the dominant wavelength and the liquid viscosity.
- 6.) The generation of large volume fluxes can cause the wavelengths in film boiling to considerably exceed the "most susceptible" wavelength. An experimental correlation of wavelength with volume flux is presented.
- 7.) The minimum heat flux has been shown to be sensitive to liquid viscosity. The nature of the influence of viscosity on  $q_{\min}$  is not presently known, however.

## V. THE PEAK HEAT FLUX IN VISCOUS LIQUIDS

The peak heat flux on any heater configuration is given in equation (3) as

$$q_{\max} = \rho_g h_{fg} (A_j/A_h) U_H$$

we shall for the moment restrict our attention to the flat plate configuration and ask how  $A_j/A_h$  and  $U_H$  change in viscous liquids.

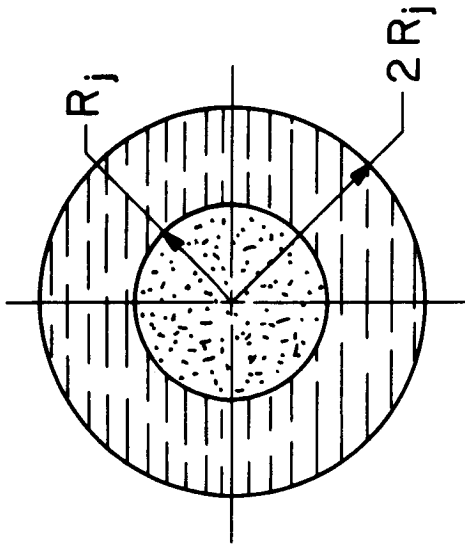
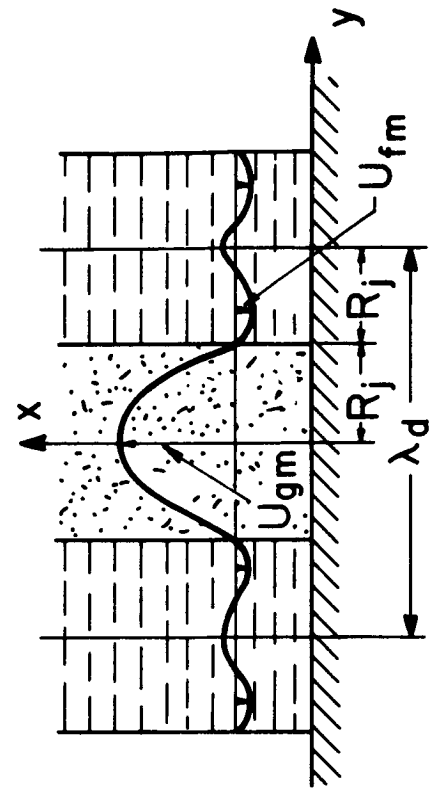
We saw in the last Chapter that the wavelength will stretch with increasing viscosity. However, the ratio  $(A_j/A_h)_F$  is independent of  $\lambda_d$  and will equal  $\pi/16$  for any flat plate. The ratio  $A_j/A_h$  may vary with  $\lambda_d$  in certain other configurations but that is a matter we shall defer for the moment.

The important variable in the problem, and the more difficult to predict, is  $U_H$ . We shall attempt first to estimate  $U_H$  for a jet leaving a flat plate.

### The Maximum Stable Vapor Velocity in a Jet

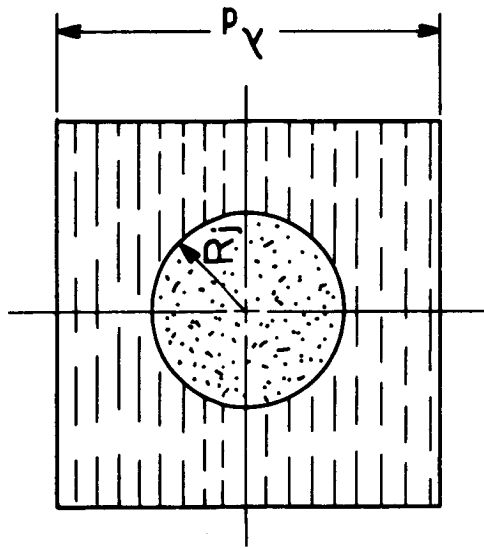
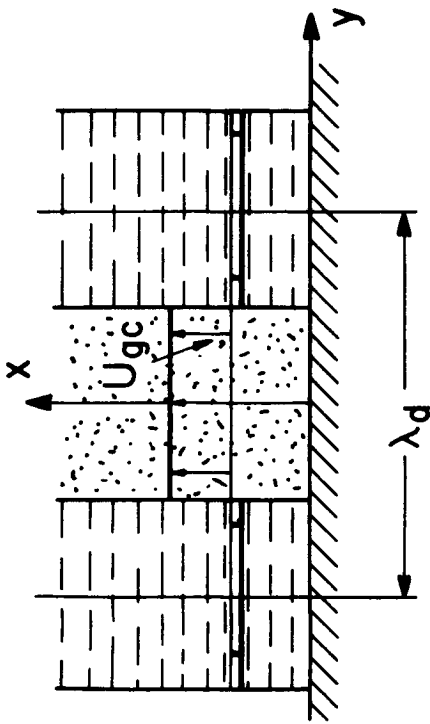
Velocity Profile for the Primary Flow in the Vapor Jet and in the Liquid Column. Figure 48 contrasts the vapor removal idealization for the inviscid case with that which we shall assume for the viscous case. In the viscous case we must avoid the configuration of a circular jet in a square area if the analysis is to be at all tractable. Thus we inscribe a circular liquid return path inside the square area. We also make the following assumptions:

- 1.) The gas velocity,  $U_g$ , and the liquid velocity,  $U_f$ , are zero on the interface.
- 2.) The Poiseuille velocity profile is valid in the vapor jet.
- 3.) The analysis is two-dimensional. However curvature of the jet will be introduced subsequently as an additional pressure contribution and velocities will be adjusted such that:
- 4.) the mass inflow of liquid in the circular annulus is matched by the gas outflow in the circular jet.  $U_f$  is locally maximum or minimum at  $y = 2R_j$ .
- 5.) The shear stresses are matched at the interface.



$$R \equiv \lambda_d / 4$$

viscous configuration



inviscid configuration

Fig. 48. Assumed theoretical models of boiling near the peak heat flux.

The resulting velocity profiles are obtained by fitting even polynomial functions in  $y/R_j$  to these conditions. For the gas we obtain

$$U_g = U_{g_m} (1 - y^2/R_j^2) \quad (89)$$

where the subscript m denotes the maximum value; and for the liquid

$$U_f = U_{g_m} \left\{ \left[ \frac{107}{54} \frac{\mu_g}{\mu_f} - \frac{11}{81} \frac{\rho_g}{\rho_f} \right] - \left[ \frac{168}{54} \frac{\mu_g}{\mu_f} - \frac{24}{81} \frac{\rho_g}{\rho_f} \right] \frac{y^2}{R_j^2} + \left[ \frac{69}{54} \frac{\mu_g}{\mu_f} - \frac{15}{81} \frac{\rho_g}{\rho_f} \right] \frac{y^4}{R_j^4} - \left[ \frac{8}{54} \frac{\mu_g}{\mu_f} - \frac{2}{81} \frac{\rho_g}{\rho_f} \right] \frac{y^6}{R_j^6} \right\} \quad (90)$$

These results incorporate considerable physical approximation and, indeed, when we complete the analysis we shall find it necessary to adjust one constant before the theory will fit the experimental results. However, the actual physical configuration is so complicated that we could hope for no more. What the present analysis will yield is the proper form of the dependence of the peak heat flux on the relevant dimensionless groups. In the light of this objective our failure to represent the configuration more precisely is of no great importance.

Equation (90) gives a maximum downward velocity of:

$$U_{f_m} = -U_{g_m} \left[ 0.3557 \frac{\mu_g}{\mu_f} + 0.0388 \frac{\rho_g}{\rho_f} \right] \quad (91)$$

which occurs at  $y = 1.28 R_j$ . We shall need these results subsequently in the analysis. It is worth noting that this maximum occurs near the interface and that there is a slight upward recirculation of liquid at  $y = 2R_j$ . We should also be aware that the constants in equation (91) fully reflect any crudity in our assumptions as to the liquid and vapor flow configurations.

Formulation of the Stability Problem. To study the stability of the interface we superpose perturbation components of velocity and pressure on the mean flow of gas. We nondimensionalize velocity, distance, pressure, and time with  $U_{f_m}$ ,  $R_j$ ,  $\rho_g U_{f_m}^2$ , and  $R_j/U_{f_m}$ ,

respectively. We then define,  $u$ ,  $v$ , and  $p$  as the dimensionless perturbation components of axial velocity, radial velocity, and pressure. And we use the subscripts  $t$ ,  $x$ , and  $y$  to denote differentiation with respect to the dimensionless dependent variables.

The continuity and Navier-Stokes equations for the perturbed flow on the gas side are then:

$$u_x + v_y = 0 \quad (92)$$

$$u_t + Uu_x + Uyv = -p_x + Re^{-1}(u_{xx} + u_{yy}) \quad (93)$$

$$v_t + Uv_x = -p_y + Re^{-1}(v_{xx} + v_{yy}) \quad (94)$$

where  $Re \equiv U_{fm} R_j \rho_g / \mu_g$ . The boundary conditions at the interface are:

$$v = 0 \quad \text{at } y = 0 \quad (95)$$

$$u_y = 0 \quad \text{at } y = 0 \quad (96)$$

$$p_g - 2Re^{-1}v_y + \sigma\eta_{xx} / (\rho_g U_{fm}^2 R_j) + \sigma\eta / (2\rho_g U_{fm}^2 R_j) = p_f \text{ complex} \quad \text{at } y = 1 \quad (97)$$

$$u_y + v_x = Re \tau_f \text{ complex} \quad \text{at } y = 1 \quad (98)$$

where  $\eta$  is the displacement of the interface between the gas jet and the liquid column from its mean position.  $p_f \text{ complex}$  and  $\tau_f \text{ complex}$  are the complex perturbation pressure and shear stress respectively from the liquid side.

Equations (92) through (94), with boundary conditions (95) through (98), have been solved for small values of  $Re$  and for wave numbers of the disturbance close to 1. Complete details of the analysis are given in reference [27]. For a neutral disturbance with a wavelength equal to the "most susceptible" Taylor wavelength in the interface of the gas jet and the liquid column, it is shown in reference [27] that:<sup>9</sup>

---

<sup>9</sup> The solution is fairly complicated. It involves putting the Navier-Stokes equation into the Orr-Sommerfeld form and obtaining the lead terms of a series solution to it.

$$1.07 \frac{\tau_f}{\eta} - \frac{p_f}{\eta} = \frac{\sigma}{2R_j} \quad (99)$$

where  $\tau_f$  represents the magnitude of the imaginary component of the complex fluctuating shear stress and  $p_f$  represents the real component of the complex fluctuating normal stress that results from the downward flow of the liquid.

The evaluations of  $\tau_f/\eta$  and  $p_f/\eta$  are extremely difficult. They involve solving the same governing equations with appropriate boundary conditions. Brooke Benjamin [67] has solved the comparable problem for a boundary layer type of exterior flow on a way wall, with no pressure gradient. For the shear stress and pressure perturbations, he obtained:

$$\frac{p_f}{\eta} = - \frac{2\pi}{\lambda_d} R_j \rho_f U_{fm}^2 \quad (100)$$

$$\frac{\tau_f}{\eta} = -1.188 \left( \frac{2\pi R_j}{\lambda_d} \right)^{5/3} \rho_f U_{fm}^2 \left( \frac{\mu_f}{\rho_f(U_f)_y R_j^2} \right)_{y=R_j}^{1/3} \quad (101)$$

We shall use these expressions in equation (99) with the realization that they represent the incorrect configuration. The liquid velocity profile in our case is more diffuse and it has a negative pressure gradient in the direction of flow. However, if we did obtain equations equivalent to (100) and (101) for our situation, they would differ only in the lead constant on the right-hand side. Substituting equations (100) and (101) in equation (99) and rearranging the result, we obtain:

$$U_{fm}^2 \left\{ 1 - 1.63 \left[ \frac{\mu_f}{\rho_f(U_f)_y R_j^2} \right]_{y=R_j}^{1/3} \right\} = \frac{\sigma}{\pi R_j \rho_f} \quad (102)$$

To get the desired expression for the maximum stable vapor velocity in the jet we combine equations (102) and (91) and replace  $R_j$  with  $\lambda_d/4$ . The result is

$$\left(\frac{U_{g_m}}{U_{H_c}}\right)^2 \left[ 0.3557 \frac{\mu_g}{\mu_f} + 0.0389 \frac{\rho_g}{\rho_f} \right] \left[ 1 - 1.01 \left( \frac{\mu_f}{\mu_g} \sqrt{\frac{\rho_g}{\rho_f}} \frac{U_{H_c}}{U_{g_m} M \Lambda_d} \right)^{1/3} \right] = \frac{2 \rho_g}{\pi^2 \rho_f \Lambda_d} \quad (103)$$

The form of equation (103) is correct within the limitations of the three constants 0.3557, 0.0388, and 1.01, which reflect the crudities of the various configurational assumptions.

### Peak Heat Flux Prediction

The average vapor velocity for Poiseuille flow in a cylindrical jet at the point of instability is  $U_{g_m}/2$ . Using  $U_{g_m}/2$  for  $U_H$  in equation (3) and  $A_j/A_h = \pi/16$  we obtain:

$$q_{\max_F} = \frac{\pi}{32} \rho_g h_{fg} U_{g_m} \quad (104)$$

Substituting equation (103) for  $U_{g_m}$  with  $\rho_g/\rho_f \simeq 0$ , and dividing by  $q_{\max_F}$  1.14  $q_{\max_Z}$  we obtain the desired expression for the dimensionless viscous peak heat flux on a flat plate. (This assumes  $\rho_g/\rho_f \ll \mu_g/\mu_f$ ):

$$\frac{q_{\max_F}}{(q_{\max_F})_{\text{inviscid}}} = \frac{0.633 \sqrt{M \Lambda_d}^{1/2}}{\sqrt{1 - 0.807 \left[ \frac{V}{M^2 \Lambda_d} \frac{(q_{\max_F})_{\text{inviscid}}}{q_{\max_F}} \right]^{1/3}}} \quad (105)$$

Our approximations as to the flow configuration are now reflected entirely in the two constants: 0.633 and 0.807.

In addition to the now-familiar dimensionless groups,  $M$  and  $\Lambda_d$ , we have now added a new one:

$$V \equiv \frac{\sqrt{\rho_g \rho_f} \sigma^{3/4}}{\mu_g \sqrt[4]{g(\rho_f - \rho_g)^3}} \quad (106)$$

It is very interesting to note at this point that Borishanskii [36] suggested in 1956 that a variety of up to 8 dimensionless groups might be involved in the viscous peak heat flux problem. These included groups which could be combined to give both  $M$  and  $V$ . However, he suggested that a group equivalent to  $M$ , alone, would be sufficient to characterize the viscous effects.

In 1970, Lienhard and Keeling [4] identified two types of viscous influences on  $q_{\max}$ . One of these was the result of induced convection which we have mentioned briefly on pages 12 and 13, and which we carefully avoided in the present experiments. The second is the direct influence of viscosity on the components of the hydrodynamic processes. Both Lienhard and Keeling, and Borishanskii sought to correlate  $q_{\max}/q_{\max_Z}$  data in terms of  $M$  (and  $R'$  in the case of finite geometries) without using additional groups. They both succeeded, but in each case they were restricted to values of  $M$  significantly greater than 100. Borishanskii's equation (10) was simply based on insufficient data, and values of his  $N$  (approximately equal to our  $M^2$ ) that were too large to reveal viscous influences with any certainty.

We have evaluated equation (105) numerically and plotted the results in Fig. 49 for four typical values of  $V$ , with  $M$  as the independent variable. In order to do this, we have used the  $R'_c = \infty$  curve from Fig. 24 to express  $\Lambda_d$  as a function of  $M$ . By following the saturated liquid-vapor line for one of our experimental fluids--cyclohexanol--at earth normal gravity, we have obtained a unique value of  $V$  for each value of  $M$ . Thus Fig. 49 displays a locus of points for cyclohexanol on dimensionless heat flux vs  $M$  coordinates. This particular curve is similar in form to equation (10) although it is higher.

### Comparison of Theory and Experiment

We have already described experiments in Chapter II which generated new data for flat plates, free of induced convection effects (recall Table I on page 20). Table VIII presents additional data obtained in this apparatus using cyclohexanol under low pressure. These data embrace values of  $M$ , sufficiently low to reflect a significant influence of viscosity.

Since we have already seen in Fig. 49 that, for a particular fluid, at one value of  $g$ , equation (105) takes the form  $q_{\max_F}/(q_{\max_F})_{\text{inviscid}} = f(M, \text{ only})$ , we plot the viscous cyclohexanol data for earth-normal gravity on these coordinates in Fig. 50. These data have been corrected

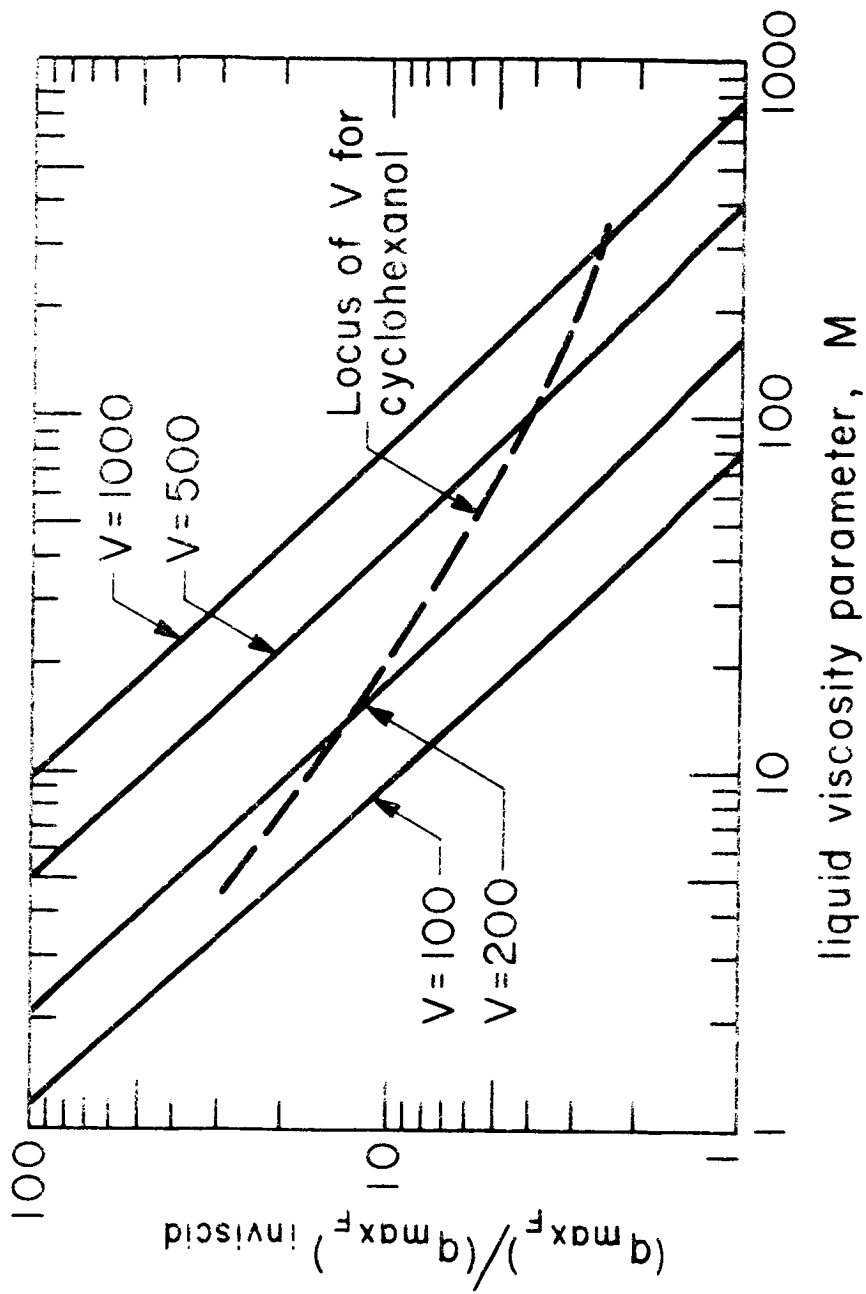


Fig. 49. Variation of dimensionless peak heat flux with  $M$  for various values of  $V$  at earth normal gravity.

Table VIII. Peak Heat Flux Data for Cyclohexanol  
for Flat Plate Heaters

| $g/g_e$ | P<br>(kPa) | M   | V   | $\frac{L'}{2\pi\sqrt{3}}$ | $q_{\max} \times 10^{-5}$<br>(W/m <sup>2</sup> ) | $\frac{q_{\max F}}{(q_{\max F})_{\text{inviscid}}}$ |
|---------|------------|-----|-----|---------------------------|--|---|
| 1       | 1.61       | 20  | 260 | 3.23                      | 1.67   | 2.19  |
|         | 3.62       | 35  | 337 | 3.31                      | 1.99   | 1.75  |
|         | 5.66       | 48  | 380 | 3.35                      | 2.10   | 1.54  |
|         | 11.73      | 100 | 490 | 3.45                      | 2.55   | 1.34  |
|         | 22.52      | 155 | 600 | 3.55                      | 2.81   | 1.25  |
|         | 99.50      | 250 | 920 | 3.86                      | 5.65   | 1.02  |
| 4.97    | 11.86      | 70  | 437 | 7.69                      | 3.75   | 1.48  |
| 8.95    | 7.31       | 38  | 350 | 10.11                     | 3.53   | 1.48  |

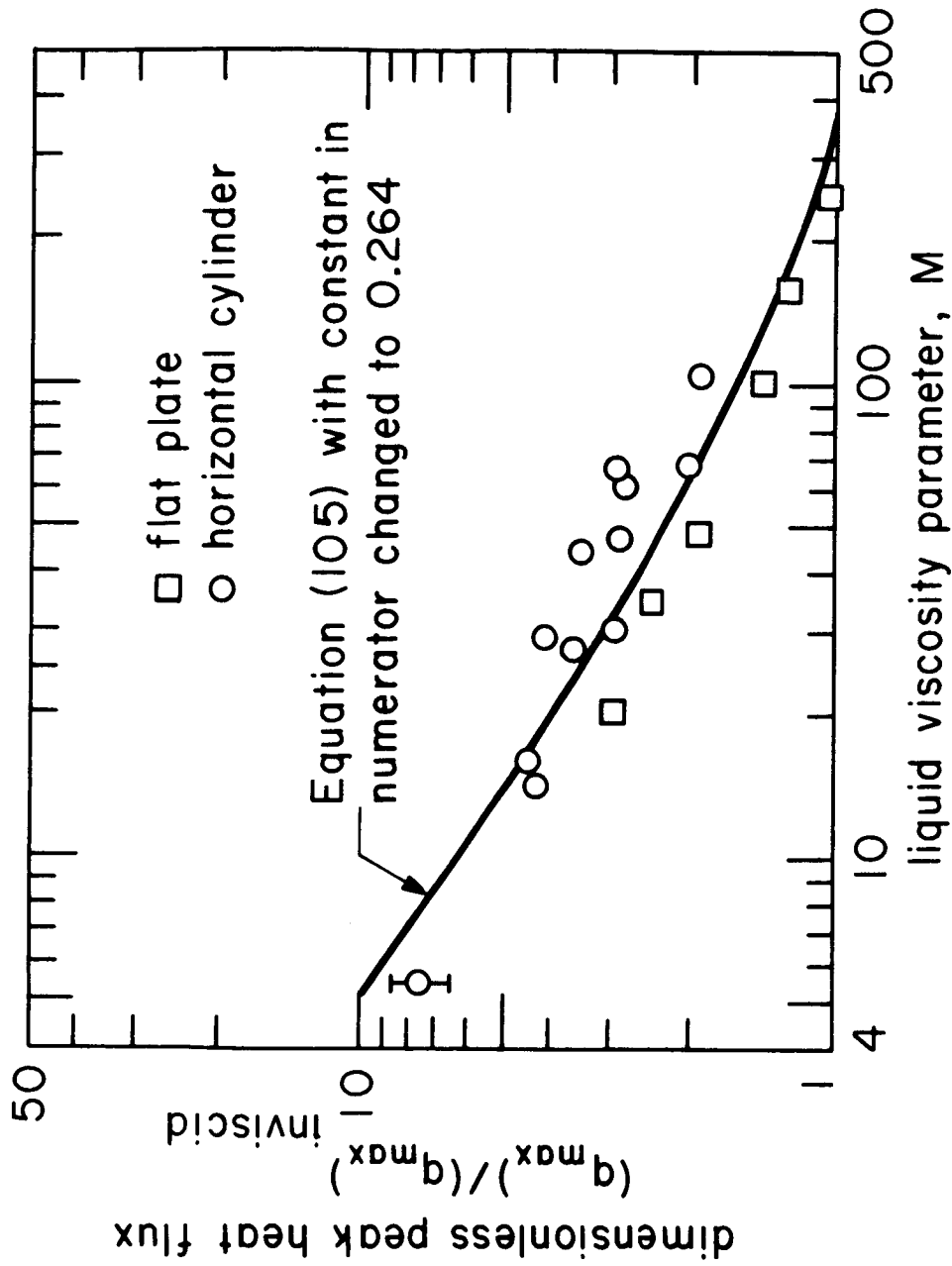


Fig. 50 Effect of liquid viscosity on peak heat flux for both flat plates and cylinders in cyclohexanol at earth normal gravity.

for the effect of finite plate size since fewer than 3 wavelengths are accommodated on the plate (recall Fig. 8) after the wavelength is corrected for viscosity (recall Fig. 24).

With these data we include original earth-normal gravity data for cyclohexanol boiling on horizontal cylindrical wires of various sizes and at various pressures. The data have been nondimensionalized by dividing them by the corresponding inviscid values. These data were obtained using exactly the same techniques as those employed by Sun and Lienhard [6], and they are presented in Table IX.

The comparison of data for cylinders with data for flat plates is justifiable if  $R'$  is near unity, and we use data in the range of  $0.22 \leq R' \leq 1.24$  here. Sun and Lienhard's [6] inviscid hydrodynamic model for the peak heat flux on small cylinders assumes the gas jets are separated by  $\lambda_d$ . They took the jet radius to be  $(R+\delta)$ , where  $\delta$  is the thickness of the vapor blanket surrounding the heater near the peak heat flux. While the radius of the jet decreases as  $(R+\delta)$ , so too does  $\lambda_H$  for small cylinders. The effect of a decrease in the liquid return velocity due to the smaller jet radius is nearly compensated by this shorter  $\lambda_H$ . Thus this model differs from our assumed flat plate model only in that the location of jets is on a line rather than on a square grid.

Figure 50 also includes equation (105) for comparison. However, as we noted in deriving this expression, the two decimal fractions in it should be regarded as free constants which might have to be altered empirically. Of these two, the value 0.807 in the denominator is relatively inconsequential, since it multiplies a term that is generally fairly small. Thus we shall not tamper with it. On the basis of the data in Fig. 50, however, we shall change the value 0.633 in the numerator to 0.264. With this adjustment, the comparison between theory and experiment in the figure is very good indeed.

When we go to variable gravity experiments in cyclohexanol,  $V$  can vary independently of  $M$ . Accordingly  $q_{\max}/(q_{\max})_{\text{inviscid}}$  becomes a function of two variables,  $M$  and  $V$ . Equation (105), with the lead constant equal to 0.264, has been plotted as a three-dimensional surface in Fig. 51. Fifteen high-gravity data for horizontal cylinders (Table IX) and one high-gravity data point from the flat plate apparatus (Table VIII) are included in the figure.

We see that these data faithfully bear out the independent influence of the parameter,  $V$ , as it is predicted by equation (105).

Table IX. Peak Heat Flux Data for Cyclohexanol Boiling  
on Horizontal Cylindrical Heaters

| R<br>(mm) | R'    | $g/g_e$ | P<br>(kPa) | M   | V   | $q_{max} \times 10^{-5}$<br>$\left(\frac{W}{m^2}\right)$ | $\frac{q_{max}}{(q_{max})_{inviscid}}$ |
|-----------|-------|---------|------------|-----|-----|--|--|
| 0.4123    | 0.216 | 1       | 0.30       | 5.4 | 125 | 3.60   | 8.00                                   |
| 0.5144    | 0.268 |         | 0.30       | 5.4 | 125 | 2.72   | 6.43                                   |
| 0.6540    | 0.343 |         | 0.30       | 5.4 | 125 | 2.74   | 6.88                                   |
| 0.8001    | 0.419 |         | 0.30       | 5.4 | 125 | 3.31   | 8.60                                   |
| 0.5144    | 0.264 |         | 2.68       | 29  | 312 | 4.60   | 4.15                                   |
|           | 0.239 |         | 5.00       | 44  | 336 | 4.89   | 3.43                                   |
|           | 0.234 |         | 7.72       | 66  | 425 | 4.79   | 2.88                                   |
| 0.6540    | 0.354 |         | 1.03       | 16  | 233 | 3.18   | 4.50                                   |
|           | 0.332 |         | 2.41       | 27  | 300 | 3.59   | 3.58                                   |
|           | 0.338 |         | 5.47       | 47  | 375 | 4.00   | 2.90                                   |
|           | 0.373 |         | 7.17       | 61  | 420 | 4.26   | 2.33                                   |
| 0.4128    | 0.222 |         | 0.94       | 14  | 215 | 3.25   | 4.34                                   |
|           | 0.228 |         | 2.76       | 30  | 317 | 3.37   | 2.87                                   |
|           | 0.233 |         | 7.86       | 67  | 429 | 3.69   | 2.01                                   |
|           | 0.241 |         | 13.31      | 104 | 500 | 4.29   | 1.92                                   |
|           | 0.669 | 8.5     | 3.54       | 20  | 196 | 5.27   | 3.01                                   |
|           | 0.997 | 18.3    | 5.34       | 23  | 181 | 6.24   | 2.66                                   |
|           | 1.194 | 25.7    | 6.83       | 26  | 182 | 8.67   | 2.96                                   |
|           | 0.680 | 8.3     | 8.00       | 37  | 247 | 5.48   | 2.23                                   |
|           | 1.020 | 18.3    | 10.41      | 37  | 218 | 7.16   | 2.24                                   |
|           | 1.220 | 25.7    | 11.99      | 36  | 203 | 8.10   | 2.29                                   |
|           | 0.672 | 8.3     | 5.45       | 28  | 224 | 5.71   | 2.76                                   |
|           | 0.998 | 17.8    | 8.00       | 30  | 205 | 7.00   | 2.50                                   |
|           | 1.207 | 25.7    | 9.44       | 32  | 193 | 7.95   | 2.44                                   |
|           | 0.687 | 8.3     | 10.40      | 44  | 262 | 5.80   | 2.13                                   |
|           | 1.011 | 17.8    | 11.58      | 39  | 221 | 6.69   | 2.08                                   |
|           | 1.220 | 25.7    | 12.82      | 39  | 209 | 8.10   | 2.19                                   |
|           | 0.702 | 8.3     | 16.52      | 63  | 295 | 5.48   | 1.65                                   |
|           | 1.032 | 17.8    | 17.99      | 55  | 251 | 7.44   | 1.90                                   |
|           | 1.240 | 25.7    | 19.23      | 53  | 239 | 8.10   | 1.90                                   |

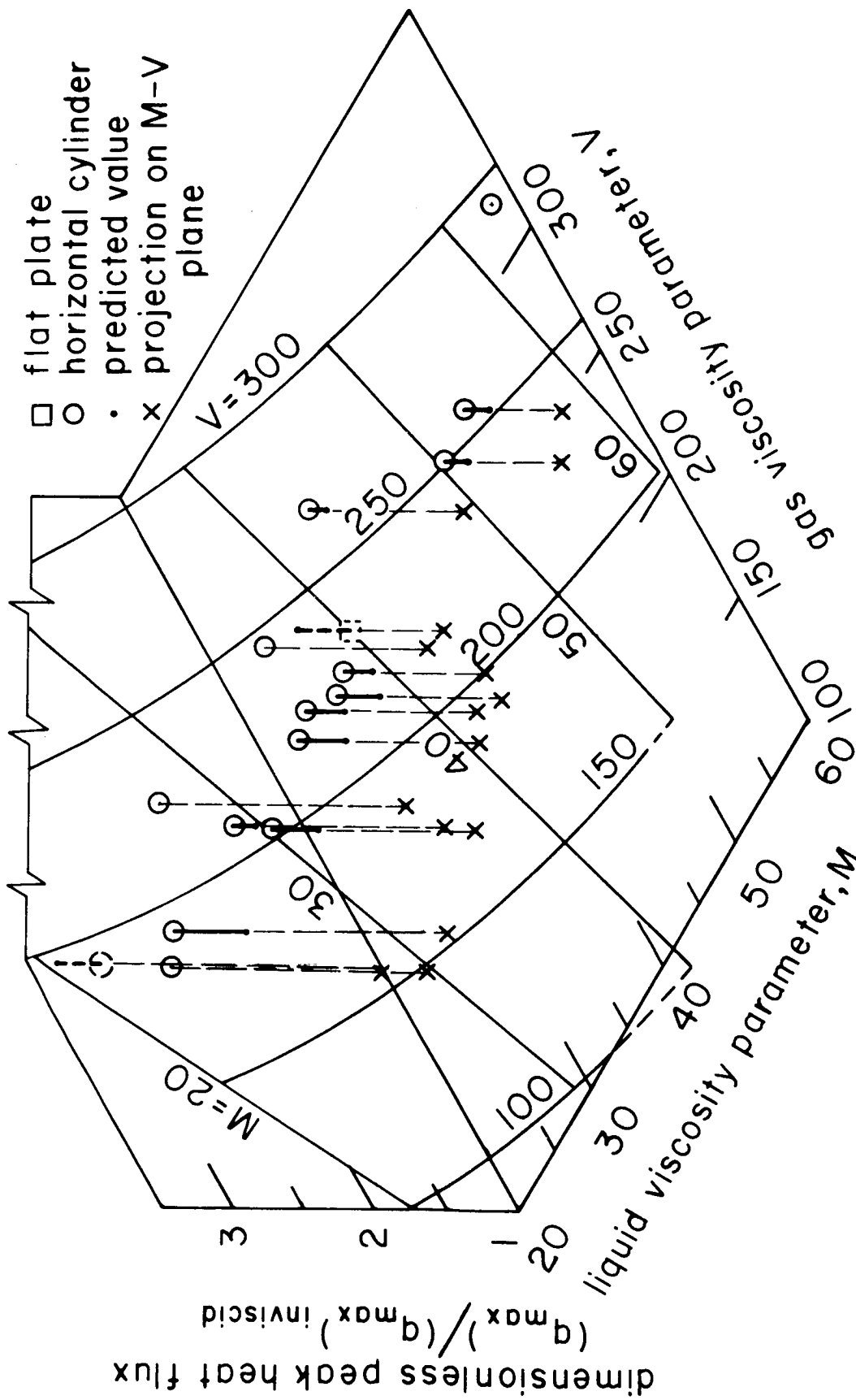


Fig. 51 Effect of liquid and gas viscosity on the peak heat flux at elevated gravities.

It is important to note that as  $M$  increases or as  $V$  decreases, the prediction of  $q_{\max}/(q_{\max})_{\text{inviscid}}$  eventually falls below unity.

At this point we simply abandon the viscous prediction and embrace the inviscid prediction. This is reasonable since a basic limitation of any viscous theory is that it does not pass to the limit of inviscid behavior as  $\mu$  is made very small.

### Conclusions

1.) We have predicted that

$$\frac{q_{\max_F}}{(q_{\max_F})_{\text{inviscid}}} = \frac{\text{Constant } V/M \Lambda_d^{1/2}}{\sqrt{1 - 0.807 \left[ \frac{V}{M^2 \Lambda_d} \frac{(q_{\max_F})_{\text{inviscid}}}{q_{\max_F}} \right]^{1/3}}}$$

for viscous liquids.

2.) The Constant has been evaluated experimentally. It is  $\approx 0.264$ .

3.) This prediction can also be applied to data for cylinders as long as  $R'$  is on the order of magnitude of unity. In this case,  $q_{\max_F}/(q_{\max_F})_{\text{inviscid}}$  should be rewritten with the appropriate values of  $q_{\max}$  and  $(q_{\max})_{\text{inviscid}}$  for cylinders.

4.) The viscous prediction is only valid when it predicts higher peak heat fluxes than the equivalent inviscid theory.

5.) The derivation of equation (105) required the solution of an original stability problem, namely the prediction of the maximum stable velocity of a gas jet in a viscous liquid. This velocity is given by equation (103). This problem might well find applications beyond the present one.

## VI. HYDRODYNAMIC THEORY OF ELECTROLYSIS

### Introduction

This chapter will deal with a non-boiling application of the principles of the hydrodynamic theory. We shall discuss the gas removal process during high current-density electrolysis with the aim of identifying hydrodynamic transitions, analogous to those which occur in boiling. This work was extracted from the Master's thesis of Bhattacharya as reported in [18] and [19].

Electrolysis has attracted increasing interest lately because of its relevance to a variety of problems of human life support and a myriad of industrial processes. References [68] and [69] provide some background as to the scope of contemporary applications of electrolysis. This particular study was part of a broader effort to establish the similarity between boiling and electrolysis. Bhattacharya generally sought to establish means for applying known methods for predicting boiling processes to the prediction of comparable processes in electrolysis. An earlier paper from his study, reference [17], dealt with bubble growth predictions for the two processes.

Figure 52 is a conventional boiling curve with a transformed ordinate. In it, the vapor volume flux,  $\dot{v}$ , (or the heat flux,  $q$ , divided by the volumetric latent heat of vaporization,  $\rho_g h_{fg}$ ) is plotted against the driving temperature difference,  $\Delta T$ . The well known transitions in the boiling mechanisms are indicated on this figure. Let us consider each one briefly:

1.) inception: This is the point at which the first bubbles appear. Since we are not concerned with predicting inception in either boiling or electrolysis, no attempt will be made here to recount the massive literature on the subject.

2.) transition from the isolated bubble region to the region of slugs and columns: This transition was identified by Zuber ([70] and [71]). It was subsequently predicted by Moissis and Berenson [32], who also advanced a variety of measurements of the transition point.

Using observations of the rise of bubbles in tubes [72] and [73], Moissis and Berenson showed that the volume flux at this transition,  $\dot{v}_{sc}$ , can be given as

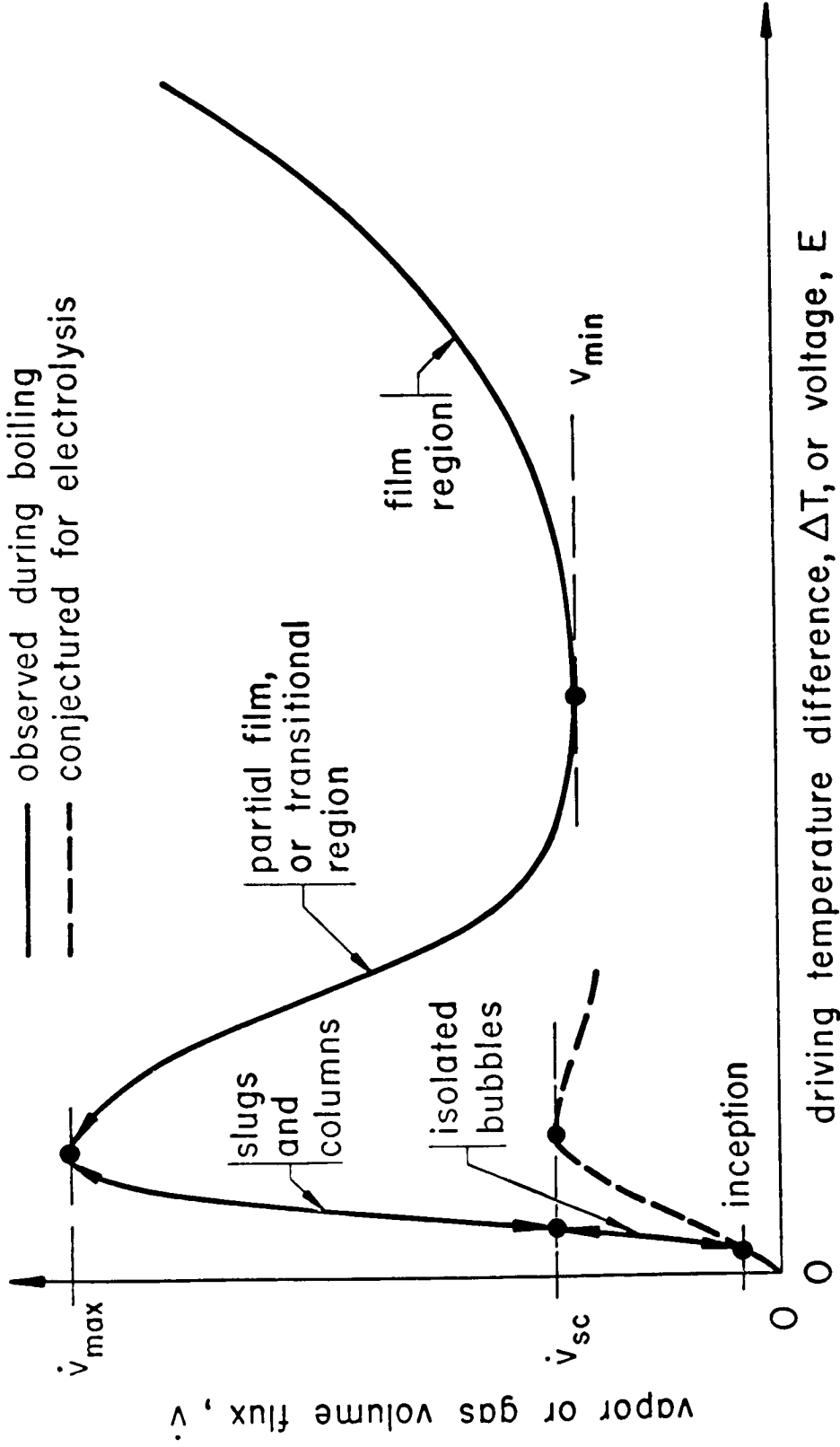


Fig. 52 Schematic boiling curve and corresponding conjectured electrolysis curve.

$$\dot{v}_{sc} = 0.56 \beta^{1/2} \sqrt[4]{g\sigma/(\rho_f - \rho_g)} \frac{A_j}{A_h} \quad (107)$$

where  $\beta$  is the contact angle of the liquid-vapor interface on the heater. Zuber's value of  $A_j/A_h = \pi/16$  for flat plates in this expression led to

$$\dot{v}_{sc} = 0.11 \beta^{1/2} \sqrt[4]{g\sigma/(\rho_f - \rho_g)} \quad (108)$$

In the published discussion of [32], both Chang and Zuber asked the authors if this transition was well defined. They replied that it was indeed slurred so that equation (108) is an approximate result. We shall return to this point later.

3.) the peak volume flux transition: Dividing Zuber's and Sun's expressions for  $q_{max}$  by  $\rho_g h_{fg}$  we obtain, respectively:

$$v_{max} = \frac{\pi}{24} \sqrt[4]{g\sigma(\rho_f - \rho_g)/\rho_g^2} \quad (109)$$

and

$$\dot{v}_{max_{cyl}} = v_{max} (0.89 + 2.27 \exp[-3.44R'^{1/2}]) \quad (110)$$

4.) the minimum heat flux transition: We likewise obtain from Zuber's and Lienhard-Wong's [33]  $q_{min}$  expressions, respectively:

$$\dot{v}_{min_Z} = C_1 \sqrt[4]{\sigma g \frac{\rho_f - \rho_g}{(\rho_f + \rho_g)^2}} \quad (111)$$

and

$$v_{min_{cyl}} = \dot{v}_{min_F} \left[ \frac{C_2}{R'^2 (2R'^2 + 1)} \right]^{1/4} \quad (112)$$

where  $C_1$  was predicted as 0.171 and  $C_2$  was found experimentally to be 1.289.

There is a general failing to these  $v_{\min}$  expressions that does not afflict  $\dot{v}_{\max}$ . As we noted earlier, Berenson [35] showed that while  $\dot{v}_{\max}$  is insensitive to surface condition,  $\dot{v}_{\min}$  can be strongly influenced by minor variations of surface condition. Kovalev [66] further amplified the point and showed that the end-mounting of cylinders also influenced  $\dot{v}_{\min_{\text{cyl}}}$ . On the basis of Kovalev's data, Lienhard [7] showed that  $C_2$  should be reduced to at least 0.0217--perhaps even further. Thus  $\dot{v}_{\min}$  predictions are generally a chancey business. What the real minimum is, cannot finally be predicted, and it is very hard to ascertain experimentally.

### The Transitions in Electrolysis

At first glance we should expect the same transitions to exist in the volume flux vs. voltage curve for electrolysis, as exist in the boiling curve (see Fig. 52). While  $\dot{v}$  is equal to  $q/\rho_g h_{fg}$  in boiling, it can be obtained from Faraday's law for electrolysis. Faraday's law expresses the mass flux of  $H_2$  dissociated at the cathode as proportional to the current flux,  $I/A$  amps per unit area, the molecular weight ( $M$ ) of  $H_2$ , and  $n^{-1}$  where  $n$  is the number of electrons transferred in the liberation of one  $H_2$  molecule (for  $H_2$ ,  $n$  and  $M$  both equal 2.) Thus:

$$\dot{v} = \frac{(I/A) M}{96500 \rho_{H_2} n} \frac{\text{cm}^3}{\text{cm}^2 \text{ sec}} \quad (113)$$

and we can reduce the current to a volume flux just as we could  $q$ .

Let us now consider a basic difference between nucleate boiling and nucleate electrolysis. The basic mechanism of heat removal in nucleate boiling was shown by Zuber [70] and [71] to be microconvection driven by the rising bubbles. In 1962 Tien [74] predicted the microconvective heat flux in the region of isolated bubbles using an inverted stagnation flow model. Boehm and Lienhard [75] summarized and extended this type of prediction in 1964 and found that in the region of isolated bubbles

$$q \sim \dot{v} \sim \Delta T^{1.18} n_s^{1/3} \quad (114)$$

where the "site density",  $n_s$ , is the number of nucleation sites per unit area.

During nucleate boiling the site density typically rises as  $\Delta T^5$  or more. Thus  $q$  or  $\dot{v}$  typically rises as  $\Delta T^3$  or 4. But during

electrolysis there should be no corresponding convective enhancement of charge removal. The diffusion coefficient for  $H_2$  created at the wall is very small (about 1/30 of the thermal diffusivity of the water). Thus the Schmidt number is on the order of 100 and the diffusion boundary layer is very much thinner than the microconvective velocity boundary layer. Furthermore, we find a heavy density of idle bubbles scattered in among the active or repeating sites during electrolysis. These create a static sublayer of fluid whose thickness is independent of the microconvective velocity, and which should totally contain the diffusion layer. Thus  $\dot{v}$  should simply increase in direct proportion to the driving voltage,  $E$ . None of the convective reinforcement by the nucleation sites, which occurs in boiling, is present. In electrolysis it is as though the sites were not there, insofar as the relation between  $v$  and  $E$  is concerned.

An important aspect of the transition from the region of isolated bubbles to the region of slugs and columns is the blanketing-over, and removal of liquid-metal contact that occurs. Throughout the isolated bubble region there is virtually no loss of contact; but as the slugs and columns evolve, there is. Zuber [71], in fact, envisioned that this loss of contact increases, honeycombing the liquid under the jets and feeding them. This can continue until more than  $\pi/16$  of the contact is eliminated and large dry patches cover the heater (see, e.g., the photographs of Kirby and Westwater [76] which dramatically show this behavior).

The heat transfer continues to increase strongly with  $\Delta T$  in the region of slugs and columns because as the vapor velocity increases and heater surface is exposed, the microconvection at the surface continues to improve. Quite the opposite should occur during electrolysis, however. As contact is lost, the electric current -- and with it,  $\dot{v}$  -- must decrease in the absence of a convective process.

We are interested, then, in learning to predict the hydrodynamic transition from the region of isolated bubbles to the region of slugs and columns, or the "first transition" as we shall call it. This transition should replace the Helmholtz unstable transition as the point of peak volume flux, in electrolysis. It can be predicted for electrolysis on a flat plate with the help of equation (108). Since the experimental work presented here is done on horizontal wires, it will next be necessary to develop an equivalent expression for cylindrical cathodes:

On a cylindrical element,  $A_j/A_h$  must be modified for use with equation (107). The bubbles rise from the wire, as indicated in Fig. 53,

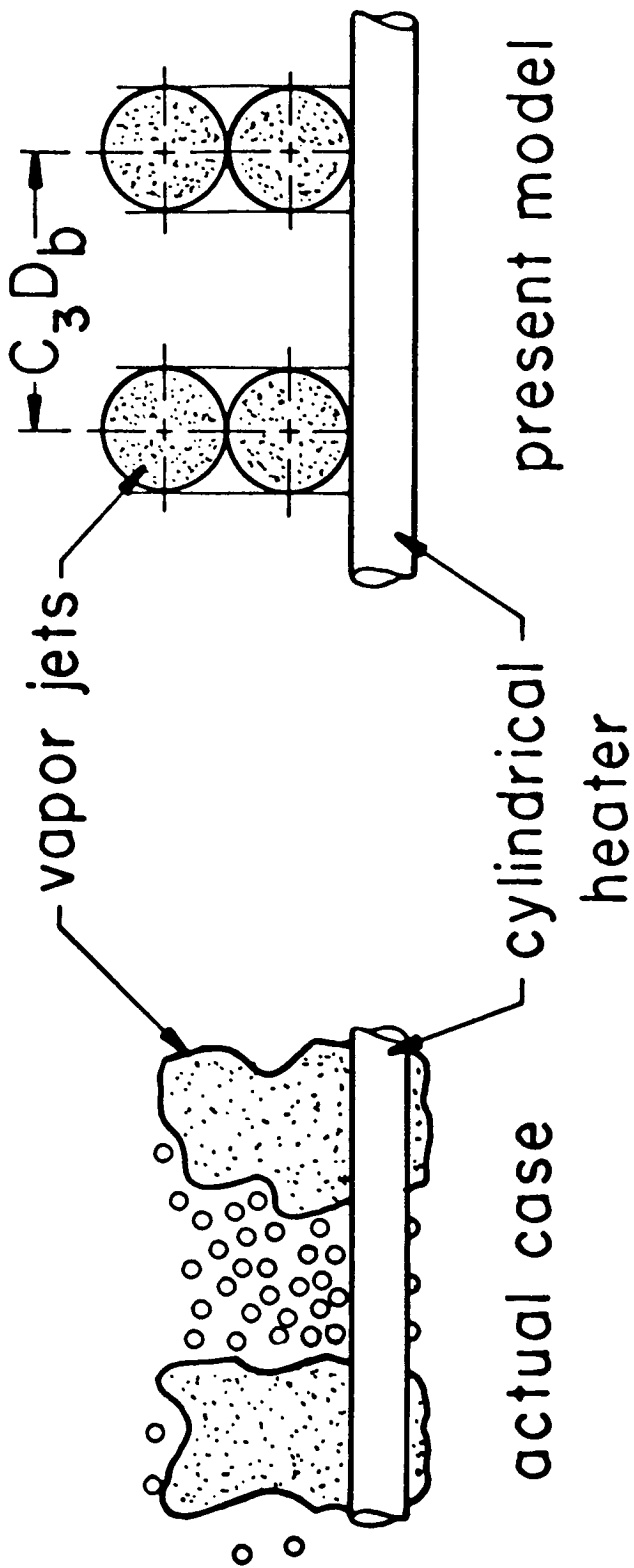


Fig. 53 Comparison of present model for cylindrical heaters, with actual case.

eventually following one another without interruption in a column of diameter,  $D_b$ , equal to that of the departing bubbles<sup>10</sup>. In this case

$$\frac{A_j}{A_h} = \frac{(\pi/4)D_b^2}{2\pi RL} = \frac{D_b}{8C_3R} \quad (115)$$

where  $L$ , the length of wire subtended by one column can no longer be assumed equal to  $\lambda_d$ , since we are far below  $\dot{v}_{\max}$ . It is therefore replaced with  $C_3D_b$ , where  $C_3$  is an unknown constant. The constant  $1/C_3$  can be viewed as the fraction of the wire's length occupied by columns. In Moissis and Berenson's model,  $C_3$  would be equal to 2, measured along the rectangular grid lines, and equal to  $2\sqrt{2}$  or 2.83 on diagonal lines through the grid. The spacing should be comparable for cylinders, but we have no way of specifying the precise value of  $C_3$  a priori.

Using Fritz's expression (quoted in [79]) for the bubble departure diameter,  $D_b$ ,

$$D_b = 0.0148 \beta \sqrt{\frac{2\sigma}{g(\rho_f - \rho_g)}} \quad (116)$$

in equation (115), and then substituting equation (116) in equation (107) we obtain

$$\dot{v}_{sc} = \frac{0.001464}{C_3} \frac{\beta^{3/2}}{R'} \sqrt[4]{\frac{g\sigma}{\rho_f - \rho_g}} \quad (117)$$

for the volume flux at the first transition on cylinders.

### Experiments

A local maximum in electrolytic gas evolution has been observed in the past. In 1950, for example, Kellog [78] reported observations of such a maximum during aqueous electrolysis from a vertical wire anode. Actually this transition was known then in connection with the "anode-effect", or the vapor blanketing of anodes which had been observed much earlier during the electrolysis of molten salts. The

---

<sup>10</sup>

This conceptualization is consistent with that of Moissis and Berenson for flat plates.

concern in this case was not with predicting (or even explaining) the peak but with identifying the phenomenon of film electrolysis and, noting that it resulted in a considerable reduction of current at a given voltage. One important en passant observation made by Kellogg was that "the current increases almost linearly with increased voltage" in the region approaching the local maximum. This concurs with the result we anticipated in the previous section.

Two basic experiments have been undertaken in the present study to test our predictions as to the nature of the electrolysis curve. In one of the tests we measured the  $I$  (or  $\dot{v}$ ) vs.  $E$  curve during electrolysis from cylinders, and obtained photographic verification of aspects of the process. In the other we measured  $\dot{v}_{SC}$  during boiling to provide additional corroboration of equation (117).

Figure 54 shows the apparatus for the electrolysis experiment. A one-tenth normal KOH electrolyte was contained in a 9 cm x 10 cm x 19 cm plexiglas box. Clean nichrome wire cathodes (14, 16, and 20 gauge and about 5 cm in length) were suspended in the electrolyte. The anode was made of clean platinum foil and suspended in the electrolyte above the cylinder. It was made considerably larger in surface area than the cathode to assure that it would function in the isolated bubble regime long after the cathode underwent any transition. Additional details relating to the experiment are given by Bhattacharya [11].

Figure 55 shows the basic output of the experiment for three of the wire sizes (14, 16, and 20 gauge). These  $\dot{v}$  vs.  $E$  curves were obtained by increasing the voltage across the test cell up to the desired value, stabilizing the temperature within an 8°C range, and measuring the current,  $I$ . Equation (113) was then used to calculate  $\dot{v}$  from  $I$ . It was necessary to operate in a fairly high temperature range because, at high currents, the capsule heated up rapidly during the course of an observation. We were generally able to hold temperatures close to 70°C when the potential was below about 100 volts; but it was increasingly hard to do so when we had to increase the voltage through the region of peak current before making an observation.

The curves were quite regular and reproducible up to a maximum value of  $\dot{v}$ . Beyond this maximum, the data exhibited a great deal of scatter and indeed the current was unsteady and tended to fluctuate at a given voltage. Nevertheless the current clearly dropped off dramatically with voltage beyond the peak. At the maximum volume flux a blue corona first formed in the vapor separating the cathode from the liquid. As the voltage was further increased the corona also increased,

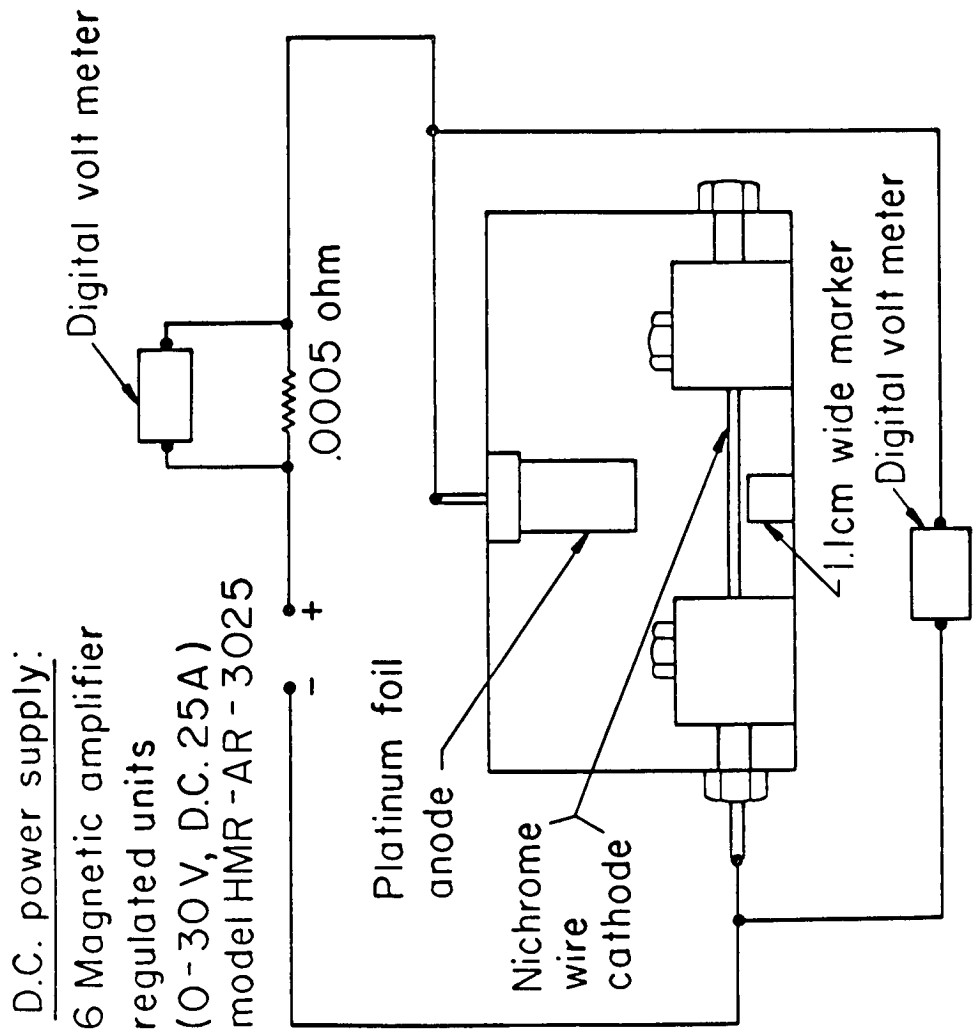


Fig. 54 A test capsule and the circuit diagram for the electrolysis experiment.

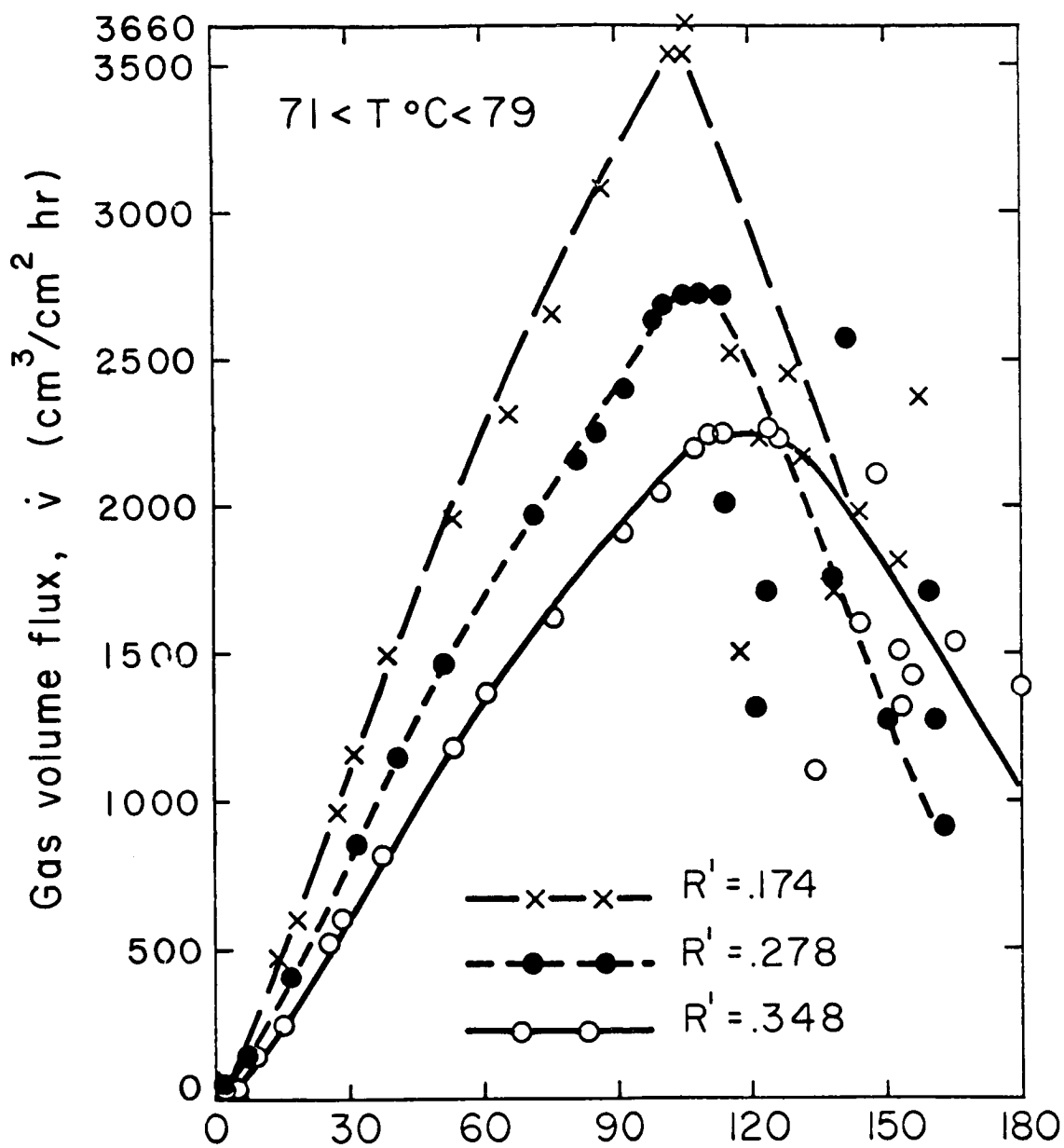


Fig. 55 Variation of volume flux with voltage during electrolysis.

and with it there developed intermittent sparking between the cathode and the electrolyte. As we approached our maximum voltage capability of about 180 volts, the sparking assumed a regular spacing and fairly great intensity.

We should emphasize that the abscissa of Fig. 55 (the voltage between the cathode and the anode) is only proportional to -- not equal to -- the driving voltage of the surface electrolysis process. This fact was clarified by a duplicate run on a 16 gage wire using a reference electrode located 13 mm below the cathode. The reference electrode reveals that about 75% of the voltage drop is being sustained across the cell, away from the cathode. The actual surface voltage drop would be still substantially less than the value,  $E_{c-b}$ , measured on the reference electrode.

Our system was therefore one in which the current varied almost entirely by virtue of changes in potential across the cathode, the remaining resistance being constant. The curves accordingly should have the right shape although the abscissas are arbitrary within a constant factor.

An additional source of error in the system is the possible contribution of vapor generation due to heating. Since this could hardly have been a significant factor before the onset of sparking and corona, and since sparking only occurred once the peak had been reached, its contribution to our observations of the peak could not have been great. However a second source of error is compensatory and comparable in magnitude. This is the fact that "current yield" efficiencies can run below 100% (see e.g. [79]) so that Faraday's Law might underestimate the hydrogen gas yield by a few percent. These effects probably give a net error somewhere between 0 and 10%. At voltages beyond the peak there might be considerable vapor generation. Probably the film electrolysis regime is, in fact, a mixed boiling and electrolysis region owing to the greatly increased surface resistance at the cathode and the resulting heat generation.

The results of the tests as plotted in Figs. 55 and 56 verify the essential linearity of current (or  $\dot{v}$ ) in voltage, after nucleate electrolysis becomes fully established. This linearity is evident only after a layer of bubbles has been established to preclude microconvection.

Figure 57 is a sequence of pictures of electrolysis on the 16 gauge wire ( $R' = 0.278$ ) beginning slightly below the maximum current and continuing to  $E = 176$  volts. The 1.1 cm wide marker is evident at

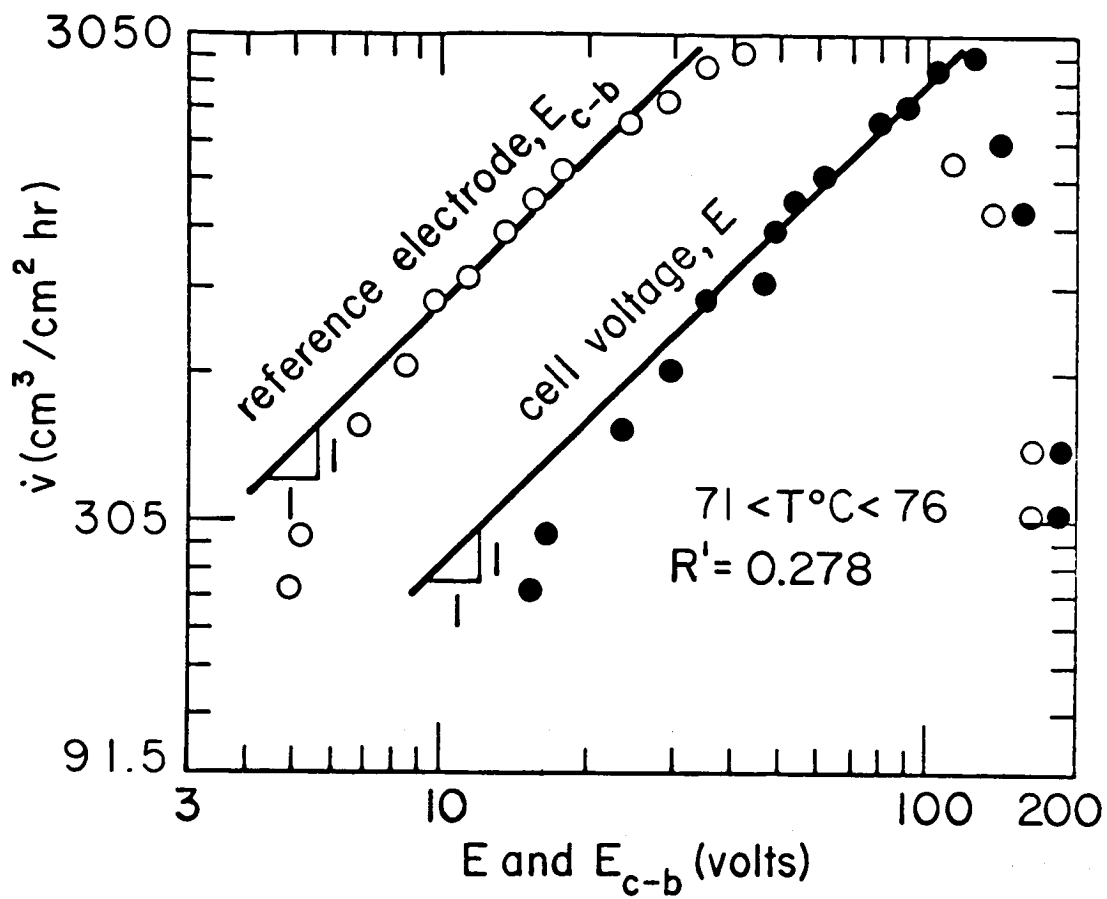
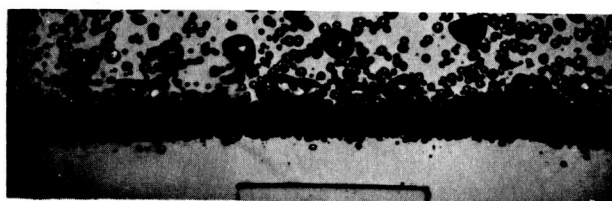
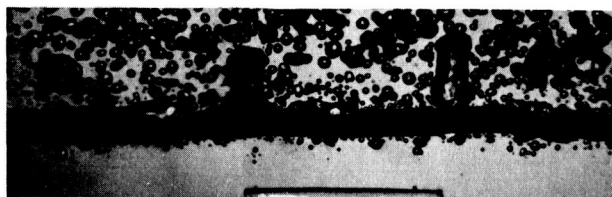


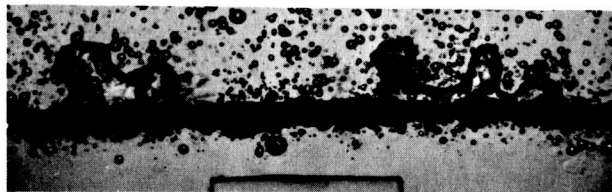
Fig. 56 Comparison of  $I(E)$  and  $I(E_{c-b})$  on logarithmic coordinates.



$$\dot{v} = 2510 \text{ cm}^3/\text{cm}^2\text{hr}, E = 95 \text{ volts}$$



$$\dot{v} = 2510 \text{ cm}^3/\text{cm}^2\text{hr}, E = 97 \text{ volts}$$



$$\dot{v} = 2670 \text{ cm}^3/\text{cm}^2\text{hr}, E = 108 \text{ volts}$$



$$\dot{v} = 880 \text{ cm}^3/\text{cm}^2\text{hr}, E = 168 \text{ volts}$$



$$\dot{v} = 760 \text{ cm}^3/\text{cm}^2\text{hr}, E = 173 \text{ volts}$$



$$\dot{v} = 1010 \text{ cm}^3/\text{cm}^2\text{hr}, E = 176 \text{ volts}$$

Fig. 57 Photographs of electrolysis in a 0.1 normal KOH solution on a 16 gauge ( $R' = 0.278$ ) wire.

the bottom of each picture. The corona and sparking are invisible in these pictures, back-illuminated with a high-intensity stroboscope. The slugs and columns are very clear on the wire in the first two pictures. As  $E$  is increased these jets appear to give way to a film process characterized by Taylor unstable waves very similar to those observed during pure film boiling (see, e.g., [33] or [5]).

The second experiment used Sun's [6] apparatus to observe  $q$  at the first transition on horizontal wires during boiling in methanol and water. Since the apparatus and basic procedure do not differ from that described in [6] we shall not reproduce details here. In this case the first transition was observed with the help of a stroboscope and checked our visual impressions with still photographs.

Table X lists the observed transition points for the two liquids and for the four wire sizes. Bhattacharya was generally able to identify the transitions reproducibly within a 6% margin, but only after identifying a particular stage (within a broader transition range) in which the first few jets appeared to take form.

### Discussion of Results

We now have the following claims as to the character of electrolysis, and data against which to test them:

1.) Microconvection does not abet the current (or volume) flux in electrolysis. A corollary of this claim was that, in the nucleate electrolysis regime,  $I$  or  $\dot{v}$  should be approximately linear in  $E$  (or  $E_{C-b}$ ) up to the point of hydrodynamic transition. Figures 55 and 56 clearly bear this out very well, as did Kellogg's experiment. Given that this is true then we expect that:

2.) The volume flux maximizes at the first transition, instead of the second, in electrolysis. Four kinds of evidence bear this out. The first is the lack of microconvective enhancement of  $I$ . The second is the visual appearance of the process (see Fig.57) which matches the appearance of the first transition in boiling.

The third piece of evidence arises from the fact that equation (110) predicts  $\dot{v}_{\max}$  in the range from  $0.975 \times 10^6$  to  $1.19 \times 10^6$   $\text{cm}^3/\text{cm}^2\text{hr}$  for our test wires. Thus  $\dot{v}_{\max}$  is predicted to be between 270 to 520 times the observed maximum, depending upon the wire size. It follows that the maximum could not possibly reflect the second transition. The reader who is acquainted with boiling might justly

Table X. Observed Heat Flux at First Transition in Boiling

| Radius<br>(cm) | Water |  | Methanol |  |
|----------------|-------|--|----------|--|
|                | R'    | $(\rho_g h_{fg}) \dot{v}_{sc} \times 10^{-5}$<br>(W/m <sup>2</sup> ) | R'       | $(\rho_g h_{fg}) \dot{v}_{sc} \times 10^{-5}$<br>(W/m <sup>2</sup> ) |
| .0406          | .174  | 2.57 + .16<br>- .15  | 2.58     | 1.39 + .019<br>- .019  |
| .0508          | .218  | 1.36 + .025<br>- .028  | .323     | 0.96 + .025<br>- .025  |
| .0648          | .278  | 1.44 + .016<br>- .016  | .412     | 0.66 + .022<br>- .025  |
| .0812          | .348  | 0.82 + .03<br>- .03  | .516     | 0.31 + .01<br>- .01  |

wonder how this ratio could reasonably be so high. The reason is that for either cylinders or flat plates the ratio of transition volume fluxes is

$$\frac{\dot{v}_{sc}}{\dot{v}_{max}} \approx f(\beta, R') \sqrt{\frac{\rho_g}{\rho_f}} \quad (118)$$

Since  $\rho_g$  is extremely small for  $H_2$  the ratio is quite small. The same would be true for boiling at low pressure.

The fourth piece of evidence lies in our third claim, namely:

3.) Equation (117) describes the first transition in both boiling and electrolysis. To apply equation (117) one must first ascertain the contact angle,  $\beta$ , for water, methanol, and tenth-normal KOH electrolyte, since  $\dot{v}_{sc} \sim \beta^{3/2}$ . Unfortunately  $\beta$  is a notoriously stochastic property. In 1959 Griffith and Wallis [80] pointed out the difficulty of reproducing  $\beta$  consistently. Table XI shows the great variability of their data with slight changes of surface condition. Trivedi and Funk [81] provided in situ measurements of contact angles under static bubbles during electrolysis in normal KOH electrolyte on platinum plates. Trivedi [82] recently measured  $\beta$  during electrolysis in tenth-normal KOH on nichrome wires. The data of [80] and [81] are included in Table XI. Both sets of data were obtained on metals that had been first cleaned in distilled water, then in methanol, and finally rinsed in the test liquid. Chang and Snyder [83] also reported values for methanol and water which they inferred from the data of earlier papers. These values are included in Table XI.

Table XI also includes original  $\beta$  values that we measured using the tilting plate method<sup>11</sup> for methanol and the sessile drop method for water. Both tests used nichrome plates cleaned in the same way that Trivedi's surfaces were.

The four measured values of  $\dot{v}_{sc}$  in electrolysis (the peaks in Figs. 55 and 56) and the eight values of  $\dot{v}_{sc}$  for boiling are given in Fig. 58. They are nondimensionalized as  $\dot{v}_{sc}/\beta^{3/2} \sqrt{4g\sigma(\rho_f - \rho_g)}$  and plotted against  $1/R'$ , since equation (117) indicates that this group should equal  $0.0001464/C_3R'$ . The observed values of  $\dot{v}_{sc}$  are spread

---

<sup>11</sup> A detailed explanation of such tests is given in Reference [80].

Table XI. Measured Contact Angles

| Liquid and Metal                       | Source  | Temp. (°C) | $\beta$ range (degrees) |
|--|---------|------------|-------------------------|
| water-stainless steel                  | [80]    | 30         | 38-78                   |
| water-stainless steel                  | [80]    | 100        | 28-82                   |
| $\frac{1}{10}$ N, KOH - platinum*      | [81]    | 23         | 15-35                   |
| $\frac{1}{10}$ N, KOH - nichrome wire* | [82]    | 23         | 10-23                   |
| water - copper                         | [83]    | 180        | 60                      |
| methanol - copper                      | [83]    | 64         | 46                      |
| water - nichrome                       | present | 27         | 60-81                   |
| methanol - nichrome                    | present | 27         | 40-52                   |

\* data for electrolytic H<sub>2</sub> bubbles in situ.

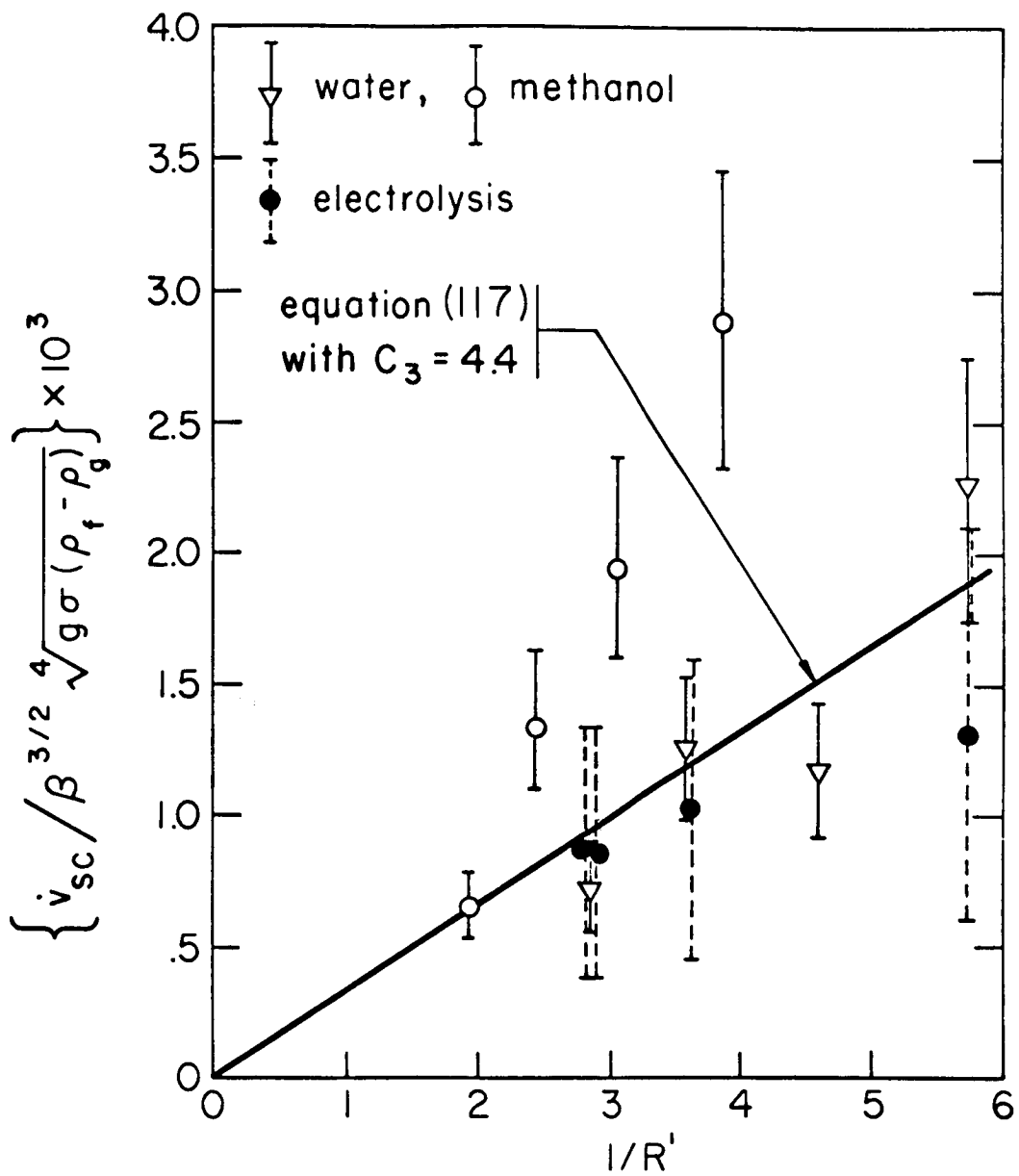


Fig. 58 Comparison of predicted first-transition data for both boiling and electrolysis.

out considerably in this representation owing to our ignorance of precise values of  $\beta$ . For the boiling results we used our own measurements of  $\beta$  and for the electrolysis data we used Trivedi's values of  $\beta$  for electrolysis on nichrome wires.

Figure 58 shows that the  $1/R'$  dependence of  $v_{sc}$  is upheld, although the slopes differ between water and methanol. The water data for both electrolysis and boiling are fairly well represented with equation (117) if  $C_3$  is taken to be 4.4. This value of  $C_3$  corresponds nicely with the proportioning of the jets that we observe in the first two pictures in Fig. 57 (taken near the point of maximum  $v$ ). A value of  $C_3$  more nearly equal to 2.5 would be required to represent the methanol data in Fig. 58.

4.) As  $E$  is increased beyond the point of peak volume flux, the process goes to a kind of film process similar to film boiling. The photographs in Fig. 57 show an evolution from gas removal by slugs-and-columns to gas-vapor removal by the cyclic collapse of Taylor-unstable waves. The wavelengths measured from the last three photographs in Fig. 57 and from other pictures not included here are:

$$(\lambda_d)_{\text{experimental}} = 1.07 \pm .25 \text{ cm}$$

while Lienhard and Wong's theory predicts  $\lambda_d = 1.04 \text{ cm}$ .

The wire appears to become almost completely blanketed in the pictures for high voltages. However a small number of departing nucleation bubbles in the pictures suggests that there is still some liquid-to-cathode contact. Despite these indications of a conventional approach to a film gas removal process, there is a difficulty in the numerical value of  $\dot{v}_{\min}$ . Equation (112), which (as we have noted) might overestimate  $\dot{v}_{\min}$ , gives:

$$\dot{v}_{\min} (R' = 0.174) = 4550 \text{ cm}^3/\text{cm}^2\text{hr}$$

$$\dot{v}_{\min} (R' = 0.348) = 3020 \text{ cm}^3/\text{cm}^2\text{hr}$$

while the corresponding experimental values of  $\dot{v}_{sc}$  are 3660 and 2280, respectively.

Thus  $\dot{v}_{sc} < \dot{v}_{\min}$ , and beyond  $E(\dot{v}_{sc})$  the calculated hydrogen gas volume flux drops still farther below  $\dot{v}_{\min}$ . This is additional evidence

that stable film electrolysis involves a substantial component of evaporated water which does not appear in the  $\dot{v}_{SC}$  calculation based on Faraday's Law.

### Conclusions

- 1.) There is an enhancement of the heat flux which occurs in boiling when nucleation sites influence one another; this does not occur in the volume flux in electrolysis. Consequently  $\dot{v} \sim E$  in the region below the first transition.
- 2.) The volume flux reaches a local maximum at the "first transition" point, or the transition from isolated bubbles to slugs-and-columns.
- 3.) The volume flux,  $\dot{v}_{SC}$ , at the first transition on horizontal cylinders is given approximately by equation (117). However, ignorance of precise values of  $\beta$  and of the precise structure of the escaping gas jets precludes accuracy beyond a factor of two in the use of equation (117). The predicted dependence of  $\dot{v}_{SC}$  on  $1/R'$  appears to be sound.
- 4.) A form of electrolysis that shows many outward appearances of film boiling, including the Taylor unstable wavelength, are established at high voltage.
- 5.) A clear understanding of transitional and film electrolysis and an identification of  $\dot{v}_{min}$  in electrolysis must await experimentation in a system with an extremely high voltage capability and a substantial cell cooling system.
- 6.) The existing body of understanding of boiling processes provides a very useful point of departure for seeking to extend our understanding of gas-forming electrolysis.

## VII. BOILING ON SMALL WIRES

### Introduction

We now turn our attention to a matter that actually lies outside of the hydrodynamic theory, as it has been described here. This chapter will describe the phenomena that replace the hydrodynamic mechanisms when a finite heater becomes very small or gravity becomes very low. These processes are extremely important in the context of aerospace applications since they will inevitably be involved as any large system passes from earth-normal gravity to the zero-gravity limit.

Under conditions of very low gravity, or for very small heaters,  $R'$  (which characterizes the ratio of buoyant forces to surface tension forces) becomes small. Figure 59 shows the same  $q_{\max}$  correlation that we showed in Fig. 13 for Sun's horizontal cylinder data, but now we have plotted the abscissa on logarithmic coordinates to illuminate small  $R'$  behavior. It is clear that  $R'$  must exceed 0.15 if the wave mechanisms which define  $q_{\max}$  are to stay intact. For smaller values of  $R'$ , surface tension so over-balances inertia that these mechanisms deteriorate, and a sampling of data by Kutateladze et al. [84], Sun [6], and Siegel and Howell [85] no longer correlate on  $q_{\max}/q_{\max Z}$  vs.  $R'$  coordinates.

It was likewise shown in [5] that there is still good visual evidence of the wave stability mechanisms for all  $R' \geq 0.12$ , during film boiling on horizontal cylinders. But for  $R' \leq 0.06$  these mechanisms cease to be identifiable.

If a correlation of the form  $q_{\max}/q_{\max Z} = f(R')$  fails, and the Zuber-Kutateladze mechanisms fail with it, what exactly happens to the boiling process at small  $R'$ ? The photographs of Sun [6], of Pitts and Leppert [86], and of Kutateladze et al. [84] for small wires provide some clue. Bubbles grow on the wire until they are large enough to buoy off and there is no evidence of the inertial waves that are apparent on large wires. The photographs of Siegel and Usiskin [87] and Siegel and Howell [85] show the same kind of process for greatly reduced gravity. The forces of surface tension and buoyancy remain important, however the process is slowed down and the effects of inertia are greatly reduced. Indeed, the soundtrack of a movie by Siegel and Keshock (associated with [88]) specifically notes the reduced inertial effects in boiling under low gravity.

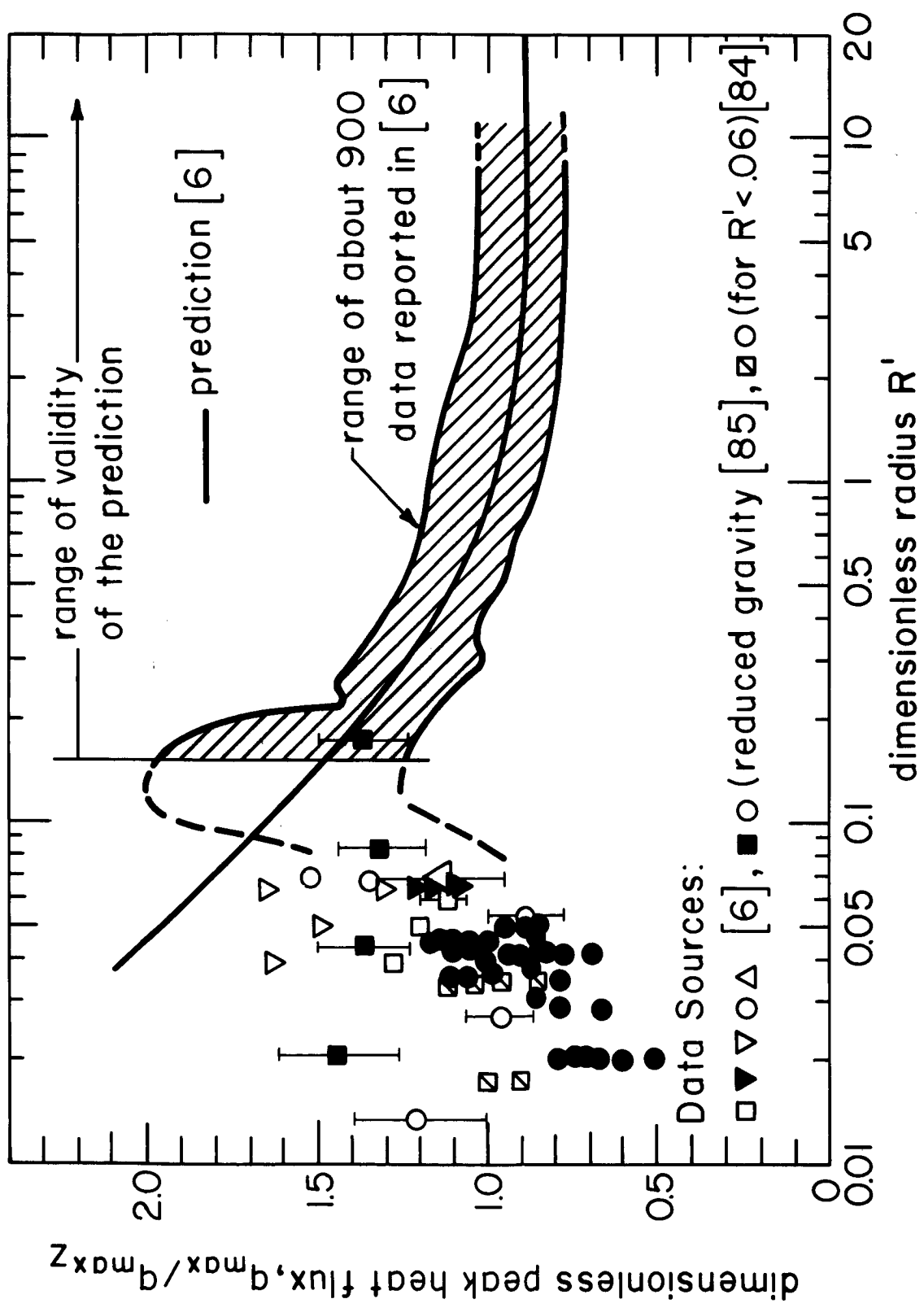


Fig. 59. Deterioration of correlation at small  $R'$ .

Another question arises: If, at low gravity or for small wires, inertia becomes insignificant and the Zuber-Kutateladze mechanisms fail, what have the investigators who have given  $q_{\max}$  data for low  $R'$  actually observed? Without the inertial wave mechanisms it is hard to see how there could have been any  $q_{\max}$  points to report.

### Experiment

To answer the questions raised in the Introduction, Bakhru [20, 21] set out to measure the full  $q$  vs.  $\Delta T$  curve for very small wires heating a variety of liquids. The apparatus used to do this is shown in Fig. 60. A small platinum wire, which served as both a resistance heater and a resistance thermometer, was suspended in the liquid of interest and boiling was observed at successive heat fluxes. The temperature of the wire was calculated from the resistance which in turn was computed from the ratio of voltage to current, using the method detailed by van Stralen and Sluyter [89]. Since complete details of the experimental method are given by Bakhru [20], we shall only list a few major features of the tests here:

The wires were cleaned in soap and then rinsed in the test liquid. Reagent grade liquids were used in all cases. During actual observations the preheater, which was used to maintain saturation conditions, was momentarily switched off. Since the wires would melt during atmospheric pressure runs in water, the water runs were all made at pressures in the neighborhood of 75 mm Hg abs. The maximum probable error in  $q$  was found to be 2-1/2%. The maximum probable error in  $\Delta T$  varied from 36% or about 3°F at the very lowest  $\Delta T$ 's to 1.8% or about 7°C at the highest  $\Delta T$ 's.

Bakhru's complete raw data are given in the form of 13 boiling curves in Figs. 61 through 72. These have been arranged in order of increasing  $R'$  from 0.0076 up to 0.0806. In each case data are presented for both increasing and decreasing heat flux to expose any hysteresis effects. Figure 63 combines data for two wires under identical conditions to assure reproducibility of results.

The major significance of Bakhru's study is readily apparent from these curves. As  $\Delta T$  is increased on the smaller wires,  $q$  rises monotonically without passing through a maximum and minimum. Only as  $R'$  increases to about 1/10 does the conventional boiling curve begin to re-establish itself.

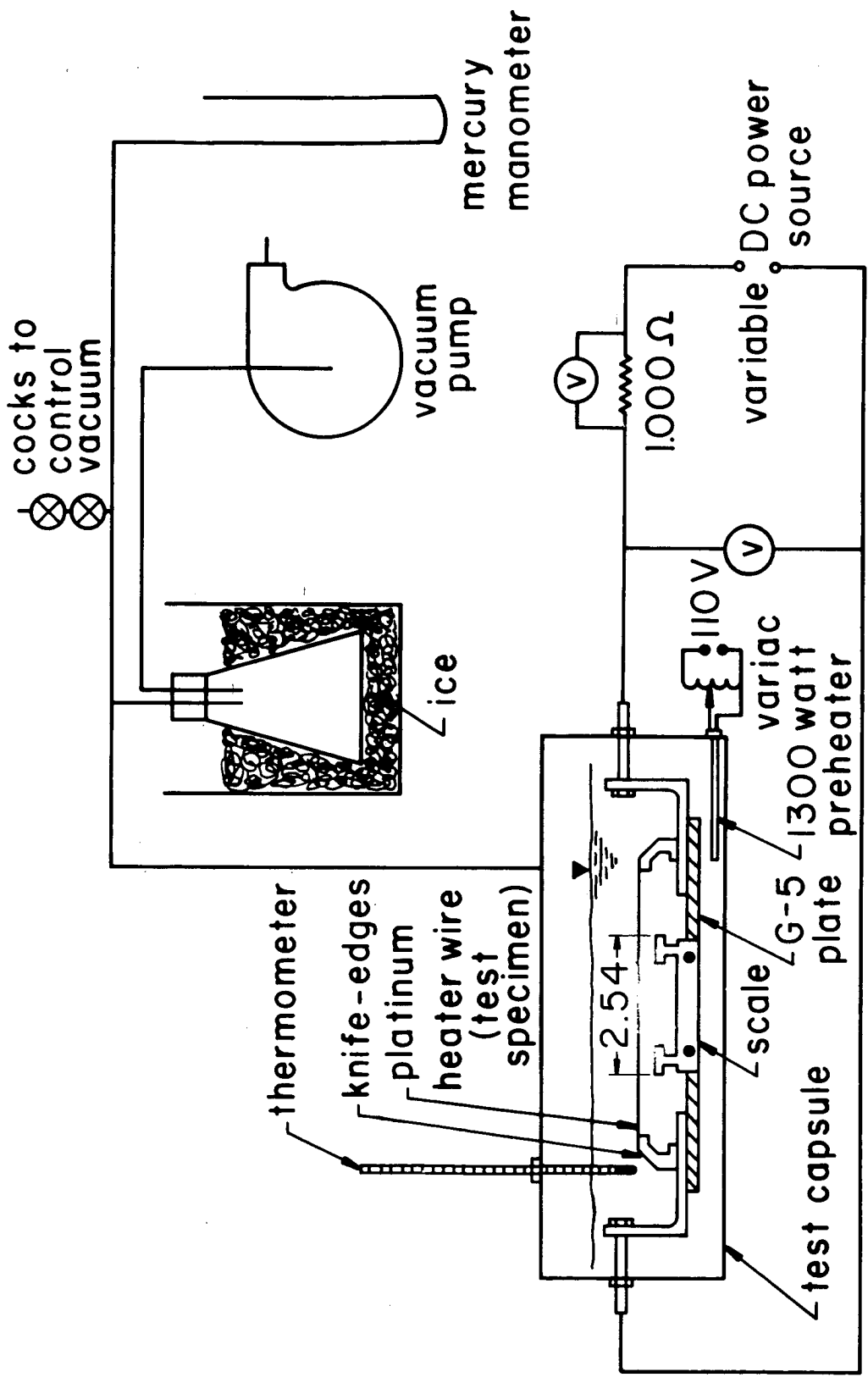


Fig. 60 Schematic representation of experimental apparatus.

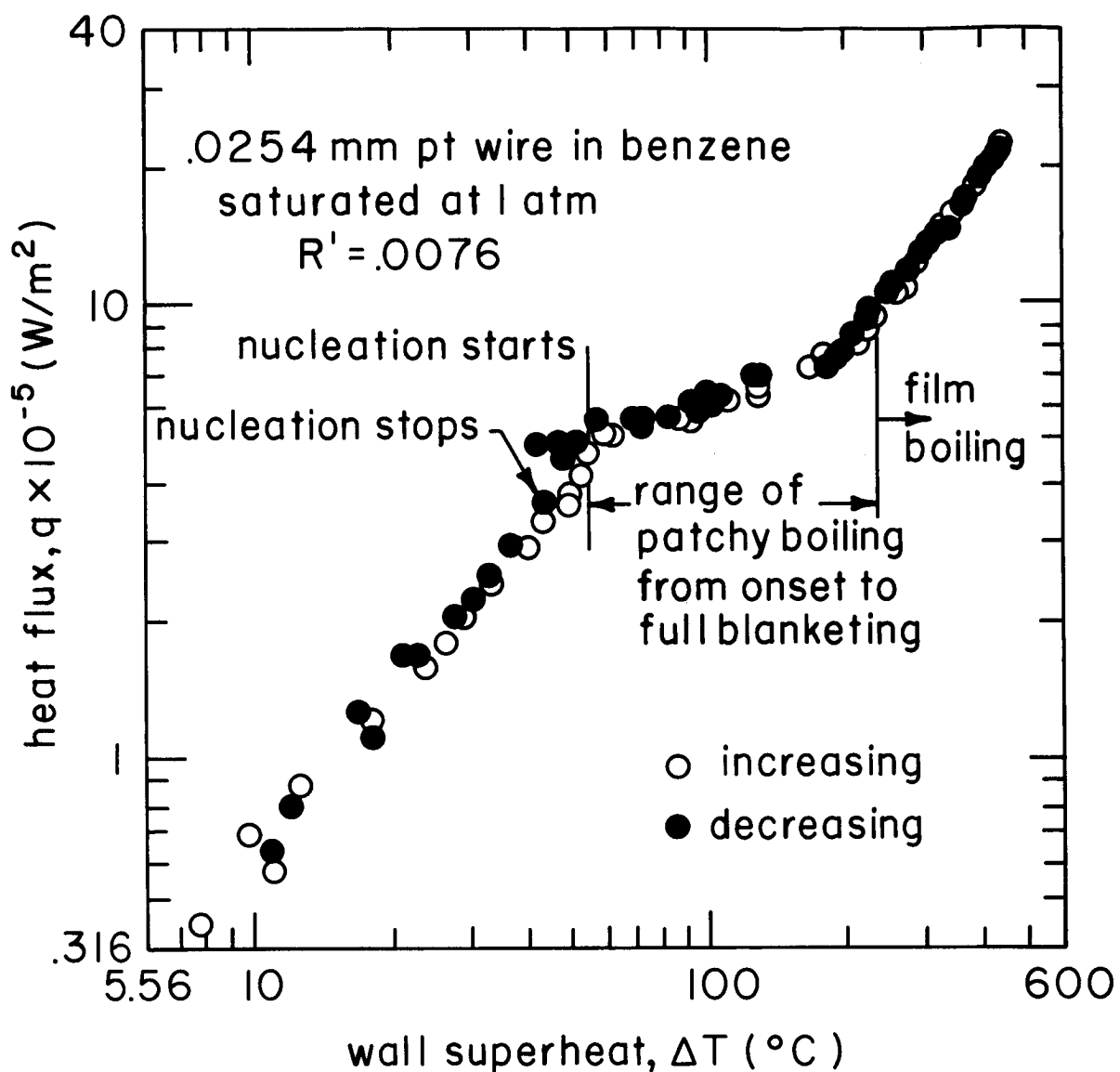


Fig. 61 Boiling curve for .0254 platinum wire in benzene.

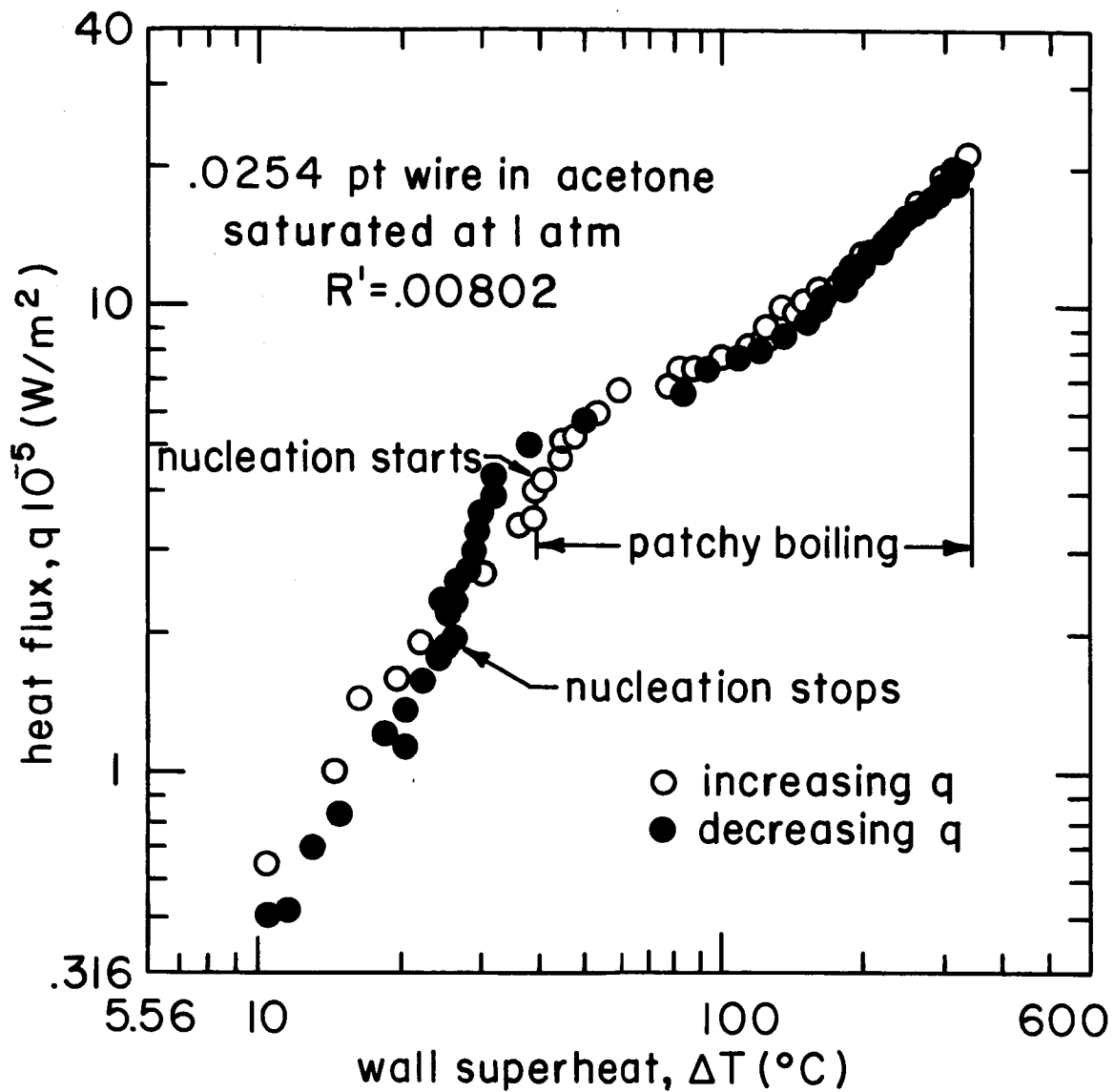


Fig. 62 Boiling curve for .0254 platinum wire in acetone.

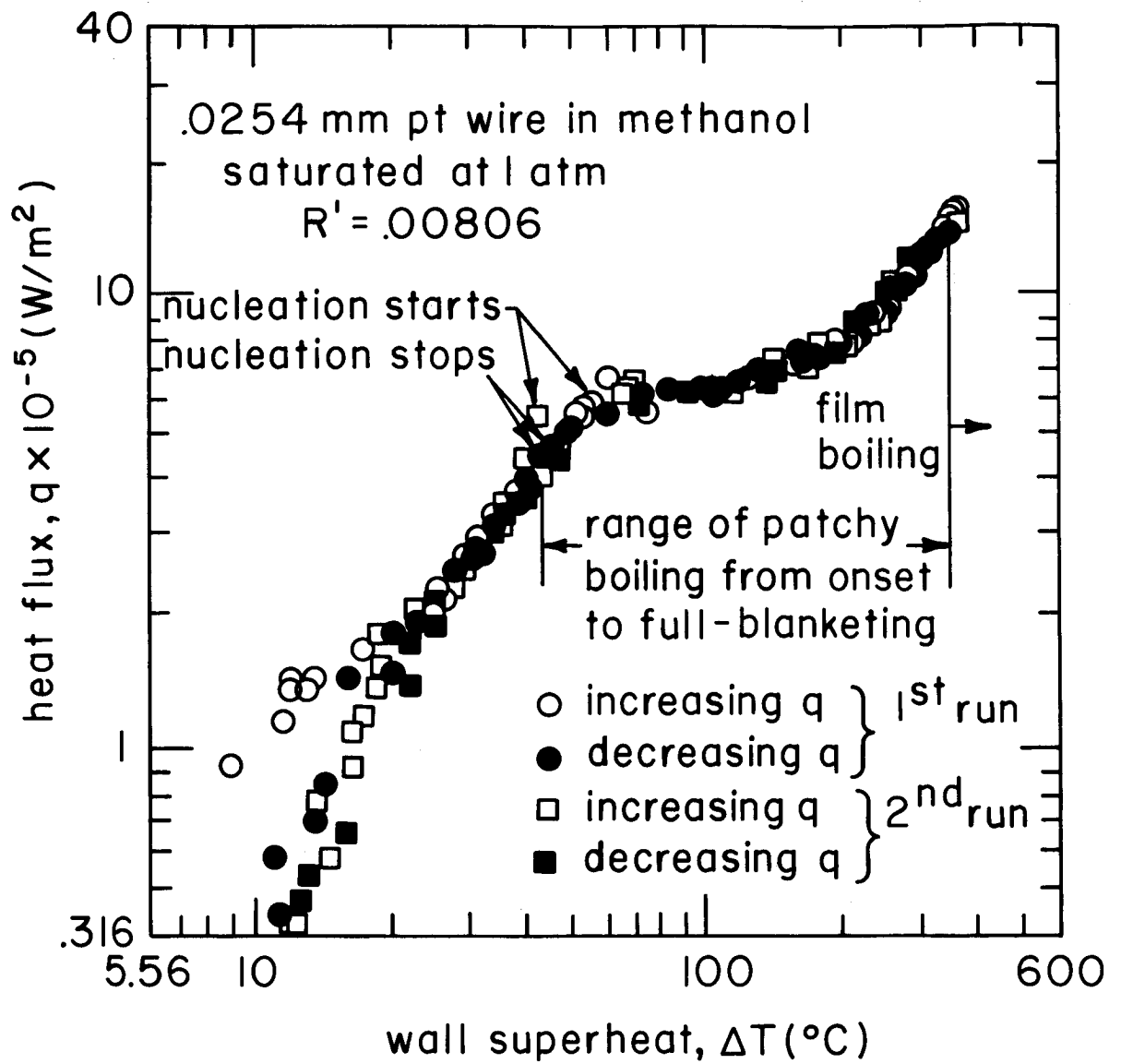


Fig. 63 Boiling curve for .0254 mm platinum wire in methanol.

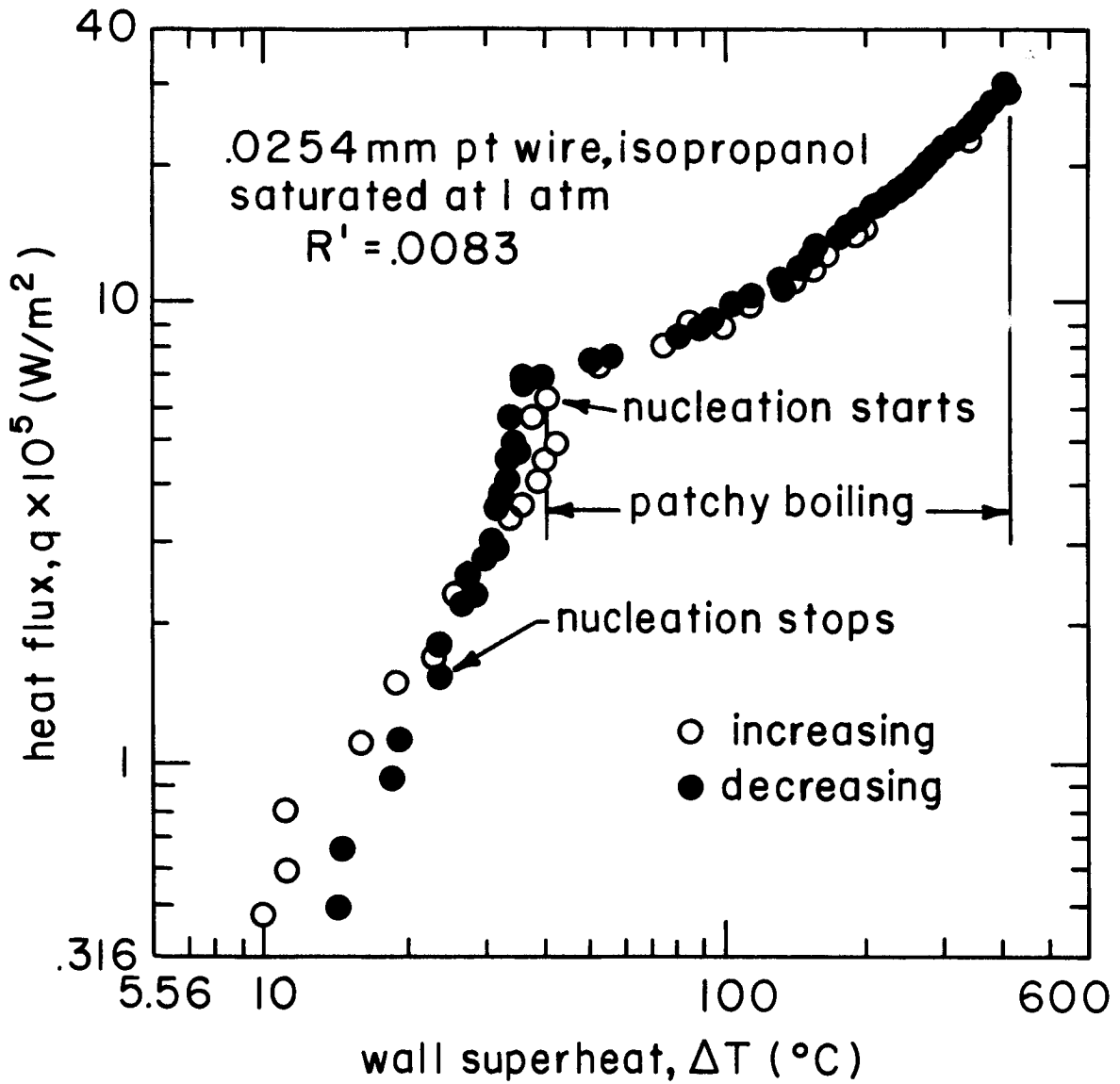


Fig. 64. Boiling curve for .0254mm platinum wire in isopropanol.

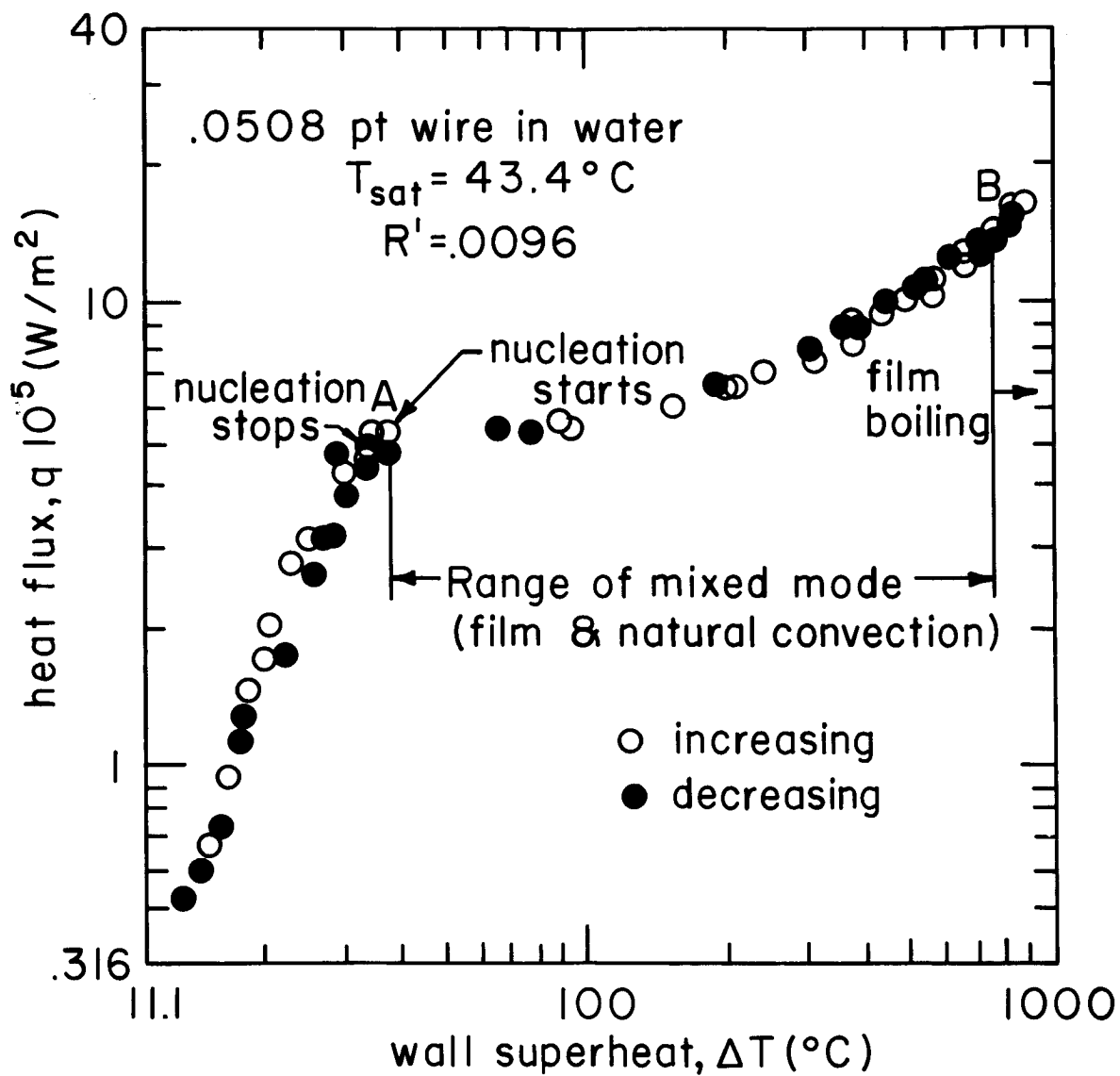


Fig. 65 Boiling curve for .0508 platinum wire in water.

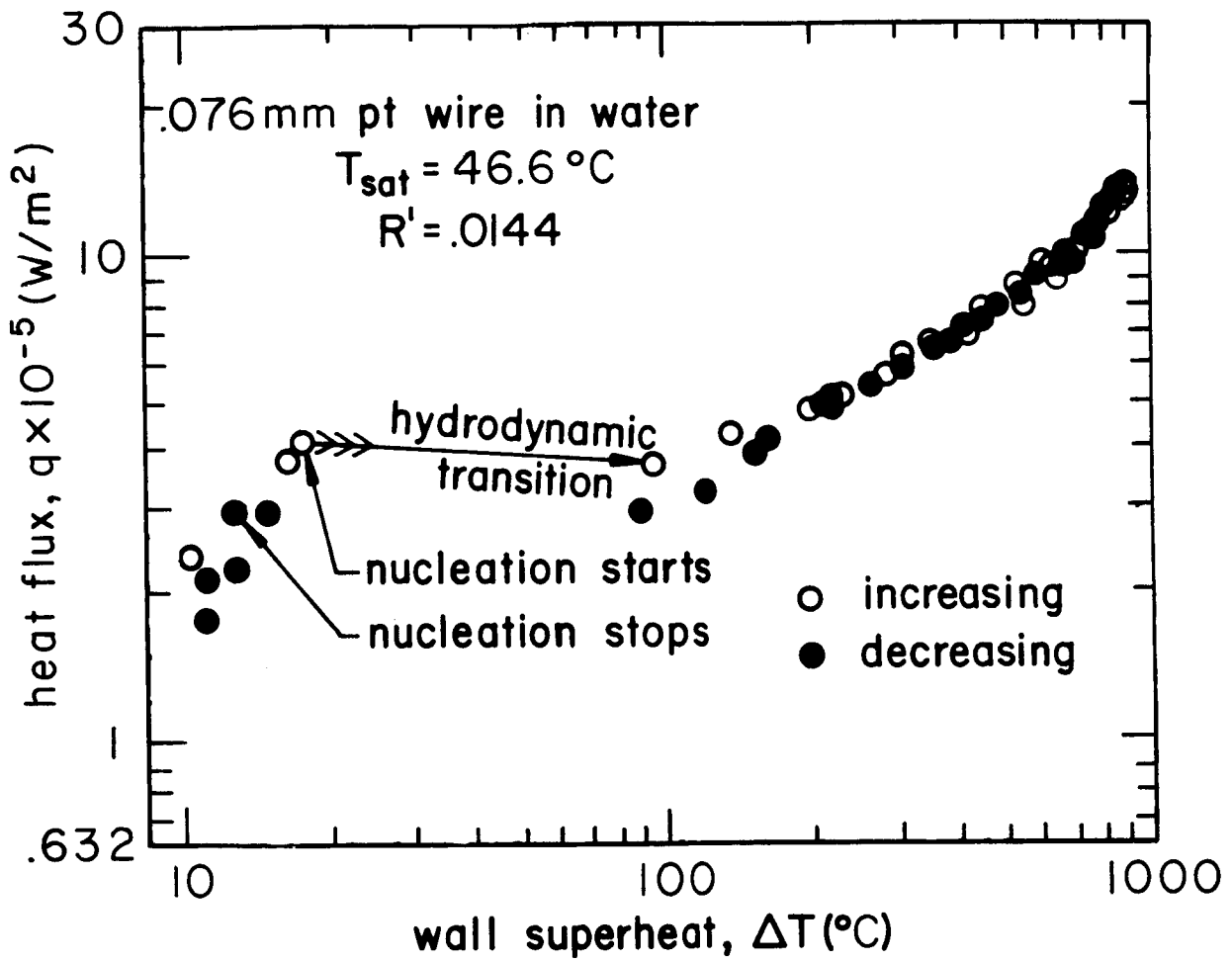


Fig. 66. Boiling curve for 0.076 mm platinum wire in water.

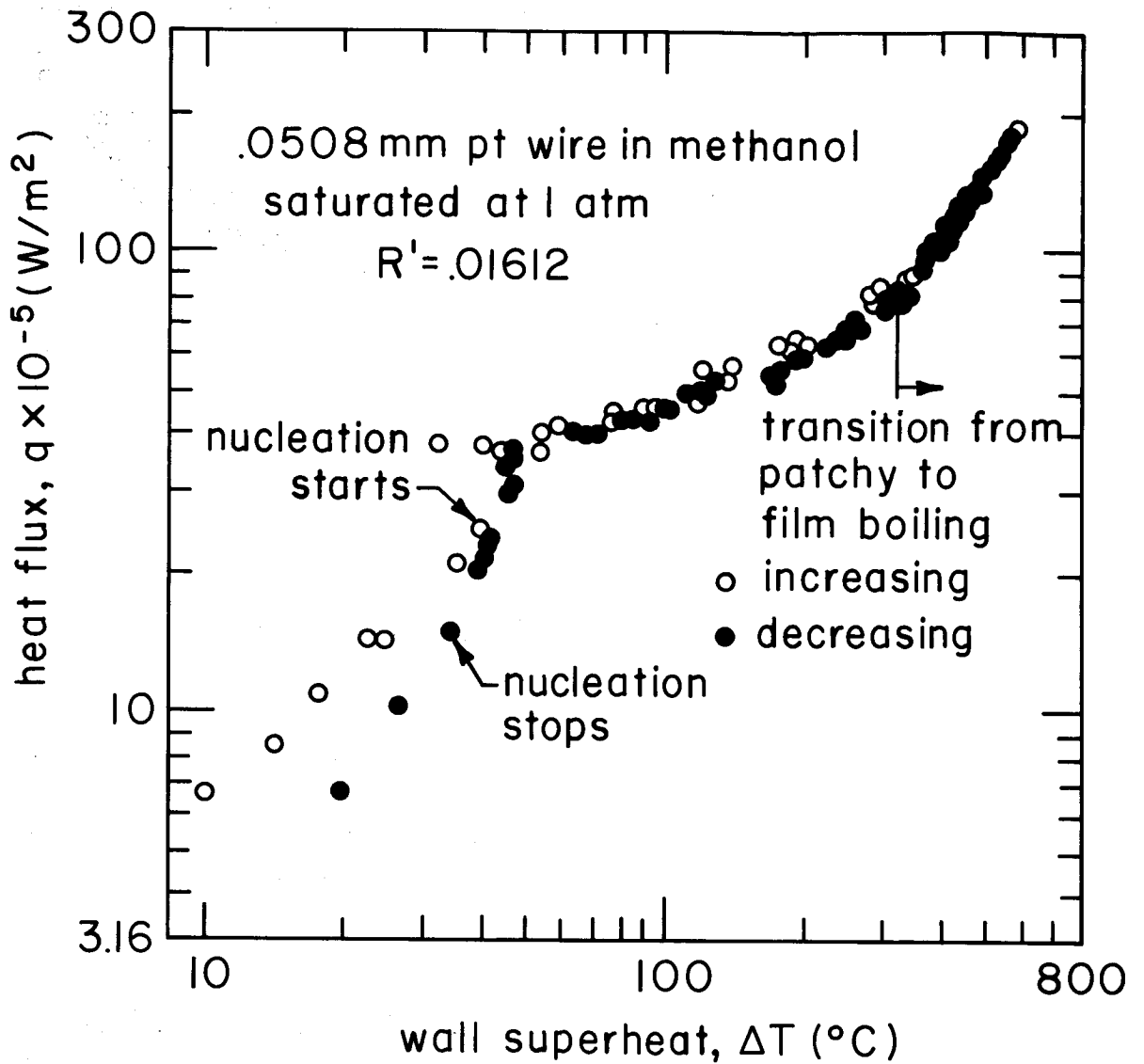


Fig. 67 Boiling curve for .0508 mm platinum wire in methanol.

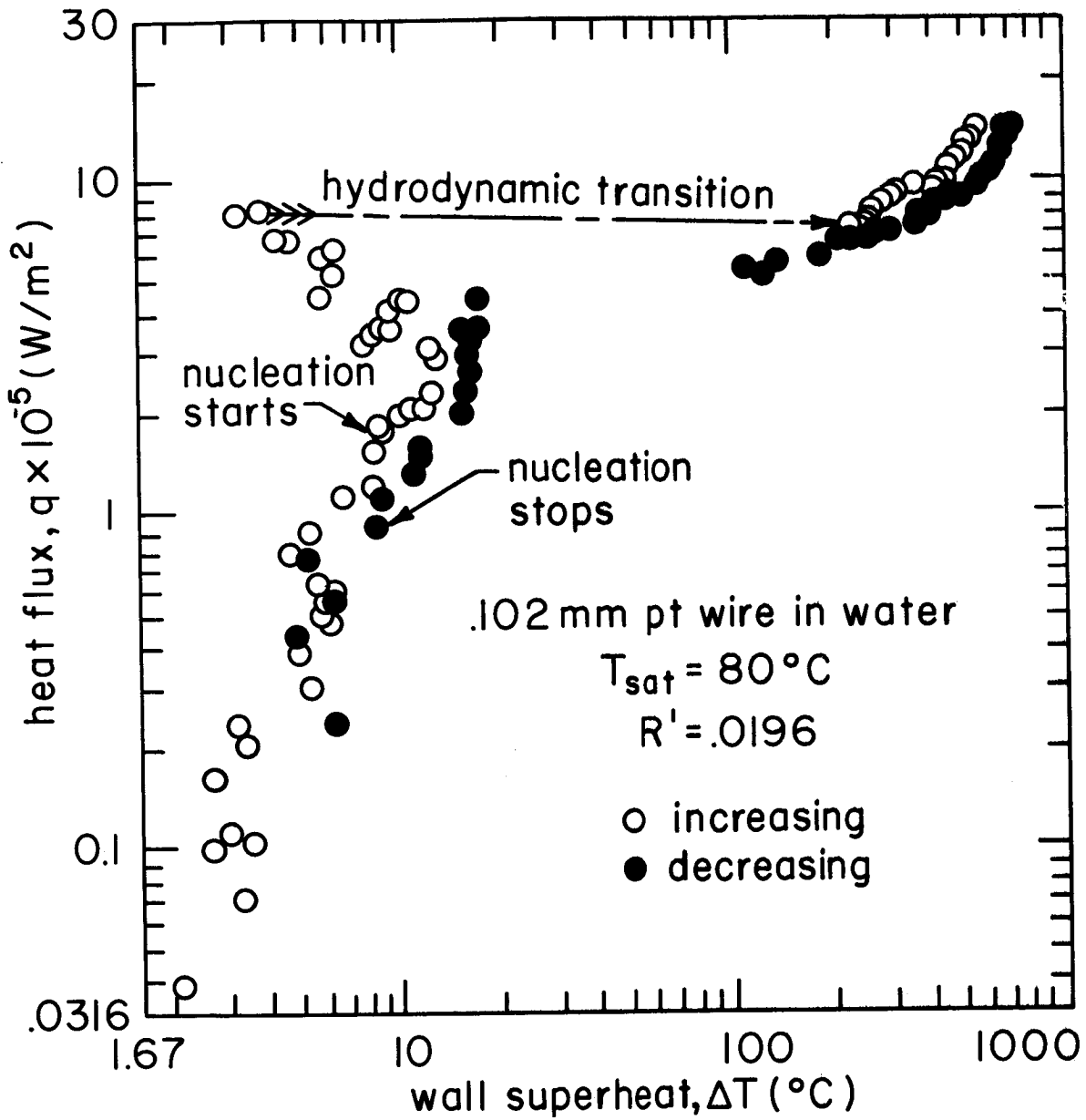


Fig. 68 Boiling curve for .102 mm platinum wire in water.

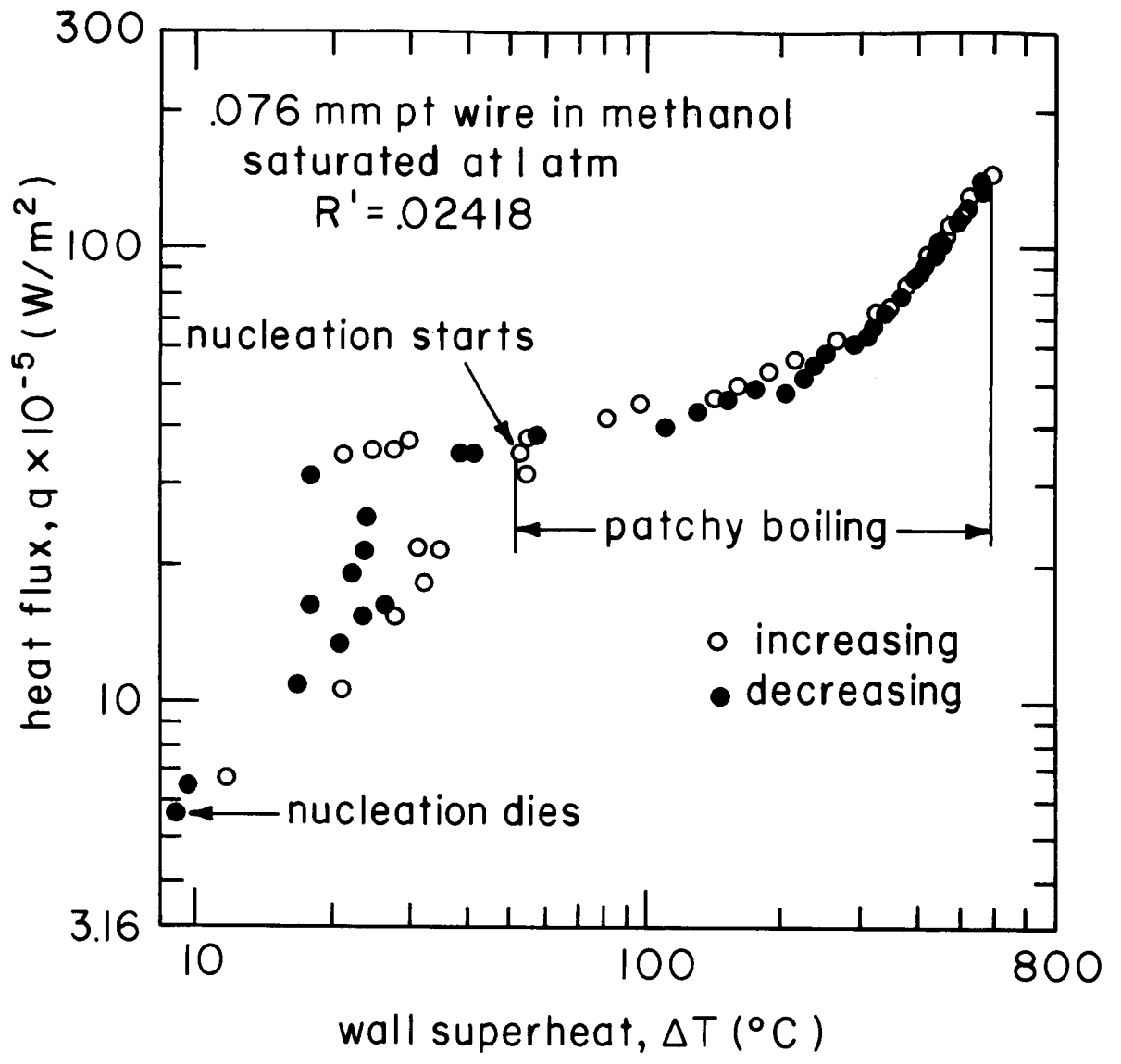


Fig. 69 Boiling curve for .076 mm platinum wire in methanol.

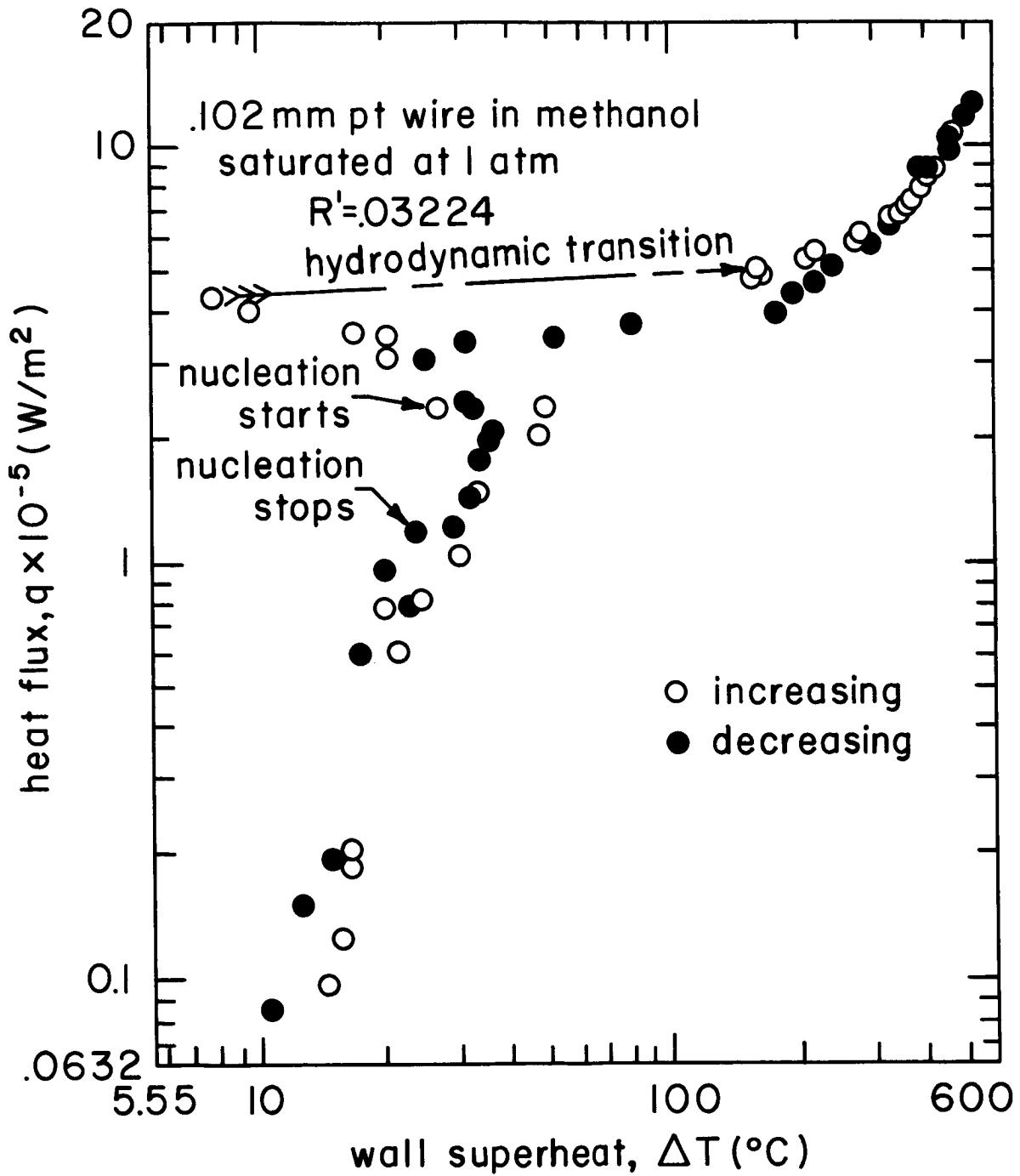


Fig. 70. Boiling curve for .102 mm platinum wire in methanol.

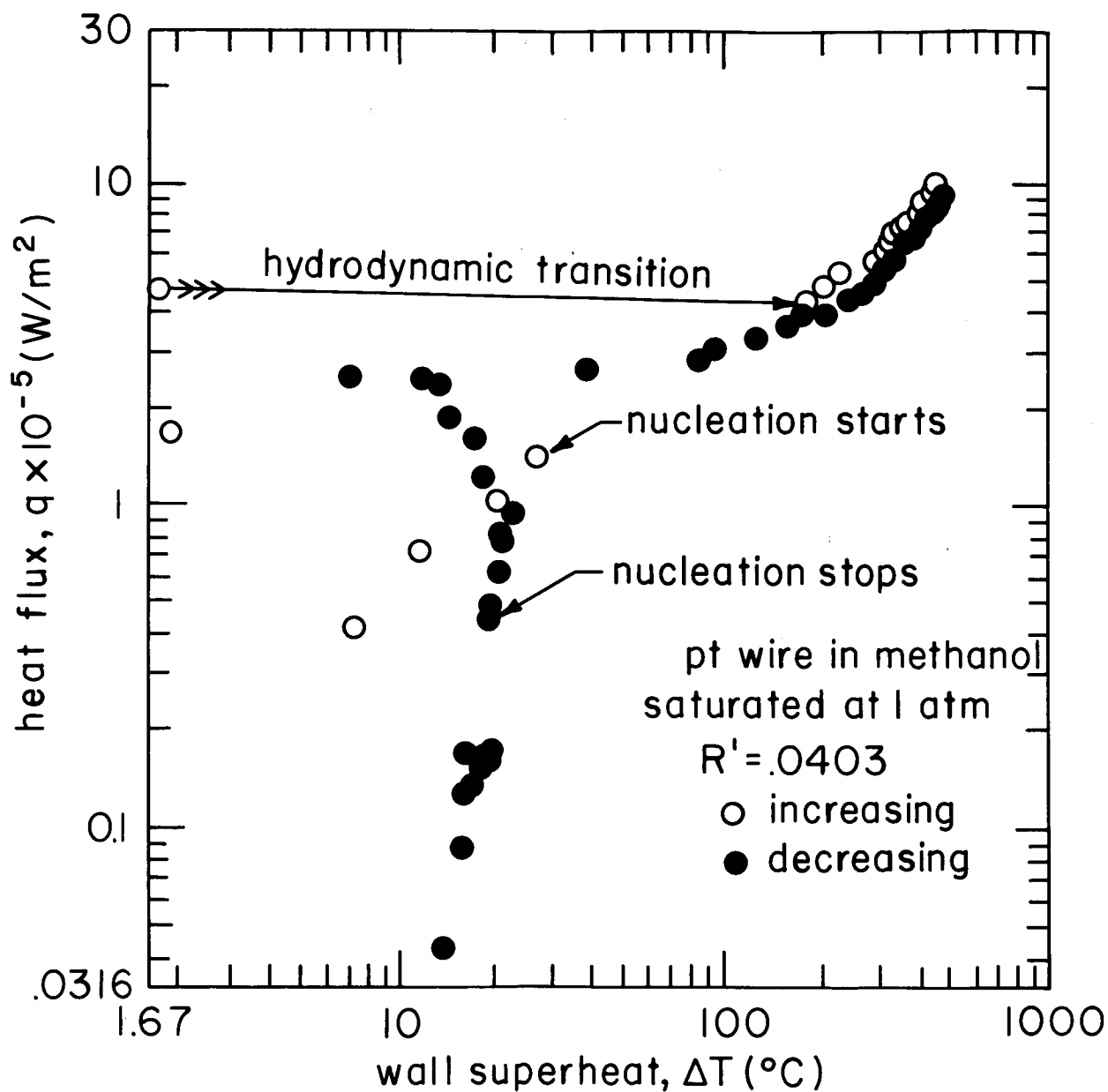


Fig. 71. Boiling curve for .127 mm platinum wire methanol.

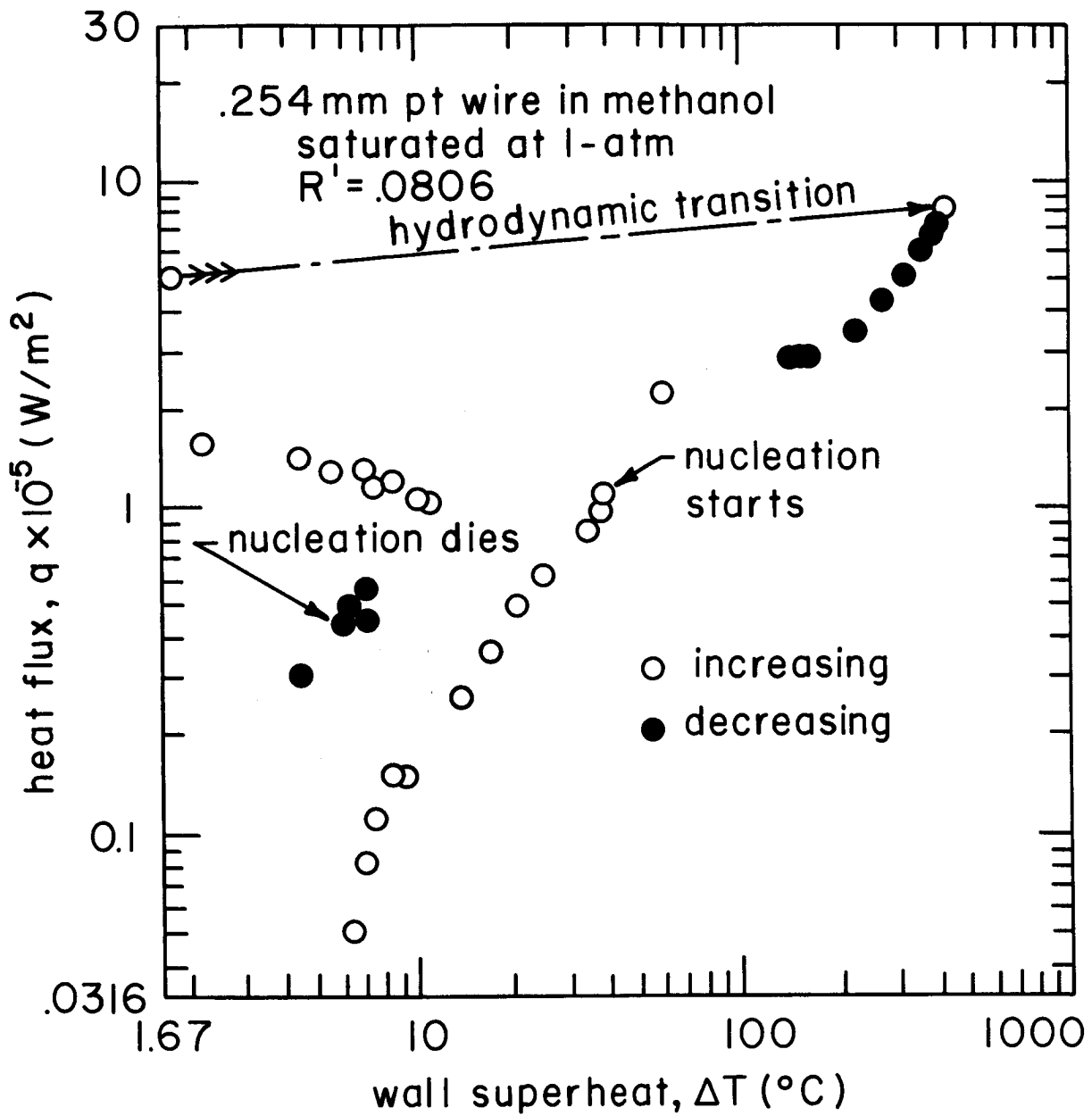


Fig. 72 Boiling curve for .254 mm platinum wire in methanol.

Still and high-speed motion pictures were made during the boiling process. For small  $R'$ , the still pictures were similar to pictures presented by several previous authors for small wires at high heat fluxes (e.g. [84] and [86]) as well as to those presented for large wires at low gravity (e.g. [85] and [87]). The first nucleation resulted in a bubble which grew and spread horizontally until the wire was partially blanketed with a vapor patch. As  $q$  was increased, the fraction of the wire covered by vapor increased until the wire was totally blanketed.

The photographs very strongly suggested that the blanketed portions of the wire were fully covered with vapor and that there was no liquid-to-heater contact within them. While these patches are properly to be called "film boiling" they exhibited none of the Taylor wave process. Instead, vapor removal was accomplished when buoyancy alone overbalanced surface tension, so that fairly large bubbles rose in an irregular way.

The motion pictures provided details of patch growth and collapse. Figure 73 shows a tracing made from a 10-frame motion picture sequence during the growth of a patch on a wire in methanol. In the organic liquids that we used, patches would rapidly grow in this way and then collapse. Thus the vapor patches would flicker on and off from place to place on the wire. However, the patches were very stable in water. They would establish themselves and then spread steadily as the heat flux was increased, until the wire was totally blanketed.

The boiling curves show that for  $R' \leq 0.01$  the monotonic small-wire mechanisms are completely established. As  $R'$  is increased from 0.01 to about 0.03, two phenomena appear: One is the onset of hydrodynamic transition in the sense that nucleate boiling occurs first, and then undergoes a discontinuous transition to film boiling. The other phenomenon is a temperature overshoot on the rising heat flux curve. The resulting hysteresis in the curve becomes quite pronounced as  $R'$  is further increased to 0.08. The hydrodynamic mechanisms, of course, will only be fully re-established for  $R'$  values of about 0.12 or 0.15 -- well beyond the range of the present tests.

There are thus four distinct processes to consider in greater detail. They are:

- 1.) Natural convection from small wires.
- 2.) The inception of boiling

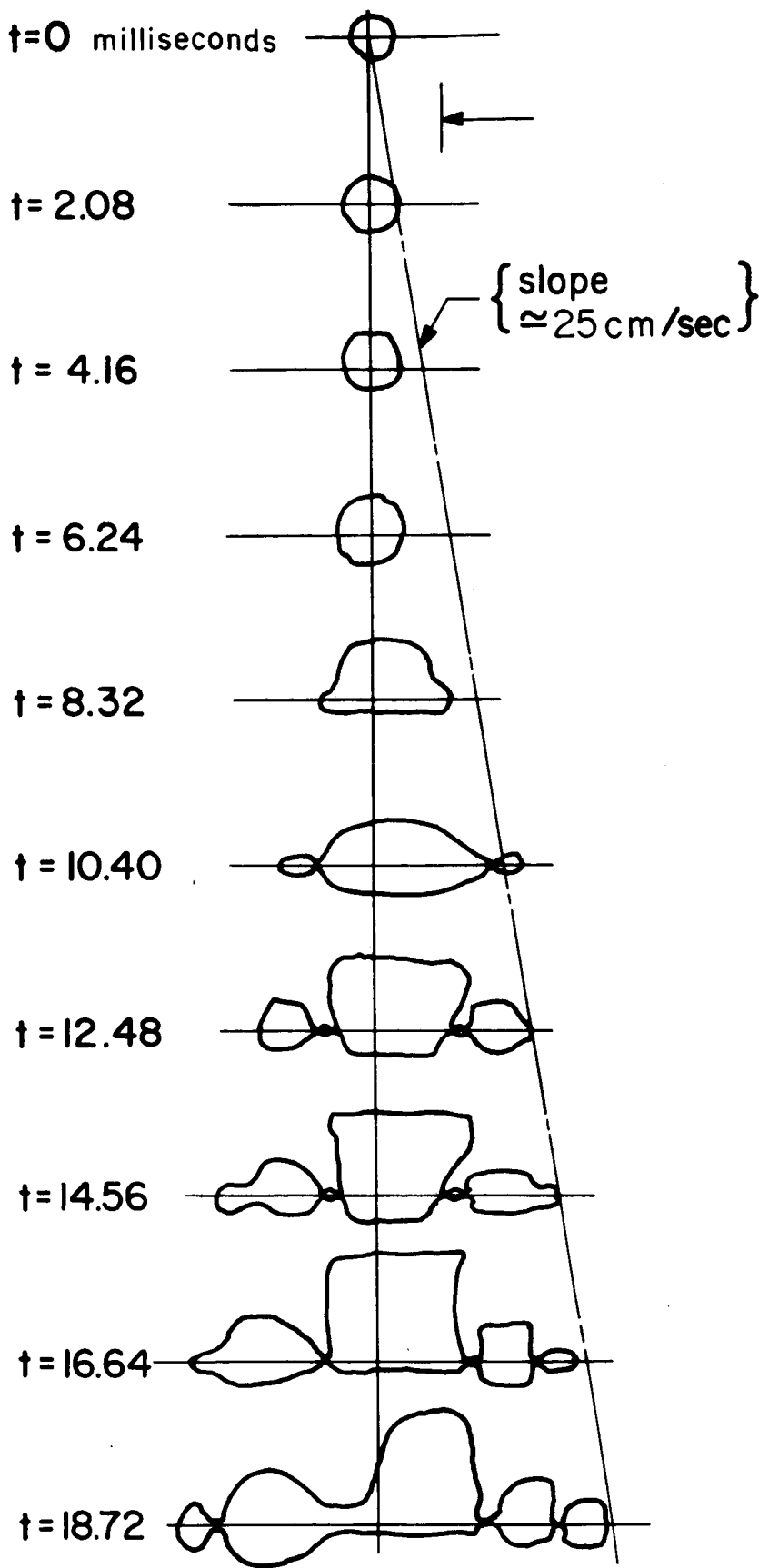


Fig. 73 A vapor patch propagation traced from a ten-frame motion picture sequence. Methanol on a 0.254 mm pt wire.  $R' = .008$ ,  $q = 521,000 \text{ W/m}^2$

3.) The mixed-mode, or combined film-boiling and natural convection, regime.

4.) Film boiling from small wires.

The nucleate and transition boiling regimes do not appear in the list since they do not occur when  $R'$  is small.

Of these processes we shall concentrate on the last three. Bakhru's [21] consideration of the natural convection data presented in Figs. 61 through 72 revealed that they were generally consistent with the results of many investigators, as have been correlated by McAdams [90], and that their scatter was generally comparable. A few points close to boiling inception fell somewhat above McAdams curve, probably owing to thermocapillary jetting from potential nucleation sites. This process is a Marangoni effect which has been discussed by a variety of investigators (see e.g. Trefethen [91], [92]). Such jetting was evident in our experiments and is discussed at greater length in [20]. For larger heaters, on which  $R'$  is small by virtue of low gravity, the conventional natural convection correlations for cylinders should apply perfectly well.

### The Inception of Boiling

Double equilibrium of unstable nuclei. In 1961, Hsu [93] pointed out that when a nucleus bubble protrudes into liquid with a non-uniform temperature profile at a wall, there are two equilibrium positions that it might assume. Brown [94] subsequently described this process for a steady temperature profile, in the following way:

The temperature profile at the wall is given in terms of the heat flux,  $q$ , and distance,  $y$ , from the wall, as

$$T = T_w - qy/k \quad (119)$$

The rate of change of temperature with pressure inside the bubble is given by the Clausius-Clapeyron equation as  $dT/dP = T_{\text{sat}} v_{\text{fg}}/h_{\text{fg}}$ . If we take the  $T_{\text{sat}} v_{\text{fg}}/h_{\text{fg}}$  as nearly constant over the small temperature ranges of interest, integrate between  $T_{\text{sat}}$  and  $T$  of interest, and finally introduce the Laplace equation ( $P - P_{\text{sat}} = 2\sigma/r$ ), we get the relation between the temperature in a bubble and its radius,  $r$ , as

$$T = T_{\text{sat}} \left[ 1 + \frac{v_{\text{fg}}}{h_{\text{fg}}} \frac{2\sigma}{r} \right] \quad (120)$$

Now, with reference to Fig. 74, let us consider a hemispherical nucleus protruding into a liquid whose temperature is given by equation (119). At a point,  $r = y$ , for which the temperatures given by equations (119) and (120) are equal, the cap of the bubble will be in equilibrium. However, the liquid around the equatorial region will be hotter than the gas inside, and evaporation will occur. This will cause the bubble to grow a little larger, forcing the cap into cooler liquid until a balance is struck between condensation at the cap and evaporation at the base of the bubble. Thus the equilibrium radius will be just a little in excess of the  $r$  for which the  $T$ 's given by equations (119) and (120) are equal.

Depending upon the parameters of equations (119) and (120), three situations can exist as suggested by Fig. 74. If there is no intersection, the shape of any liquid-vapor interface that might exist in the cavity is determined, not by equations (119) and (120), but by such features of the cavity as the contact angle and the presence of non-condensable gases. If the curves simply fall tangent there is a single equilibrium radius, a little larger than  $r_2$ . If the temperature distribution in the liquid near the wall is still steeper, there will then be two possible equilibrium points one of which will be a little larger than  $r_3$ . The other equilibrium radius is smaller than the existing site in this case; hence it would have been triggered already in the cavity depicted. If the cavity were smaller, either site could exist.

The double radii are stable with respect to slow changes of  $q$  (and of the temperature gradient) until the smaller radius becomes too small for the cavity. The larger radius will trigger if its size is somehow altered quickly enough that inertia will cause it to overshoot its equilibrium. Accordingly the group at M.I.T. named these larger nuclei, "metastable bubbles" and they noted experimental examples of their metastable behavior [94, 95]. We shall have two occasions in the present discussion to point out their influence.

Nucleation<sup>12</sup> hysteresis. In all cases, nucleation occurred in Bakhr'u's tests at temperatures well in excess of that predicted by equations (119) and (120) for  $r_2$ . Furthermore nucleation always began at temperatures a good deal larger than those at which it stopped.

---

<sup>12</sup>We use the word "nucleation" to denote the inception of bubble growth whether it leads (as in the case of small  $R'$ ) directly to film boiling or (as in the case of larger  $R'$ ) to nucleate boiling.

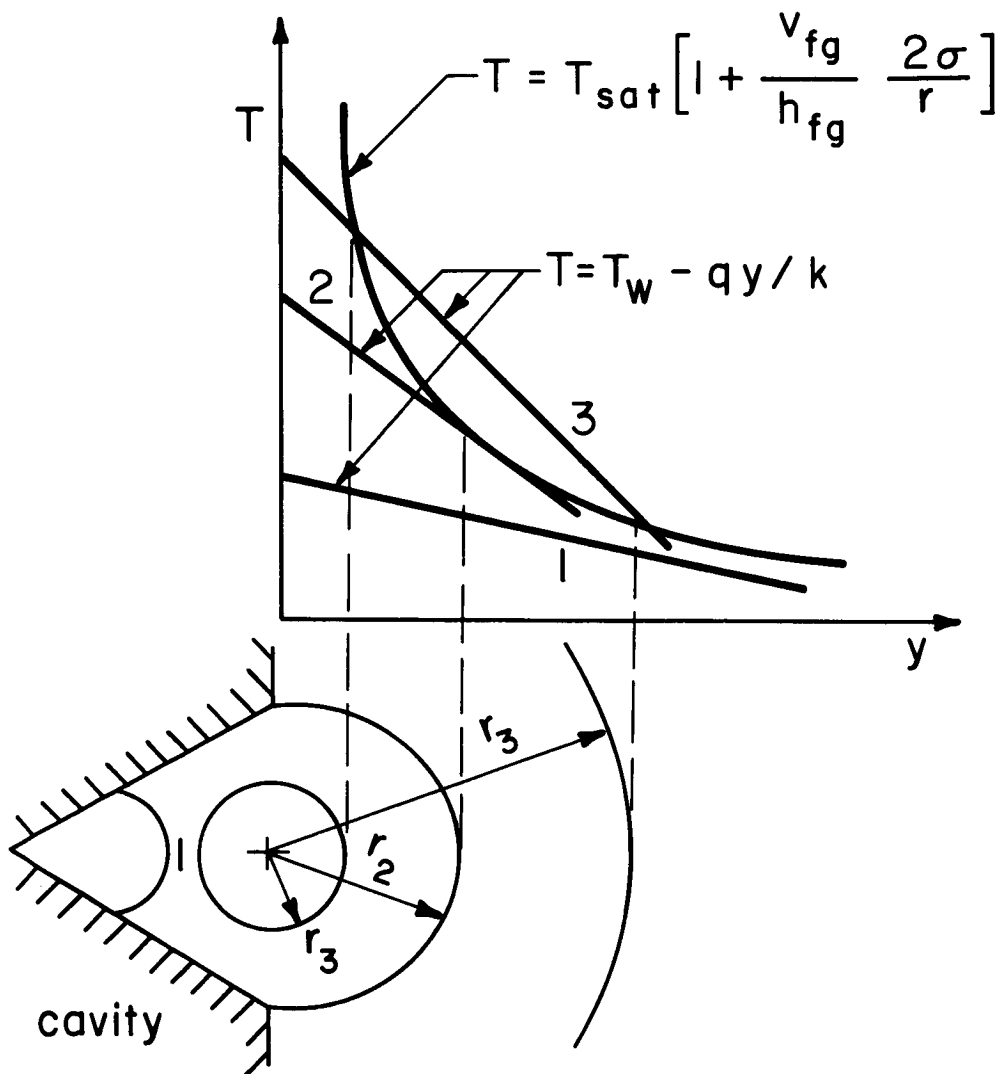


Fig.74. Equilibrium nucleus radii in a temperature gradient near a wall.

Thus a "metastable bubble" undoubtedly gave rise to nucleation, and nucleation terminated when the temperature fell below the triggering temperature for the cavity. The disparity between the two points is called "nucleation hysteresis".

Temperature overshoot hysteresis. The phenomenon of temperature overshoot is well known. In prior studies, both Bakhru and Lienhard noted [95, 96] that when nucleation occurs the temperature sometimes drops back before continuing to rise with  $q$ . Then, the decreasing heat flux traverse usually drops to the right of the nucleation heat flux and meets the convection regime with much less discontinuity. Several other authors, all the way back to Corty and Faust [97], have noted this hysteresis. In the present case the magnitude of the temperature overshoot diminishes with wire size as is shown in Fig. 75--a plot of the temperature drop at inception,  $\Delta T_{OV}$ , against wire size.

It is commonly argued (see, e.g. [97, 98]) that the overshoot occurs because the first nucleation triggers many adjacent sites and a sudden onset of widespread boiling cools the heater. Before the first boiling occurs, the larger nucleation sites which would normally have triggered inception, are initially filled with liquid and they do not function at low temperatures. But as the heat flux is decreased the sites, having filled with vapor and begun to function, will continue to function down to low temperatures, thus shifting the return traverse to the right and causing a hysteresis. That the temperature overshoot vanishes with decreasing wire size simply reflects the fact that there are fewer and fewer large sites on finely drawn wires.

Thus the nucleation hysteresis should be the same for large wires at low gravity as for these small wires. But the temperature overshoot hysteresis, on the other hand, could not be expected to vanish on large wires at low gravity the way it does here.

### Mixed-Mode Boiling

Vapor front propagation. Figure 73 suggests an important aspect in the growth of a vapor patch, namely that it spreads with a constant velocity. This behavior was reproducible in many motion picture runs for wires in methanol and it was evident in the other organic liquids, but not in water. Since this spreading behavior is a primary feature of the mixed-mode regime it should be treated in detail.

Figure 76 shows the advancing vapor patch in a coordinate frame

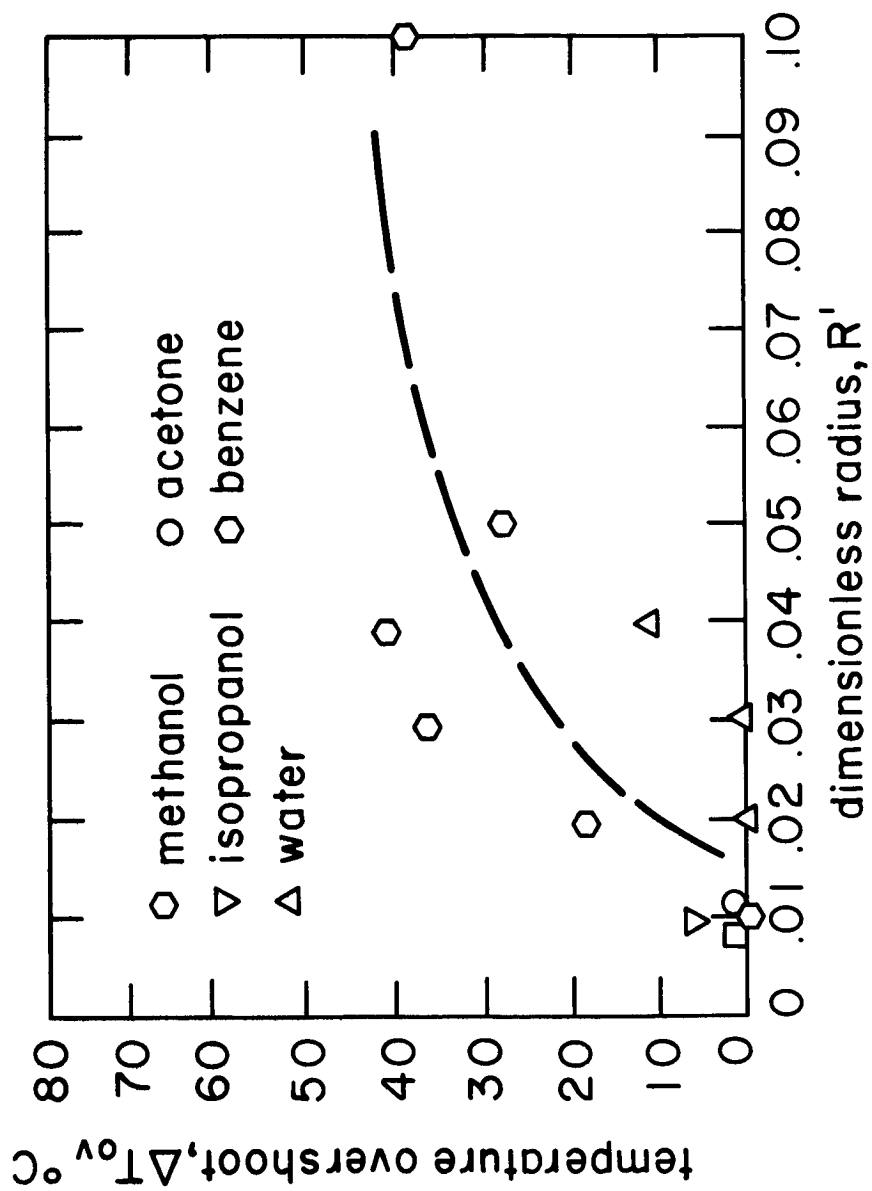


Fig. 75 Influence of heater size on temperature overshoot.

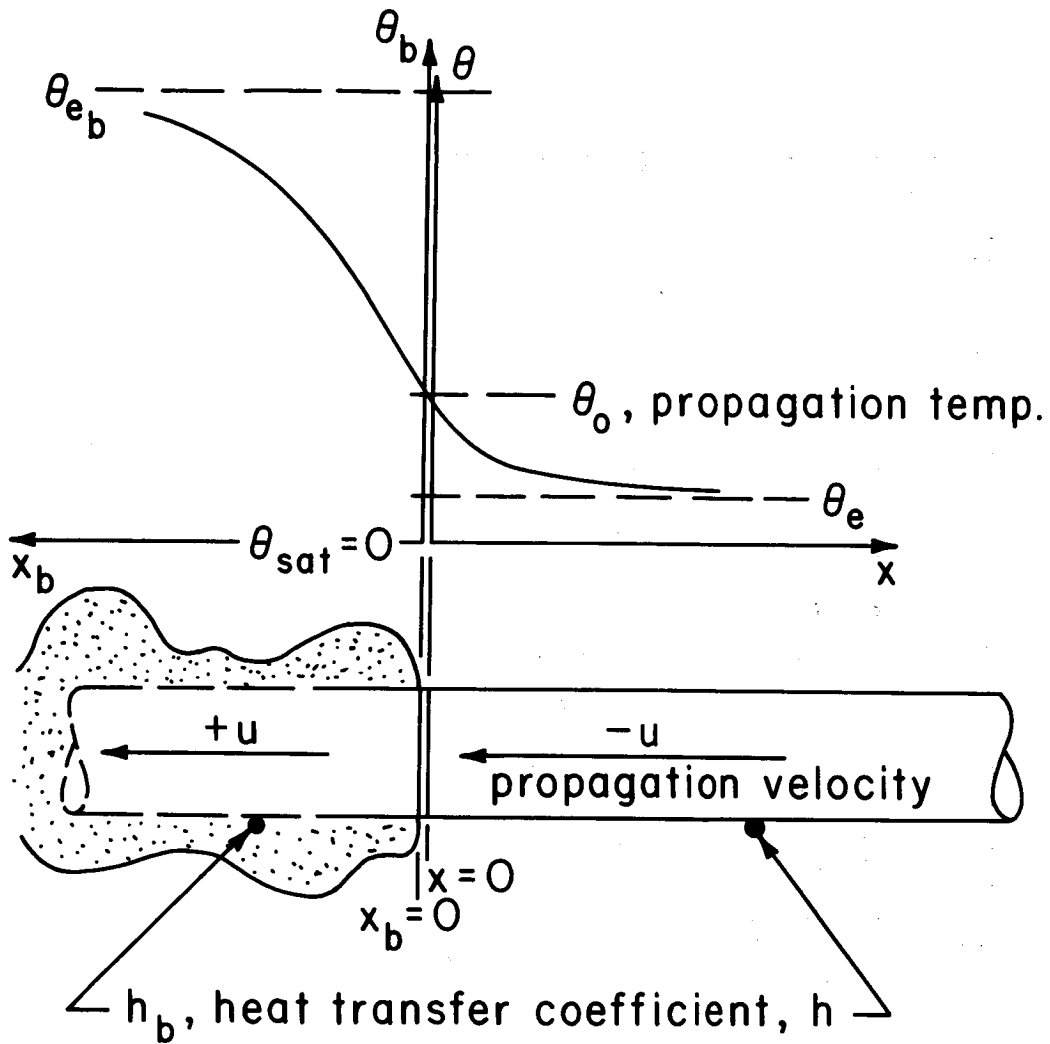


Fig. 76 Steady-state representation of advance of a vapor patch.

that moves with the speed of propagation,  $u$ . Thus the liquid-vapor interface is fixed while the wire moves into it with a speed,  $u$ . Defining  $\theta \equiv T - T_{\text{sat}}$ , one can write the equilibrium wire temperatures under the patch and in the liquid as  $\theta_{e_b}$  and  $\theta_e$ , respectively.

The aim now is to determine the propagation or "triggering" temperature  $\theta_o$ , that is consistent with an observed propagation speed. This will then help to reveal the mechanism of propagation. In particular, it should reveal whether the interface propagates at the Leidenfrost temperature or at a nucleation temperature.

The heat conduction equation for the wire is easily obtained from the familiar fin equation as long as the transverse Biot number,  $hR/k$ , is small:

$$-\frac{u}{\alpha} \frac{d\theta}{dx} = \frac{d^2\theta}{dx^2} + \frac{2q}{k_w R} - \frac{2h}{k_w R} \theta \quad (121)$$

where  $q$  here designates the local heat flux. It will be less in the unblanketed portion of the wire since the temperature (and electrical resistance) are lower in that portion. Equation (121) will apply to either the blanketed portion of the wire (hereafter designated with the subscript,  $b$ ) or to the unblanketed portion. The boundary conditions are

$$\theta(\infty) = \theta_e; \quad \theta_b(\infty) = \theta_{e_b}; \quad \left. \frac{d\theta}{dx} \right|_{x=0} = \left. \frac{d\theta_b}{dx} \right|_{x_b=0}; \quad \theta(0) = \theta_b(0) = \theta_o \quad (122)$$

The dependence of the propagation velocity upon system variables is given by  $u = u(\alpha, q, q_b, k_w, R, h, h_b, \theta_o)$  where  $\theta_e$  and  $\theta_{e_b}$  are dependent variables since they equal  $q/h$  and  $q_b/h_b$ , respectively. There are thus 9 variables expressible in 4 dimensions, so the problem reduces to 5 independent dimensionless groups:

$$\theta_o \equiv \frac{\theta_o}{q/h} = \frac{\theta_o}{\theta_e}; \quad Pe \equiv \frac{u}{\alpha\sqrt{2h/k_w R}}; \quad Bi \equiv \frac{hR}{2k_w}; \quad \frac{h_b}{h}; \quad \frac{q_b}{q} \quad (123)$$

The first group is a dimensionless triggering temperature. The second group is a kind of Peclet number involving the familiar fin constant,  $\sqrt{2h/k_w R}$ . It compares the propagation capacity of the vapor front to the conduction capacity of the wire. The Biot number,  $Bi$ , is

typically on the order of  $10^{-3}$  in the present problem, and should therefore exert no influence other than assuring us that radial conduction can be ignored in the total problem. Thus we anticipate a functional equation of the form:  $\theta_o = \theta_o (Pe, h_b/h, q_b/q)$ .

The analytical problem then reduces to a pair of coupled ordinary differential equations:

$$\begin{aligned} \theta'' + Pe \theta' - \theta &= -1 \\ \theta_b'' - Pe \sqrt{\frac{h}{h_b}} \theta_b' - \theta_b &= -\frac{h}{h_b} \frac{q_b}{q} = -\theta_{e_b} / \theta_e \end{aligned} \quad (124)$$

with boundary conditions:

$$\theta(\infty) = 1; \quad \theta_b(\infty) = \frac{q_b h}{q h_b}; \quad \theta'(0) = -\sqrt{\frac{h_b}{h}} \theta_b'(0); \quad \theta(0) = \theta_b(0) = \theta_o \quad (125)$$

where the dimensionless dependent variable is  $\xi \equiv x\sqrt{2h/k_w R}$  or  $\xi_b \equiv x_b\sqrt{2h_b/k_w R}$ . The solution is straight forward and the result is

$$\theta_o = \frac{1 - \frac{h}{h_b} \frac{q_b}{q} \left[ \frac{1 - \sqrt{1 + 4h_b/hPe^2}}{1 + \sqrt{1 + 4/Pe^2}} \right]}{1 - \left[ \frac{1 - \sqrt{1 + 4h_b/hPe^2}}{1 + \sqrt{1 + 4/Pe^2}} \right]} \quad (126)$$

Equation (126) will (by way of an example) now be compared with methanol data for a .0254 mm platinum wire (Figs. 61 and 73). To make the comparison, the blanketed and unblanketed conditions are taken to correspond approximately with the points at either end of the mixed-mode regime in Fig. 61. Here,  $h = 4650$  and  $h_b = 2160 \text{ W/m}^2$ , so  $h_b/h = 1/2.26$ . The temperatures at the end points are such that  $q_b/q = 1.95$ .

Figure 77 displays equation (126) for this  $q_b/q$  and for three values of  $h_b/h$ : 0, 1/8, and the value of 1/2.26 given above. It is clear from

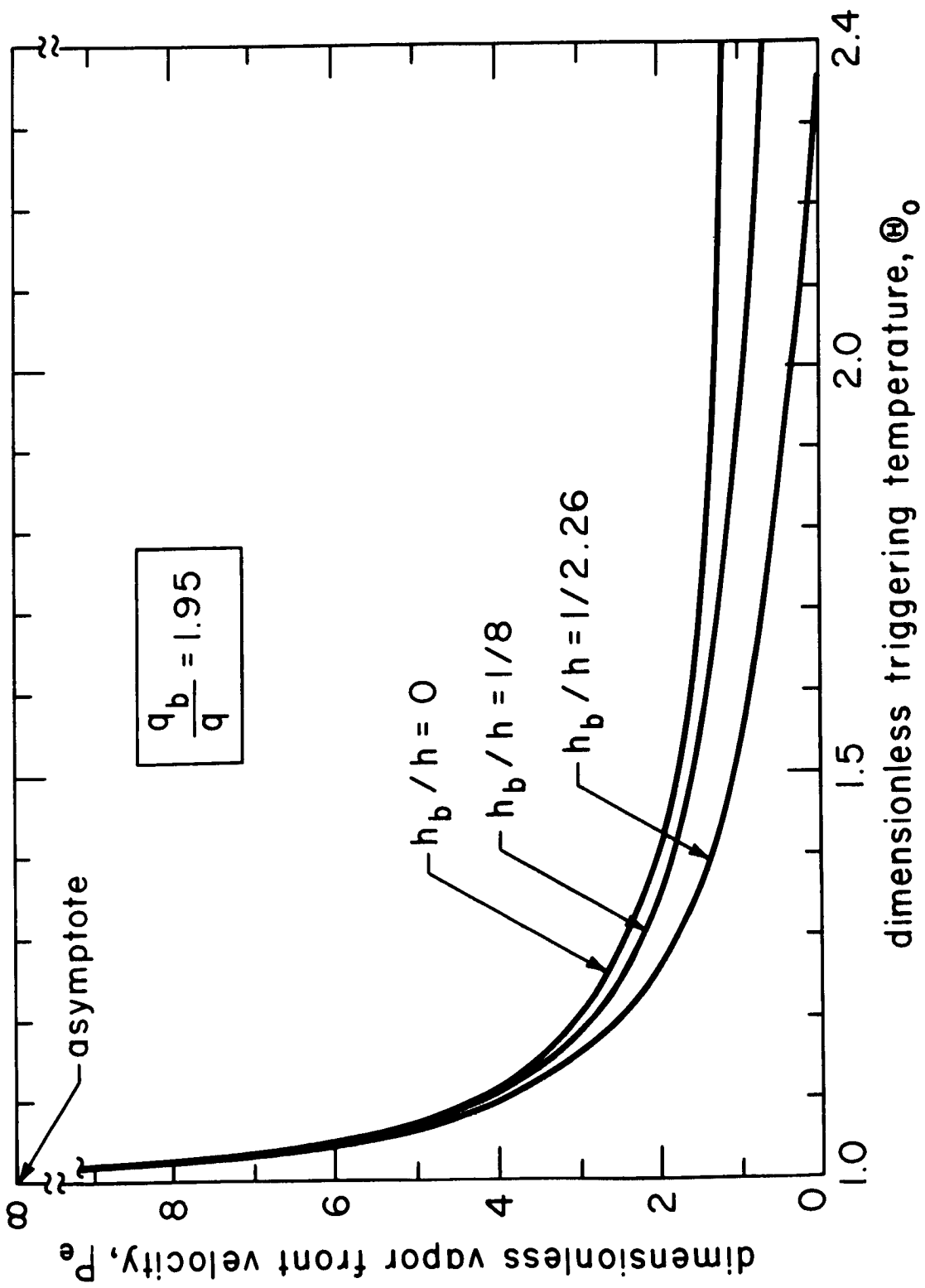


Fig. 7.77 Influence of triggering temperature on vapor front velocity.

the curve that the relation between the dimensionless propagation velocity,  $Pe$ , and the triggering temperature,  $\Theta_0$ , is not too sensitive to  $h_b/h$ . In this case the average value of  $u$  was found to be about 26.2 cm/sec (cf. Fig. 15 where  $u = 25$  cm/sec.) which gives  $Pe = 2.48$ . The corresponding value of  $\Theta_0$  is 1.19, so the vapor front propagates by virtue of a triggering temperature only 19% higher than that which gives rise to the first nucleation.

The triggering temperature for methanol is thus comparatively low -- a typical nucleation temperature -- and definitely not the Leidenfrost temperature. Figure 73 bears this out in that the front appears to be moving by triggering a succession of new bubbles immediately adjacent to it. The patch spreads until so much of the wire is insulated and heated-up that the resistance rises, throttling the current. This reduces the heat flux and the patch must again retreat. The result is the rapid, and apparently random, growth and collapse of patches on the wire.

Non-propagation of the vapor front. One of the liquids used in Bakhru's study -- distilled water -- did not show the propagation of the vapor patch. The patch (or patches) formed in water and spread in direct proportion to  $q$ . The flickering behavior was not present as it was in the various organic liquids.

To see why this should be, one should recall (Figs. 61 through 72) that the nucleation hysteresis was far less pronounced in water than in the organic liquids. But nucleation hysteresis should depend on the presence of "metastable bubbles". Then, equating  $T$  as given by equations (119) and (120), setting  $y = r$  and solving the result for  $r$ , one finds

$$\frac{hr}{k} = \frac{1}{2} \pm \sqrt{\frac{1}{4} - \Lambda} \quad (127)$$

where

$$\Lambda \equiv 2\sigma h v_{fg} T_{sat} / kh_{fg} \Delta T \quad (128)$$

The ratio of the two possible radii given by equation (127) will be real if nucleation occurs. Thus:

$$\frac{r_{big}}{r_{little}} = \frac{1 + \sqrt{1 - 4\Lambda}}{1 - \sqrt{1 - 4\Lambda}} ; \quad \Lambda \leq 1/4 \quad (129)$$

Equation (129) is plotted in Fig. 78. Values of  $\Lambda$  based on the inception point for the smallest wire in each of the five liquids have been calculated and plotted on this curve. It turns out that the ratio  $r_{\text{big}}/r_{\text{little}}$  ranges between about 60 and 130 for the organic liquids but it is only about 4 for water. Thus there are many large "metastable bubbles" in the organic liquids. These tend to be triggered by the disturbances associated with the advancing vapor front, so the patch keeps over-running itself and then collapsing. Since any metastable bubbles in water differ relatively little from ordinary nuclei, the front can trigger only the nuclei very near the vapor-front and the advance is stable.

Using Fig. 63 Bakhru found  $h_b/h = 1/8$  for water on a 0.0508 mm wire. Entering equation (11) with this value and a zero propagation speed (i.e.,  $Pe = 0$ ) he found  $\theta_o \simeq 6.6$  or (since  $\theta_e \simeq 21^\circ\text{C}$ )  $\theta_o \simeq 240^\circ\text{C}$ . The front can thus be at any temperature upto  $\theta = 240^\circ\text{C}$  but it still is not triggering nuclei. Thus, without large metastable bubbles on the wire, only those nuclei immediately adjacent to the vapor-front will be triggered. Furthermore  $\theta_o$  is too low to trigger a Liedenfrost front. This is why the patch doesn't move in this case.

Large cylinders at low gravity would behave like those described here with two possible changes: 1.) The Biot number might become large enough to make the heat conduction problem two-dimensional. This would require a considerably more complicated set of predictive relations than we have offered, possibly without great change in the results. 2.) With more nucleation sites on the cylinder,  $\theta_o$  would probably tend to be lower than it is on small wires.

### Film Boiling

Bromley [99] provided the first analytical prediction of heat transfer from cylinders in 1950. He found that:

$$N_u / (Ra^*)^{1/4} = 0.62 \quad (130)$$

where:

$$Ra^* \equiv \rho_g (\rho_f - \rho_g) h_{fg}^* g (2R)^3 / \mu_g k_g \Delta T \quad (131)$$

In 1962, Breen and Westwater [59] provided a semi-empirical modification of Bromley's equation. For  $2R' < 0.8$  they recommended:

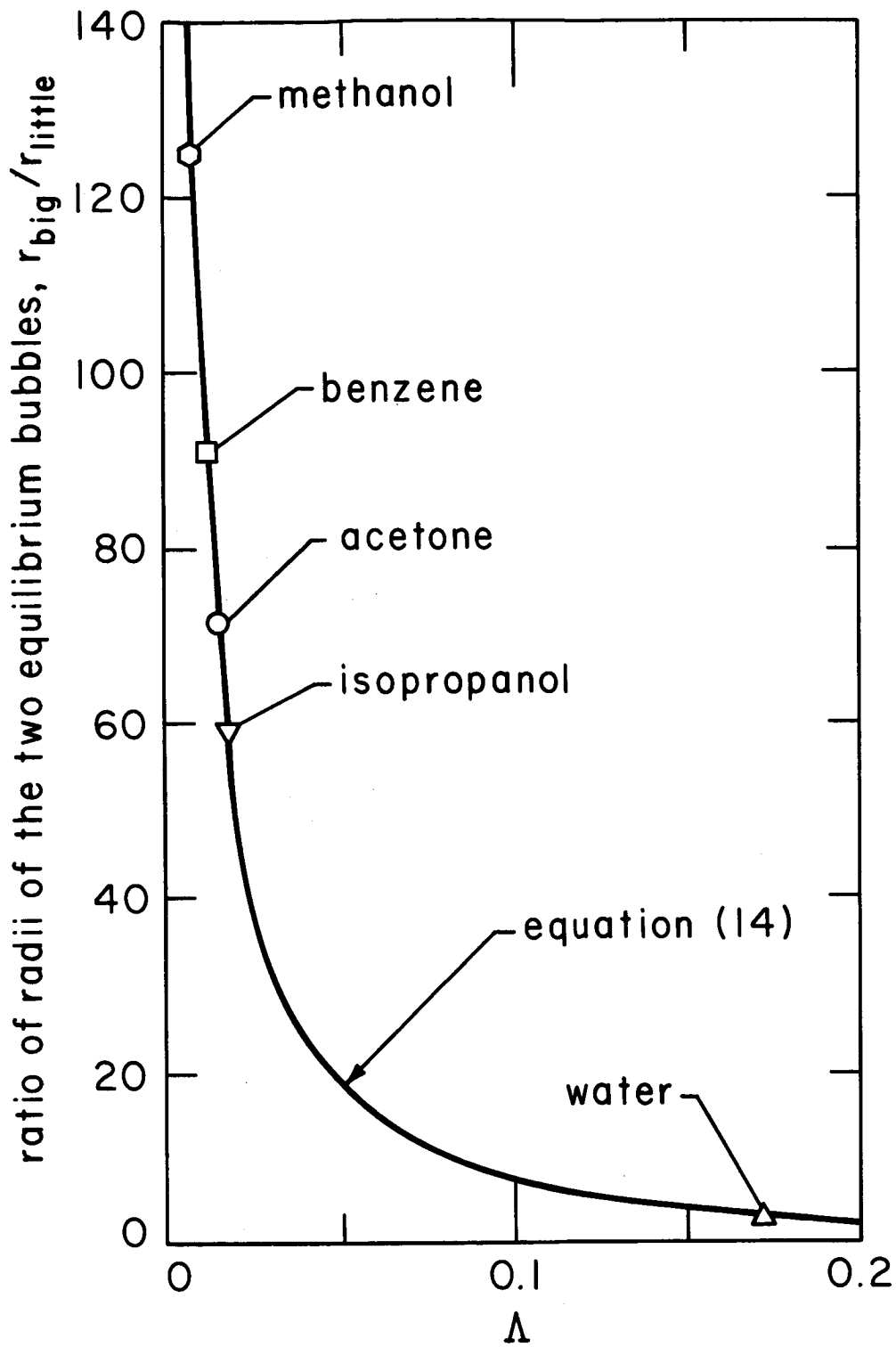


Fig. 78 Radius ratio of equilibrium bubbles at inception for liquids on small wires.

$$\text{Nu}/(\text{Ra}^*)^{1/4} = 0.372(2R')^{1/4} + 0.274/(2R')^{3/4} \quad (132)$$

Finally, in 1967 Baumeister and Hamill [58] derived the following relation

$$\text{Nu}/(\text{Ra}^*)^{1/4} = 0.373 \left[ (2R') + 3.68 + \frac{1.088}{(2R')^2} \right]^{1/4} \quad (133)$$

Bakhru plotted his film boiling data on  $\text{Nu}/(\text{Ra}^*)^{1/4}$  vs.  $(2R')$  coordinates as shown in Fig. 79, and included the preceding three expressions for comparison. Bromley's prediction is, of course, low for small  $R'$  and the other two expressions were developed with the objective of improving it. Equations (132) and (133) are a little high and a little low respectively, but either is in reasonable agreement with the available data. Since Baumeister and Hamill's expression is based upon an analytical rationalization that applies to wires of any size, the correlation in Fig. 79 should be valid for either large wires at low gravity or small wires under higher gravity.

It is, of course, possible to fit an empirical curve to the data in Fig. 79 and obtain higher accuracy than either equation (132) or (133) will give. For example

$$\text{Nu}/(\text{Ra}^*)^{1/4} \simeq 0.7(2R')^{1/3} \quad (134)$$

will fit the data nicely.

### Conclusions

1.) The local maxima and minima in the boiling curve which are dictated by hydrodynamic instabilities vanish for all  $R' \leq 0.01$ . The region  $0.01 < R' < 0.15$  is a transition regime in which the hydrodynamic mechanisms re-establish themselves.

2.) Nucleate boiling also vanishes when  $R'$  becomes small.

3.) Natural convection and film boiling on small wires (or on larger cylinders at low gravity) are predictable by conventional methods.

4.) The nature of a monotonic boiling curve between first nucleation and full film boiling has been traced in detail and many of its features have been analyzed. This has been done for the constant electrical current case on small wires. The region is one in which

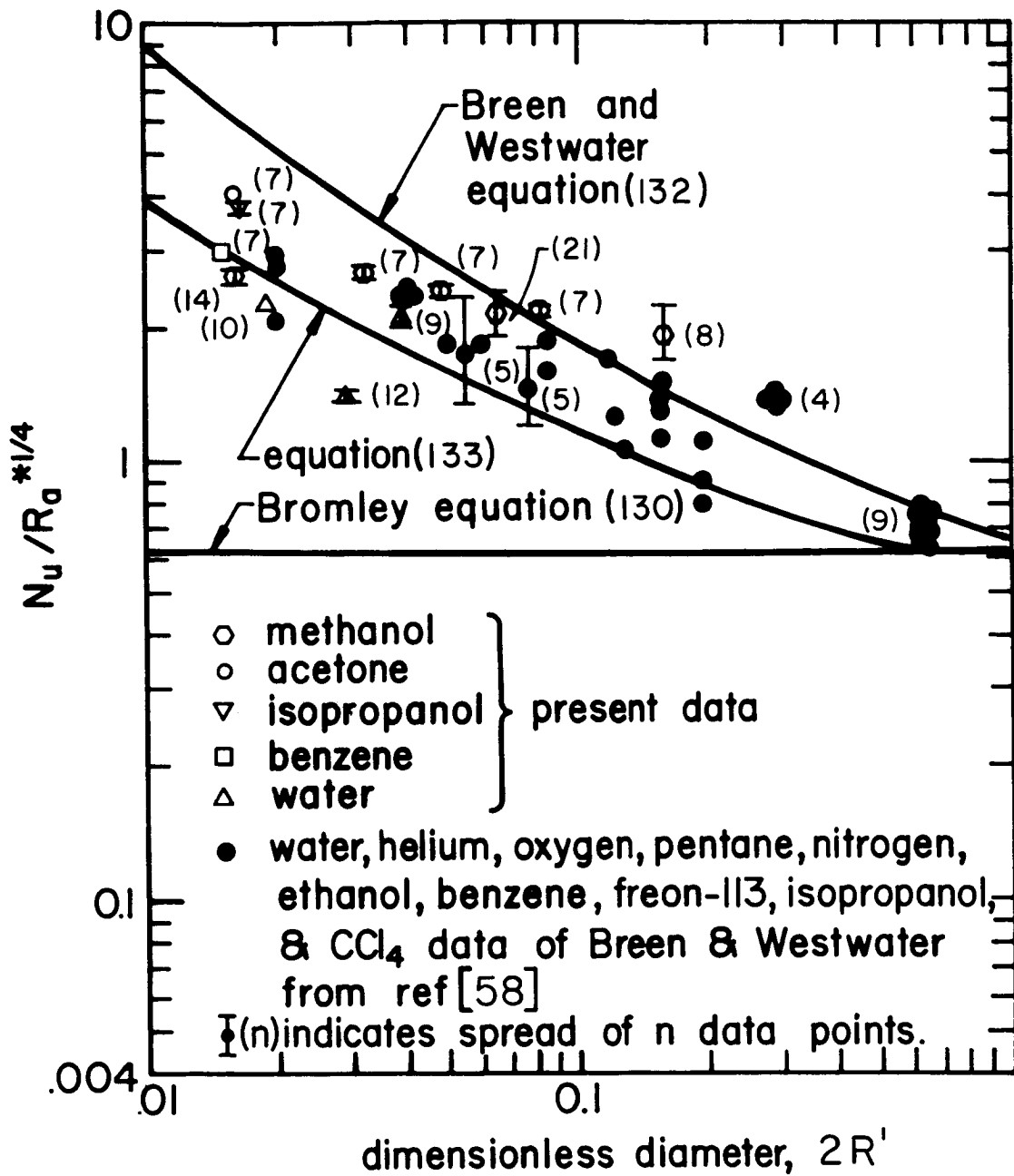


Fig. 79 Correlation for film boiling on small wires.

film boiling and natural convection coexist on the wire. If the parameter  $\Lambda$  is on the order of a few hundredths or less, patches of film boiling flicker on and off over the wire. If  $\Lambda$  is larger than one or two tenths, the patches are steady and grow only with increasing heat flux. The analytical descriptions of the mixed-mode regime can generally be applied to large cylinders at low gravity as well.

5.) Values of  $q_{\max}$  hitherto reported by many investigators (e.g. [84], [85], [86] for  $q_{\max}$  at  $R' < 0.03$  have probably been either  $q$  at the inception of film boiling, or values of  $q$  for which the temperature first began to increase rapidly, or possibly values of  $q$  for which the heater first glowed red. In any case, such data are not meaningful since there is no longer a real local maximum to measure.

## VIII. CONCLUSIONS

Motivated by a need to know the influence of gravity on the boiling transitions, we have spent five years exploring the hydrodynamic mechanisms giving rise to these transitions. During the past three years these studies have been quite fruitful. In particular they have yielded major extensions of the hydrodynamic theory which, we believe, make a powerful problem-solving tool of the theory. The work has led to the following specific results:

A. A broad scheme for predicting the peak pool boiling heat fluxes on a variety of heaters in low viscosity liquids. This material is developed in Chapters II and III. Predictions involving few or no empirical constants are developed for the following configurations:

- 1.) Horizontal flat plates without induced side flow:
  - a) "infinite" plates (equation (15), Fig. 7)
  - b) finite plates (equation (16), Figs. 8 and 9)
- 2.) Horizontal circular cylinders
  - a) large (equation (31), Fig. 13)
  - b) small (equation (37), Fig. 13)
- 3.) Spheres
  - a) large (equation (38), Fig. 16)
  - b) small (equation (30), Fig. 16)
- 4.) Horizontal ribbons, vertically oriented
  - a) both sides uninsulated
    - (i) large (equation (34), Fig. 18)
    - (ii) small (equation (41), Fig. 18)
  - b) one side insulated
    - (i) large (equation (34), Fig. 19)
    - (ii) small (equation (42), Fig. 19)

In addition to making these predictions we have provided:

- 5.) Copious experimental verification of each prediction.
- 6.) Theoretical and experimental values of the vapor blanket thickness at the peak heat flux. (Fig. 12 and pg. 31).

- 7.) General guidelines for predicting  $q_{\max}$  on a variety of finite heater configurations. For these generalizations the reader should see pages 48 and 50 of the Conclusions of Chapter III.

B. Theoretical descriptions of the Taylor and Helmholtz stability mechanisms underlying the hydrodynamic theory of the boiling transitions. Solutions of these problems, although developed for application to boiling heat transfer, have potential application in any of a large variety of two-phase dynamical configurations. The two problems are:

- 1.) the prediction of Taylor instability in the top of the interface between a horizontal gaseous cylinder and the surrounding viscous liquid. The horizontal plane interface between a gas (below) and a viscous liquid (above) is obtained as the special case for large radius. The analytical solution is given in Figs. 23 through 26. The results show that viscosity slows the growth rate of Taylor waves and considerably increases their length.
- 2.) the prediction of the maximum velocity of gas for which a vertical jet in a viscous liquid remains stable. This result is given by equation (105) in which the three decimal-constants must be viewed as arbitrary.

C. Experimental studies of film boiling. A variety of new data have made possible:

- 1.) a verification of the predicted Taylor wavelengths and frequencies for viscous liquids. (Figs. 35 through 38).
- 2.) an empirical correlation of vapor blanket thickness during film boiling. (Fig. 28).
- 3.) an empirical correlation of an observed stretching of the wavelength at high vapor volume fluxes, independent of the influence of viscosity. (Fig. 45).
- 4.) verification of the lack of correlation between bubble frequency and wave "frequency" in film boiling. (pgs. 91 and 97, and Fig. 44).

D. Peak and minimum pool boiling heat fluxes in viscous liquids.

- 1.) Item B-2, above, was used in the formulation of a theoretical expression for  $q_{\max}$  in viscous liquids. (equation (105))
- 2.) Original data provided verification of the viscous  $q_{\max}$  theory. (See Figs. 50 and 51 and Conclusions on page 117).
- 3.) It is shown, analytically, that viscosity influences  $q_{\min}$  in complicated and conflicting ways (pg. 101). This problem is left unresolved.

E. Hydrodynamic theory of high current-density electrolysis. Like the pool boiling heat flux, the current density during electrolysis passes through a peak, after which a film electrolysis region is established. It is predicted, by Bhattacharya, and verified experimentally, that this peak corresponds with Moissis and Berenson's "first hydrodynamic transition". A prediction for the peak current density (equation (117)) is formulated and verified experimentally (Fig. 58). More detailed conclusions are given on pg. 137.

F. The vanishing of the hydrodynamic mechanisms at low gravity and for small sizes of heaters. It is shown by the extensive experiments of Bakhru that the hydrodynamic stability mechanisms vanish as  $R'$  is reduced from 0.15 to about 0.01. For  $R' \lesssim 0.01$  the conventional boiling curve with its well-known maxima and minima is replaced with a monotonic curve. This curve passes from natural convection directly into film boiling without a nucleate or transitional boiling regime. Full conclusions relating to the prediction of the heat flux in this case are given in the conclusions on pages 168 and 170.

G. "Spinoff". A variety of studies completed under the present grant, but not immediately related to the hydrodynamic theory, are excluded from this report. These studies of condensation, convection, fins, and computer coding are described briefly on pages 2 and 3, and full references are given to published work.

The initial aim of determining the influence of gravity has been fully met in this work since every one of these results includes gravity in the analysis or in the non-dimensional correlation of data. The influence of gravity is thus made clear in all cases.

## APPENDIX A NOMENCLATURE

|                 |   |
|-----------------|---|
| $A_h$           | area of heater (or of cathode in the context of electrolysis)   |
| $A_j$           | cross-sectional area of vapor jets escaping from $A_h$  |
| B               | ratio of viscous to surface tension force in vapor blanket, $q\mu_g/(\rho_g h_{fg}^* \sigma)$                 |
| Bi              | Biot number, $hR/k_w$ in context of Chapter III and $hR/2k_w$ in context of Chapter VII.                      |
| Bo              | the Bond number, ratio of buoyant to surface tension forces, $R_c^2(\rho_f - \rho_g)g/\sigma \equiv R'_c{}^2$ |
| $C_1$           | constant in $\dot{v}_{\min F}$ expression, equation (111)   |
| $C_2$           | constant in $\dot{v}_{\min cyl}$ expression, equation (112)   |
| $C_3$           | fraction of axial distance, on cathode or heating element, occupied by gas or vapor jets                      |
| c               | speed of a disturbance in a liquid-vapor interface  |
| $c_p(T)$        | specific heat of heater material, a function of T   |
| $c_v$           | specific heat of vapor  |
| $D_b$           | bubble diameter at departure from cathode or heating element  |
| $d_f, d_g$      | depth of liquid and vapor phases, respectively  |
| E               | voltage drop between cathode and anode  |
| $E_{c-b}$       | voltage drop from cathode to nearby liquid bulk   |
| $f(\text{---})$ | any function of ---   |
| $f_b$           | number of bubbles released per second   |
| g               | actual gravity (or body) force acting on a heater or cathode  |

|               |   |
|---------------|---|
| $g_e$         | earth-normal gravity  |
| H             | vertical dimension of a horizontal ribbon   |
| $h_{fg}$      | latent heat of vaporization   |
| $h_{fg}^*$    | latent heat of vaporization corrected for sensible heat,<br>$h_{fg} [1 + 0.34 c_v \Delta T / h_{fg}]^2$   |
| h             | heat transfer coefficient   |
| I             | electrical current  |
| i             | $\sqrt{-1}$   |
| K             | dimensionless wave number, $k \sqrt{\sigma / [g(\rho_f - \rho_g)]}$ . Also denotes dimensionless group defined in Fig. 28   |
| $k, k_g, k_w$ | thermal conductivity of liquid, vapor, and heater, respectively   |
| L             | a characteristic dimension (= H or R in certain of the present applications). Also used in Chapter VI to denote spacing between adjacent vapor jets                                       |
| M             | liquid viscosity parameter, defined in equation (75). Also used to designate molecular weight (of $H_2$ ) in Chapter VI   |
| N             | Borishanski number, defined in equation (11)  |
| $N_j$         | number of vapor jets on a heater of area, $A_h$   |
| Nu            | Nusselt number, $2hR/k$   |
| n             | number of electrons (equal to 2) per $H_2$ atom formed by electrolysis  |
| $n_s$         | nucleation site density   |
| P             | absolute pressure (at surface of heater in context of Chapters IV and V). Also used in context of Chapter III to denote length of perimeter of the cross-section of a long slender heater |

|                      |  |
|----------------------|--|
| $Pe$                 | dimensionless velocity, or Peclet number, defined by equation (123)  |
| $P_g$                | pressure in a gas jet  |
| $p_f, p_g$           | perturbation pressure in liquid and gas, respectively  |
| $p_o$                | total perturbation pressure  |
| $q$                  | average heat flux on an entire heater. Also heat flux on the unblanketed portion of the heater when used with $q_b$ in Chapter VI          |
| $q_{max}, q_{max_F}$ | peak heat flux for a particular heater geometry and for an "infinite" flat plate, respectively   |
| $q_{max_Z}$          | a characteristic heat flux defined by equation (1), equal to Zuber's prediction for infinite horizontal flat plates                        |
| $q_{min}, q_{min_F}$ | minimum heat flux on a cylindrical heater and on an infinite flat plate, respectively  |
| $q_r$                | radiant heat flux  |
| $R$                  | radius of spherical or cylindrical heating element or of cylindrical cathode   |
| $Ra^*$               | modified Rayleigh number defined in equation (131)   |
| $R_c$                | radius of a cylindrical heater corrected for the vapor blanket thickness around it   |
| $Re$                 | Reynold's number as defined below equation (94) in the context of Chapter V, and as defined in equation (86) in the context of Chapter IV. |
| $R_j$                | radius of an escaping vapor jet  |
| $r$                  | radius of a bubble   |
| $T$                  | temperature  |
| $\Delta T_{ov}$      | temperature overshoot, $T$ at nucleation minus minimum $T$ for $q$ beyond nucleation   |

|   |  |
|---|--|
| $T_{\text{sat}}$  | saturation temperature of a liquid   |
| $T_w$   | temperature of heater wall   |
| $t$   | time   |
| $U_f$   | primary velocity of the liquid in a liquid column  |
| $U_{f_m}$   | maximum primary downward velocity in the liquid  |
| $U_g$   | primary velocity of the gas in a gas jet   |
| $U_{g_m}$   | maximum primary velocity of the gas  |
| $U_H$   | vapor velocity in a jet, for which jet becomes Helmholtz unstable  |
| $u$   | speed of vapor patch propagation. Also used to denote perturbation velocity of gas in x-direction in Chapter V   |
| $u_g, u_f$  | perturbation velocity of gas and liquid, respectively, in the x-direction. Used in Chapter IV  |
| $V$   | dimensionless gas viscosity parameter, defined in equation (106)   |
| $v$   | perturbation velocity of gas in the y-direction. Used in Chapter V   |
| $\dot{v}$   | vapor or gas volume flux   |
| $v_f, v_g$  | perturbation velocity of liquid and gas, respectively, in the y-direction. Used in Chapter IV  |
| $\dot{v}_{\text{max}}, \dot{v}_{\text{min}}, \dot{v}_{\text{sc}}$ | volume flux at the "second" (or Helmholtz unstable) transition, at the minimum film electrolysis or boiling transition, and at the "first" (or isolated-bubbles to slugs-and-columns) transition, respectively |
| $x, x_b$  | axial distance coordinate; subscript b denotes reversed coordinate under the blanketed portion of the wire   |
| $y$   | distance measured normal to axial direction  |

## Greek Letters

|                        |  |
|------------------------|--|
| $\alpha$               | thermal diffusivity of heater  |
| $\beta$                | contact angle or angle between liquid-vapor (or gas) interface and heater (or cathode) surface, measured on the liquid side  |
| $\Gamma$               | dimensionless density, $(\rho_f - \rho_g) / (\rho_f + \rho_g)$   |
| $\delta$               | vapor blanket thickness near the peak heat flux  |
| $\Delta$               | dimensionless vapor blanket thickness in film boiling, $d_g/R$ . Also designates $\delta\sqrt{g(\rho_f - \rho_g)/\sigma}$  |
| $\Delta T$             | temperature difference between a heater wall and a liquid  |
| $\Delta t, \Delta r$   | increments of time and sphere radius in numerical computation  |
| $\eta$                 | ordinate of an interface measured from its mean position   |
| $\theta, \theta_o$     | dimensionless temperatures, $\theta/\theta_e$ and $\theta_o/\theta_e$ , respectively   |
| $\theta$               | temperature measured above $T_{sat}$   |
| $\theta_e$             | equilibrium temperature in the wire, $q/h$   |
| $\theta_o$             | vapor patch triggering temperature   |
| $\Lambda$              | dimensionless wavelength, $(\lambda/2\pi)\sqrt{g(\rho_f - \rho_g)/3\sigma} = 1/K\sqrt{3}$ . Also denotes a dimensionless function, $2\sigma h_{fg} T_{sat} / \Delta T h_{fg} k$ in Chapter VII |
| $\Lambda_d$            | dimensionless "most susceptible" wavelength  |
| $\lambda$              | wavelength   |
| $\lambda_c, \lambda_d$ | the "critical" or minimum and "most susceptible" or most rapidly growing wavelengths, respectively   |

|                  |   |
|------------------|---|
| $\lambda_H$      | Helmholtz unstable wavelength   |
| $\mu_f, \mu_g$   | viscosity of liquid and vapor, respectively   |
| $\xi, \xi_b$     | dimensionless axial parameters defined after equation (125)   |
| $\rho_f$         | density of saturated liquid or of electrolyte   |
| $\rho_g$         | density of saturated vapor or of gas generated at cathode   |
| $\rho_h$         | density of heater material  |
| $\rho_{H_2}$     | density of gaseous hydrogen (special case for $\rho_g$ in the context of electrolysis)  |
| $\sigma$         | surface tension between a liquid and its vapor  |
| $\tau_f, \tau_g$ | perturbation shear stress in liquid and vapor, respectively   |
| $\Phi$           | perturbation potential function as defined in equation (57)   |
| $\Psi$           | perturbation function as defined in equation (52)   |
| $\Omega$         | dimensionless frequency, $\omega \sqrt[4]{\sigma/g^3(\rho_f - \rho_g)}$   |
| $\Omega_d$       | dimensionless "most susceptible" frequency  |
| $\omega$         | angular frequency (complex). Denotes $\omega(\omega)$ in Chapter IV.  |
| $\omega_d$       | maximum or "most susceptible" angular frequency   |
| $\omega_{dF}$    | "most susceptible" angular frequency on a flat plate when both the liquid and gas are considered inviscid,<br>$0.620 \sqrt[4]{g^3(\rho_f - \rho_g)/\sigma}$ |

### General Subscripts

- b denoting conditions related to the portion of heater blanketed by vapor
- c denotes a critical, or maximum stable, condition
- cyl denotes horizontal cylinder
- F "infinite" flat plate

### General Superscript

denotes a length multiplied by  $\sqrt{g(\rho_f - \rho_g)/\sigma}$

## REFERENCES

- [1] Lienhard, J.H. and Carter, W.M., "Gravity Boiling Studies-- First Annual Report," University of Kentucky, College of Engineering, Tech. Rept. 1-68-ME-1, July 1968.
- [2] Sun, K.H. and Lienhard, J.H., "The Peak Pool Boiling Heat Flux on Horizontal Cylinders," College of Engineering Bulletin No. 88, University of Kentucky, May 1969.
- [3] Keeling, K.B., "Effect of Gravity Induced Convection Upon the Peak Boiling Heat Flux on Horizontal Strip Heaters," University of Kentucky, College of Engineering, Tech. Rept. 11-69-ME-4, Feb. 1969.
- [4] Lienhard, J.H. and Keeling, K.B., "An Induced Convection Effect Upon the Peak Heat Flux," Jour. Heat Transfer, vol. 92, No. 1, 1970, pp. 1-5.
- [5] Lienhard, J.H. and Sun, K.H., "Effects of Gravity and Size Upon Film Boiling from Horizontal Cylinders," Jour. of Heat Transfer, vol. 92, No. 2, 1970, pp. 292-298.
- [6] Sun, K.H. and Lienhard, J.H., "The Peak Pool Boiling Heat Flux on Horizontal Cylinders," Int. Jour. Heat, Mass Transfer, vol. 13, 1970, pp. 1425-1439.
- [7] Lienhard, J.H., "Interacting Effects of Gravity and Size Upon the Peak and Minimum Pool Boiling Heat Fluxes," NASA CR 1551, May 1970.
- [8] Lienhard, J.H. and Funk, J.E., "Design of a Perfectly 'Effective' Boiling Fin," Jour. of Basic Eng., vol. 93, No. 2, 1971, pp. 328-329.
- [9] Bakhru, N. and Lienhard, J.H., "On the Non-Existence of Peak and Minimum Boiling Heat Fluxes at Low Gravity," University of Kentucky, College of Engineering, Tech. Rept. 18-70-ME-5, March 1970.
- [10] Dhir, V. and Lienhard, J.H., "Laminar Film Condensation on Plane and Axi-Symmetric Bodies in Non-Uniform Gravity," Jour. Heat Transfer, vol. 93, No. 1, 1971, pp. 97-100.

- [11] Bhattacharya, A. and Lienhard, J.H., "The Similarity of Bubble Growth in Boiling and Electrolysis," University of Kentucky, College of Engineering, Tech. Rept. UKY-23-70-ME-7, May 1970.
- [12] Dhir, V., "Some Notes on the Development of the Hydrodynamic Theory of Boiling," (based on 3 lectures by J. H. Lienhard), University of Kentucky, College of Engineering, Tech. Rept. UKY-19-70-ME-6, March 1970.
- [13] Reich, R.A. III, and Lienhard, J.H., "Computerized Reduction of Pool Boiling Data," Boiling and Phase Change Laboratory Report, College of Engineering, 1970, University of Kentucky.
- [14] Ded, J.S., "The Peak Boiling Heat Flux on Spheres in Saturated Liquids," University of Kentucky, College of Engineering, Tech. Rept. UKY-39-71-ME-12, July 1971.
- [15] Ded, J.S. and Lienhard, J.H., "The Peak Pool Boiling Heat Flux from a Sphere," AICHE Jour., vol. 18, No. 2, 1972, pp. 337-342.
- [16] Dhir, V.K. and Lienhard, J.H., discussion (and application to film boiling) of ASME paper No. 71-FE-7, Jour. Basic Engr., vol. 94, No. 1, 1972, pp. 160-162.
- [17] Bhattacharya, A. and Lienhard, J.H., "Similarity of Vapor and Gas Bubble Growth," Iranian Jour. Sci. and Tech., vol. 1, No. 2, 1971, pp. 113-129.
- [18] Bhattacharya, A., "The Analogy Between Gas Removal Processes in Boiling and Electrolysis," University of Kentucky, College of Engineering, Tech. Rept. UKY-35-71-ME-10, July 1971.
- [19] Bhattacharya, A. and Lienhard, J.H., "Hydrodynamic Transition in Electrolysis," Jour. Basic Engr., vol. 94, No. 4, 1972, p. 804.
- [20] Bakhru, N., "Heat Transfer and Boiling from Cylinders of Small Size or Under Reduced Gravity," University of Kentucky, College of Engineering, Tech. Rept. UKY-38-71-ME-11, July 1971.
- [21] Bakhru, N. and Lienhard, J.H., "Boiling from Small Cylinders", Int. Jour. Heat & Mass Transfer, vol. 15, No. 11, 1972, p. 2011.

- [22] Lienhard, J.H., Eichhorn, R., Dhir, V.K., "Laminar Natural Convection Under Nonuniform Gravity," Jour. Heat Transfer, vol. 94, No. 1, 1972, pp. 80-86.
- [23] Lienhard, J.H. and Dhir, V.K., "A Simple Analysis of Laminar Film Condensation with Suction," Jour. Heat Transfer, vol. 94, No. 3, 1972, pp. 334-336.
- [24] Lienhard, J.H. and Dhir, V.K., "Hydrodynamic Prediction of Peak Pool Boiling Heat Fluxes from Finite Bodies," Paper No. 72-WA/HT-10, ASME Winter Annual Meeting, New York, 1972.
- [25] Lienhard, J.H. and Dhir, V.K., "On Making Hydrodynamic Predictions of the Peak and Minimum Pool Boiling Heat Fluxes," Paper No. 2.48, IVth All-Union Heat and Mass Transfer Conference, Minsk, USSR, May 1972.
- [26] Dhir, V.K. and Lienhard, J.H., "The Influence of Viscosity and Other System Variables Upon the Taylor Wavelength in Pool Boiling," XVth Siberian Thermophysical Seminar on Critical Phenomena in Two-Phase Systems, Novosibirsk, USSR, May 1972.
- [27] Dhir, V.K., "Viscous Hydrodynamic Instability Theory of the Peak and Minimum Heat Fluxes," College of Engineering, Bulletin No. UKY-100, University of Kentucky, November 1972, (Ph.D. Dissertation, August 1972).
- [28] Three manuscripts, related to [27], published by University of Kentucky in 1973.
- a. Lienhard, J.H., Dhir, V.K., and Rihard, D.M., "Peak Pool Boiling Heat Flux Measurements on Finite Horizontal Flat Plates."
  - b. Dhir, V.K., and Lienhard, J.H., "Taylor Stability of Viscous Fluids with Application to Film Boiling."
  - c. Dhir, V.K., and Lienhard, J.H., "Peak Pool Boiling Heat Flux in Viscous Liquids."
- [29] Zuber, N., "Hydrodynamic Aspects of Boiling Heat Transfer," AEC Report No. AECU-4439, Physics and Mathematics, 1969.
- [30] Kutateladze, S.S., "On the Transition to Film Boiling Under Natural Convection," Kotloturbostroenie, No. 3, 1948, p. 10.
- [31] Bellman, R. and Pennington, R.H., "Effects of Surface Tension and Viscosity on Taylor Instability," Quart. App. Math., vol. 12, 1954, pp. 151-162.

- [32] Moissis, R. and Berenson, P.J., "On the Hydrodynamic Transition in Nucleate Boiling," Jour. Heat Transfer, vol. 85, No. 3, 1963, pp. 53-78.
- [33] Lienhard, J.H. and Wong, P.T.Y., "The Dominant Unstable Wavelength and Minimum Heat Flux During Film Boiling on a Horizontal Cylinder," Jour. Heat Transfer, vol. 86, No. 2, 1964, pp. 220-226.
- [34] Lamb, Sir H., Hydrodynamics, 6th ed., Dover, New York, 1945.
- [35] Berenson, P.J., "Transition Boiling Heat Transfer from a Horizontal Surface," M.I.T. Heat Transfer Laboratory Tech. Report No. 17, 1960.
- [36] Borishanski, V.M., "An Equation Generalizing Experimental Data on the Cessation of Bubble Boiling in a Large Volume of Liquid," Zhurnal Technicheski Fiziki, vol. 25, 1956, pg. 252.
- [37] Chang, Y.P., "A Theoretical Analysis of Heat Transfer in Natural Convection and in Boiling," Trans. ASME, vol. 79, 1957, pg. 1501.
- [38] Zuber, N., Tribus, M., and Westwater, J.W., "The Hydrodynamic Crisis in Pool Boiling of Saturated Liquids," #27, International Developments in Heat Transfer, ASME, New York, 1963, pp. 230-236.
- [39] Bobrovich, G.I., Gogonin, I.I. and Kutateladse, S.S., "Influence of Size of Heater Surface on the Peak Pool Boiling Heat Flux," Jour. App. Mech. and Tech. Phys., (ТМТ), No. 4, 1964, pp. 137-138.
- [40] Lienhard, J.H. and Watanabe, K., "On Correlating the Peak and Minimum Boiling Heat Fluxes with Pressure and Heater Configuration," Jour. Heat Transfer, Trans. ASME, Series C, vol. 88, No. 1, 1966, pp. 94-100.
- [41] Costello, C.P., Bock, C.O., and Nichols, C.C., "A Study of Induced Convection Effects on Pool Boiling Burnout", CEP Symposium Series, vol. 61, 1965, pp. 271-280.
- [42] Cichelli, M.T. and Bonilla, C.F., "Heat Transfer to Liquids Boiling Under Pressure," Trans. A.I.Ch.E., vol. 41, 1945, p.755.

- [43] Riherd, D.M., "The Effect of Size on Peak Heat Flux for Small, Horizontal, Square Heaters," unpublished undergraduate research project in course ME 395, Univ. of Ky., Mech. Engr. Dept., July 1972.
- [44] Westwater, J.W. and Santangelo, J.G., "Photographic Study of Boiling", Ind. and Engr. Chem., vol. 47, 1955, p. 1605.
- [45] Costello, C.P. and Adams, J.M., "The Interrelation of Geometry, Orientation and Acceleration in the Peak Heat Flux Problem", Mech. Engr. Dept. Report, University of Washington, Seattle, 1963.
- [46] Hendricks, R.C., Private Communication of unpublished data related to the paper by Hendricks and Baumeister, "Film Boiling from Submerged Spheres", NASA TND-5124, June 1969.
- [47] Bergles, A.E. and Thompson, W.G., Jr., "The Relationship of Quench Data to Steady-State Pool Boiling Data," Int. J. Heat Mass Transfer, vol. 13, 1970, pp. 55-68.
- [48] Veres, D.R. and Florschuetz, L.W., "A Comparison of Transient and Steady-State Pool-Boiling Data Obtained Using the Same Heating Surface," Jour. Heat Transfer, Trans. ASME, Series C, vol. 93, No. 2, 1971, pp. 229-232.
- [49] Merte, H. Jr. and Clark, J.A., "Boiling Heat Transfer with Cryogenic Fluids at Standard, Fractional and Near-Zero Gravity," Jour. Heat Transfer, Trans. ASME, Series C, vol. 86, No. 3, August 1964, pp. 351-359.
- [50] Bradfield, W.S., "On the Effect of Subcooling on Wall Superheat in Pool Boiling," Jour. Heat Transfer, Trans. ASME, Series C, vol. 89, 1967, pp. 269-270.
- [51] Houchin, W.R. and Lienhard, J.H., "Boiling Burnout in Low Thermal Capacity Heaters," ASME Paper 66-WA/HT-40, Winter Annual ASME Meeting, New York, N.Y., Nov. 1966.
- [52] Lienhard, J.H. and Schrock, V.E., "The Effect of Pressure, Geometry, and the Equation of State upon the Peak and Minimum Boiling Heat Flux," Jour. Heat Transfer, Trans. ASME, Series C, vol. 85, No. 3, 1963, pp. 261-272.

- [53] Adams, J.M., "A Study of the Critical Heat Flux in an Accelerating Pool Boiling System," Ph.D. Thesis, Univ. of Wash., Seattle, September 1, 1962. Also released as Univ. of Wash. Mech. Eng. Dept. Report to NSF, September 1, 1962.
- [54] Taylor, G.I., "The Instability of Liquid Surfaces When Accelerated in a Direction Perpendicular to Their Plane," Proc. Roy. Soc. London, A-201, 1950, p. 192.
- [55] Hsieh, D.Y., "Effects of Heat and Mass Transfer on Rayleigh-Taylor Instability," Jour. Basic Engineering, Trans. ASME, Series D, vol. 94, No. 1, March 1972, pp. 156-162.
- [56] Dhir, V. and Lienhard, J.H., discussion of "Effects of Heat and Mass Transfer on Rayleigh-Taylor Instability," by D.Y. Hsieh, Jour. Basic Engineering, Trans. ASME, Series D, vol. 94, No. 1, March 1972, pp. 161-162.
- [57] Numerical Analysis Library for the S/360. University Computing Center, University of Kentucky, Lexington, Kentucky, December 1970.
- [58] Baumeister, K.J. and Hamill, T.D., "Film Boiling from a Thin Wire as an Optim Boundary-Value Process", ASME Paper 67-HT-62 ASME-AIChE Heat Transfer Conference, Seattle, Wash., 1967.
- [59] Breen, B.P. and Westwater, J.W., "Effects of Diameter of Horizontal Tubes on Film Boiling Heat Transfer," Chem. Engr. Prog., vol. 58, No. 7, 1962, pp. 67-72.
- [60] Touloukian, Y.S. and Dewitt, D.Y., Thermal Radiative Properties of Metallic Elements and Alloys, IFI/Plenum-New York, 1970.
- [61] Guboreff, G.G., Jansen, J.E. and Torborg, R.H., "Thermal Radiative Properties Survey", 2nd ed., Honeywell Research Center, Minneapolis-Honeywell Regulator, Minneapolis, 1960.
- [62] Lienhard, J.H. and Wong, P.T.Y., "The Dominant Unstable Wavelength During Film Boiling", ASME/ESL Film Library.
- [63] Nishikawa, K., Shimomura, R., Hatano, M. and Negatomo, H., "Investigation of Surface Boiling Under Free Convection", Bulletin of the JSME, vol. 10, No. 37, 1967, pp. 123-131.

- [64] Grigull, U. and Abadzic, E., "Heat Transfer From a Wire in the Critical Region," Proc. Inst. Mech. Engrs., vol. 182, Pt. 31, 1967-8, pp. 52-57.
- [65] Abadžić, E. and Goldstein, R.J., "Film Boiling and Free Convection to Carbon Dioxide Near the Critical State", Int. Jour. Heat Mass Transfer, vol. 13, 1970, pp. 1163-1175.
- [66] Kovalev, S.A., "An Investigation of Minimum Heat Fluxes in Pool Boiling of Water," Int. Jour. Heat Mass Transfer, vol. 9, 1966, p. 1219.
- [67] Brooke Benjamin, T., "Shearing Flow Over a Wavy Boundary", J. Fluid Mech., vol. 6, 1959, pp. 161-205.
- [68] Wydeven, T. and Jonson, R.W., "Water Electrolysis: Prospects for the Future," Jour. Engr. for Ind., vol. 90, 1968, p. 531.
- [69] Secord, T.C. and Ingelfinger, A.L., "Life Support for Large Space Stations," Astronautics and Aeronautics, Feb. 1970, p.56.
- [70] Zuber, N., "Hydrodynamic Aspects of Nucleate Pool Boiling -- Part I," Report No. RW-RL-164, Ramo Wooldridge Research Laboratory, Conoga Park, Calif., Jan. 1960.
- [71] Zuber, N., "Nucleate Boiling. The Region of Isolated Bubbles and the Similarity with Natural Convection," Int. J. Heat Mass Transfer, vol. 6, 1963, pp. 53-78.
- [72] Moissis, R. and Griffith, P., "Entrance Effects in a Two-Phase Slug Flow," Journal of Heat Transfer, ASME Trans., Series C, vol. 84, 1962, pp. 29-39.
- [73] Griffith, P. and Wallis, G., "Slug Flow", M.I.T. Div. of Spons. Res., Rept. No. 15, Project 7-7673, 1959.
- [74] Tien, C.L., "A Hydrodynamic Model for Nucleate Pool Boiling," Int. Jour Heat Mass Transfer, vol. 5, 1962, p. 533.
- [75] Boehm, R.F. and Lienhard, J.H., "Transient Effects in Tien's Nucleate Boiling Model," ASME paper no. 64-WA/HT-34, ASME Winter Annual Meeting, New York, Dec. 1964.

- [76] Kirby, D.B. and Westwater, "Bubble and Vapor Behavior on a Heated Horizontal Plate During Pool Boiling Near Burnout," Chem. Engr. Prog., vol. 61, no. 57, 1965, pp. 238-248.
- [77] Jakob, M., Heat Transfer, vol. 1, John Wiley and Sons, New York, 1955, p. 630.
- [78] Kellogg, H.H., "Anode Effect in Aqueous Electrolysis," Jour. Electrochemical Soc., vol. 97, 1950, pp. 133-142.
- [79] Meyer, R.E., "Faraday's Laws," Encyclopedia of Electrochemistry, (C.A. Hampel, ed.), Reinhold Pub. Co., 1969, pp. 592-594.
- [80] Griffith, P. and Wallis, J.D., "The Role of Surface Conditions in Nucleate Boiling," Chemical Engineering Symposium Series, Storrs, Conn., no. 30, vol. 56, 1960, pp. 49-63.
- [81] Trivedi, G. and Funk, J.E., "Dynamics and Stability of Electrolytic Bubbles: Bubble Departure Diameters," University of Kentucky, College of Engineering, Tech. Rept. UKY 28-70-ME8, 1970.
- [82] Trivedi, G., unpublished results, University of Kentucky Boiling and Phase-Change Laboratory, 1971.
- [83] Chang, Y.P. and Snyder, N.W., "Heat Transfer in Saturated Boiling," Chemical Engineering Symposium Series, Storrs, Conn., no. 30, vol. 56, 1960, pp. 25-38.
- [84] Kutateladze, S.S., Valukuna, N.V., and Gogonin, I.I., "Influence of Heater Size on the Peak Heat Flux in Saturated Liquids," Inzhenerno Fizicheskii Zhurnal, vol. 12, no. 5, 1967, pp. 569-575.
- [85] Siegel, R. and Howell, J.R., "Critical Heat Flux for Saturated Pool Boiling from Horizontal and Vertical Wires in Reduced Gravity," NASA Tech. Note TND-3123, Dec. 1965.
- [86] Pitts, C.C. and Leppert, G., "The Critical Heat Flux for Electrically Heated Wires in Saturated Pool Boiling," Int. J. Heat Mass Transfer, vol. 9, 1966, pp. 365-377.

- [87] Siegel, R. and Usiskin, C., "Photographic Study of Boiling in the Absence of Gravity," Jour. Heat Transfer, Trans. ASME, Series C, vol. 81, no. 3, 1959, pp. 230-236.
- [88] Siegel, R. and Keshock, E.G., "Effects of Reduced Gravity on Nucleate Boiling Bubble Dynamics in Saturated Water," AICHE Jour., vol. 10, no. 4, 1964, pp. 509-516.
- [89] van Stralen, S.J.D. and Sluyter, W.M., "Investigation on the Critical Heat Flux of Pure Liquids and Mixtures Under Various Conditions," Int. J. Heat Mass Transfer, vol. 12, 1969, pp. 1353-1384.
- [90] McAdams, W.H., Heat Transmission, 3rd Edition, McGraw Hill Book Co., New York, 1954.
- [91] Trefethen, L., Surface Tension in Fluid Mechanics, film distributed by Educational Services Inc., Watertown, Mass.
- [92] Trefethen, L., "On the Jet Propulsion of Bubbles in a Heated Liquid," Tufts University, Mechanical Engineering, Report No. 61-S-1, August 1961.
- [93] Hsu, Y.Y., "On the Range of Active Nucleation Cavities on a Heating Surface," Jour. Heat Transfer, Trans. ASME, Series C, vol. 84, no. 3, 1962, pp. 207-216.
- [94] Brown, W.T., Jr., "A Study of Flow Surface Boiling," Ph.D. Thesis, Mech. Eng. Dept., Massachusetts Institute of Technology, 1967.
- [95] Bergles, A.E., Bakhru, N. and Shires, J.W., Jr., "Cooling of High Power Density Computer Components," Tech. Rept. No. 70712-60, Heat Transfer Lab., Mech. Engr. Dept., M.I.T., Nov. 1968.
- [96] Johnson, H.A., Schrock, V.E., Selph, F.B., Lienhard, J.H. and Rosztoczy, Z.R., "Temperature Variation, Heat Transfer, and Void Volume Development in the Transient Atmospheric Boiling of Water," AEC Rept.: SAN-1001, 1961.
- [97] Corty, C. and Faust, A.S., "Surface Variables in Nucleate Boiling," Chemical Engineering Progress Symposium Series, vol. 51, no. 17, 1955, pp. 1-12.

- [98] Rohsenow, W.M., "Heat Transfer with Boiling," Chapter in Modern Developments in Heat Transfer, W.M. Rohsenow, ed., The M.I.T. Press, 1964.
- [99] Bromley, L.A., "Heat Transfer in Stable Film Boiling," Chem. Engr. Prog., vol. 46, no. 5, 1950, pp. 221-227.